eISSN 2500-0632

MINING SCIENCE AND TECHNOLOGY (RUSSIA)

ТОМ
VOL. 7, №2
2022

GORNYE NAUKI I TEKHNOLOGII

ГОРНЫЕ НАУКИ И ТЕХНОЛОГИИ

MISIS
НАЦИОНАЛЬНЫЙ ИССЛЕДОВАТЕЛЬСКИЙ ТЕХНОЛОГИЧЕСКИЙ УНИВЕРСИТЕТ «МИСИС»
NATIONAL UNIVERSITY OF SCIENCE AND TECHNOLOGY MISIS

MINING SCIENCE AND TECHNOLOGY (Russia)

Горные науки и технологии

SCIENTIFIC AND PRACTICAL E-JOURNAL

eISSN 2500-0632

2022

Vol. 7, no. 2

https://mst.misis.ru/

Activities of the ***Mining Science and Technology (Russia) (Gornye nauki i tekhnologii)*** international journal are aimed at developing international scientific and professional cooperation in the field of mining.

The journal target audience comprises researchers, specialists in the field of mining, representatives of academic and professional communities.

The journal publishes original papers describing research findings, experience in the implementation of projects in mining industry, review publications.

The journal seeks to develop interdisciplinary areas that contribute to progress in mining, for example, technological and environmental safety, project organization and management in mining industry, development of territories, legal aspects of natural resource use, and other areas studied by researchers and practitioners. The journal always welcomes new developments. Papers are accepted in English or Russian.

QUARTERLY

FOUNDED in 2016

REGISTRATION

The journal science and applied research journal is registered by the Federal Service for Communication, IT and Mass Communication Control on August 10, 2015.
Registration Certificate E-No. ФС77-62652

INDEXATION

Scopus, CAS, EBSCO, DOAJ, РИНЦ, ВИНИТИ РАН, Dimensions, BASE, J-Gate, Jisc Library Hub Discover.

FOUNDER AND PUBLISHER

The National University of Science and Technology MISiS (NUST MISiS)

CONTACT

4 Leninsky Prospect, Moscow 119049, Russian Federation
Phone: +7 (495) 955-00-77
e-mail: send@misis.ru

ГОРНЫЕ НАУКИ И ТЕХНОЛОГИИ

Mining Science and Technology (Russia)

ЭЛЕКТРОННЫЙ НАУЧНО-ПРАКТИЧЕСКИЙ ЖУРНАЛ

eISSN 2500-0632

2022

Т. 7, № 2

https://mst.misis.ru/

Деятельность научно-практического журнала «Горные науки и технологии» (Mining Science and Technology (Russia)) направлена на развитие международного научного и профессионального сотрудничества в области горного дела.

Целевая аудитория журнала – исследователи, специалисты в области горного дела, представители академического и профессионального сообществ.

В журнале публикуются оригинальные статьи, описывающие результаты исследований, опыт реализации проектов в горнопромышленном комплексе, обзорные публикации.

Журнал стремится развивать такие междисциплинарные направления, как технологическая и экологическая безопасность, организация и управление проектами в горной промышленности, развитие территорий, правовые аспекты использования природных ресурсов и другие, которые способствуют прогрессу в горном деле и реализуются исследователями и практиками.

ПЕРИОДИЧНОСТЬ 4 раза в год

ОСНОВАН в 2016 году

РЕГИСТРАЦИЯ

Зарегистрирован Федеральной службой по надзору в сфере связи, информационных технологий и массовых коммуникаций 10 августа 2015 года.
Свидетельство о регистрации Эл № ФС77-62652.

ИНДЕКСИРОВАНИЕ

Scopus, CAS, EBSCO, DOAJ, РИНЦ, ВИНИТИ РАН, Dimensions, BASE, J-Gate, Jisc Library Hub Discover.

OPEN ACCESS Журнал открытого доступа.

УЧРЕДИТЕЛЬ И ИЗДАТЕЛЬ

МИСиС Национальный исследовательский технологический университет «МИСиС» (НИТУ «МИСиС»)

АДРЕС УЧРЕДИТЕЛЯ И ИЗДАТЕЛЯ

119049, г. Москва, Ленинский проспект, д. 4

КОНТАКТЫ РЕДАКЦИИ

Адрес: 119049, г. Москва, Ленинский проспект, д. 4
Телефон: +7 (495) 955-00-77
e-mail: send@misis.ru

MINING SCIENCE AND TECHNOLOGY (Russia)
Горные науки и технологии
SCIENTIFIC AND PRACTICAL E-JOURNAL
eISSN 2500-0632
2022
Vol. 7, no. 2
https://mst.misis.ru/

CONTENTS

ГОРНЫЕ НАУКИ И ТЕХНОЛОГИИ
Mining Science and Technology
ЭЛЕКТРОННЫЙ НАУЧНО-ПРАКТИЧЕСКИЙ ЖУРНАЛ
eISSN 2500-0632
2022
Т. 7, № 2
https://mst.misis.ru/

СОДЕРЖАНИЕ

MINERAL RESOURCES EXPLOITATION

Research article

https://doi.org/10.17073/2500-0632-2022-2-93-99

Substantiation of pillar parameters in mining of inclined coal seams in Quang Ninh Province, Vietnam

V. N. Nguyen[1], T. N. Pham[1], P. Osinski[2], T. C. Nguyen[1], L. H. Trinh[3]
[1] *Hanoi University of Mining and Geology, Hanoi, Vietnam*
[2] *Institute of Civil Engineering, Warsaw University of Natural Science, Warsaw, Poland*
[3] *Le Quy Don Technical University, Hanoi, Vietnam*
✉ *phamthinhan@humg.edu.vn*

Abstract
Design and operation of auxiliary underground workings in coal mines involves substantiation of parameters of coal pillars and requires development of new approaches to substantiate their geometrics. On the one hand, sufficient stability of a "rock mass – working – coal pillar" system should be ensured. On the other hand, the parameters of "frozen" coal reserves in the pillars should be justified. The joint solution of these two problems requires accurate forecasting based on modern digital models of a rock mass. In this study, a model of rock mass and mine workings with different dimensions of a coal pillar is presented with the use of Flac3D software. The simulation findings showed that when developing sloping coal seams, the volume of coal extraction in a longwall has an effect on the stress-strain state of the enclosing rock mass. During the study different factors having effect on geometrics of a coal pillar were analyzed, and their influence on the field of stresses and shear of inclined layers in a rock mass was studied, and the size of the plastic deformation zone around an auxiliary mine working was also determined. The study findings are also of practical importance in terms of substantiating the parameters of a working support design. The size of coal pillar is also connected with the support type. It should be taken into account that bolts should be of sufficient length to ensure firm fixing and located in the zone of intact rocks. The research showed that a coal pillar should be 10 to 15 m wide in order to ensure optimal mining conditions and safety.

Keywords
Mining, coal mining, coal pillar, rock mass, working, rock mass stress, stability, numerical model, Quang Ninh, Vietnam, Flac3D

Acknowledgments
This study was supported by the project "A study on the application of a numerical method to predict instability of a tunnel under dynamic load in deep mining environment and propose reasonable support system", coded 191/HĐ-KHCN-KC.01.DD03-18/16-20.

For citation
Nguyen V.N., Pham T.N., Osinski P., Nguyen T.C., Trinh L.H. Substantiation of pillar parameters in mining of inclined coal seams in Quang Ninh Province, Vietnam. *Mining Science and Technology* (*Russia*). 2022;7(2):93–99. https://doi.org/10.17073/2500-0632-2022-2-93-99

РАЗРАБОТКА МЕСТОРОЖДЕНИЙ ПОЛЕЗНЫХ ИСКОПАЕМЫХ

Научная статья

Обоснование параметров целиков при отработке наклонных угольных пластов в условиях шахт провинции Куангнинь Вьетнама

В.Н. Нгуен[1], Т.Н. Фам[1], П. Осинский[2], Т.К. Нгуен[1], Л.Х. Чинь[3]
[1] *Ханойский горно-геологический университет, Ханой, Вьетнам*
[2] *Варшавский университет естественных наук, Варшава, Польша*
[3] *Технический университет им. Ле Куи Дон, Ханой, Вьетнам*
✉ *phamthinhan@humg.edu.vn*

Аннотация
Проектирование и эксплуатация вспомогательных подземных выработок при разработке угольных месторождений предполагают обоснование параметров целиков угля и требуют разработки новых подходов для обоснования их геометрических параметров. С одной стороны, необходимо обеспечить достаточную устойчивость системы «массив горных пород – выработка – угольный целик», с другой –

обосновать параметры «замороженных» в целиках запасов угля. Совместное решение этих двух задач требует точного прогнозирования на основе современных цифровых моделей массива горных пород. В настоящем исследовании авторы публикации, используя программное обеспечение Flac3D, представили модель массива горных пород и выработок с различными размерами угольного целика. Результаты моделирования показали, что в условиях наклонного залегания угольных пластов и массива горных пород объём добычи угля в забое влияет на напряженно-деформированное состояние массива горных пород. В ходе исследования были проанализированы различные факторы, влияющие на геометрические параметры угольного целика, изучено их влияние на поле напряжений и смещений горных пород, происходящих в условиях их наклонного залегания в массиве, а также определена величина зоны пластической деформации вокруг вспомогательной выработки. Результаты исследования имеют практическое значение и в части обоснования параметров конструкции крепи выработки. Размер угольного целика также связан с типом крепи выработки. Следует учитывать, что анкер должен иметь достаточную для прочного крепления длину и располагаться в зоне ненарушенных горных пород. Исследования показали, что для обеспечения оптимальных условий ведения горных работ и безопасности ширина угольного целика должна составлять от 10 до 15 м.

Ключевые слова
горное дело, добыча угля, угольный целик, массив горных пород, выработка, напряжения в массиве горных пород, устойчивость, цифровая модель, провинция Куангнинь, Вьетнам, Flac3D

Финансирование
Это исследование было поддержано проектом «Исследование применения численного метода для прогнозирования стабильности горных выработок в условиях динамических нагрузок при глубокой разработке, а также для обоснования конструкции горных выработок», код 191/HĐ-KHCN-KC.01.DD03-18/16-20.

Для цитирования
Nguyen V.N., Pham T.N., Osinski P., Nguyen T.C., Trinh L.H. Substantiation of pillar parameters in mining of inclined coal seams in Quang Ninh Province, Vietnam. *Mining Science and Technology* (*Russia*). 2022;7(2):93–99. https://doi.org/10.17073/2500-0632-2022-2-93-99

Introduction

The Vietnamese coal industry aims to improve the methods of underground coal mining while improving the technical and economic level of mine development and mining safety. Quang Ninh Province has significant reserves of coal for underground mining. By 2025, the underground mining volume is expected to reach 63.1 mln t of coal. Although the underground coal mining is the most difficult technologically, underground mining of the most valuable coal grades for the industry is quite justified.

For several decades, coal industry has been conceptually developing using “mine – longwall” process principle, which ensures high productivity and competitiveness of mining enterprises. Such solutions are successfully applied at advanced coal mines in Russia, China, India, USA, Australia, and many other countries. The greatest effect of this approach is achieved while developing extraction panels of more than 1000 m long at longwall length of not less than 250–400 m. For the conditions of inclined coal seams typical for Quang Ninh Province, the implementation of high-productivity solutions on the basis of the previously voiced principles is complicated to a great extent. However, since more than 24 % of the total coal balance reserves occur under these conditions, it is necessary to solve the whole set of problems to provide effective operation of mines. One of the key problems to be solved when justifying mining processes and parameters is substantiating the size of pillars, ensuring the stability of mine workings. The search for process solutions in this field for the conditions of Vietnam’s coal mining is described in [1–4]. Although safety pillars became widely used in underground coal mining in Quang Ninh Province of Vietnam, no clear techniques for calculating and substantiating their parameters are available. In most cases, assessment of pillar parameters was based on empirical dependencies, which led to overestimation of pillar widths and, consequently, reduced the efficiency of coal extraction. In some cases, at the design stage, decisions were made without preliminary calculations, based on analogies, which also provided overstated values of pillar parameters. In conditions of longwall (mechanized) coal extraction from inclined coal seams, the task becomes even more complicated [5]. The approaches described in [6, 7] allowed to make calculations of safety pillars in conditions of Khe mine [6], where the pillar width of 6 m was substantiated, but the criteria related to ensuring stability of an auxiliary mine working, as well as a longwall parameters and characteristics were not taken into account [6]. The main idea of the present study is to determine the parameters of safety pillars by the criteria of stability of an auxiliary working [8], as well as taking into account the characteristics of a longwall in the conditions of inclined coal seams. The methods of numerical simulation of stress-strain state of rock mass on the basis of finite-difference models [9, 10] were used as a toolkit in the study. Flac3D was used as a software environment.

1. Simulation model parameters

Geometrics: length, 220 m; width, 120 m; height, 150 m.

The rock mass model includes 14 different rock layers with different properties. The rocks mechanical properties are presented in five categories (Table 1).

A force simulating the mass rock pressure acts on the top of the model. The formalized boundary conditions of the model are shown in Fig. 1.

When creating a model of the coal mining area, the following was taken into account: rock layer sloping occurrence; dimensions of coal pillars, including coal seam thickness; parameters and characteristics of rocks (consisting of sandstone, siltstone, and coal) occurring between coal seams (see Table 1) [11]. Numerical parameters of the model take into account a coal seam dip angle of 20°, thickness of 3.5 m, and the rock mass thickness (from a working bottom) of 300 m. The mine working support is presented by CBII-27 steel arched support, spaced at intervals of 0.7 m in a working.

The workings are shaped as a rectilinear semicircular arch 5.0 m wide and 3.5 m high (a working parameters are also relevant for solving the task [12]). The model includes two longwalls, LC1 and LC2, 190 m long, two ventilation drifts 01, 03, and a haulage roadway 02. The model coordinate center is located in the center of the lower ventilation drift. The simulation grid becomes denser while approaching the workings that allows more accurate studying stress-strain state of the rock mass, having effect on the workings stability (Fig. 2).

2. The main stages of model development

Based on actual tunneling data and processing results obtained by experimental method of observation, an algorithm for conducting the study was derived:

Step 1: Model development: establishing the values of stress at the measurement points in the rock mass and running the model until the equilibrium state is reached.

Step 2: Workings #1 and #2 tunneling up to the boundary of the mine field. Running the model until equilibrium state is reached.

Step 3: LC1 longwall operation. Running the model until equilibrium state is reached.

Step 4: Working #3 tunneling. Running the model until equilibrium state is reached.

Step 5: Collecting parametric modeling data. Determination of the stress-strain state of a rock mass

Table 1

Mechanical properties of rock layers

Layer	Compressive Strength σ, MPa	*E*, GPa	Density γ, *t/m*^{3}	Bedding angle φ, degrees	Rock deformability *C*, MPa
Sandstone (*f* = 6–8)	96.64	20	2.67	34	33.6
Siltstone (*f* = 4–6)	47.79	18	2.73	32	14.6
Gritstone (*f* = 8–10)	138.13	22	2.59	34	47.2
Coal (*f* = 1–2)	15	5	1.50	20	2.2

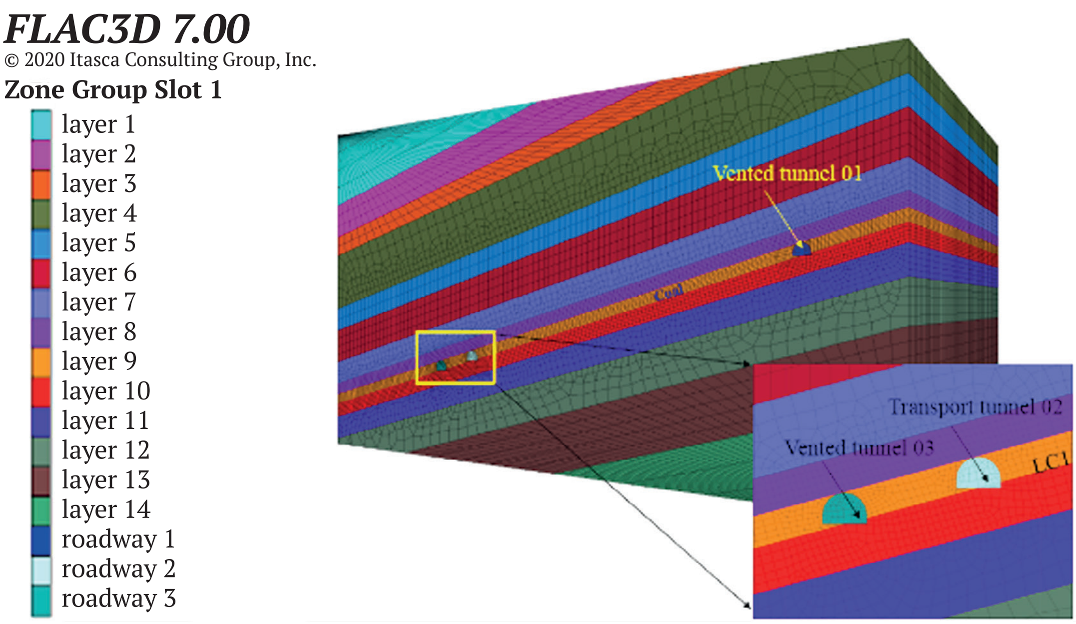

Fig. 1. Boundary conditions and model of force distribution

eISSN 2500-0632
https://mst.misis.ru/

for subsequent analysis and determination of mine workings stability.

Calculation of stress-strain state models of rock mass was carried out at different widths of coal pillars: 5, 8, 10, 15, 20, 30 m. Stability of mine working No. 3 was assessed.

3. Analysis of modeling findings

Distribution of stresses in a rock mass represented in Fig. 3 shows that coal extraction in LC1 longwall has a significant effect on distribution of vertical stress components in the rock mass around LC2 longwall. In this case, the maximum stress in the rock mass, about 25 MPa, is achieved in the coal seam within the longwall contour. The zone of maximum support pressure in the vicinity of LC2 longwall is located at a distance of about 7.5 m from the edge of coal pillar.

Distribution of stresses in a rock mass at a working roof is shown in Fig. 3. The stresses distribution in rock mass is asymmetrical in relation to the working. Thus the size of coal pillar has a significant effect on geotechnical conditions in LC2 vicinity.

The results of mathematical simulation data processing showed that when coal pillar width increases, the maximum compressive stress in the rock mass to the left of a working tends to shift towards the mined-out space of LC1 longwall. Decrease in coal pillar size results in gradual decreasing its carrying capacity that leads to shifting the maximum compressive stress towards the zone below LC1 longwall.

Fig. 5 shows the positions of rock mass plastic fracture zone around auxiliary working #3. This was used for analyzing these zones distribution. The data were also obtained on the basis of the above model.

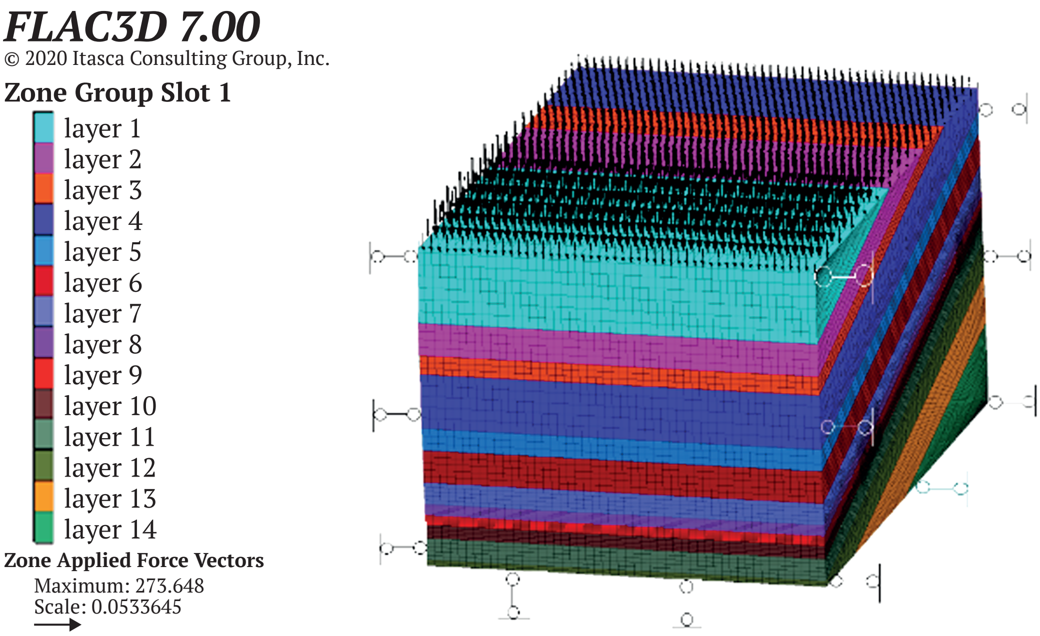

Fig. 2. Model in Flac3D

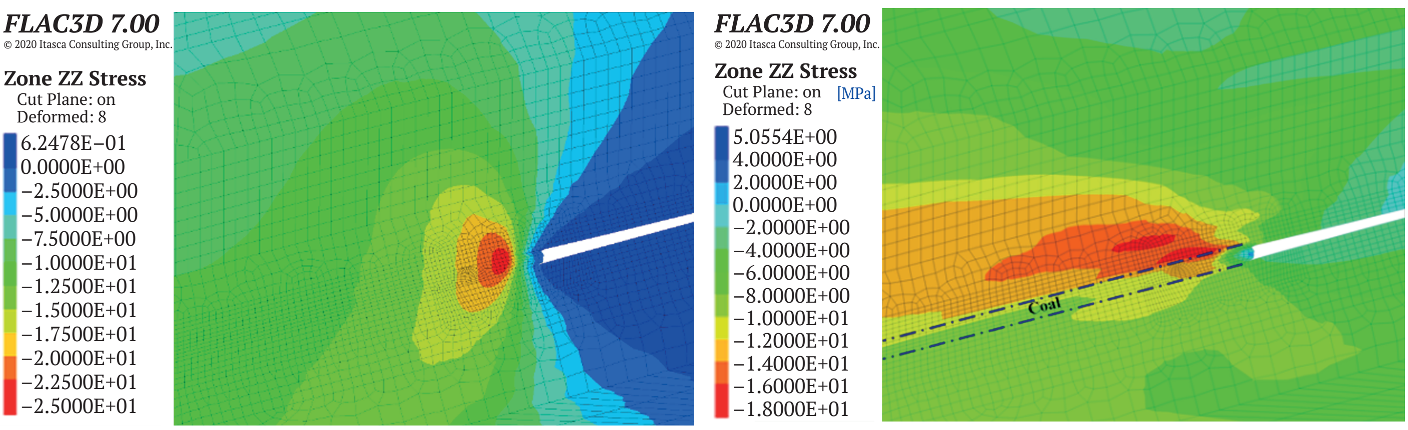

a *b*

Fig. 3. Distribution of vertical (*a*) and horizontal (*b*) stresses in rock mass

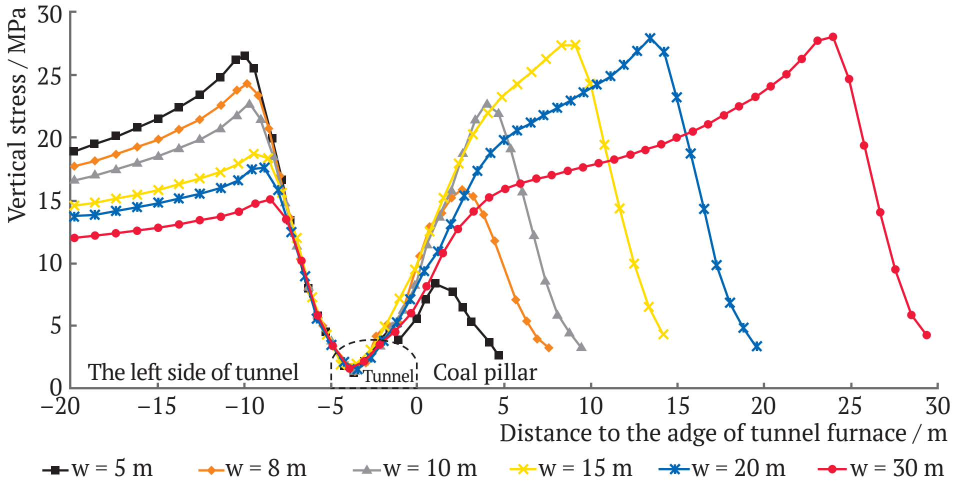

Fig. 4. Distribution of stresses at a working roof at different sizes of coal pillar

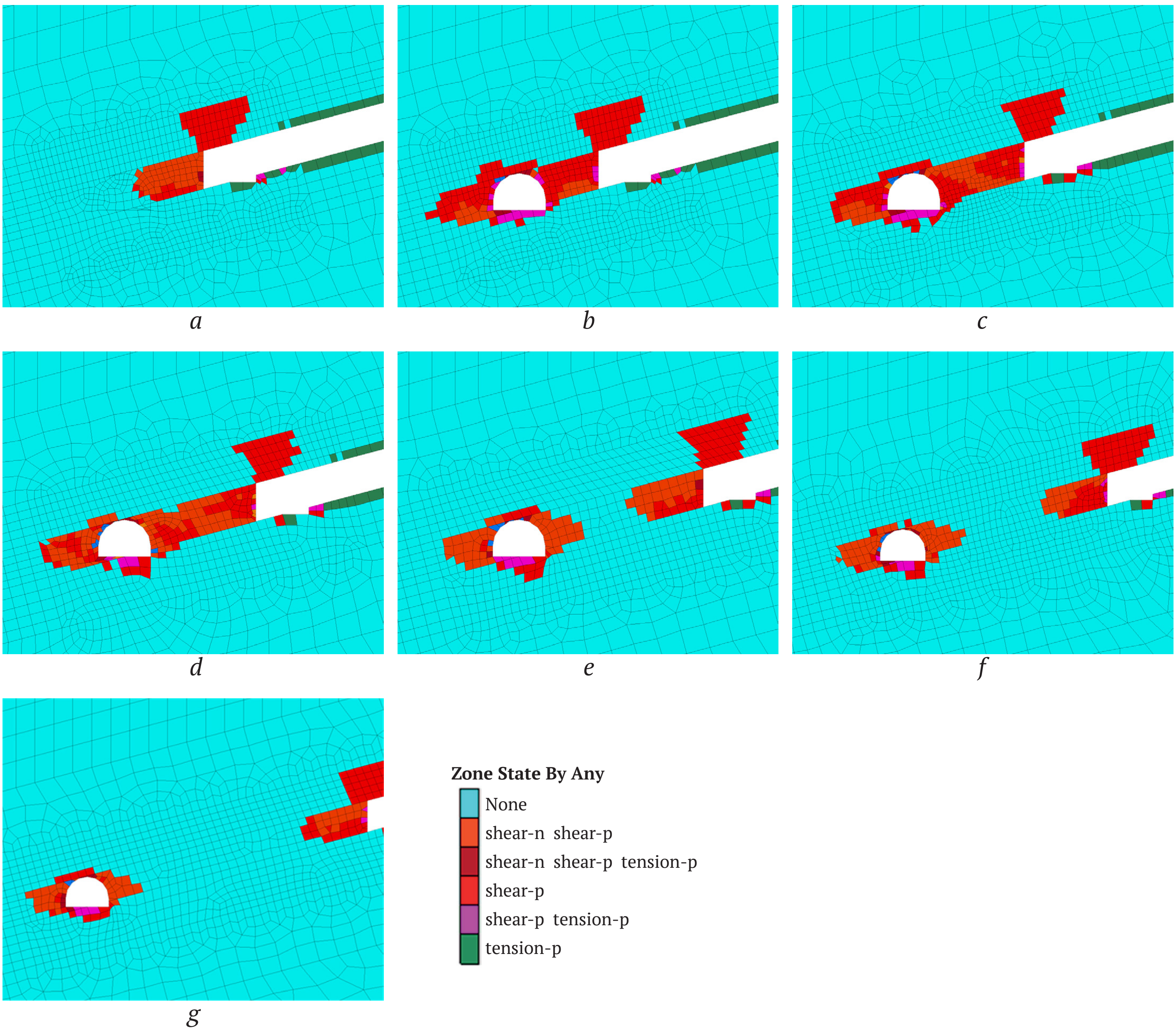

Fig. 5. Characteristics of rock mass shift around auxiliary working #3 at different sizes of coal pillar: *a* – 5 m; *b* – 8 m; *c* – 10 m; *d* – 15 m; *e* – 20 m; *f* – 25 m; *g* – 30 m

The simulation findings showed that mining operations in LC1 longwall resulted in fracturing the rock mass around working #2. As the size of the simulated coal pillar gradually increased, the linear dimensions of the zone of the coal pillar plastic deformation changed ("continuous zone" — "discontinuous zone") (Fig. 5, *a*–*d*) and reached 7 m.

It is known that when using working bolting, a bolt rests on intact rock mass [13–15], so the size of coal pillar must be sufficient to install and fix a bolt in intact stable rock. Taking into account this requirement, width of a coal pillar should be at least 2.5 m. If the auxiliary tunnel is placed in the zone of decreasing stresses, the tunnel support stability and the coal pillar stability will be ensured.

When driving an auxiliary working based on bolting support, geotechnical conditions of a coal pillar must provide sufficient strength for bolting. If coal pillar stability (rock strength) is too low (increased fracturing or deformation of the rock mass), it is incapable to provide reliable operation of bolting support. Therefore, bolts should be positioned outside the fracture zone, potentially caused by the influence of LC1 longwall. Consequently, the decision to select the size of a coal pillar should ensure not only the stability of a working, but also its effective operation.

Conclusions

1. For the conditions of inclined coal seams extraction, rock mass pressure on a working roof and stresses distribution on both sides of a working are asymmetrical.

2. As the size of coal pillar increases, the position of maximum vertical stress shifts to the side of coal pillar. This phenomenon demonstrates in fact a transition of the system from one steady state to another one.

3. If the rock mass is insufficiently stable, a special attention should be paid to strengthening support to increase the corresponding stability.

4. The selection of a coal pillar size should be based not only on the analysis of the rock mass deformation behavior, stress distribution, and the interval of plastic fracture zone, but also on the need to maximize coal reserve extraction.

5. The size of coal pillar is also connected with the support type. While supporting a working by bolting, one should take into account that bolts should be of sufficient length to ensure firm fixing and be located in the zone of intact rocks.

6. The research showed that a coal pillar should be 10 to 15 m wide (in the conditions of the presented model) in order to ensure optimal mining conditions and safety.

References

1. Ming J. Numerical simulation of narrow coal pillars at fully-mechanized caving face with driving roadway along goaf. *Coal Technology*. 2010;29(12):71–73.

2. Ullah M.F., Alamri A.M., Mehmood K., et al. Coal mining trends, approaches, and safety hazards: a brief review. *Arabian Journal of Geosciences*. 2018;11(21):651. https://doi.org/10.1007/s12517-018-3977-5

3. Qu Q. Study on destressing technology for a roadway driven along goaf in a fully mechanized top coal caving face. *Journal of Coal Science & Engineering*. 2003;9(1):33–37.

4. Zhang K.X. Determining the reasonable width of chain pillar of deep coal seams roadway driving along next goaf. *Journal of China Coal Society*. 2011;36(1):29–35.

5. Sun Y., Li G., Zhang J., Qian D. Experimental and numerical investigation on a novel support system for controlling roadway deformation in underground coal mines. *Energy Science & Engineering*. 2020;8(2):490–500. https://doi.org/10.1002/ese3.530

6. Nam P.Q., Minh T.T. Studying the stability and determining the reasonable location of auxiliary mining tunnels with the steep condition coal seam in Quang Ninh. In: *National Mining Science and Technical Conference. Quang Ninh. 2018.*

7. Doan D.V. Research on determining the size of coal pillar for the auxiliary mining tunnels at level – 300 in Khe Cham coal mine using FLAC3D software. *Mining Industry Journal*. 2016;5.

8. Pham N.T., Nguyen N.V. The effects of dynamic pressure on the stability of prepared drifts near the working surface areas. *Journal of Mining and Earth Sciences*. 2021;62(1):85–92. (In Vietnamese). https://doi.org/10.46326/JMES.2021.62(1).10

9. Le D.T., Bui T.M. Numerical modelling techniques for studying longwall geotechnical problems under realistic geological structures. *Journal of Mining and Earth Sciences*. 2021;62(3):87–96. (In Vietnamese). https://doi.org/10.46326/JMES.2021.62(3).10

10. Voznesensky A.S., Kidima-Mbombi L.K. Formation of synthetic structures and textures of rocks when simulating in COMSOL Multiphysics. *Mining Science and Technology (Russia)*. 2021;6(2):65–72. https://doi.org/10.17073/2500-0632-2021-2-65-72

11. Hung V.M. Study on the law of occurrence of mine pressure and rock deformation in mechanized underground coal mining in Quang Ninh. *Research project under the Ministry of Industry and Trade*. 2015.

12. Pham N.T., Qi F. Application of the numerical method to analyze the effect of cross-sectional type in stabilizing the coal mine tunnel. *Journal of Mining and Earth Sciences*. 2022;63(2):62–70. (In Vietnamese) https://doi.org/10.46326/JMES.2022.63(2).06

13. Zhang K., Zhang Y., Ma Z., et al. Determination of the narrow pillar width of gob-side entry driving. *Journal of Mining & Safety Engineering*. 2015;32(3):447–452.

14. Xie G.X., Yang K., Chang J. C. Influenced of coal pillar width on deformation and fracture of gateway surrounding rocks in fully mechanized top-coal caving mining. *Journal of Liaoning Technical University*. 2007;26(2):173–176. (In Chinese). https://doi.org/10.3969/j.issn.1008-0562.2007.02.004

15. Yao G.M., Kang L.J., Study on the chain pillar stability of the developing entry in longwall top-coal mining. *Journal of China Coal Society*. 2002;027(001):6–10. (In Chinese). https://doi.org/10.3321/j.issn:0253-9993.2002.01.002

Information about the authors

Viet Nghia Nguyen – Lecturer, Hanoi University of Mining and Geology, Hanoi, Vietnam; ORCID 0000-0001-7010-8613, Scopus ID 57204141788; e-mail nguyenvietnghia@gmail.com

Thi Nhan Pham – Lecturer, Hanoi University of Mining and Geology, Hanoi, Vietnam; Scopus ID 57369754200; e-mail phamthinhan@humg.edu.vn

Piotr Osinski – Assistant, Department of Geotechnical Engineering, Warsaw University of Life Science, Warsaw, Poland; ORCID 0000-0003-1503-7650, Scopus ID 55929586000, ResearcherID N-5911-2015

Thi Cuc Nguyen – Lecturer, Hanoi University of Mining and Geology, Hanoi, Vietnam; Scopus ID 57450931300; e-mail nguyenthicuc.nn@humg.edu.vn

Le Hung Trinh – Lecturer, Le Quy Don Technical University, Hanoi, Vietnam; ORCID 0000-0002-2403-063X, Scopus ID 57035066200; e-mail trinhlehung@lqdtu.edu.vn

Received 01.05.2022
Revised 20.05.2022
Accepted 28.05.2022

MINING SCIENCE AND TECHNOLOGY (RUSSIA)
ГОРНЫЕ НАУКИ И ТЕХНОЛОГИИ
2022;7(2):100–110
eISSN 2500-0632
https://mst.misis.ru/

GEOLOGY OF MINERAL DEPOSITS

Research paper

https://doi.org/10.17073/2500-0632-2022-2-100-110

Identification of geochemical anomalies associated with Sn-W mineralization in the Dong Van region, North-Eastern Vietnam, using statistical methods

K. T. Hung
Hanoi University of Mining and Geology, Hanoi, Vietnam
khuongthehung@humg.edu.vn

Abstract
Sn-W multimetal mineralization in the Dong Van region, North-Eastern Vietnam was studied using statistical and multivariate approaches based on 890 samples of stream bottom sediments collected for assaying for 27 elements. The findings of frequency analysis demonstrated that Pb, As, Bi, Li, Sn, W, Ta, Ce, Ag, Sb, and Be have close ties with multimetal ores, implying that these elements can be used as prospecting indicators for multimetal mineralization. In addition, correlation matrix and dendrogram studies were also applied to subdivide the elements in the stream bottom sediment samples assays into two groups: associated with multimetal mineralization (Be-Sn-W-Bi, and, to a lesser extent, Li-Pb sub-groups) and not associated with the mineralization: (As-Cd-Sc-Cr-Ce-La, Co-Ni-V, and Ga-Ge-Ba sub-groups). Sn and W were found to be the best indicator elements for the mineralization, according to the findings of geochemical modeling and location of their anomalies in the region. Furthermore, extensive Sn and W anomalies were identified in the Dong Van region (using threshold values (mean ± 3 STD), providing the most important indications for multimetal mineralization prospecting in the region. The studies also suggest genetic ties between the region's multimetal mineralization and the northwest-southeast fault system and concealed granitoid blocks. Finally, the performed statistical analyses (with the use of threshold values) of stream bottom sediments assays allowed revealing indicator elements and their geochemical anomalies and using them as an effective tool in further prospecting and exploration for multimetal mineralization in the region.

Keywords
geochemical anomalies, Sn-W mineralization, statistical methods, Dong Van region, North-Eastern Vietnam

For citation
Hung K.T. Identification of geochemical anomalies associated with Sn-W mineralization in the Dong Van region, North-Eastern Vietnam, using statistical methods. *Mining Science and Technology* (*Russia*). 2022;7(2):100–110. https://doi.org/10.17073/2500-0632-2022-2-100-110

ГЕОЛОГИЯ МЕСТОРОЖДЕНИЙ ПОЛЕЗНЫХ ИСКОПАЕМЫХ

Научная статья

Выявление геохимических аномалий, связанных с Sn-W минерализацией в провинции Донг Ван, северо-восточный Вьетнам, с использованием статистических методов

Х. Т. Хунг
Ханойский университет горного дела и геологии, г. Ханой, Вьетнам
khuongthehung@humg.edu.vn

Аннотация
Изучение Sn-W комплексной (поликомпонентной) минерализации в провинции Донг Ван, северо-восточный Вьетнам, проводилось с использованием статистических и мультивариантных подходов на основе 890 проб донных отложений водных потоков, отобранных для анализа на 27 элементов. Результаты частотного анализа показали, что Sn, W, Pb, As, Bi, Li, Ta, Ce, Ag, Sb и Be имеют тесные связи с комплексными рудами, что означает, что эти элементы могут быть использованы в качестве поисковых индикаторов комплексной (поликомпонентной) минерализации. Кроме того, были проведены исследования с использованием корреляционных матриц и дендрограмм для разделения элементов в анализах проб донных отложений на две группы: связанные с комплексной минерализацией (подгруппы Be-Sn-W-Bi и, в меньшей степени, Li-Pb) и не связанные с минерализацией (подгруппы As-Cd-Sc-Cr-Ce-La, Co-Ni-V и Ga-Ge-Ba). Sn и W были признаны лучшими элементами-индикаторами минерализации, согласно результатам геохимического моделирования и расположению их аномалий в провинции. Более того, в провинции Донг Ван были выявлены обширные геохимические

аномалии Sn и W (с использованием пороговых значений содержаний (среднее ± 3 STD)), что дает наиболее важные указания для поисков комплексной минерализации в провинции. Исследования также указывают на генетические связи между комплексной минерализацией провинции и системой разломов направления северо-запад – юго-восток и скрытыми гранитоидными блоками. В итоге проведенный статистический анализ содержаний (с использованием пороговых значений) в пробах донных отложений позволил выявить индикаторные элементы и их геохимические аномалии и использовать их в качестве эффективных инструментов при дальнейших поисках и разведке комплексной минерализации в провинции.

Ключевые слова
геохимические аномалии, Sn-W минерализация, статистические методы, Geostatistic, провинция Донг Ван, северо-восточный Вьетнам

Для цитирования
Hung K.T. Identification of geochemical anomalies associated with Sn-W mineralization in the Dong Van region, North-Eastern Vietnam, using statistical methods. *Mining Science and Technology* (*Russia*). 2022;7(2):100–110. https://doi.org/10.17073/2500-0632-2022-2-100-110

Introduction

Mineral resource research relies heavily on stream sediment surveys. In fact numerous types of deposits have been identified by this way in North-Eastern Vietnam [1, 2]. However, the processing of such data to find multivariate geochemical patterns and signals linked to mineralization is a complicated problem [3]. Principal component analysis is a useful data analysis technique for reducing the number of variables in a dataset or identifying components to reveal hidden patterns in multivariate data [4, 5]. In addition to basic principal component analysis, there are several other types of principal component analysis [6, 7]. These methods may be used with raw data, log-transformed data, selected data, and other types of data [8].

Traditional statistical analysis tools such as probability graphs, univariate and multivariate analysis methods [8–10], and fractal and multifractal models have all been proposed to differentiate geochemical anomalies from background [11–14]. Reimann et al. [15] compared various statistical methods for determining element concentration threshold values. They found that the box plots, median ± 2 median absolute deviations, and empirical cumulative distribution functions work better than mean ± 2 standard deviations for estimating anomaly threshold values. Fractal and multifractal algorithms have frequently been used to identify geochemical anomalies due to spatial autocorrelation nature of data [16–18].

The Dong Van region in northeastern Vietnam is regarded as a significant prospective area for multimetal ores (i.e., Fe, Mn, Sn, W, and Au) [1]. Furthermore, since tin, tungsten, and gold commonly occur in association with arsenic mineralization, such as As-Sn-W-Au Nam Khi, Lang Xum, Lang Me, and Lang Lup deposits, mineralization plays an important role as a source of precious metals for industry[1] [19]. From 1965 until the present, this region was surveyed at a scale of 1:500,000–1:50,000 for geological mapping and mineral exploration [20–23]. However, geological sample collecting and geochemical data processing are insufficient to identify prospective Sn-W mineralization areas. As a result, more research needs to be undertaken in the Dong Van region of northeastern Vietnam, in order to identify new multimetal ore areas.

Statistic and multivariate analysis were used to process 890 geochemical samples, in order to identify multimetal mineralization/ore occurrences in the Dong Van region.

1. Geological setting

The Song Hien zone is located within the northeast block of the Vietnam's segment. It is a 200 kilometer-long NW-SE trending tectonic zone, which hosts the Song Hien Permian-Triassic and Triassic volcanic-sedimentary strata with subordinate middle-late Paleozoic terrigenous-carbonate rocks (Fig. 1). The Song Hien zone is thought to be a pre-late Paleozoic-early Mesozoic intracontinental rift basin related to the Emeishan plume [24–27], or a pre-late Paleozoic-early Mesozoic back-arc basin formed by rifting within the merged Indochina-South China plate [28].

The study area belongs to the Song Hien zone of Northeast Vietnam (Fig. 1, A). The lithology of the Dong Van region comprises mostly Triassic sedimentary rocks (marlaceous shale, oolithic limestone, siltstone, tuffaceous sandstone, shale, sandstone), Devonian, Carboniferous, and Permian sedimentary rocks (i.e., conglomerate, clay shale, carbonate rocks, and marly sandstone). Cambrian, and Ordovician sedimentary rocks are also present in the Song Hien margin. Triassic gabbro and unknown age granitoid rocks occur in the central and western part of the zone [21–23, Fig. 1, B]. Quaternary sediments are mostly found along valleys (i.e., sandstone and gravelstone). The Dong Van region is located in the northern part of the Song Hien zone extending from northwest to

[1] USGS. Minerals Yearbook. United States Geological Survey: Reston, VA, USA; 2014. https://doi.org/10.3133/mybvI

MINING SCIENCE AND TECHNOLOGY (RUSSIA)
ГОРНЫЕ НАУКИ И ТЕХНОЛОГИИ
2022;7(2):100–110
eISSN 2500-0632
https://mst.misis.ru/

southeast (Fig. 1, B). The Cao Bang-Lang Son-Tien Yen strike-slip fault zone in the northern part and the Duong Thuong-Du Gia reverse fault in the southern part play an important role in controlling the Song Hien structural zone [20]. The intrusive magmatic rocks in this area were considerably controlled by these faults and other minor fault systems, contributing to the area's more intricate structure [22].

There is a primary multimetal mineralization zone in the studied area, namely Dong Van, extending from northwest to southeast and covers 1,190 square kilometers. The zone I mainly encompassed by Triassic sedimentary rocks [21–23, Fig. 1, B]. According to Truyen et al. [22], uneven concentrations of Sn, W, and As were found in this mineralized zone, as illustrated by Thang et al. [29].

2. Materials and methodologies

2.1. Collection and preparation of bottom sediment samples

Geochemical exploration techniques for exploring mineral deposits usually use bottom sediment samples. For this study, eight hundred ninety geochemical samples of recent bottom sediments were collected along river and streams at 25–50 m intervals. Surface sediments (0–3 cm deep) were collected by means of hand shovel from all points (on both river sides) with low current velocities, in order to take fine and recent material. Each sample contained around 25–130 g of recent bottom sediment, depending on a sediment sample particle size (Fig. 2).

The sample sets were processed based on distinct characterizations of the zone's bottom sediments.

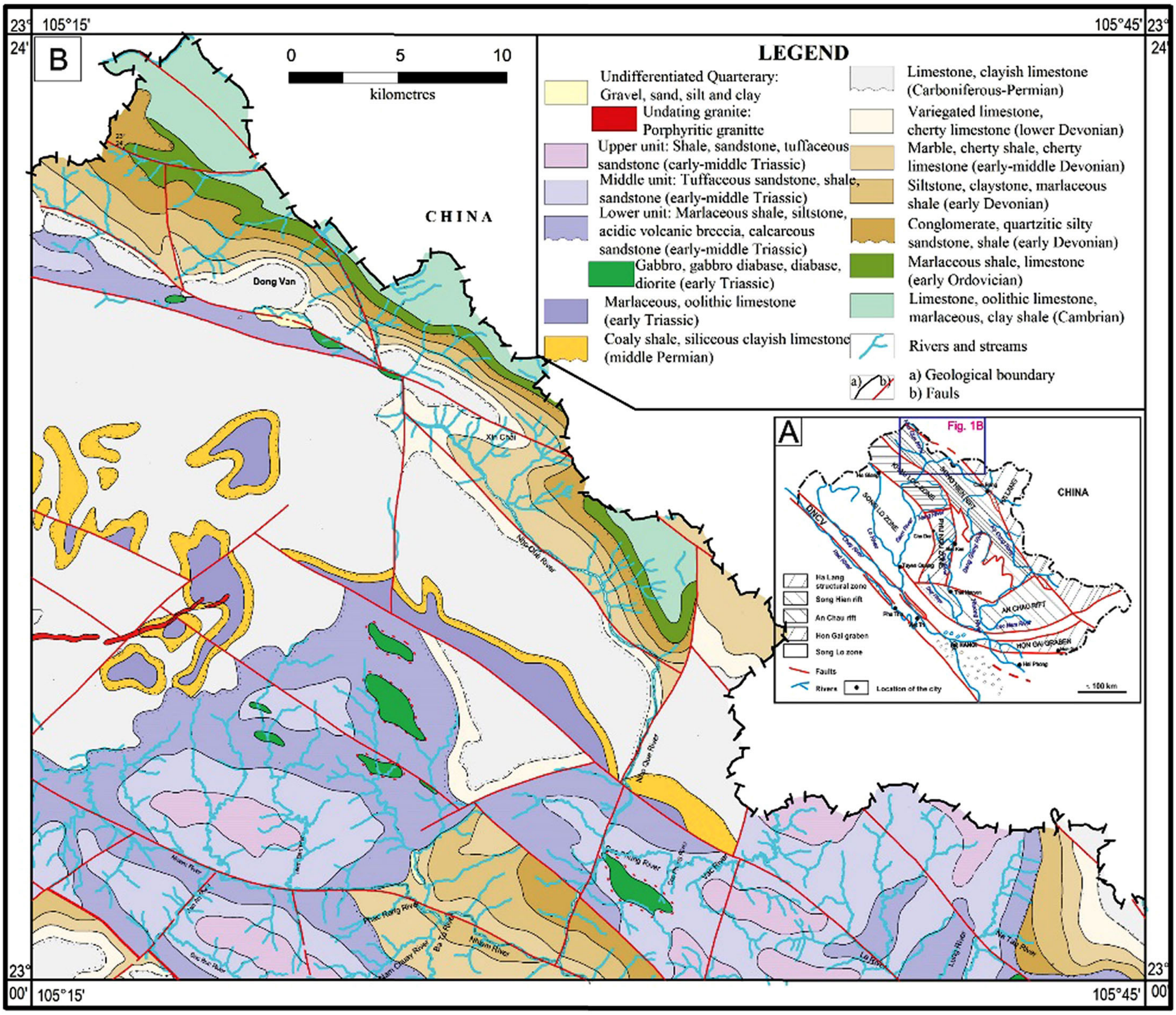

Fig. 1. Tectonic sketch map of northeastern Vietnam, showing the study area (*A*) [20]; Simplified geological map of the Dong Van region (*B*) (modified from [22])

In addition, the contents of 27 chemical components (elements) were measured using Inductively Coupled Plasma Mass Spectrometry (ICP-MS) (i.e., Ag, As, Be, Ba, Bi, Cd, Ce, Co, Cr, Cu, Ga, Ge, La, Li, Mo, Nb, Ni, Pb, Sb, Sc, Sn, Sr, Ta, V, W, Y, and Zn).

2.2. Data transformation

In this study, a total of 27 elements (variables) (i.e., Ag, As, Be, Ba, Bi, Cd, Ce, Co, Cr, Cu, Ga, Ge, La, Li, Mo, Nb, Ni, Pb, Sb, Sc, Sn, Sr, Ta, V, W, Y, and Zn) in the bottom sediment samples were processed. If the variables did not demonstrate asymmetric distribution, skewness (statistical distribution test) and transformed variables were used to assess the normal distribution of each variable [30]. Furthermore, ten distribution models (geometric, special discrete, uniform, triangular, Pareto, binomial, exponential, lognormal, normal, and transformed gamma) were developed to achieve normality and transition for skewed variables [8, 31–33].

2.3. Multivariate analysis

Multivariate analysis methods are used to clarify and explain correlations between multiple factors linked with statistical data throughout the assessment and collecting of this data.

Geostatistic 9.0 is used to examine the findings of correlation coefficients and cluster studies, which assist in analyzing links between elements and element grouping.

The purpose of cluster analysis is to reduce the number of significant subgroups of people or things in an extensive data collection. Data subdivision (grouping) is performed on the basis of the items' similarity, based on predetermined characteristics.

Ward (1963) describes Ward's mathematical technique as a criterion for studying hierarchical clusters. Ward [34] introduced a universal agglomerative hierarchical clustering technique, in which the criteria for picking the pair of clusters to be joined at each level are based on the optimal value of an objective function.

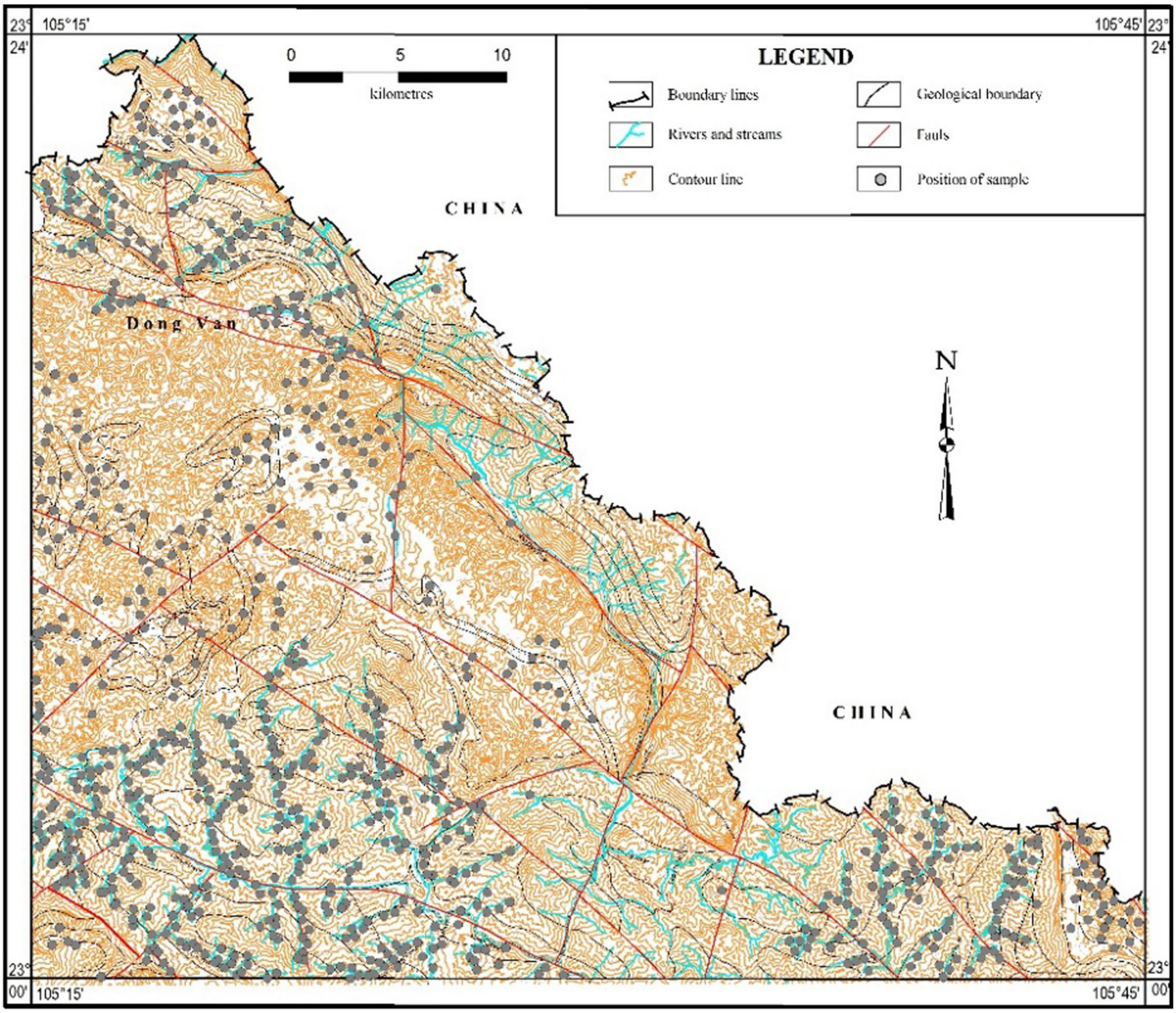

Fig. 2. General map of the Dong Van region, northeastern Vietnam showing bottom sediment sample points (shown as black dots)

eISSN 2500-0632
https://mst.misis.ru/

Eigenvalues and eigenvectors are used to generally express covariance and correlation coefficient matrices.

In the meanwhile Varimax rotation was performed to enhance the factor loads. Ward's approach was used to carry out Pearson's correlation coefficients cluster analysis (or hierarchical cluster analysis), and the results were shown in a dendrogram.

3. Results and discussion

3.1. The characteristics of statistical element distribution

Statistical distribution models for elements of multimetal ores and associated elements can be used to identify the laws of their statistical distribution. Results of geochemical data statistical analysis for the whole region were displayed separately. The resulting element contents hierarchy in the whole region was as follows: Pb > As > Bi > Li > Sn > W > Ta > Ce > Ag > Sb > Be > Mo > La > Nb > Cr > Ni > Cd > Y > Cu > Ba > Co >Sc> Zn > Sr > V (Table 1). Moreover, Pb, As, Bi, Li, Sn, W, Ta, Ce, Ag, Sb, and Be constituted more than 90 % of the total, indicating obvious association with multimetal ores. Finally, these elements can be used as indicators when prospecting for multimetal mineralization.

Using the three-sigma limit method, the geochemical samples were statistically processed in this study (Table 2). We used mean value, variance, and coefficient of variation as the basic statistical metrics. In addition, skewness and kurtosis techniques were used to test the element distribution models and the majority of the element contents on the basis of geometric distribution criteria (Table 3). Geostatistic 9.0 software program evaluated the distribution models and statistical analysis [35].

The distribution rules of the indicator elements did not adhere to the normal standard distribution and were modified to geometric distribution, pursuant to the characterization of the statistical distribution of Sn and W in secondary geochemical dispersion haloes (Table 3). The overall contents of Sn and W are higher than crustal abundance (Sn* = 2.5 ppm, W* = 1.3 ppm [36]), while the distributions of the Sn

Table 1

Frequency analysis of the elements contents [ppm] in the sediment samples

Element	Amount of Information (AI)	Information Combination (IC)	Probability (%)	Element	Amount of Information (AI)	Information Combination (IC)	Probability (%)
Pb	0.573	0.573	**30.02**	Nb	0.337	1.842	96.49
As	0.572	0.810	**42.41**	Cr	0.313	1.868	97.87
Bi	0.564	0.987	**51.69**	Ni	0.235	1.883	98.64
Li	0.561	1.135	**59.46**	Cd	0.197	1.893	99.18
Sn	0.546	1.260	**65.98**	Y	0.190	1.903	99.68
W	0.527	1.365	**71.52**	Cu	0.095	1.905	99.80
Ta	0.512	1.458	**76.39**	Ba	0.082	1.907	99.89
Ce	0.492	1.539	**80.62**	Co	0.069	1.908	99.96
Ag	0.471	1.609	**84.31**	Sc	0.046	1.909	99.99
Sb	0.439	1.668	**87.39**	Zn	0.029	1.909	100
Be	0.435	1.724	**90.31**	Sr	0.000	1.909	100
Mo	0.413	1.773	92.87	V	0.000	1.909	100
La	0.369	1.811	94.86				

Note: AI and IC are described by Hung et al. (2020) [2].

Table 2

Statistical characteristics of the indicator elements (ppm) in the Dong Van region

Parameters	Ag	As	Be	Pb	Bi	Sb	Ce	Sn	Ta	W	Ge	Li
Mean	1.27	49.39	5.67	27.9858	0.98	19.2444	87.55	14.6279	23.0603	19.7104	5.5618	46.403
Median	0.33	27.63	1.90	23.31	0.47	3.2	78.15	8.805	5.255	5.87	5	33.715
Mode	18.54	49.00	31.60	10.77	4.03	37.24	64.05	49.07	20.63	48.02	0	40.19
Standard deviation	13.10	75.83	29.49	21.7042	3.62	60.9511	40.018	45.4845	46.9017	61.1201	1.579	47.3386
Variance	171.60	5750.53	869.61	471.0731	13.09	3715.039	1601.45	2068.839	2199.772	3735.672	2.4934	2240.944
Coefficient of variation (%)	1029.03	153.55	520.29	77.55	371.94	316.72	45.71	310.94	203.39	310.09	28.39	102.02
Skewness	25.87	6.32	14.85	2.252	18.13	6.19	2.35	14.913	4.109	9.053	2.463	7.51
Kurtosis	717.33	52.41	270.95	9.444	384.99	47.879	7.91	273.92	22.217	106.11	4.073	83.746
Minimum	0.04	2.00	0.10	0.77	0.03	0.24	16.05	0.07	0.13	0.02	5	5.69
Maximum	370.70	945.65	636.31	209.29	85.61	743.58	337.75	986.44	415.76	967.95	10	703.89
Summary	1132.97	43954	5044.38	24907.39	865.90	17127.49	77916.67	13018.85	20523.7	17542.25	4950	41298.7

and W contents vary from uneven to extremely uneven. On this basis, the different geochemical anomalies can be identified at a local scale. This indicates that Sn and W can form small primary geochemical anomalies. This data can allow primary geochemical dispersion haloes to be detected. This in turn can be used to identify prospective targets for Sn-W mineralization in the Dong Van region.

3.2. Correlation and cluster analyses application

The correlation analysis findings allow a pair correlation matrix of the best indicator elements to be created for the geochemical landscape (pattern) of the entire region. Table 4 shows the elements pair correlation matrix. Among the indicator elements, Be, Sn, W, and Bi demonstrate obvious correlation. Sn and W especially establish the element association as an indication for multimetal ore prospecting. Li also demonstrated marked correlation with Be and Bi, indicating Li participation in ore-forming processes.

Thus, the calculations showed close correlation ties between Be, Sn, W, and Bi, thus indicating that they formed stable association.

A dendrogram was created, in order to determine the correlation ties between the studied elements in the secondary geochemical haloes in the Dong Van region based on the pair-correlation analysis findings (Fig. 3). Pearson's correlation coefficients were used to statistically measure the ties.

The dendrogram depicts associations between the elements studied and allows for their grouping/subgrouping. Multimetal mineralization-associated elements are represented by two sub-groups, Be-Sn-W-Bi, and, to a lesser extent, Li-Pb. At the same time, three other sub-groups, i.e., As-Cd-Sc-Cr-Ce-La, Co-Ni-V, and Ga-Ge-Ba, not associated with the mineralization, can be distinguished. For instance, the dendrogram also defines a local Co-Ni-V branch, which indicates that Co, Ni, and V are not syngenetic components of the multimetal ores in the region.

Table 3

Testing of Sn, W statistical distribution models

Distribution model	Sn (ppm)							W (ppm)						
	Deviation	Actual deviation	Chi square (18.307)	Conforming to Chi square test	λ (1.358)	Conforming to Kolmogorov-Smirnov test	Synthesizer	Deviation	Actual deviation	Chi square (18.307)	Conforming to Chi square test	λ (1.358)	Conforming to Kolmogorov-Smirnov test	Synthesizer
Geometric	2.486	1	3.267	1-Yes	0.160	**1-Yes**	0.300	5.045	1	31.429	1-No	0.345	**1-Yes**	1.973
Gamma	24.441	2	61.592	2-No	1.562	2-No	4.515	22.369	2	51.685	2-No	1.470	2-No	3.906
Lognormal	61.402	3	164.788	3-No	3.412	3-No	11.514	32.496	3	88.052	3-No	1.889	3-No	6.201
Special discrete	104.029	5	459.352	4-No	7.294	5-No	30.463	58.635	4	147.230	4-No	3.282	4-No	10.459
Pareto	115.827	6	487.814	5-No	7.537	6-No	32.196	98.299	5	412.558	5-No	6.929	5-No	27.638
Exponential	94.306	4	606.050	6-No	6.356	4-No	37.7853	111.040	6	449.417	6-No	7.227	6-No	29.871
Binomial	287.065	10	926.397	7-No	20.737	10-No	65.874	281.168	10	1223.811	7-No	20.239	10-No	81.753
Normal	266.722	9	2150.286	8-No	14.912	7-No	128.438	260.992	9	2059.889	8-No	14.689	7-No	123.336
Triangular	234.503	7	4426.587	9-No	17.320	8-No	254.552	231.131	7	4598.079	9-No	17.081	8-No	263.743
Uniform	251.125	8	8564.185	10-No	18.822	9-No	481.669	244.535	8	8120.654	10-No	18.324	9-No	457.075

Note: The Kolmogorov-Smirnov test was implemented in Chakravarti et al. [31].

Table 4

The correlation coefficient for indicator elements (ppm) in the sediment samples

	Ag	As	Be	Bi	Ce	Li	Pb	Sb	Sn	Ta	W
Ag	1										
As	0.032	1									
Be	0.062	0.445	1								
Bi	0.051	0.205	**0.711**	1							
Ce	0.026	0.262	0.082	0.142	1						
Li	0.044	0.425	**0.569**	**0.542**	0.386	1					
Pb	−0.009	0.310	0.173	0.057	0.331	0.333	1				
Sb	0.071	0.407	0.392	0.499	0.437	0.465	−0.027	1			
Sn	0.006	**0.623**	**0.645**	0.213	−0.027	0.377	0.325	0.106	1		
Ta	−0.021	−0.019	−0.045	−0.036	−0.000	−0.078	0.110	−0.073	0.041	1	
W	0.018	0.438	**0.588**	0.412	−0.048	0.400	0.264	0.176	**0.666**	0.138	1

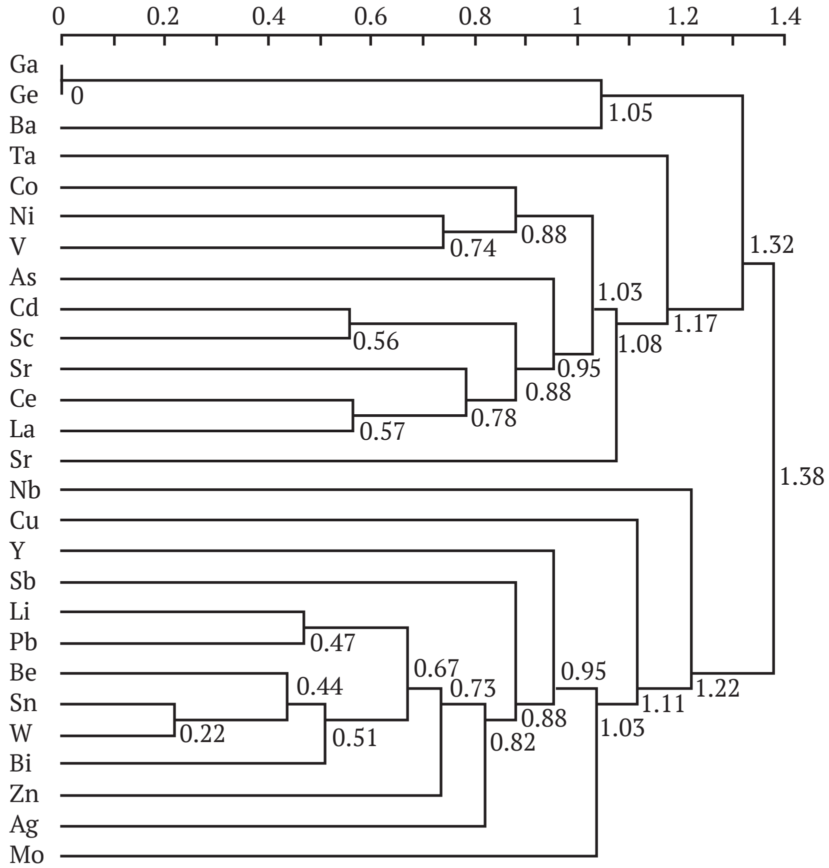

Fig. 3. Dendrogram of elements contents in the Dong Van region's geochemical landscape (ppm). Numbers indicate cluster analysis linkage distances based on Ward's agglomerative clustering algorithm

A combination of multivariate correlation and dendrogram analysis was used, in order to determine the relevance of syngenetic element association for prospecting multimetal ores in the study region. As a result, Be, Sn, W, and Bi were recognized as a members of the syngenetic association. Despite the high contents of some other elements in the samples, they cannot be considered as indicators of multimetal mineralization (or some other mineralization) in this region.

3.3. Geochemical anomaly modeling

Secondary geochemical dispersion is the movement of elements at or just below the Earth's surface, which results from weathering, erosion, and deposition. External circumstances can damage and modify ore bodies, mineralization zones, and change geochemical landscape of a region. Some minerals can be dissolved, washed-out, some elements can migrate, while others can be accumulated with an increase of their contents. The material elements of the secondary geochemical haloes are redistributed in the weathering conditions. The haloes can be considerably larger than primary ore bodies. The secondary geochemical haloes and geochemical anomalies are of crucial importance in prospecting concealed mineral deposits in the region. Geochemical anomaly diagrams were used to represent the spatial variation of the element contents in the region and predict prospective areas for multimetal mineralization.

Secondary geochemical anomalies of Sn and W were constructed, in order to represent the spatial distribution of these good indicator elements for multimetal ore prospecting in the Dong Van region. Creating such geochemical anomaly diagrams is aimed at establishing the distribution and accumulation of indicator elements in certain locations (Figs. 4, 5). This allows for the interpretation and selection of anomalies connected with mineralization, while eliminating anomalies that provide no information about any mineralization.

In order to reveal prospective anomalies, isolines for Sn and W (the indicator elements) contents based on three preset anomaly thresholds were constructed and mapped taking into account geochemical background values. The anomaly thresholds of the first order (mean ± 1 STD), second order (mean ± 2 STD), and third order (mean ± 3 STD) were selected using the statistical processing findings to estimate geochemical background values based on the local average values (Table 5, Figs. 4, 5). For this purpose, mean and STD

MINING SCIENCE AND TECHNOLOGY (RUSSIA)
ГОРНЫЕ НАУКИ И ТЕХНОЛОГИИ
2022;7(2):100–110
eISSN 2500-0632
https://mst.misis.ru/

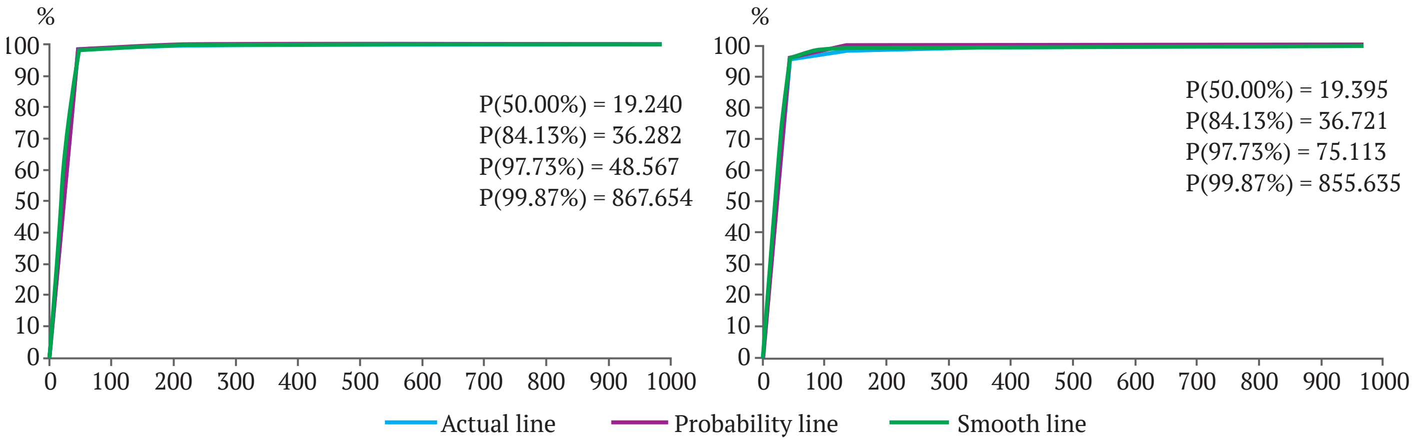

a *b*

Fig. 4. Sn (*a*) and W (*b*) occurrence graphs based on their distribution in the Dong Van region, showing probability at three anomaly thresholds and background

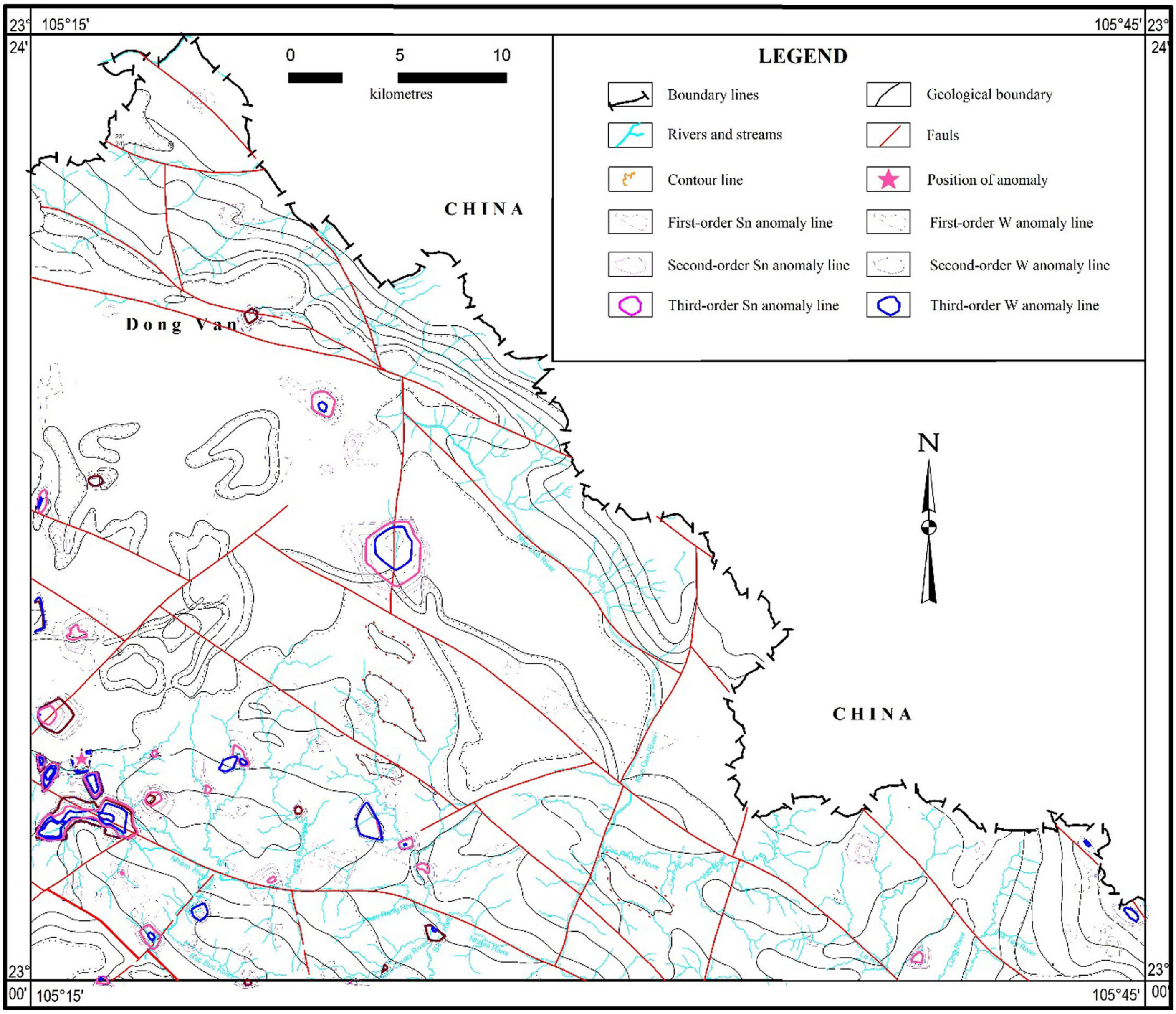

Fig. 5. General map of the Dong Van region showing Sn-W anomaly indicating prospective area

Table 5

Anomaly contents of Sn, W in the Dong Van region based on anomaly thresholds using calculated, theoretical, and probability standard deviation

Element (ppm)	Method	Crustal abundance	Back-ground	First-order anomaly	Second-order anomaly	Third-order anomaly	Anomaly
Sn	Calculated standard deviation (CSD)	2.5	19	65	110	156	156
	Theoretical standard deviation (TSD)	2.5	19	19	20	20	20
	Probability standard deviation (PSD)	2.5	19	38	57	76	76
	Probability distribution (PPD)	2.5	19	36	49	868	868
W	Calculated standard deviation (CSD)	1.3	19	81	142	203	203
	Theoretical standard deviation (TSD)	1.3	19	20	20	20	20
	Probability standard deviation (PSD)	1.3	19	38	56	75	75
	Probability distribution (PPD)	1.3	19	37	75	856	856

Note: Crustal abundance values for the indicator elements (Sn* = 2.5 ppm, W* = 1.3 ppm) were taken from Fortescue [32].

values were calculated on the basis of geometric distribution. Geochemical anomalies associated with multimetal mineralization can be selected, while geochemical anomalies not connected with the mineralization can be rejected based on the geochemical anomaly diagrams for the indicator elements, in combination with prospecting data to ascertain the geochemical anomalies.

Tin occurrence locations in the mineralized zone are expressed in the geochemical anomalies of Sn and W. The geochemical anomalies of the indicator elements were identified in three separate areas, as shown in Fig. 5. The anomalies are often elliptical, extending northwest-southeast in accordance with the established mineralization zone orientation. Most of the geochemical anomalies are confined to the Song Hien formation area. The geochemical anomalies identified, particularly those of tin and tungsten adjacent to the mineralized zone, are relatively large and have a complex shape. This indicates the potential presence of concealed ore bodies associated with the granitoid massive. Geochemical anomalies with no ties to mineralization are often presented by limited secondary accumulations located on local slopes and similar land forms.

Conclusions

Multimetal mineralization in the Dong Van region, northeastern Vietnam was studied using statistical and multivariate analytic approaches based on 890 geochemical sediment samples. The findings of frequency analysis demonstrated that Pb, As, Bi, Li, Sn, W, Ta, Ce, Ag, Sb, and Be have close ties with multimetal ores. This implies that these elements can be used as prospecting indicators for multimetal mineralization. Furthermore, extensive Sn and W anomalies were identified in the Dong Van region, providing the most important indications for multimetal mineralization prospecting in the region. In the region under examination, correlation matrix and dendrogram studies were also used to subdivide elements in the stream sediment samples assays into two groups: those associated with multimetal mineralization (Be-Sn-W-Bi, and, to a lesser extent, Li-Pb sub-groups); and those not associated with the mineralization: (As-Cd-Sc-Cr-Ce-La, Co-Ni-V, and Ga-Ge-Ba sub-groups).

Threshold value (mean ± 3 STD) was then applied to identify the indicator elements anomaly locations (and background levels) associated with known multimetal mineralization in the region. Thus, such anomalies can be a promising tool for further multimetal mineralization prospecting and exploration.

According to the findings of geochemical modeling and location of the anomalies in the region, Sn and W are the best indicator elements for the mineralization. The studies also suggest genetic ties between the region's multimetal mineralization and the northwest-southeast fault system and concealed granitoid blocks.

Finally, the statistical analysis (with the use of threshold values) of stream bottom sediments assays enabled indicator elements and their geochemical anomalies to be established, and for them to be used as an effective tool in further prospecting and exploration for multimetal mineralization in the region.

References

1. Tri T.V., Khuc V. (eds.). *Geology and Earth Resources of Vietnam*. General Department of Geology and Minerals of Vietnam: Publishing House for Science and Technology. 2011. 645 p.

2. Hung K.T., Sang P.N., Phuong N. et al. Statistical evaluation of the geochemical data for prospecting complex mineralization in the Suoi Thau-Sang Than region, Northeast Vietnam. *Geology, Geophysics and Environment*. 2020;46(4):285–299. https://doi.org/10.7494/geol.2020.46.4.285

3. Carranza E. J. M. Usefulness of stream order to detect stream sediment geochemical anomalies. *Geochemistry: Exploration, Environment, Analysis*. 2005;4(4):341–352. https://doi.org/10.1144/1467-7873/03-040

4. Cheng Q., Jing L., Panahi A. Principal component analysis with optimum order sample correlation coefficient for image enhancement. *International Journal of Remote Sensing*. 2006;27(16):3387–3401. https://doi.org/10.1080/01431160600606882

5. Reimann C., Filzmoser P., Garrett R. G., Dutter R. *Statistical Data Analysis Explained: Applied Environmental Statistics with R*. Wiley, Chichester, UK; 2008. 362 p. https://doi.org/10.1002/9780470987605

6. Cheng Q., Bonham-Carter G., Wang W., Zhang S., Li W., Qinglin X. A spatially weighted principal component analysis for multi-element geochemical data for mapping locations of felsic intrusions in the Gejiu mineral district of Yunnan, China. *Computers and Geosciences*. 2011;37(5):662–669. https://doi.org/10.1016/j.cageo.2010.11.001

7. Zuo R. Identification of geochemical anomalies associated with mineralization in the Fanshan district, Fujian, China. *Journal of Geochemical Exploration*. 214;139:170–176. https://doi.org/10.1016/j.gexplo.2013.08.013

8. Aitchison J. *The Statistical Analysis of Compositional Data*. Chapman & Hall, London; 1986. 416 p. https://doi.org/10.1002/bimj.4710300705

9. Tukey J. W. *Exploratory data analysis*. Reading, Massachusetts: Addison-Wesley Publishing Company; 1977. 688 p. https://doi.org/10.1177/014662167800200115

10. Sun X., Deng J., Gong Q. et al. Kohonen neural network and factor analysis based approach to geochemical data pattern recognition. *Journal of Geochemical Exploration*. 2009;103(1):6–16. https://doi.org/10.1016/j.gexplo.2009.04.002

11. Mandelbrot B. B. *The fractal geometry of nature*. Freeman, San Francisco; 1983. 468 p.

12. Agterberg F. P. Multifractal modeling of the sizes and grades of giant and supergiant deposits. *International Geology Review*. 1995;37(1):1–8. https://doi.org/10.1080/00206819509465388

13. Wang Q. F., Deng J., Zhao J. et al. Tonnage-cutoff model and average grade-cutoff model for a single ore deposit. *Ore Geology Reviews*. 2010;38(1–2):113–120. https://doi.org/10.1016/j.oregeorev.2010.07.003

14. Yang L. Q., Wang Q. F., Liu X. F. Correlation between mineralization intensity and fluid-rock reaction in the Xinli gold deposit, Jiaodong Peninsula, China: constraints from petrographic and statistical approaches. *Ore Geology Reviews*. 2015;71:29–39. https://doi.org/10.1016/j.oregeorev.2015.04.005

15. Reimann C., Filzmoser P., Garrett R. G. Background and threshold: critical comparison of methods of determination. *Science of the Total Environment*. 2005;346(1–3):1–16. https://doi.org/10.1016/j.scitotenv.2004.11.023

16. Cheng Q. Mapping singularities with stream sediment geochemical data for prediction of undiscovered mineral deposits in Gejiu, Yunnan Province, China. *Ore Geology Reviews*. 2007;32(1–2):314–324. https://doi.org/10.1016/j.oregeorev.2006.10.002

17. Sun X., Gong Q., Wang Q. et al. Application of local singularity model to delineate geochemical anomalies in Xiong'ershan gold and molybdenum ore district,Western Henan province, China. *Journal of Geochemical Exploration*. 2010;107(1):21–29. https://doi.org/10.1016/j.gexplo.2010.06.001

18. Zuo R., Xia Q., Zhang D. A comparison study of the C–A and S–A models with singularity analysis to identify geochemical anomalies in covered areas. *Applied Geochemistry*. 2013;33:165–172. https://doi.org/10.1016/j.apgeochem.2013.02.009

19. Graedel T. E., Harper E. M., Nassar N. T., Reck B. K. On the materials basis of modern society. *Proceedings of the National Academy of Sciences*. 2013;112(20):6295–6300. https://doi.org/10.1073/pnas.1312752110

20. Dovzhikov A. E., My B. P., Vasilevskaya E. D. et al. *Geology of North Vietnam*. Hanoi: Science and Technology Publishing House; 1965. 650 p. (In Russ.)

21. Tinh H. X. (ed.). *Report on results of geological mapping and mineral investigation of Bao Lac sheet at 1:200.000 scale*. Geological Department of Vietnam, Ha Noi; 1976. (In Vietnamese)

22. Truyen M. T. (ed.). *Report on results of geological mapping and mineral investigation of Bao Lac sheet at 1:50.000 scale*. Geological Department of Vietnam, Ha Noi; 1977. (In Vietnamese)

23. Tri T. V. (ed.). *Report on results of geological and mineral potential mapping of Bao Lac-Bac Quang-Ma Quang at 1:200.000 scale*. Geological Department of Vietnam, Ha Noi; 2000 (In Vietnamese)

24. Izokh A. E., Polyakov G. V., Hoa T. T., Balykin P. A., Phuong N. T. Permian–Triassic ultramafic–mafic magmatism of Northern Vietnam and Southern China as expression of plume magmatism. In: *32nd International Geological Congress*. 2005;46:942–951. (In Russ.)

25. Hoa T. T., Anh T. T., Phuong N. T. et al. Permo-Triassic intermediate–felsic magmatism of the Truong Son belt, eastern margin of Indochina. *ComptesRendus Geoscience*. 2008;340(1–2):112–126. https://doi.org/10.1016/j.crte.2007.12.002

26. Polyakov G. V., Shelepaev R. A., Hoa T. T. et al. The Nui Chua layered peridotitegabbro complex asmanifestation of Permo-Triassic mantle plume in northern Vietnam. *Russian Geology and Geophysics*. 2009;50(6):501–516. https://doi.org/10.1016/j.rgg.2008.10.002

27. Vladimirov A.G., Balykin P.A., Anh P.L. et al. The Khao Que-Tam Tao gabbro-granite massif, Northern Vietnam: a petrological indicator of the Emeishan plume. *Russian Journal of Pacific Geology*. 2012;6:395–411. https://doi.org/10.1134/S1819714012050065

28. Hai T.T., Thanh N.X., Halpin J.A., Zaw K. The occurrence of ophiolite-style assemblages along Sino-Vietnam border, Northeastern Vietnam and its implication to the tectonic evolution of Northeastern Indochina. In: *Proceedings of the International Conference on Geology. Geotechnology and Mineral Resources of Indochina (GEOINDO 2011), KhonKaen*. 2011. Pp. 479–488.

29. Thang P.V. (ed.). *Report on the results of prospecting Sn-W mineralization and accompaning minerals in the northwestern Ha Giang area*. Geological Department of Vietnam, Ha Noi; 1988. (In Vietnamese)

30. Reimann C., Filzmoser P. Normal and lognormal data distribution in geochemistry: death of a myth. Consequences for the statistical treatment of geochemical and environmental data. *Environmental Geology*. 2000;39:1001–1014. https://doi.org/10.1007/s002549900081

31. Chakravarti R., Laha G., Roy J. *Handbook of Methods of Applied Statistics. Volume I*. John Wiley and Sons; 1967. 160 p.

32. Egozcue J.J., Pawlowsky-Glahn V., Mateu-Figueras G., Barceló-Vidal C. Isometric logratio transformations for compositional data analysis. *Mathematical Geology*. 2003;35:279–300. https://doi.org/10.1023/A:1023818214614

33. Carranza E.J.M. Analysis and mapping of geochemical anomalies using logratiotransformed stream sediment data with censored values. *Journal of Geochemical Exploration*. 2011;110(2):167–185. https://doi.org/10.1016/j.gexplo.2011.05.007

34. Ward J.H.Jr. Hierarchical grouping to optimize an objective function. *Journal of the American Statistical Association*, 1963;58:236–244. https://doi.org/10.1080/01621459.1963.10500845

35. Robertson G.P. *GS+: Geostatistics for the Environmental Sciences*. Gamma Design Software, Plainwell: Michigan USA; 2008. URL: https://softbooks.pl/gammadesign/files/download/gsplususerguide.pdf

36. Fortescue J.A.C. Landscape geochemistry-retrospect and prospect–1990. *Applied Geochemistry*. 1992;7(1):1–53. https://doi.org/10.1016/0883-2927(92)90012-R

Information about the author

Khuong The Hung – Dr. Sci. (Earth Sci.), Lecturer, Department of Prospecting and Exploration Geology, Hanoi University of Mining and Geology, Hanoi, Vietnam; ORCID 0000-0003-1544-6470, Scopus ID 36716173500; e-mail khuongthehung@humg.edu.vn

Received 21.01.2022
Revised 17.05.2022
Accepted 18.05.2022

SAFETY IN MINING AND PROCESSING INDUSTRY AND ENVIRONMENTAL PROTECTION

Research paper
https://doi.org/10.17073/2500-0632-2022-2-111-125

Forecasting $PM_{2.5}$ emissions in open-pit minesusing a functional link neural network optimized by various optimization algorithms

X.-N. Bui[1] ✉, H. Nguyen[1], Q.-T. Le[1], T.-N. Le[2]
[1] *Hanoi University of Mining and Geology, Hanoi, Vietnam*
[2] *Vinacomin – Minerals Holding Corporation, Hanoi, Vietnam*
✉ *buixuannam@humg.edu.vn*

Abstract
$PM_{2.5}$ air pollution is not only a significant hazard to human health in everyday life but also a dangerous risk to workers operating in open-pit mines OPMs), especially open-pit coal mines (OPCMs). $PM_{2.5}$ in OPCMs can cause lung-related (e.g., pneumoconiosis, lung cancer) and cardiovascular diseases due to exposure to airborne respirable dust over a long time. Therefore, the precise prediction of $PM_{2.5}$ is of great importance in the mitigation of $PM_{2.5}$ pollution and improving air quality at the workplace. This study investigated the meteorological conditions and $PM_{2.5}$ emissions at an OPCM in Vietnam, in order to develop a novel intelligent model to predict $PM_{2.5}$ emissions and pollution. We applied functional link neural network (FLNN) to predict $PM_{2.5}$ pollution based on meteorological conditions (e.g., temperature, humidity, atmospheric pressure, wind direction and speed). Instead of using traditional algorithms, the Hunger Games Search (HGS) algorithm was used to train the FLNN model. The vital role of HGS in this study is to optimize the weights in the FLNN model, which was finally referred to as the HGS-FLNN model. We also considered three other hybrid models based on FLNN and metaheuristic algorithms, i.e., ABC (Artificial Bee Colony)-FLNN, GA (Genetic Algorithm)-FLNN, and PSO (Particle Swarm Optimization)-FLNN to assess the feasibility of $PM_{2.5}$ prediction in OPCMs and compare their results with those of the HGS-FLNN model. The study findings showed that HGS-FLNN was the best model with the highest accuracy (up to 94–95 % in average) to predict $PM_{2.5}$ air pollution. Meanwhile, the accuracy of the other models ranged 87 % to 90 % only. The obtained results also indicated that HGS-FLNN was the most stable model with the lowest relative error (in the range of −0.3 to 0.5 %).

Keywords
open-pit coal mine, air pollution, dust, $PM_{2.5}$, human health, hunger games search, functional link neural network, optimization, Coc Sau open-pit coal mine, Quang Ninh province, Vietnam

Acknowledgments
This study was financially supported by the Ministry of Education and Training (MOET) of Vietnam under grant number B2018-MDA-03SP. The authors also thank the Center for Mining, Electro-Mechanical Research of Hanoi University of Mining and Geology (HUMG), Vietnam; the engineers and managers of the Coc Sau open-pit coal mine, Quang Ninh province, Vietnam for their help and cooperation.

For citation
Bui X.-N., Nguyen H., Le Q.-T., Le T.-N. Forecasting $PM_{2.5}$ emissions in open-pit mines using a functional link neural network optimized by various optimization algorithms. *Mining Science and Technology* (*Russia*). 2022;7(2):111–125. https://doi.org/10.17073/2500-0632-2022-2-111-125

ТЕХНОЛОГИЧЕСКАЯ БЕЗОПАСНОСТЬ В МИНЕРАЛЬНО-СЫРЬЕВОМ КОМПЛЕКСЕ И ОХРАНА ОКРУЖАЮЩЕЙ СРЕДЫ

Научная статья

Прогнозирование выбросов пыли ($PM_{2.5}$) на угольных разрезах с помощью нейронной сети с функциональными связями, оптимизированной различными алгоритмами

С.-Н. Буи[1] ✉, Х. Нгуен[1], К.-Т. Ле[1], Т.-Н. Ле[2]
[1] *Ханойский университет горного дела и геологии, Ханой, Вьетнам*
[2] *Vinacomin – Minerals Holding Corporation, Ханой, Вьетнам*
✉ *buixuannam@humg.edu.vn*

Аннотация
Загрязнение воздуха $PM_{2.5}$ (твердые частицы размером 2,5 мк и менее) представляет собой не только значительную опасность для здоровья человека в повседневной жизни, но и опасный риск для рабочих при открытых горных работах, особенно на угольных разрезах. $PM_{2.5}$ на угольных разрезах могут вызывать за-

болевания легких (например, пневмокониоз, рак легких) и сердечно-сосудистые заболевания из-за длительного воздействия вдыхаемой пыли. Поэтому точное прогнозирование $PM_{2.5}$ имеет большое значение для минимизации загрязнения $PM_{2.5}$ и улучшения качества воздуха на рабочих местах. В данном исследовании изучались метеорологические условия и выбросы $PM_{2.5}$ на угольном разрезе во Вьетнаме с целью разработки новой интеллектуальной модели для прогнозирования выбросов и загрязнения $PM_{2.5}$, применялась нейронная сеть с функциональными связями (FLNN) для прогнозирования загрязнения $PM_{2.5}$ в зависимости от метеорологических условий (в частности, температуры, влажности, атмосферного давления, направления и скорости ветра). Вместо традиционных алгоритмов для обучения модели FLNN был использован алгоритм поиска методом голодных игр (HGS). Важнейшая роль HGS в данном исследовании заключается в оптимизации весов в модели FLNN, которая была названа моделью HGS-FLNN. Также были рассмотрены три другие гибридные модели, основанные на FLNN и метаэвристических алгоритмах, т.е. ABC (искусственная пчелиная колония)-FLNN, GA (генетический алгоритм)-FLNN и PSO (оптимизация роя частиц)-FLNN, для оценки возможности прогнозирования $PM_{2.5}$ на угольных разрезах и сравнения их результатов с результатами модели HGS-FLNN. Исследования показали, что HGS-FLNN является лучшей моделью с самой высокой точностью прогнозирования загрязнения воздуха $PM_{2.5}$ (в среднем до 94–95 %, при этом точность других моделей варьировалась от 87 до 90 %), а также наиболее стабильной моделью с наименьшей относительной ошибкой (в диапазоне от –0,3 до 0,5 %).

Ключевые слова
угольный разрез, загрязнение воздуха, пыль, $PM_{2.5}$, здоровье человека, поиск методом голодных игр, нейронная сеть с функциональными связями, оптимизация, разрез Кок Сау, провинция Куангнинь, Вьетнам

Благодарности
Данное исследование было финансово поддержано Министерством образования и профессиональной подготовки (MOET) Вьетнама в рамках гранта № B2018-MDA-03SP. Авторы также благодарят Центр горных и электромеханических исследований Ханойского университета горного дела и геологии (HUMG), Вьетнам; инженеров и руководителей угольного разреза Кок Сау, провинция Куангнинь, Вьетнам, за помощь и сотрудничество.

Для цитирования
Bui X.-N., Nguyen H., Le Q.-T., Le T.-N. Forecasting $PM_{2.5}$ emissions in open-pit mines using a functional link neural network optimized by various optimization algorithms. *Mining Science and Technology* (*Russia*). 2022;7(2):111–125. https://doi.org/10.17073/2500-0632-2022-2-111-125

Introduction

"Mining is not everything, but without mining, everything is nothing", Max Planck, famous German theoretical physicist, said. Practically everything, for example, metals, cement, construction materials, bridges, glass, towers/buildings, coal, power plans, etc., originate initially from mining. Such activities have a positive economic effect on development of countries worldwide and energy security of each country. However, mining operations also have significant negative environmental impacts, especially air pollutants (e.g., total suspended particulate (TSP), inhalable dust particles with diameters that are generally 1.0, 2.5, and 10 micrometers and smaller ($PM_{1.0}$, $PM_{2.5}$, PM_{10})) [1–3] Fig. 1). Open-pit mines (OPMs) have a more serious environmental impact compared with underground mines because of the outdoor work implementation. Depending on the particle size, the adverse effects on human health and occupational exposure may be more or less significant [4, 5]. Among the particles generated by OPM operations, OPCM-produced particles are considered as the most dangerous due to their different sizes and chemical and mineralogical composition (e.g., coal, minerals, organic compounds, etc.) [6].

In OPCMs, many activities can produce dust (i.e., $PM_{2.5}$), for instance, drilling, blasting, excavation, hauling, and transportation among others. The dust impact radius can increase due to specific meteorological conditions (e.g., wind direction and speed). In recent years, with exponential increase in energy consumption, OPCM operation has deepened to increase coal production [8]. Deeper OPCMs are unable to use natural ventilation efficiently. This results in availability of huge amount of thin particles in mining medium. These particles can be dangerous for miners and cause severe health impacts [9, 10].

To manage OPM dust emission, many researchers have measured and analyzed the amount of PM of different sizes, in order to evaluate the impacts of PM depending on size. They have proposed solutions for reductions of air pollution [11–13]. Dr. Emanuele Caudaet al. (NIOSH Center for Direct Reading and Sensor Technologies) investigated the distribution of PMs from different sources, and their findings showed that coal mine dust emission is a significant PM source (Fig. 2), and its forecast and control is an actual challenge.

Another approach to solving the dust pollution problem is estimating/forecasting the dust emission/concentration in OPCMs. Most historical studies related to PM emissions from OPCM have focused on estimating PM concentration in these operations [14, 15]. In recent years, artificial intelligence (AI) has

Fig. 1. Open-pit mines air pollution from various sources:
a – Transportation air pollution [7]; *b* – Shovel air pollution; *c* – Air pollution by various operations; *d* – Blasting air pollution

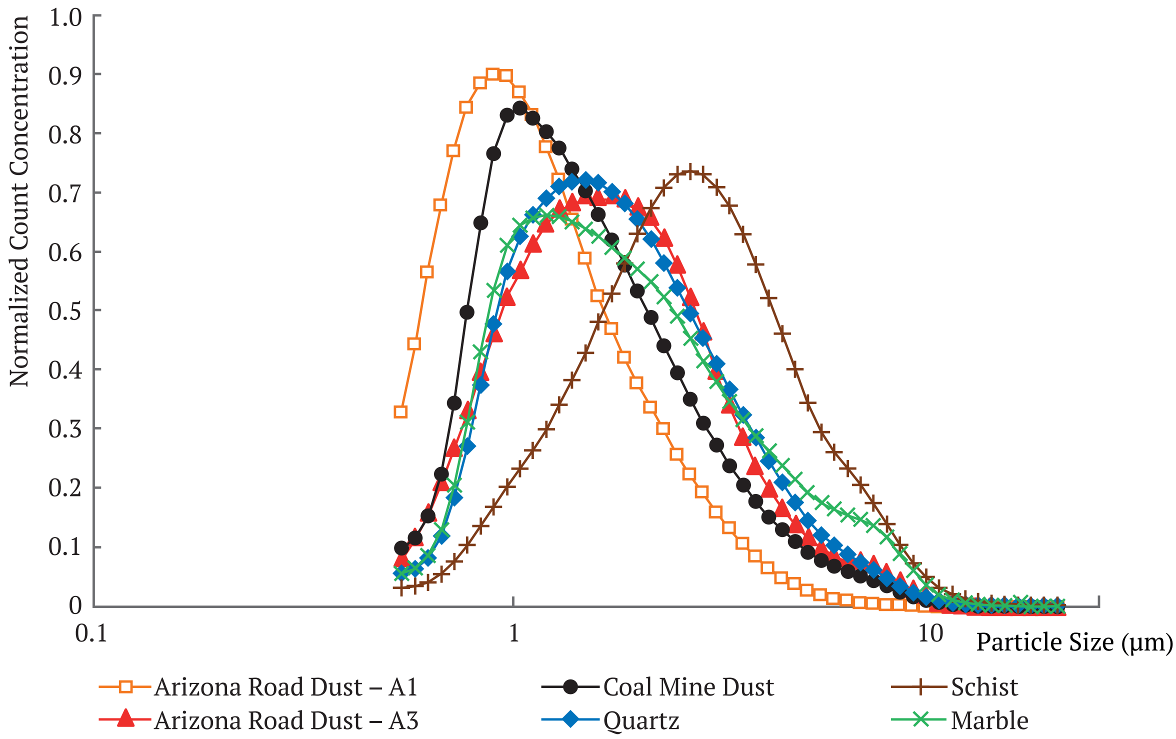

Fig. 2. Distribution of dust from various sources by size
Source: Nanozen (the official site). Dust specific calibrated real-time particle monitors.
https://nanozen.com/nanozette-q120/[Accessed: 03/10/2021]

been widely applied to predict dust concentrations/emissions in OPM. It is also recommended as a robust tool for use in other sectors [16–20]. In the aims of forecasting OPCM air pollution Lal B. and Tripathy S.S. [21] applied a multiple layers perceptron (MLP) neural network model to predict dust concentration in an Indian OPCM. Their study confirmed the high accuracy of the MLP model in predicting dust concentration. Bakhtavar E. et al. [22] also applied an artificial causality-weighted neural network (ACWNN) model for predicting OPM blasting dust emissions. They applied a fuzzy cognitive map to extract the weights of inputs for the dust emission prediction neural network. However, the study only predicted horizontal and vertical dust distributions. Considering other activities in OPCM (i.e., drilling), Bui H.-N. et al. [23] predicted PM10 emission by means of the support vector regression model optimized by particle swarm optimization (PSO). Using deep learning technique (e.g., long short-term memory – LSTM), Li L. et al. [24] predicted the $PM_{2.5}$ and PM_{10} emissions in OPMs at RMSE (root-mean-square error) of 29.517 and 23.204, MAPE (mean absolute percentage error) of 11.573 % and 8.537 %, respectively. Lu X. et al. [25] proposed a hybrid PSO-GBM (Gradient Boosting Machine) model for forecasting $PM_{2.5}$ concentrations based on other machine learning algorithm. High convergence was observed in their study with the correlation coefficient ranged 0.920 to 0.942.

The dust concentrations/emissions were studied in terms of measurement and prediction. In most cases they were measured and forecasted based on single activity in OPMs. Although several AI models were proposed and successfully applied to forecasting dust emissions/concentrations, their validity was limited due to the range of meteorological conditions in different areas and the robustness of different intelligent models. In OPMs, $PM_{2.5}$ was evaluated as much more dangerous than PM10 in the working environment. They can cause restrictive respiratory disorder and diseases related to lung and cardiovascular system [26–28]. Therefore, in this study we designed an air quality evaluation intelligent system to measure $PM_{2.5}$ emission in OPMs. We used the internet of things method for data transfer to workstations. Subsequently, a novel hybrid-neural network model based on functional linked neural network (FLNN) and hunger games search (HGS) algorithm, abbreviated as HGS-FLNN model, was developed, in order to forecast $PM_{2.5}$ emission in a deep OPCM. It is worth mentioning that the proposed HGS-FLNN model was never developed and applied previously for forecasting OPM dust emission. The obtained HGS-FLNN model results were then compared with three other hybrid models, i.e., ABC (artificial bee colony)-FLNN, GA (genetic algorithm)-FLNN, and PSO-FLNN to highlight outstanding performance of the HGS-FLNN model.

1. Data collection

In order to estimate $PM_{2.5}$ emission in OPMs, the Coc Sau OPCM in Vietnam was investigated (Fig. 3). This is one of Vietnam's largest and deepest OPCMs with a depth of 300m below sea level in July 2021[1]. Due

[1] Coc Sau Coal Company. Summary report of production in 2021, Coc Sau. 2021 (In Vietnamese).

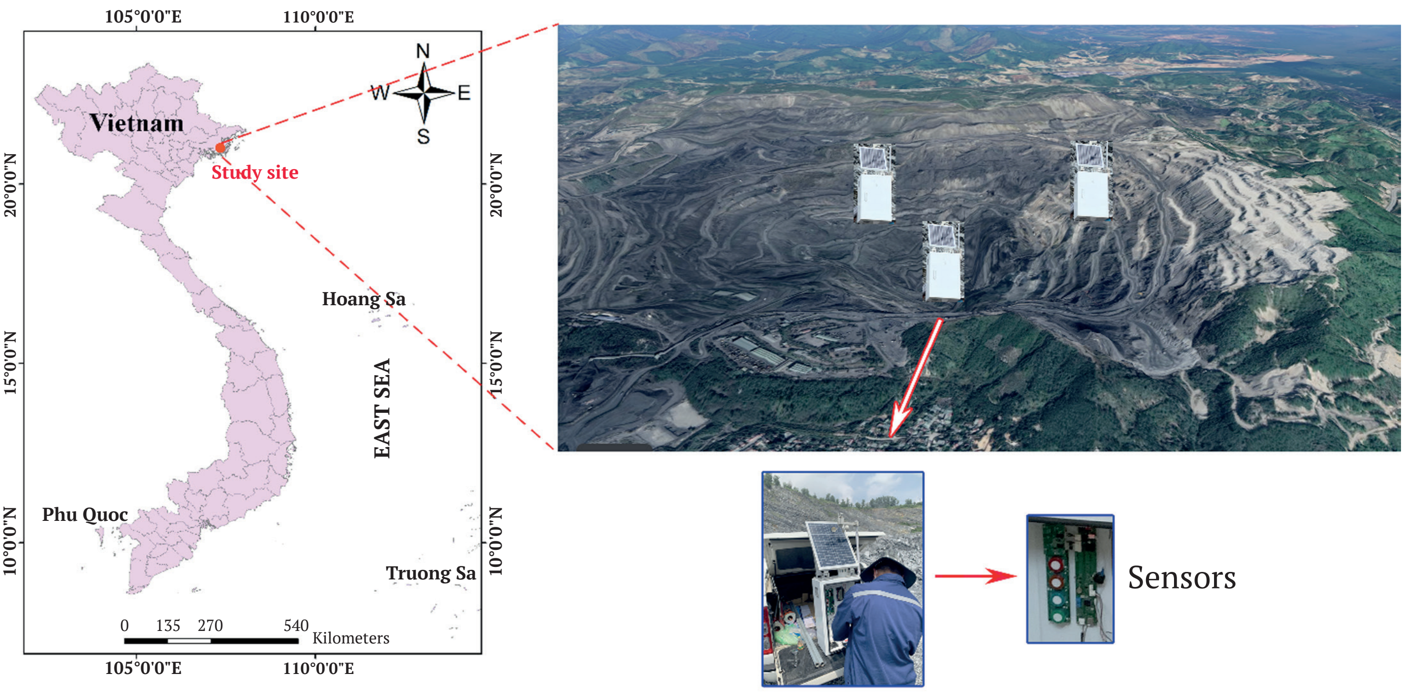

Fig. 3. Study area and air quality measurement stations locations

to the irregular shape and great depth, the mine air quality, especially in terms of $PM_{2.5}$, is very bad. Due to the great depth, the mine is unable to use natural ventilation. Therefore, the impact of high $PM_{2.5}$ concentrations is significant. As described above, $PM_{2.5}$ is one of the most adverse particles capable of causing occupational diseases. Hence, predicting $PM_{2.5}$ in this mine is aimed at finding suitable solutions to reduce the air pollution (e.g., $PM_{2.5}$) in the mine working environment.

In the aims of developing AI models to predict $PM_{2.5}$, the dataset was collected using three measuring stations (Fig. 3). Each station was designed as an air quality measuring system capable of measuring not only $PM_{2.5}$ but also meteorological conditions, such as temperature (T), atmospheric pressure (AP), humidity (H), wind direction and speed (WD, WS). These stations measured all the parameters hourly and transferred the data to the mine's technical department via the 4G network. Historical studies indicated that meteorological conditions significantly affect OPM dust emission [29, 30]. Therefore, they were used as the input variables to predict $PM_{2.5}$ in the present study. Since the mine geometry does not change significantly with deepening, the mine $PM_{2.5}$ pollution over the operation time is considered to be stable. It is worth noting that WD (e.g., West, East, North, South) was converted to numeric for solving regression problem in this study. The dataset is presented in Table 1.

Table 1

$PM_{2.5}$ emission and meteorology conditions in the study area

Category	$PM_{2.5}$	T	H	AP	WD	WS
Min.	10	18.5	83.4	985.5	1	0.1
1st Qu.	23	22.4	91.7	1,000.3	3	2.4
Median	34	23.4	94.7	1,004.4	10	3.3
Mean	34.98	23.43	94.3	1,004.3	8.534	3.285
3rd Qu.	44	24.5	97.1	1,008.2	12	4.2
Max.	90	28.8	100	1,023.9	16	7.5

2. HGS-FLNN model design for predicting $PM_{2.5}$

In the aims of predicting $PM_{2.5}$, FLNN, a kind of ANN, was selected as a single-layer architecture in this study [31, 32]. The unique mechanism of this network is based on the input variables and non-linear functional expansions [33]. It can generate hidden neurons and calculate the sum of weights. This approach enables complexity associated with regression problems [34] to be reduced. For training the FLNN model, the simple least mean square (LMS), back propagation (BP), or gradient descent-based methods can be applied to update the model's weights. The FLNN model architecture is illustrated in Figure 4.

The FLNN model (Figure 4) has many nodes generated with a large number of weights. In connection with this, updating weights to the network is challenging for a FLNN model with traditional training

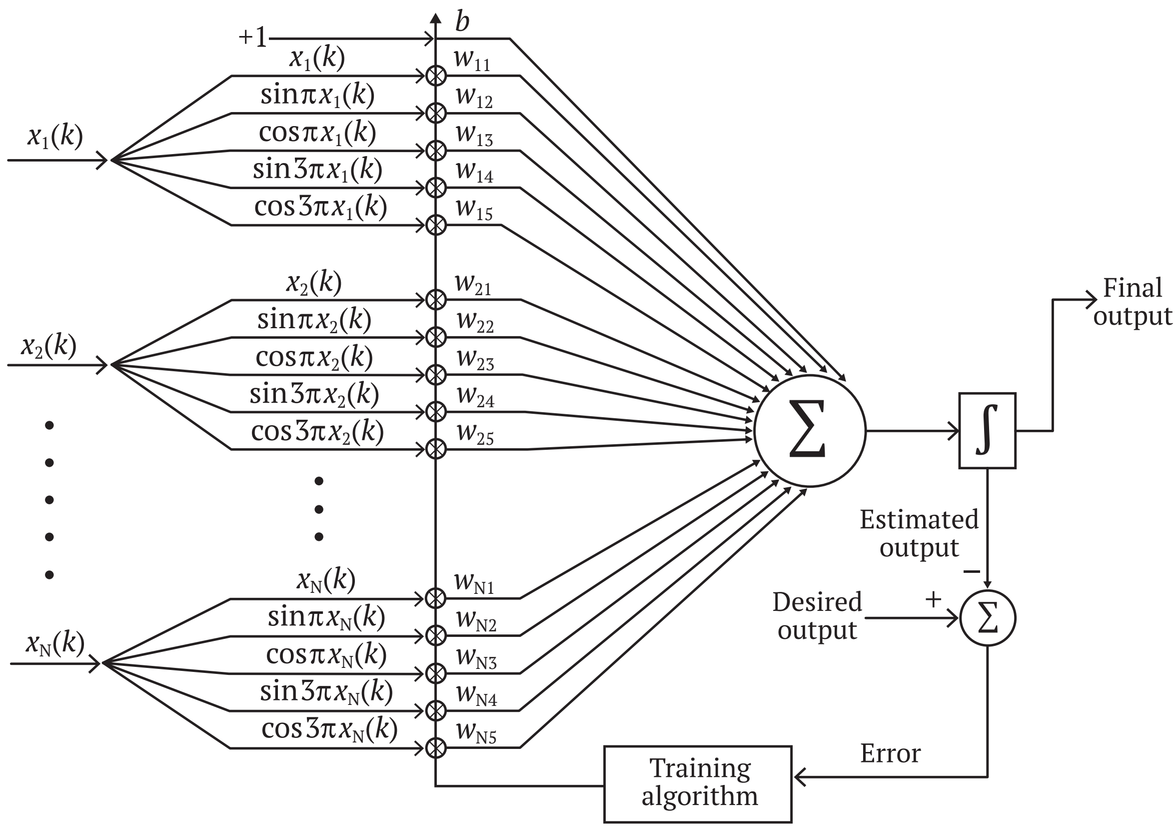

Fig. 4. FLNN model architecture

algorithms (e.g., BP, LMS) [35]. Local optima may occur while training the FLNN model with traditional training algorithms. This can reduce FLNN model performance in predicting $PM_{2.5}$.

In order to overcome this problem, optimization algorithms can be used for network training in the aims of optimizing the FLNN model weights. Metaheuristic algorithms are a good choice since they enable the FLNN model to reach the global optimum [36, 37]. In this study, HGS, a new metaheuristic algorithm proposed by Yang Y. et al. [38], was selected to train the FLNN model instead of traditional algorithms. The HGS is highly competitive algorithm in resolving optimization problems [39]. It was designed on the basis of hunger-driven activities of individuals in a swarm while hunting prey or looking for food. The HGS details are available in the original study [38]. The HGS flowchart is presented in Figure 5.

A novel hybrid AI model was designed based on the FLNN and the HGS algorithm for predicting $PM_{2.5}$ in OPCMs, referred to as the HGS-FLNN model. The HGS algorithm was developed and used to train and generate the weights for the FLNN model based on hunger-driven activities. Subsequently, the weights were updated for the network, and the model error was calculated. While optimizing the FLNN model for predicting $PM_{2.5}$, RMSE was used as the loss function for evaluating the model's performance, to determine whether the criterion is met or not. The proposed HGS-FLNN model framework is presented in Figure 6.

3. Development of the HGS-FLNN model for predicting $PM_{2.5}$

The HGS-FLNN model for predicting OPCM $PM_{2.5}$ was developed as described in Figure 6. Before developing the HGS-FLNN and other models, the dataset was randomly divided into two parts in the ratio of 4:1 for developing and testing the models, respectively. In addition, the datasets were also normalized by scaling between 0 and 1, in order to improve the models accuracy and minimize errors.

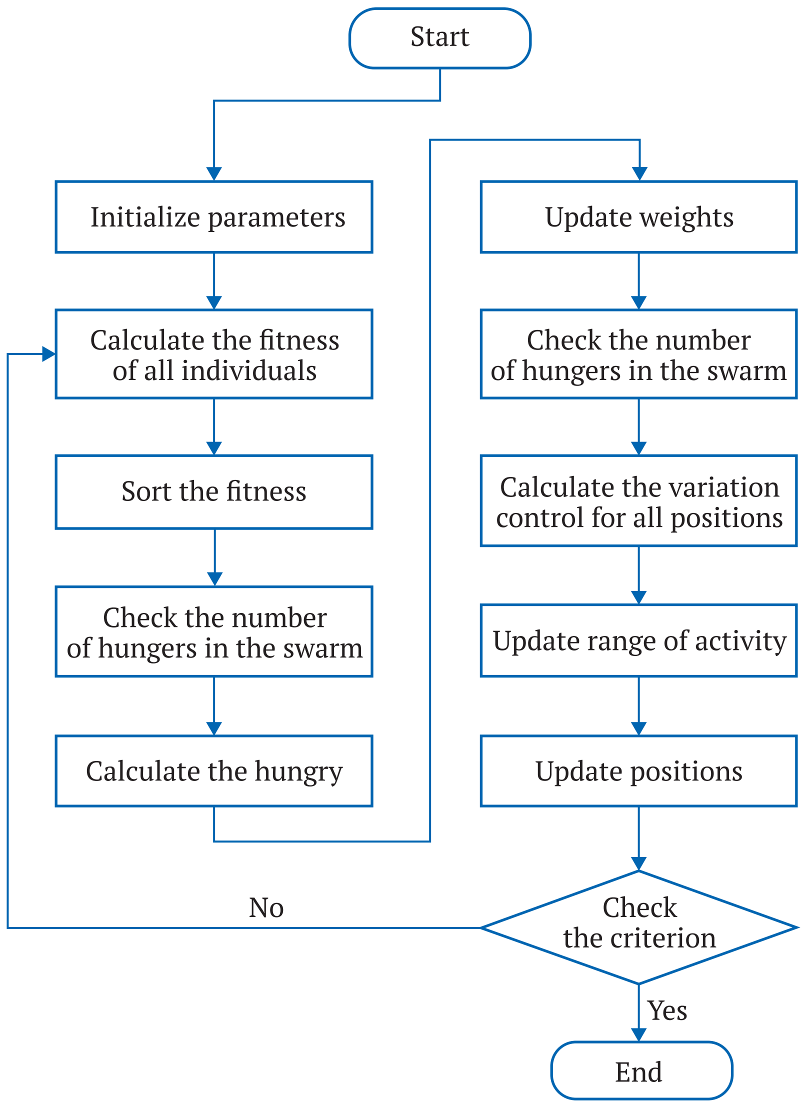

Fig. 5. HGS optimization algorithm simplified flowchart

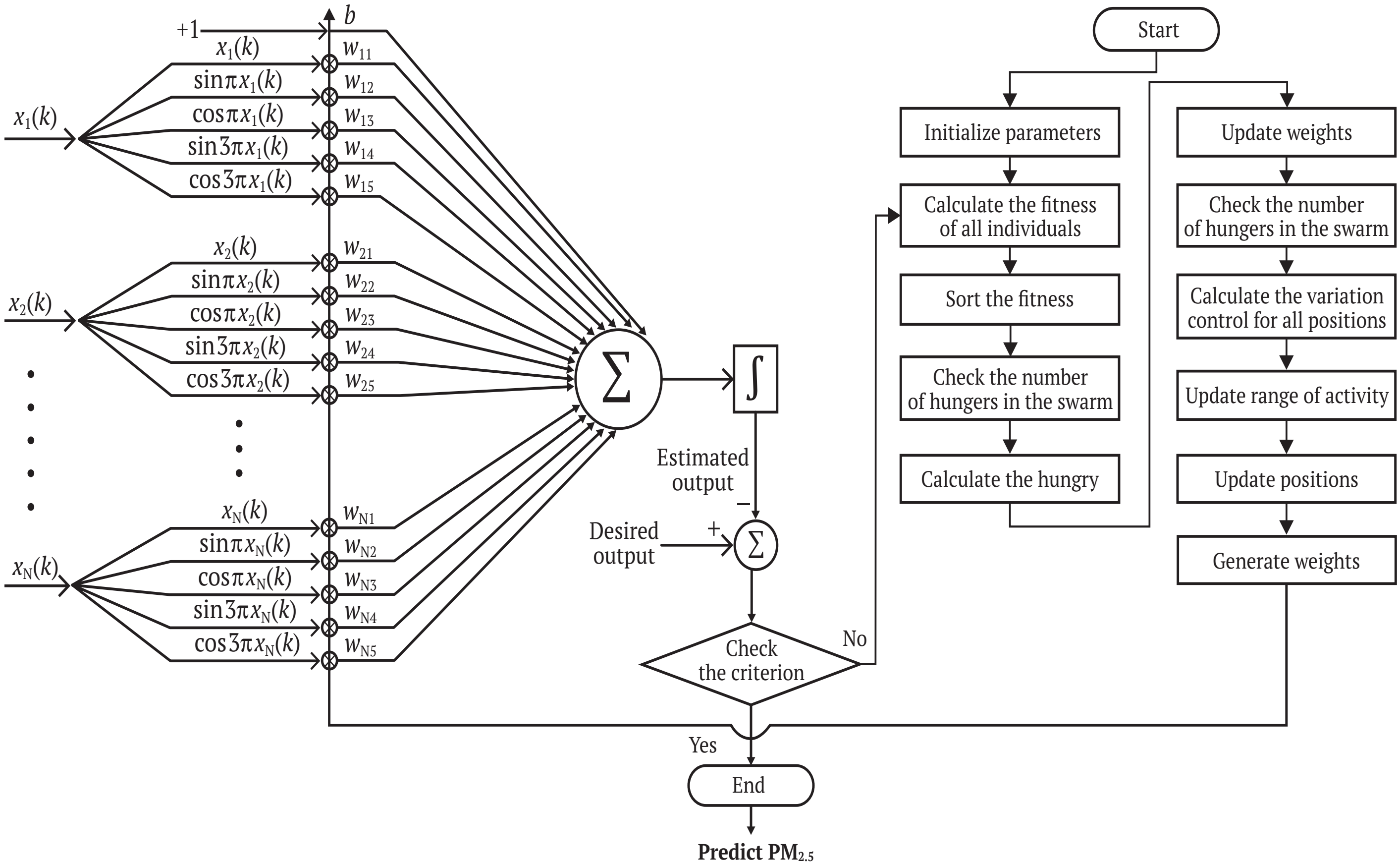

Fig. 6. Proposed HGS-FLNN model for predicting $PM_{2.5}$ in OPMs

Prior to optimizing the FLNN model, the functional expansion and HGS's parameters were established and calibrated. The Chebyshev function was selected as the FLNN model expansion function for transferring the input variables data (i.e., T, H, AP, WD, WS) to the hidden nodes. In addition, ReLu (Rectified Linear Unit) activation function was used to transform the data (weights) in the FLNN model nodes. For the HGS optimizer, different numbers of hungers were considered, e.g., 50, 100, 150, 200, 250, 300, 350, 400, 450, 500 for evaluating the optimizer performance. The switching updating position probability was selected equal to 0.03 with the threshold of 1000. For each hunger and its position, the HGS created weights and then updated them to the FLNN model. Finally, the RMSE values were calculated, and the best model with the lowest RMSE was selected, as shown in Figure 7. For this purpose, the Mealpy library developed by Thieu N.V.[2] was used. The performance curves show that the HGS-FLNN model training performance and RMSE are excellent. The next chapter is devoted to the performance testing and evaluation.

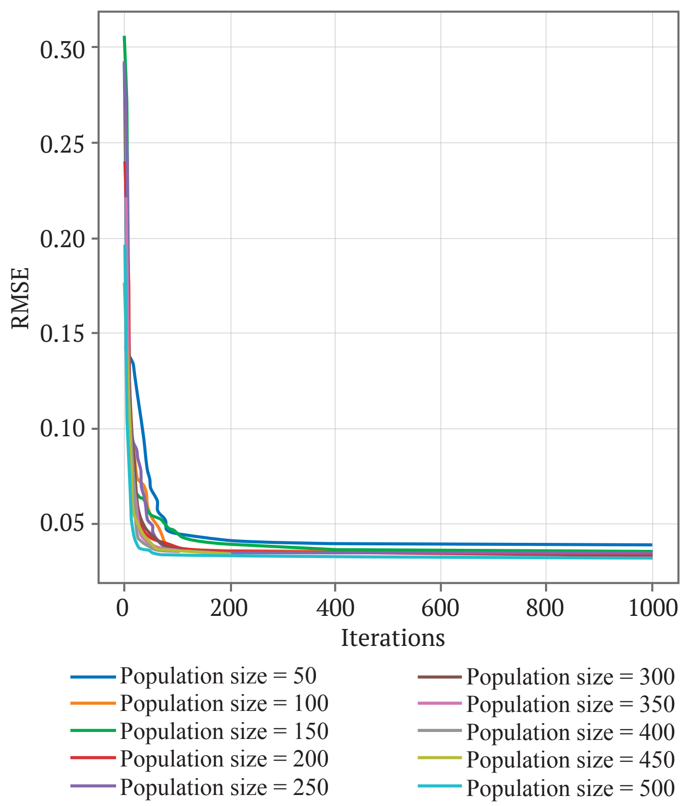

Fig. 7. Optimization performance of the HGS-FLNN model for predicting $PM_{2.5}$

[2] Thieu N.V. A collection of the state-of-the-art meta-heuristics algorithms in Python: Mealpy. 2020.

4. Development of other models for predicting $PM_{2.5}$

PSO, GA, and ABC well-known metaheuristic algorithms are widely used for resolving optimization problems [40–48]. In this study, we hybridized FLNN model (for predicting PM2.5 in OPCMs) with these algorithms to produce so-called PSO-FLNN, GA-FLNN, and ABC-FLNN models. It should be noted that they are also novel hybrid models related to air pollution prediction, especially for $PM_{2.5}$ predicting. The PSO, GA, and ABC basic principles are available in the following studies [49–61]. It is worth mentioning also that the role of the PSO, GA, and ABC is similar to the HGS optimizer in this study, and the development of the PSO-FLNN, GA-FLNN, and ABC-FLNN models is similar to that of the HGS-FLNN model.

4.1. PSO-FLNN

In order to develop the PSO-FLNN model, the same framework with Chebyshev function and ReLu activation function was used (similar to that used for the HGS-FLNN model). Different numbers of swarms were also set in interval of 50–500 similarly to those used for the HGS-FLNN model. The PSO's parameters were set as follows: $C_1 = 1.2$, $C_2 = 1.2$, $W_{\min} = 0.4$, $W_{\max} = 0.9$. The PSO was also implemented with 1000 iterations through RMSE objective function. The best PSO-FLNN model was then defined based on the lowest RMSE (Fig. 8).

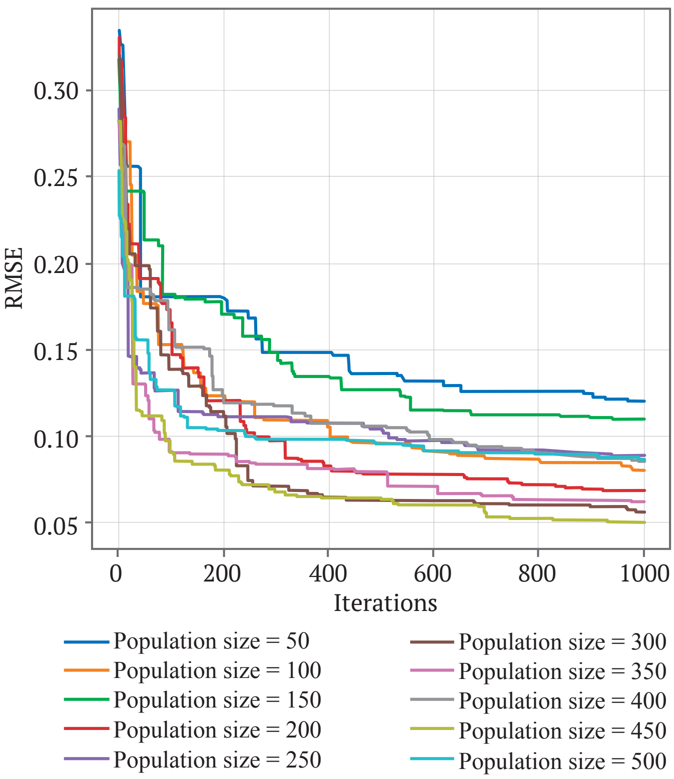

Fig. 8. Optimization performance of the PSO-FLNN model for predicting $PM_{2.5}$

4.2. GA-FLNN

In order to develop the GA-FLNN model, the same framework with Chebyshev function and ReLu activation function was used (similar to that used for the HGS-FLNN and PSO-FLNN models). Different numbers of swarms were also set in interval of 50–500 similarly to those used for the HGS-FLNN and PSO-FLNN models. The GA's parameters were set as follows: $P_c = 0.85$, $P_m = 0.05$. The GA was also implemented with 1000 iterations through RMSE objective function. The best GA-FLNN model was then defined based on the lowest RMSE (Fig. 9).

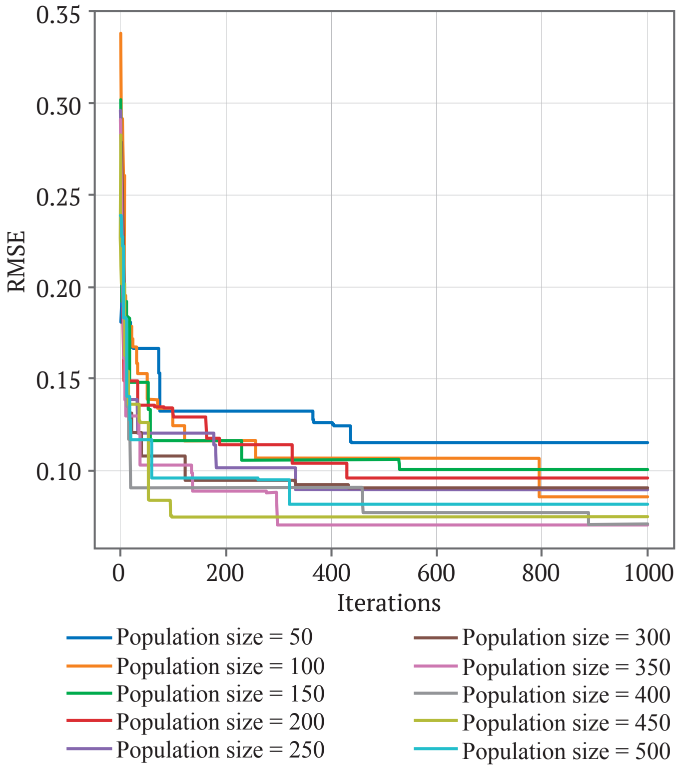

Fig. 9. Optimization performance of the GA-FLNN model for predicting $PM_{2.5}$

4.3. ABC-FLNN

Similar to the PSO-FLNN and GA-FLNN models, the ABC-FLNN model to predict $PM_{2.5}$ was also developed based on the same approaches. The same framework of the initial FLNN model (i.e. the inputs, expansion function, activation function) was used. Next, the ABC optimizer implemented global search to provide the set the number of weights. Subsequently, they were updated to the initial FLNN model and the error (i.e., RMSE) was calculated. Different numbers of bees were also set equal to 50–500, as those used for the HGS-FLNN, PSO-FLNN, and GA-FLNN models. The size of neighborhood for the elite and other bees (as the ABC's parameter) was set at 16.4. The ABC algorithm optimized the initial FLNN model with 1000 iterations through the RMSE objective function, as shown in Figure 10. Ultimately, the best ABC-FLNN model was defined based on the lowest RMSE. Training curves in Figure 10 show that the learning performance of the ABC-FLNN model is good. The next chapter describes the performance testing and evaluation.

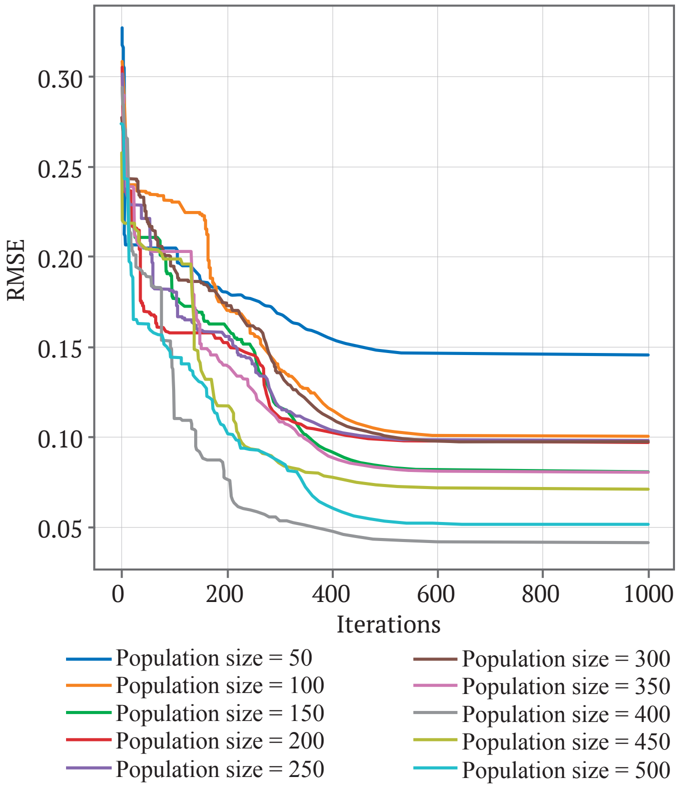

Fig. 10. Optimization performance of the ABC-FLNN model for predicting $PM_{2.5}$

5. Findings and discussion

Figures 5–8 demonstrate that the HGS-FLNN, ABC-FLNN, PSO-FLNN, and GA-FLNN models are well-trained with good convergence. However, it is difficult to indicate which model is the best for predicting $PM_{2.5}$ using these Figures only. We used statistical indices, such as MAE, RMSE, R^2, and MAPE to estimate the accuracy of the developed hybrid FLNN-based models. They are useful not only in estimating the accuracy of the models but also for determining the properties of the developed models (e.g., overfitting, underfitting). The results are presented in Table 2.

Table 2 shows that the HGS-FLNN model is obviously superior to the other models. In the HGS-FLNN model, the MAE ranges 1.405 to 1.497 only, whereas the ABC-FLNN, PSO-FLNN, and GA-FLNN models provided higher errors (MAE of 1.776, 2.326, 3.693, respectively, in the training dataset, and MAE of 2.246, 2.453, 3.602, respectively, in the testing dataset. Similarly to MAE, the RMSE values in the HGS-FLNN model amounting to 2.652 and 2.700 (in training and testing phases, respectively) are lower than those in other models. The training and testing phases of the other models yielded higher RMSE values (ranged 3.298–5.938 and 3.857–5.672, respectively). It is remarkable that MAPE was 0.054 only in the HGS-FLNN model training and 0.057 in testing of the corresponding dataset. In other words, the MAPE in the HGS-FLNN model-based predicting $PM_{2.5}$ ranged at 5.4–5.7 % only taking into account the meteorological conditions.

With regard to the level of regression in the models (i.e., correlation factor R^2), the results also indicated that the HGS-FLNN model demonstrated the highest R^2 in both phases. Furthermore, as observed, the developed models did not demonstrate overfitting. In other words, the training and testing phases showed practically similar accuracy of the results on predicting PM2.5 in this study. The visualization of the models regression levels in Figures 9 and 10 shows the best correlation between the predicted and measured data in the HGS-FLNN model, when compared to the other models. Whereas the correlation in the HGS-FLNN model is perfect, the other models (i.e., ABC-FLNN, PSO-FLNN, and GA-FLNN) demonstrate lower correlation, especially the GA-FLNN model. The GA-FLNN model demonstrated the lowest performance in predicting $PM_{2.5}$ in this study. The PSO-FLNN and ABC-FLNN models demonstrated better correlation/performance than the GA-FLNN model.

Turning to the FLNN-based models training performance (Figures 5–8), and taking a closer look at the performance lines and RMSE values, one can see that the HGS-FLNN model training performance is much better than that of the other models with lower RMSE values. This finding confirms the results presented in Table 2 and Figures 9–10. In other words, this con-

Table 2

Statistical indices for examination of the FLNN-based models for predicting $PM_{2.5}$

Model	Training				Testing			
	MAE	RMSE	R^2	MAPE	MAE	RMSE	R^2	MAPE
HGS-FLNN	1.405	2.652	0.967	0.054	1.497	2.700	0.966	0.057
ABC-FLNN	1.776	3.298	0.949	0.070	2.246	3.857	0.931	0.097
PSO-FLNN	2.326	3.968	0.930	0.087	2.453	3.962	0.933	0.091
GA-FLNN	3.693	5.938	0.837	0.125	3.602	5.672	0.852	0.129

firms that the HGS algorithm performs better than the other algorithms (i.e., ABC, PSO, and GA) in this case. This statement does not mean that the HGS algorithm is better than the ABC, PSO, and GA algorithms in all cases. It depends on datasets used in each case study. Nevertheless, the HGS algorithm is considered as the best for predicting $PM_{2.5}$ in the OPCM at least in the present study. In order to measure the accuracy of the HGS-FLNN model in practice, the relative error (RE) was calculated, as shown in Figure 13. As can be seen, in the HGS-FLNN model, RE is very small. Most of the RE values ranges −0.3 to 0.5. Only one data point is out of this range, but this RE value is also low at 0.699. At the same time, the other models demonstrated higher REs, ranged −0.63 to 2.194. Notice that the ABC-FLNN model statistical indices (Table 2) indicated its better performance, when compared to the PSO-FLNN and GA-FLNN models. However, the ABC-FLNN model provided some data points with the highest RE, as shown in Figure 13. Finally, this study allowed a confident conclusion to be made that the HGS-FLNN model was the best technique to predict $PM_{2.5}$.

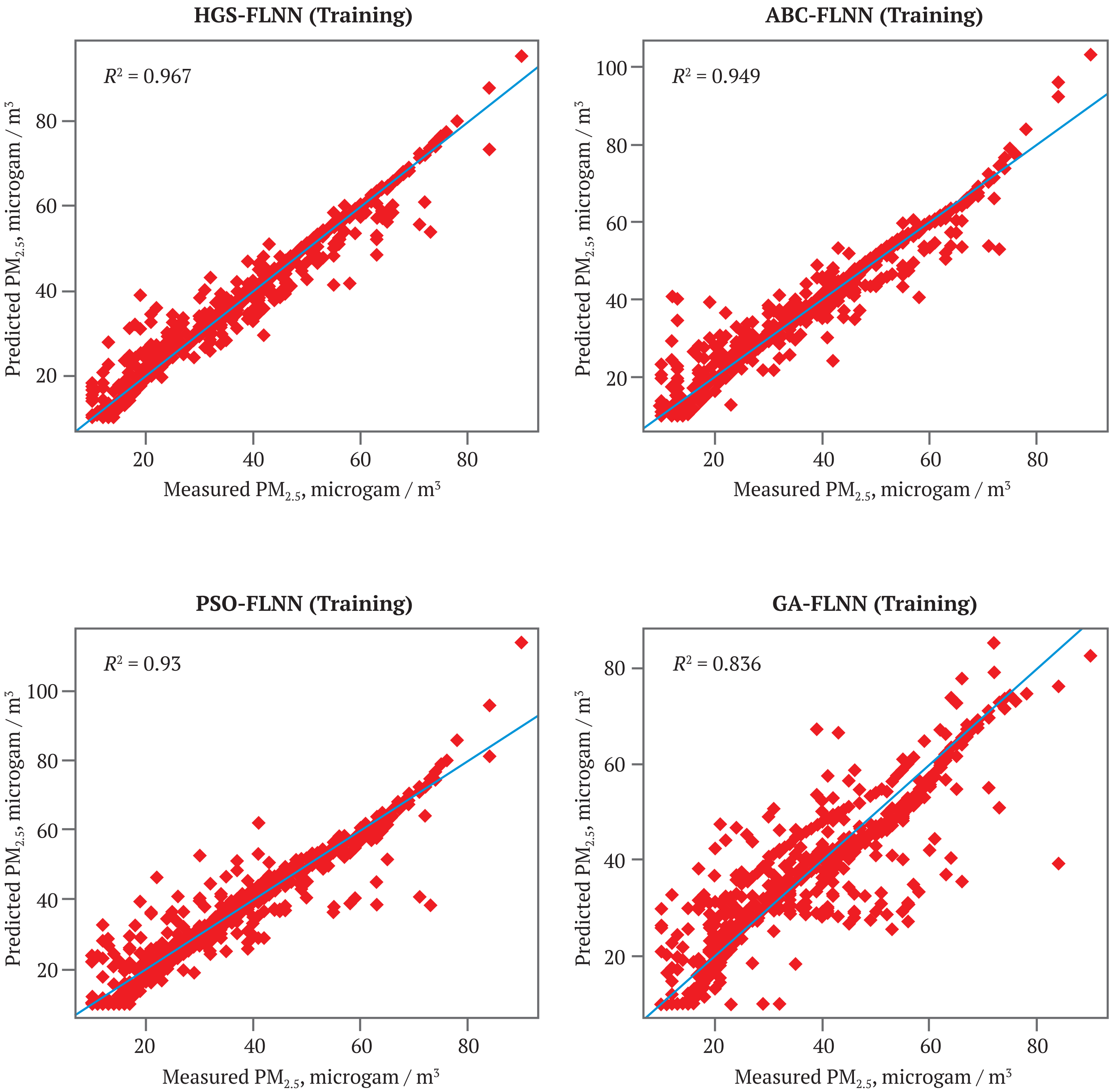

Fig. 11. Correlation between the predicted and measured data in the FLNN models (training dataset) under swarm-based algorithms optimization

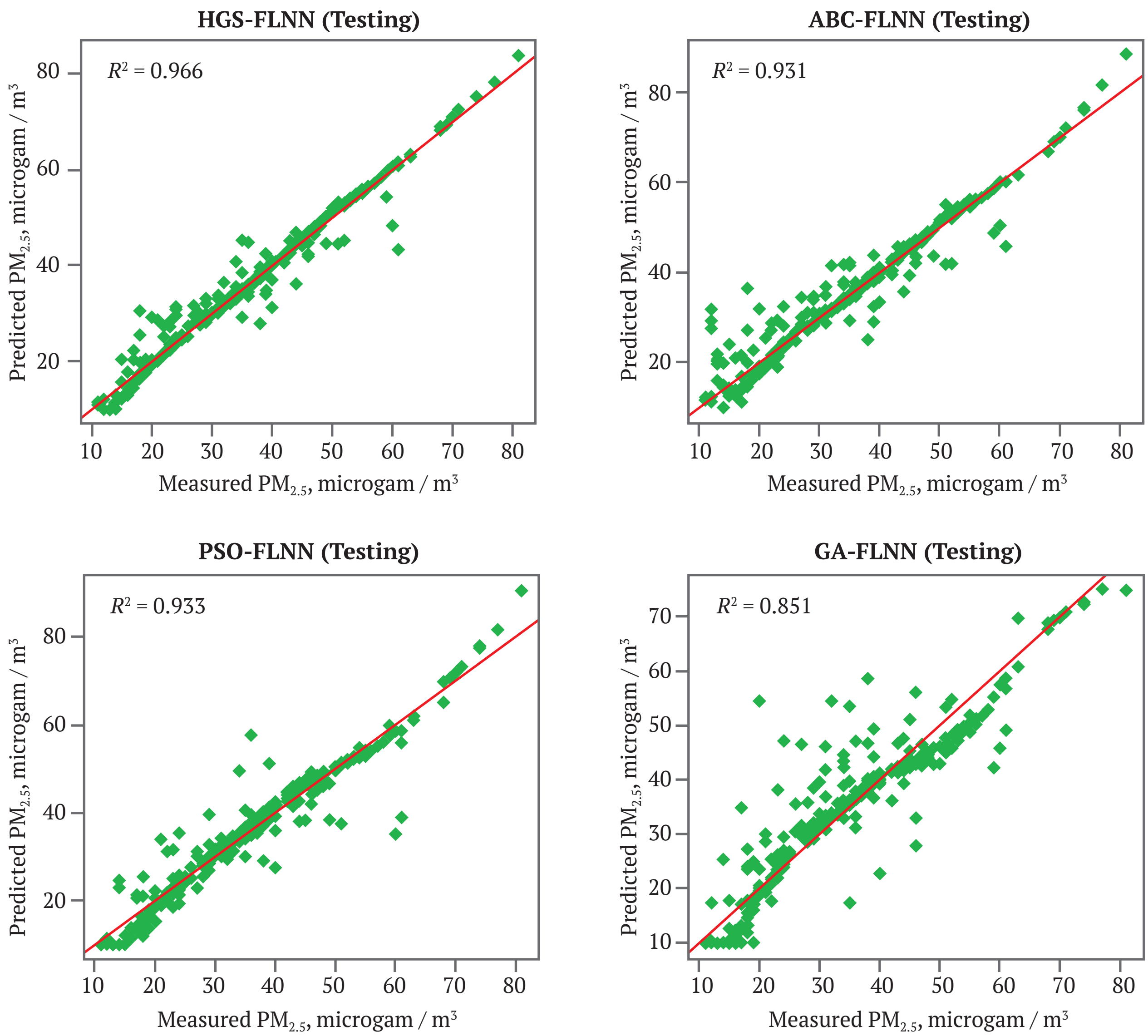

Fig. 12. Correlation between the predicted and measured data in the FLNN models (testing dataset) under swarm-based algorithms optimization

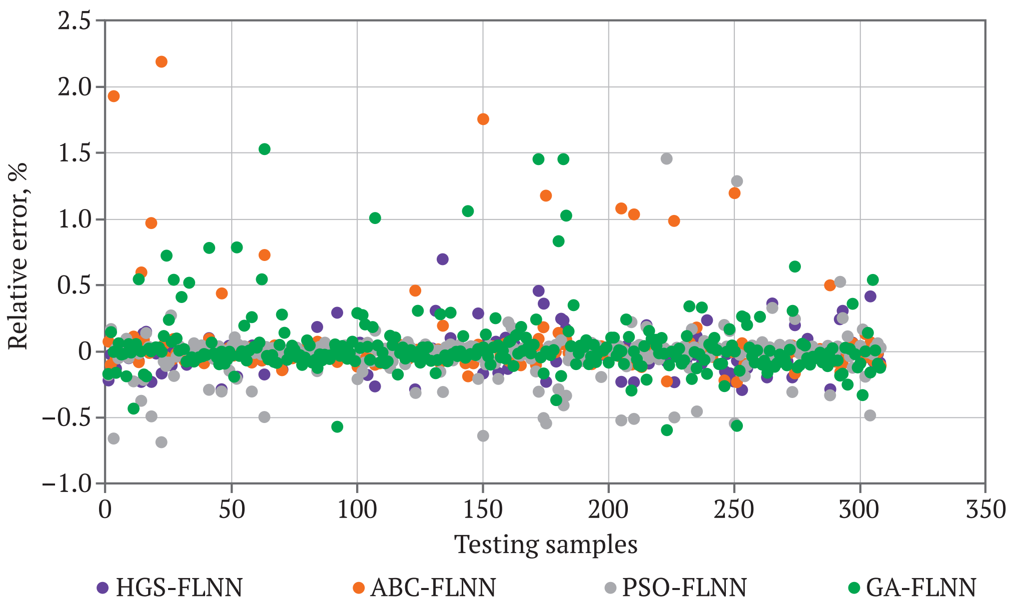

Fig. 13. Comparison of relative errors of the considered models

eISSN 2500-0632
https://mst.misis.ru/

Conclusion

$PM_{2.5}$ in OPCMs is a serious occupational hazard to miners' health. It can cause respiratory, lung, cardiovascular, and cancer diseases. Historical reports indicate that increasing air PM2.5 pollution concentration by 10 μg/m³ results in an increase in lung cancer rate by 36 %. Meanwhile, OPCM $PM_{2.5}$ emissions measured in this study ranged 10 to 90 μg/m³. These are really hazardous levels for the health of miners. Therefore, accurate air $PM_{2.5}$ pollution prediction is of crucial importance in terms of occupational health and selecting solutions to reduce OPCM $PM_{2.5}$ pollution. This study proposed the novel HGS-FLNN model for predicting $PM_{2.5}$ pollution in OPCMs with an average accuracy of 94–95 %. In addition, three other hybrid models were developed, reviewed, and evaluated in terms of $PM_{2.5}$ prediction. However, their accuracy proved in the range of 87 % to 90 % only. The obtained results also indicated that the HGS-FLNN model was the most stable model with a very low relative error. It can be used in mining engineering to predict and control $PM_{2.5}$ pollution in OPCMs.

References

1. Aneja V.P., Isherwood A., Morgan P. Characterization of particulate matter (PM_{10}) related to surface coal mining operations in Appalachia. *Atmospheric Environment*. 2012;54:496–501. https://doi.org/10.1016/j.atmosenv.2012.02.063

2. Chakraborty M., Ahmad M., Singh R. et al. Determination of the emission rate from various opencast mining operations. *Environmental Modelling & Software*. 2002;17(5):467–480. https://doi.org/10.1016/S1364-8152(02)00010-5

3. Nie B.-S., Li X.-C., Yang T. et al. Distribution of $PM_{2.5}$ dust during mining operation in coal workface. *Journal of China Coal Society*.2013;38(1):33–37. (In Chinese) URL: https://www.ingentaconnect.com/content/jccs/jccs/2013/00000038/00000001/art00006#

4. Kurth L.M., McCawley M., Hendryx M., Lusk S. Atmospheric particulate matter size distribution and concentration in West Virginia coal mining and non-mining areas. *Journal of Exposure Science & Environmental Epidemiology*. 2014;24:405–411. https://doi.org/10.1038/jes.2014.2

5. Li Z., Ma Z., van der Kuijp T.J. et al. A review of soil heavy metal pollution from mines in China: pollution and health risk assessment. *Science of the Total Environment*. 2014;468–469:843–853. https://doi.org/10.1016/j.scitotenv.2013.08.090

6. Dos Santos Pedroso-Fidelis G., Farias H.R., Mastella G.A. et al. Pulmonary oxidative stress in wild bats exposed to coal dust: A model to evaluate the impact of coal mining on health. *Ecotoxicology and Environmental Safety*. 2020;191:110211. https://doi.org/10.1016/j.ecoenv.2020.110211

7. Hendryx M., Islam M.S., Dong G.-H., Paul G. Air pollution emissions 2008–2018 from australian coal mining: implications for public and occupational health. *International Journal of Environmental Research and Public Health*. 2020;17(5):1570. https://doi.org/10.3390/ijerph17051570

8. Luo H., Zhou W., Jiskani I.M., Wang Z. Analyzing characteristics of particulate matter pollution in open-pit coal mines: Implications for Green Mining. *Energies*. 2021;14(9):2680. https://doi.org/10.3390/en14092680

9. Moreno T., Trechera P., Querol X. et al. Trace element fractionation between PM_{10} and $PM_{2.5}$ in coal mine dust: Implications for occupational respiratory health. *International Journal of Coal Geology*. 2019;203:52–59. https://doi.org/10.1016/j.coal.2019.01.006

10. Song Y., Wang X., Maher B.A. et al. The spatial-temporal characteristics and health impacts of ambient fine particulate matter in China. *Journal of Cleaner Production*. 2016;112:1312–1318. https://doi.org/10.1016/j.jclepro.2015.05.006

11. Alvarado M., Gonzalez F., Fletcher A., Doshi A. Towards the development of a low cost airborne sensing system to monitor dust particles after blasting at open-pit mine sites. *Sensors*. 2015;15(8):19667–19687. https://doi.org/10.3390/s150819667

12. Nambiar M.K., Robe F.R., Seguin A.M. et al. Diurnal and seasonal variation of area-fugitive methane advective flux from an open-pit mining facility in Northern Canada using WRF. *Atmosphere*. 2020;11(11):1227. https://doi.org/10.3390/atmos11111227

13. Trechera P., Moreno T., Córdoba P. et al. Comprehensive evaluation of potential coal mine dust emissions in an open-pit coal mine in Northwest China. *International Journal of Coal Geology*. 2021;235:103677. https://doi.org/10.1016/j.coal.2021.103677

14. Chaulya S. Assessment and management of air quality for an opencast coal mining area. *Journal of Environmental Management*. 2004;70(1):1–14. https://doi.org/10.1016/j.jenvman.2003.09.018

15. Patra A.K., Gautam S., Kumar P. Emissions and human health impact of particulate matter from surface mining operation – A review. *Environmental Technology & Innovation*. 2016;5:233–249. https://doi.org/10.1016/j.eti.2016.04.002

16. Alam G., Ihsanullah I., Naushad M., Sillanpää M. Applications of artificial intelligence in water treatment for optimization and automation of adsorption processes: recent advances and prospects. *Chemical Engineering Journal*. 2022;427:130011. https://doi.org/10.1016/j.cej.2021.130011

17. Li B.-H., Hou B.-C., Yu W.-T., Lu X.-B., Yang C.-W. Applications of artificial intelligence in intelligent manufacturing: a review. *Frontiers of Information Technology & Electronic Engineering*. 2017;18:86-96. https://doi.org/10.1631/FITEE.1601885

18. Nguyen H., Bui N.X., Tran H.Q., Le G.H.T. A novel soft computing model for predicting blast – induced ground vibration in open – pit mines using gene expression programming. *Journal of Mining and Earth Sciences*. 2020;61:107–116. (In Vietnamese) https://doi.org/10.46326/jmes.ktlt2020.09

19. Nguyen L.Q. A novel approach of determining the parameters of Asadi profiling function for predictiong ground subsidence due to inclied coal seam mining at Quang Ninh coal basin. *Journal of Mining and Earth Sciences*. 2020;61:86–95. (In Vietnamese) https://doi.org/10.46326/jmes.2020.61(2).10

20. Tayarani-N M.-H. Applications of artificial intelligence in battling against COVID-19: a literature review. *Chaos, Solitons & Fractals*. 2020;142:110338. https://doi.org/10.1016/j.chaos.2020.110338

21. Lal B., Tripathy S.S. Prediction of dust concentration in open cast coal mine using artificial neural network. *Atmospheric Pollution Research.* 2012;3(2):211–218. https://doi.org/10.5094/APR.2012.023

22. Bakhtavar E., Hosseini S., Hewage K., Sadiq R. Green blasting policy: simultaneous forecast of vertical and horizontal distribution of dust emissions using artificial causality-weighted neural network. *Journal of Cleaner Production*. 2021;283:124562. https://doi.org/10.1016/j.jclepro.2020.124562

23. Bui X.-N., Lee C.W., Nguyen H. et al. Estimating PM_{10} concentration from drilling operations in open-pit mines using an assembly of SVR and PSO. *Applied Sciences*. 2019;9(14):2806. https://doi.org/10.3390/app9142806

24. Li L., Zhang R., Sun J. et al. Monitoring and prediction of dust concentration in an open-pit mine using a deep-learning algorithm. *Journal of Environmental Health Science and Engineering*. 2021;19:401–414. https://doi.org/10.1007/s40201-021-00613-0

25. Lu X., Zhou W., Qi C. et al. Prediction into the future: A novel intelligent approach for $PM_{2.5}$ forecasting in the ambient air of open-pit mining. *Atmospheric Pollution Research*. 2021;12(6):101084. https://doi.org/10.1016/j.apr.2021.101084

26. Gautam S., Prasad N., Patra A.K. et al. Characterization of $PM_{2.5}$ generated from opencast coal mining operations: A case study of Sonepur Bazari Opencast Project of India. *Environmental Technology & Innovation*. 2016;6:1–10. https://doi.org/10.1016/j.eti.2016.05.003

27. Huang Y., Bao M., Xiao J. et al. Effects of $PM_{2.5}$ on cardio-pulmonary function injury in open manganese mine workers. *International Journal of Environmental Research and Public Health*. 2019;16(11):2017. https://doi.org/10.3390/ijerph16112017

28. Wanjun T., Qingxiang C. Dust distribution in open-pit mines based on monitoring data and fluent simulation. *Environmental Monitoring and Assessment*. 2018;190:632. https://doi.org/10.1007/s10661-018-7004-9

29. Oguntoke O., Ojelede M.E., Annegarn H.J. Frequency of mine dust episodes and the influence of meteorological parameters on the Witwatersrand area, South Africa. *International Journal of Atmospheric Sciences*. 2013;2013:128463. https://doi.org/10.1155/2013/128463

30. Silvester S., Lowndes I., Hargreaves D. A computational study of particulate emissions from an open pit quarry under neutral atmospheric conditions. *Atmospheric Environment*. 2009;43(40):6415–6424. https://doi.org/10.1016/j.atmosenv.2009.07.006

31. Pao Y. *Adaptive pattern recognition and neural networks*. CWRU: Case Western Reserve University; 1989. https://doi.org/10.5860/choice.26-6311

32. Patra J.C., Pal R.N. A functional link artificial neural network for adaptive channel equalization. *Signal Processing*. 1995;43(2):181–195. https://doi.org/10.1016/0165-1684(94)00152-P

33. Nguyen T., Tran N., Nguyen B.M., Nguyen G. A resource usage prediction system using functional-link and genetic algorithm neural network for multivariate cloud metrics. In: *2018 IEEE 11th Conference on Service-Oriented Computing and Applications (SOCA)*. 2018. Pp. 49–56. https://doi.org/10.1109/SOCA.2018.00014

34. Majhi B., Naidu D. Pan evaporation modeling in different agroclimatic zones using functional link artificial neural network. *Information Processing in Agriculture*. 2021;8(1):134–147. https://doi.org/10.1016/j.inpa.2020.02.007

35. Nguyen T., Nguyen B.M., Nguyen G. Building Resource Auto-scaler with Functional-Link Neural Network and Adaptive Bacterial Foraging Optimization. In: Gopal TV, Watada J (eds.) *Theory and Applications of Models of Computation. TAMC 2019. Lecture Notes in Computer Science*. Springer, Cham. 2019. Pp. 501–517. https://doi.org/10.1007/978-3-030-14812-6_31

36. Kaveh A. *Advances in metaheuristic algorithms for optimal design of structures*. Springer, Cham; 2014. https://doi.org/10.1007/978-3-319-05549-7

37. Ting T., Yang X.-S., Cheng S., Huang K. Hybrid metaheuristic algorithms: past, present, and future. In: Yang X. S. (ed.) *Recent Advances in Swarm Intelligence and Evolutionary Computation. Studies in Computational Intelligence*. Springer, Cham; 2015. Pp. 71–83. https://doi.org/10.1007/978-3-319-13826-8_4

38. Yang Y., Chen H., Heidari A.A., Gandomi A.H. Hunger games search: Visions, conception, implementation, deep analysis, perspectives, and towards performance shifts. *Expert Systems with Applications*. 2021;177:114864. https://doi.org/10.1016/j.eswa.2021.114864

39. Nguyen H., Bui X.-N. A novel hunger games search optimization-based artificial neural network for predicting ground vibration intensity induced by mine blasting. *Natural Resources Research*. 2021;30:3865–3880. https://doi/org/10.1007/s11053-021-09903-8

40. Chen W., Sarir P., Bui X.-N. et al. Neuro-genetic, neuro-imperialism and genetic programing models in predicting ultimate bearing capacity of pile. *Engineering with Computers*. 2020;36:1101–1115. https://doi.org/10.1007/s00366-019-00752-x

41. Erkoc M.E., Karaboga N. A novel sparse reconstruction method based on multi-objective Artificial Bee Colony algorithm. *Signal Processing*. 2021;189:108283. https://doi.org/10.1016/j.sigpro.2021.108283

42. Fang Q., Nguyen H., Bui X.-N., Tran Q.-H. Estimation of blast-induced air overpressure in quarry mines using cubist-based genetic algorithm. *Natural Resources Research*. 2020;29:593–607. https://doi.org/10.1007/s11053-019-09575-5

43. Liu L., Moayedi H., Rashid A.S.A. et al. Optimizing an ANN model with genetic algorithm (GA) predicting load-settlement behaviours of eco-friendly raft-pile foundation (ERP) system. *Engineering with Computers*. 2020;36:421–433. https://doi.org/10.1007/s00366-019-00767-4

44. Nguyen H., Bui H.-B., Bui X.-N. Rapid determination of gross calorific value of coal using artificial neural network and particle swarm optimization. *Natural Resources Research*. 2021;30:621–638. https://doi.org/10.1007/s11053-020-09727-y

45. Peng B., Wu L., Wang Y., Wu Q. Solving maximum quasi-clique problem by a hybrid artificial bee colony approach. *Information Sciences*. 2021;578:214–235. https://doi.org/10.1016/j.ins.2021.06.094

46. Xu Y., Wang X. An artificial bee colony algorithm for scheduling call centres with weekend-off fairness. *Applied Soft Computing*. 2021;109:107542. https://doi.org/10.1016/j.asoc.2021.107542

47. Zhang X., Nguyen H., Bui X.-N. et al. Evaluating and predicting the stability of roadways in tunnelling and underground space using artificial neural network-based particle swarm optimization. *Tunnelling and Underground Space Technology*. 2020;103:103517. https://doi.org/10.1016/j.tust.2020.103517

48. Zhang X., Nguyen H., Bui X.-N. et al. Novel soft computing model for predicting blast-induced ground vibration in open-pit mines based on particle swarm optimization and XGBoost. *Natural Resources Research*. 2020;29:711–721. https://doi.org/10.1007/s11053-019-09492-7

49. Akay B., Karaboga D., Gorkemli B., Kaya E. A survey on the artificial bee colony algorithm variants for binary, integer and mixed integer programming problems. *Applied Soft Computing*. 2021;106:107351. https://doi.org/10.1016/j.asoc.2021.107351

50. Aygun H., Turan O. Application of genetic algorithm in exergy and sustainability: A case of aero-gas turbine engine at cruise phase. *Energy*. 2022;238:121644. https://doi.org/10.1016/j.energy.2021.121644

51. Bai B., Zhang J., Wu X. et al. Reliability prediction-based improved dynamic weight particle swarm optimization and back propagation neural network in engineering systems. *Expert Systems with Applications*. 2021;177:114952. https://doi.org/10.1016/j.eswa.2021.114952

52. Kennedy J., Eberhart R. Particle swarm optimization. In: *Proceedings of ICNN'95 – International Conference on Neural Networks*. 1995. Pp. 1942–1948. https://doi.org/10.1109/ICNN.1995.488968

53. Kiran M.S., Hakli H., Gunduz M., Uguz H. Artificial bee colony algorithm with variable search strategy for continuous optimization. *Information Sciences*. 2015;300:140–157. https://doi.org/10.1016/j.ins.2014.12.043

54. Liang B., Zhao Y., Li Y. A hybrid particle swarm optimization with crisscross learning strategy. *Engineering Applications of Artificial Intelligence*. 2021;105:104418. https://doi.org/10.1016/j.engappai.2021.104418

55. Mirjalili S. Genetic algorithm. In: *Evolutionary Algorithms and Neural Networks. Studies in Computational Intelligence*. Springer, Cham; 2019. Pp. 43–55. https://doi.org/10.1007/978-3-319-93025-1_4

56. Pourzangbar A., Vaezi M. Optimal design of brace-viscous damper and pendulum tuned mass damper using Particle Swarm Optimization. *Applied Ocean Research*. 2021;112:102706. https://doi.org/10.1016/j.apor.2021.102706

57. Roy A., Dubey C.P., Prasad M. Gravity inversion of basement relief using Particle Swarm Optimization by automated parameter selection of Fourier coefficients. *Computers & Geosciences*. 2021;156:104875. https://doi.org/10.1016/j.cageo.2021.104875

58. Tapia A.R., del Nozal A., Reina D.G., Millán P. Three-dimensional optimization of penstock layouts for micro-hydropower plants using genetic algorithms. *Applied Energy*. 2021;301:117499. https://doi.org/10.1016/j.apenergy.2021.117499

59. Wang C., Guo C., Zuo X. Solving multi-depot electric vehicle scheduling problem by column generation and genetic algorithm. *Applied Soft Computing*. 2021;112:107774. https://doi.org/10.1016/j.asoc.2021.107774

60. Wang S.-C. Genetic algorithm. In: *Interdisciplinary Computing in Java Programming. The Springer International Series in Engineering and Computer Science*. Springer, Boston; 2003. Pp. 101–116. https://doi.org/10.1007/978-1-4615-0377-4_6

61. Xiang W.-L., Li Y.-Z., He R.-C., An M.-Q. Artificial bee colony algorithm with a pure crossover operation for binary optimization. *Computers & Industrial Engineering*. 2021;152:107011. https://doi.org/10.1016/j.cie.2020.107011

Information about the authors

Huan-Nam Bui – Dr.-Ing, Professor, Department of Surface Mining, Mining Faculty, Hanoi University of Mining and Geology; Research Group of Innovations for Sustainable and Responsible Mining (ISRM), Hanoi University of Mining and Geology; ORCID 0000-0001-5953-4902, Scopus ID 36892679300; e-mail buixuannam@humg.edu.vn

Hoang Nguyen – Department of Surface Mining, Mining Faculty, Hanoi University of Mining and Geology; Research Group of Innovations for Sustainable and Responsible Mining (ISRM), Hanoi University of Mining and Geology; ORCID 0000-0001-6122-8314, Scopus ID 57209589544; e-mail nguyenhoang@humg.edu.vn

Qui-Thao Le – Department of Surface Mining, Mining Faculty, Hanoi University of Mining and Geology; Research Group of Innovations for Sustainable and Responsible Mining (ISRM), Hanoi University of Mining and Geology; Scopus ID 57209279515; e-mail lequithao@humg.edu.vn

Tuan-Ngoc Le – Deputy General Director, Vinacomin – Minerals Holding Corporation, Hanoi, Vietnam; e-mail letuanngoc@vimico.vn

Received 17.01.2022
Revised 22.02.2022
Accepted 25.05.2022

SAFETY IN MINING AND PROCESSING INDUSTRY AND ENVIRONMENTAL PROTECTION

Research article

https://doi.org/10.17073/2500-0632-2022-2-126-136

Rock burst forecasting technique and selecting a safe coal face advance direction

S.S. Kobylkin ✉, **A.S. Pugach**

National University of Science and Technology "MISiS" (NUST MISiS), Moscow, Russian Federation

✉ *kobylkin.s@misis.ru*

Abstract

Mine planning involves selecting an optimal mine layout. At the same time key factors, including those influencing mining safety, should be comprehensively taken into account. A developed rock burst forecasting technique taking into account mine workings of an extraction area and a mine goaf enables determining the safe direction of a coal face. The proposed technique also takes into account all faulting/joint systems, occurring beyond a mine field. The distribution of specific potential energy in an intact rock mass is proposed to be used as the basis of the input data required for rock burst forecasting. The forecast is carried out via estimating the Lode-Nadai coefficient at different directions of coal face advancing. The stress (intensity) coefficient is proposed to be used as a criterion in order to determine a safe direction. We determined the safety criterion is equal to 10 in the Komsomolskaya Mine conditions. Besides, the safest direction of a coal face advance to mitigate the risks of rock burst was determined for this mine. The direction between 138° and 128° counter-clockwise from the north direction was identified to be the safest for the Komsomolskaya Mine conditions for any values of deformation modulus and Poisson's ratio.

Keywords

coal mine, safety, rock burst, forecast, extraction area, algorithm

For citation

Kobylkin S.S., Pugach A.S. Rock burst forecasting technique and selecting a safe coal face advance direction. *Mining Science and Technology* (*Russia*). 2022;7(2):126–136. https://doi.org/10.17073/2500-0632-2022-2-126-136

ТЕХНОЛОГИЧЕСКАЯ БЕЗОПАСНОСТЬ В МИНЕРАЛЬНО-СЫРЬЕВОМ КОМПЛЕКСЕ И ОХРАНА ОКРУЖАЮЩЕЙ СРЕДЫ

Научная статья

Методика прогноза горных ударов и выбора безопасного направления фронта очистных работ

С.С. Кобылкин ✉, **А.С. Пугач**

Национальный исследовательский технологический университет «МИСиС» (НИТУ МИСиС), г. Москва, Российская Федерация

✉ *kobylkin.s@misis.ru*

Аннотация

Планирование горных работ связано с выбором оптимальных решений по раскройке шахтного поля. При этом необходимо комплексно учитывать основные факторы, влияющие в том числе на безопасность ведения горных работ. Разработанная методика прогноза горных ударов в процессе ведения горных работ, учитывающая горные выработки выемочного участка и выработанное пространство, позволяет определить безопасное направление фронта очистных работ. Предлагаемая методика учитывает также все геологические нарушения, которые находятся и за пределами шахтного поля. В основе исходных данных, необходимых для осуществления прогноза горных ударов, предлагается использовать распределение удельной потенциальной энергии в нетронутом массиве. Прогноз осуществляется путем оценки параметра Надаи–Лоде (Lode–Nadai coefficient) при различных направлениях движения фронта очистных работ. Для определения безопасного направления предлагается в качестве критерия использовать коэффициент напряженности. В статье определен критерий безопасности для условий ш. Комсомольская, равный 10. Также для данной шахты было определено направление фронта очистных работ, при котором существенно снижаются риски проявления горных ударов. Наиболее безопасным для условий ш. Комсомольская является вариант направления между 138° и 128° против часовой стрелки от Северного направления для любых реализаций модуля деформации и коэффициента Пуассона.

Ключевые слова

угольная шахта, безопасность, горный удар, прогноз, выемочный участок, алгоритм

Для цитирования

Kobylkin S.S., Pugach A.S. Rock burst forecasting technique and selecting a safe coal face advance direction. *Mining Science and Technology* (*Russia*). 2022;7(2):126–136. https://doi.org/10.17073/2500-0632-2022-2-126-136

Introduction

Mining safety assurance is a complex, system task to be solved long before drivage. At the same time different factors should be taken into account at different stages of a mining enterprise existence. Geotechnical safety is governed by a large number of influencing variables: physical properties of a rock mass, mining depth, occurrence of geological faults and their influence on stressed state of a coal seam [1, 2], structural features of a rock mass [3, 4, 5], influence of tectonic forces [6], etc. There are complex approaches to forecasting hazardous zones on the basis of assessing the stability (faulting) of a rock mass[1]. A mining area (mining allotment or mine field) is selected in locations with the least amount of major geological faults. In coal mining the influence of such faults located outside a mine field is not controlled. We propose a rock burst forecasting technique taking into account all adjacent geological faults with the aim of increasing mining safety. It is applicable in mining conditions when at least one geodynamic event has been recorded. The given technique allows determining a safe direction of coal face advance.

Input data for rock burst forecasting

One of the most attractive techniques for forecasting rock bursts is the evaluation of events based on the concept of seismicity of events [7]. According to the documents [8, 9] regulating the operation of seismic stations, 4 energy levels are distinguished. Energy level II corresponds to fracturing (disturbance) in the near-contour rock mass enclosing mine workings and is defined at 3500 J and more. Energy level III corresponds to the impact of coal-face work and is defined at 6000 J and more. Introducing such energy levels is based on selection of a safety criterion and recommendations of seismic services. This study considers energy levels II and III, while the others are excluded because rock burst manifestation hazard is assessed starting from energy level 3500 J and more. Energy levels II and III serve as threshold values for manifestation of minimum disturbance (fracturing), because an impact of coal-face work when extracting coal will take place in any case. Thus, we determine the boundary zone between the zone of fracturing in the near-contour rock mass enclosing mine workings and the coal-face impact zone. Application of energy level IV will overestimate the safety criterion value. In this case, one can note a general trend in the distribution of energies (determined based on seismic station data), calculated for an intact coal seam in accordance with a mathematical model developed by the authors. The mathematical model is based on the concepts of the nature of tectonic forces [6], the models of rock mass behavior [10, 11, 12], the results of laboratory sample testing [13] and the samples physical properties [14]. The authors [15] note that the accuracy of describing the behavior of a rock mass depends on the correct selection of a model. We summarized these approaches and integrated them into a single forecasting technique. The seismic energy values obtained for the Komsomolskaya Mine (Fig. 1, *a*) were compared with the calculated values of specific potential energy in an intact coal seam (Fig. 1, *b*).

The resulting distribution of specific potential energy in an intact rock mass is the basis of the inputs required for rock burst forecasting. In addition, the inputs should contain a mine plan.

Technique for determining a safe direction of a coal face advance

When solving the problem of rock burst forecasting at different values of deformation modulus E_{ur} and Poisson's ratio ν for an intact rock mass in a faulting (disturbance) zone, assessment of stress-strain state of a coal seam should be performed. Rock physical properties for the model are determined in accordance with the technical documentation of a mine and [16]. The most characteristic options of tasks are selected in accordance with a stress map. At the first stage, different tasks with different set of the values of deformation modulus and Poisson's ratio are solved, and the specific potential energy is determined. Then the solutions with the greatest qualitative differences are selected. For the example under consideration (Komsomolskaya Mine) the following options correspond to the characteristic solutions: 1) E_{ur} = 1,489 MPa, ν = 0.211; 2) E_{ur} = 1,335 MPa, ν = 0.181; 3) E_{ur} = 1,037 MPa, ν = 0.203; 4) E_{ur} = 1,305 MPa, ν = 0.232; 5) E_{ur} = 1,296 MPa, ν = 0.162; 6) E_{ur} = 1,395 MPa, ν = 0.224; 7) E_{ur} = 1,524 MPa, ν = 0.179; 8) E_{ur} = 1,036 MPa, ν = 0.160; 9) E_{ur} = 1,331 MPa, ν = 0.171; 10) E_{ur} = 1,433 MPa, ν = 0.174.

Then the considered extraction area comprising a set of mine workings (a coal face and adjoining drifts, as well as mined-out space) was added into the simulation model. For each set of the parameters, we estimated the Lode–Nadai coefficient to compare with that of an intact coal seam (see Fig. 1, *b*). Fig. 2 shows a map of the Lode–Nadai coefficient values depending on the location of an extraction area for the 1st direction of coal face advancing (218° from the north direction). In the model plane, the direction change in increments of 10° was selected (from the initial position of 218° clockwise from the north direction). At the Komsomolskaya Mine, the direction of coal face advance is selected depending on the mine field boundaries (in a direction orthogonal to the boundaries). The boundaries, as a rule, correspond to the geometry of faults/joint systems. A coal face in this case falls on the 5–6th directions in accordance with the chosen designations (168–158° clockwise from the north direction).

[1] Forecasting possible faulting zones. 2017. URL: https://www.micromine.ru/possible-zones-of-tectonic-fault-prediction/ (accessed date: 31.12.2021)

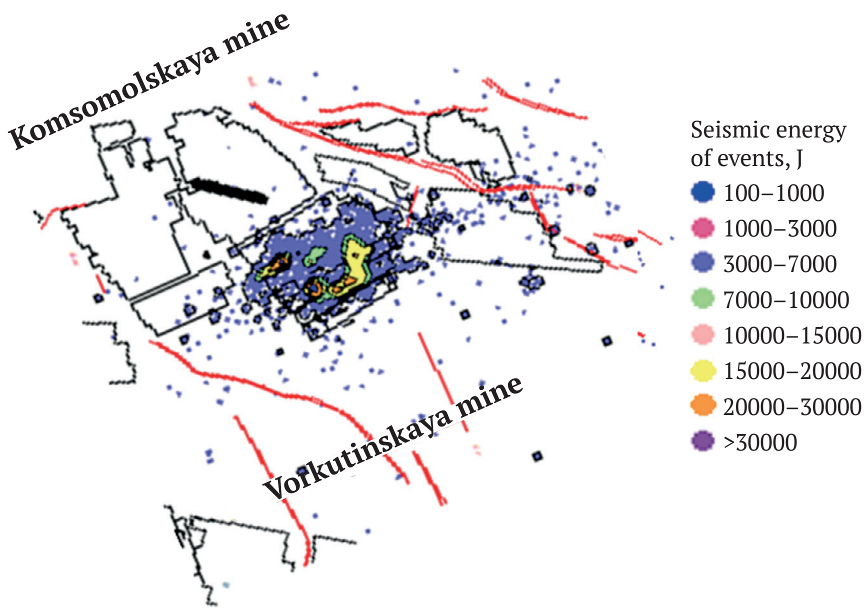

a

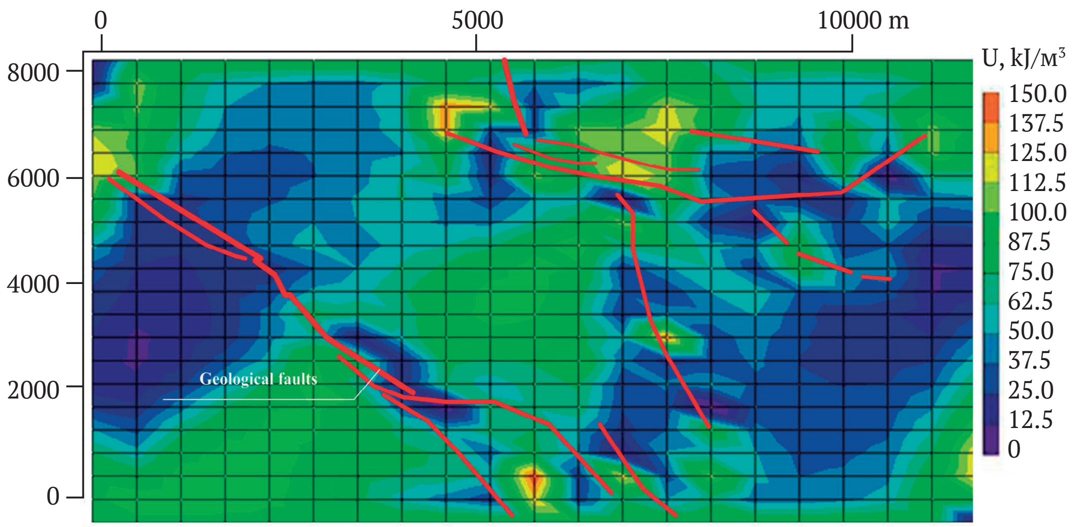

b

Fig. 1. Data of seismic observations (*a*); map of specific potential energy in intact rock mass (*b*)

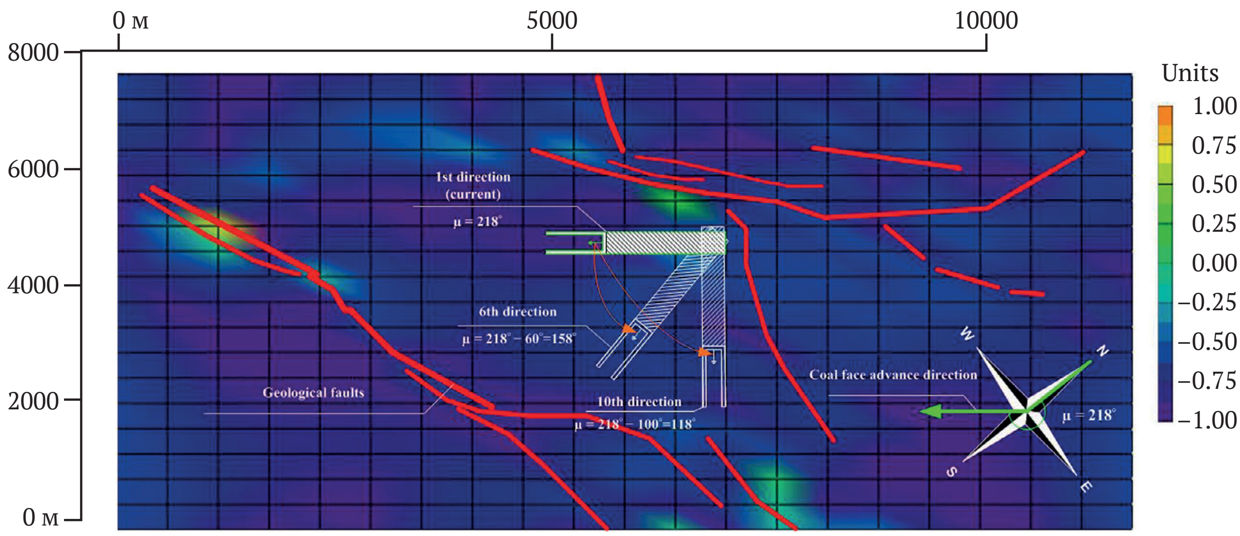

Fig. 2. Map of Nadai-Lode coefficient values at the 1st direction of coal face advancing

eISSN 2500-0632
https://mst.misis.ru/

Fig. 4 shows the distribution of maximum and minimum principal stresses along a coal face advance direction (Fig. 5) inward the rock mass at different combinations of the physical properties.

Interpreting graphs in Fig. 4 via the representation of specific potential energy allows determining the gradient between the maximum principal stress and the stress on the boundary of the simulated coal face. The sandstone rock pressure is represented in the form of gravity per unit area (a stress equivalent). On this basis specific energy is calculated as follows:

$$E_{grav\_sandst} = \frac{(\rho_{sandst}\, gH)^2}{2E_{sandst}}, \qquad (1)$$

where ρ_{sandst} is the sandstone density, kg/m^3; g is the gravitational acceleration, m/s^2; H is a depth of coal extraction, m; E_{sandst} is the sandstone modulus of deformation, MPa.

The ratio of the specific activation energy W_a, representing the gradient from the maximum or minimum stresses (two curve behavior types in Fig. 4) towards the free surface, to the specific potential energy of the overlying rocks weight E, is a value characterizing the degree of rock burst hazard used when selecting an option of coal face advance direction in the framework of designing optimal mine layout. The obtained value should be compared with the critical value corresponding to the safe specific potential energy. This ratio can be called as a stress coefficient K.

Depending on the maximum principal stresses observed at a coal face (local maximums or local minimums) we present two options of calculations.

The formulas describing a local stress maximum on the boundary of a simulated coal face are presented below. The model solutions with E_{ur} = 1,036 MPa, ν = 0.160 (Fig. 6) correspond to this case.

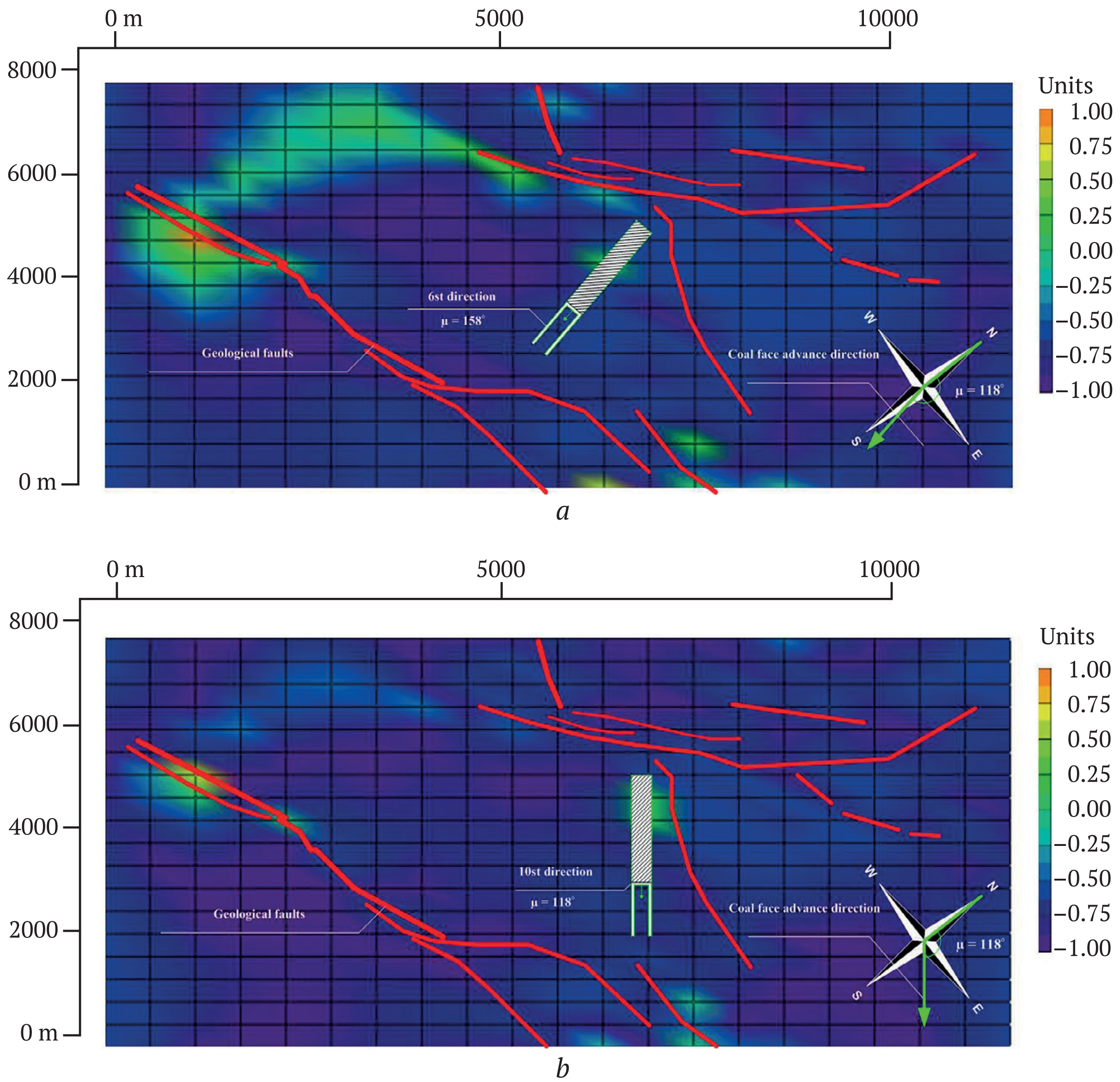

Fig. 3. Map of Nadai-Lode coefficient values at different positions of a mine working: (*a*) the 6th direction (158°) [current], (*b*) the 10th direction (118°)

Stress coefficient at the local maximums of stresses observed on the boundary of the simulated coal face

$$K_1 = \frac{W_{a_1}}{E_{grav\_sandst}}. \quad (2)$$

Specific potential activation energy at local maximums of stresses observed on the boundary of the simulated coal face

$$W_{a_1} = 0.5\left(\frac{[\sigma_1^{\text{max face}} - \sigma_3^{\text{max face}}]^2}{E_i} - \frac{[\sigma_1^{\text{min}} - \sigma_3^{\text{min}}]^2}{E_i}\right); \quad (3)$$

stress gradient at local maximums of stresses observed on the boundary of the simulated coal face

$$grad_1 = \frac{\sigma_1^{\text{min}} - \sigma_1^{\text{max face}}}{r^{\text{min}}}, \quad (4)$$

where $\sigma^{\text{max face}}$ are the local maximums of stresses on the boundary of the simulated coal face, MPa; σ^{min} are the local minimums of stress inward the rock mass, MPa; E_i is the calculated modulus of deformation at the i-th point of the rock mass corresponding to maximums/maximums of stresses, MPa; r^{min} is the distance from the

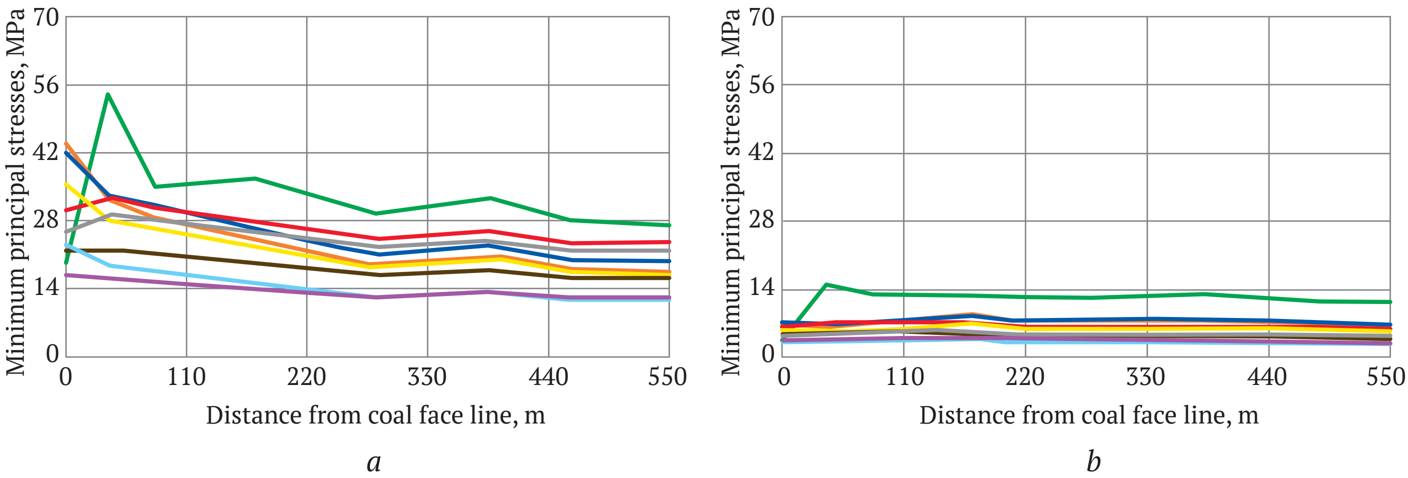

Fig. 4. Distribution of principal stresses along a coal face advance direction inward the rock mass for the 1st direction: *a* – for the maximum principal stresses σ_1; *b* – for the minimum principal stresses σ_3

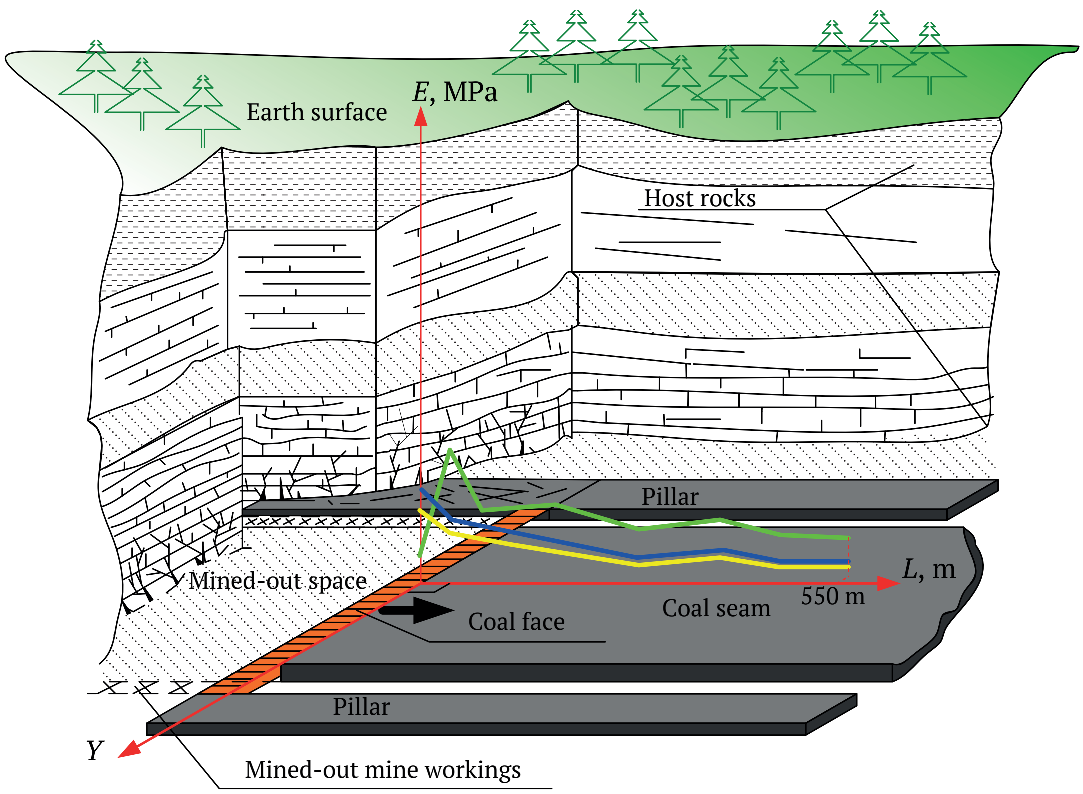

Fig. 5. Schematic diagram for determining the distribution of maximum and minimum principal stresses along a coal face advance direction

boundary of the simulated coal face to a local minimum of stresses, m.

Table 1 presents the values used for the distribution determination.

The value $r = 0$ is the boundary of the simulated coal face (the face plane). For the graph of the presented form, we determined $\sigma_1^{\text{max face}} = 43.86$ MPa, $\sigma_1^{\min} = 18.41$ MPa, $r^{\min} = 280$ m and made calculations according to formulas (2)–(4).

Then, we considered the second case, when local minimums occur on the boundary of the simulated face. The model solutions with $E_{ur} = 1{,}037$ MPa, $\nu = 0.203$ correspond to this case (Fig. 7).

Stress coefficient at the local minimums of stress observed on the boundary of the simulated coal face is equal to:

$$K_2 = \frac{W_{a_2}}{E_{grav\_sandst}}. \quad (5)$$

Specific potential activation energy at the local maximums of stresses observed on the boundary of the simulated coal face is equal to:

$$W_{a_2} = 0.5\left(\frac{[\sigma_1^{\max} - \sigma_3^{\max}]^2}{E_i} - \frac{[\sigma_1^{\text{min face}} - \sigma_3^{\text{min face}}]^2}{E_i}\right); \quad (6)$$

stress gradient at the local maximums of stresses observed on the boundary of the simulated coal face is equal to:

$$grad_2 = \frac{\sigma_1^{\max} - \sigma_1^{\text{min face}}}{r^{\max}}, \quad (7)$$

where $\sigma^{\text{min face}}$ are the local minimums of stresses on the boundary of the simulated coal face, MPa; $\sigma^{\max}$ are the local maximums of stress inward the rock mass, MPa; E_i is the calculated modulus of deformation at the i-th point of the rock mass corresponding to maximums/maximums of stresses, MPa; $r^{\max}$ is the distance from the boundary of the simulated coal face to a local maximum of stresses, m.

Table 1

Data for plotting maximum principal stresses as a function of the distance from the boundary of the simulated coal face (inward the rock mass) (for E_{ur} = 1,036 MPa, ν = 0.160)

Parameters	Values									
Maximum principal stresses σ_1, MPa	43.86	32.38	28.51	23.53	21.78	18.41	20.26	17.62	16.96	16.67
The distance from the boundary of the simulated coal face (inward the rock mass) r, m	0	38	79	172	212	280	387	459	564	649

Table 2

Data for plotting maximum principal stresses as a function of the distance from the boundary of the simulated coal face (inward the rock mass) (for E_{ur} = 1,037 MPa, ν = 0.203)

Parameters	Values									
Maximum principal stresses σ_1, MPa	20.97	54.54	35.14	36.92	34.1	29.67	32.85	28.39	26.94	25.98
The distance from the boundary of the simulated coal face (inward the rock mass) r, m	0	38	79	172	212	280	387	459	564	649

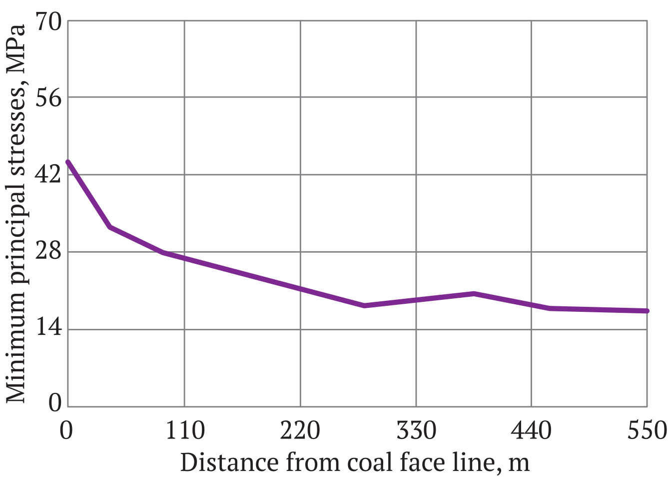

Fig. 6. Distribution of the principal stresses along a coal face advance direction inward the rock mass by the example of the 1st direction for E_{ur} = 1,036 MPa, ν = 0.160

Fig. 7. Distribution of the principal stresses along the coal face advance direction inward the rock mass by the example of the 1st direction for E_{ur} = 1,037 MPa, ν = 0.203

Table 2 presents the values used for the distribution determination for this option.

Then $\sigma_1^{\text{min face}}$ = 20.97 MPa, σ_1^{max} = 54.54 MPa, r^{max} = 38 m were inserted into formulas (5)–(7), and calculations were made.

Referring graphs in Fig. 4 to the first or second options, we made the corresponding calculations and obtained 10 values of activation energy for the maximum principal stresses and 10 values of stress gradient.

Similarly, the minimum principal stresses were determined for the graphs of each considered coal face advance direction (angle μ in Fig. 2). Within a direction, we obtained 10 values of activation energy for the maximum principal stresses and 10 values of stress gradient. Stress coefficients K_1 and K_2 were calculated for each option. Further K_1 and K_2 were represented as one characteristic K. We performed the above-described calculations for each of the directions presented in Fig. 2. The results were summarized and integrated into a single matrix. This matrix of the values was used to draw an isogram (Fig. 8).

The isogram is a surface of the stress coefficients. In the matrix's rows, the gradient values determined by formulas (5) and (7) depending on the type of distribution are presented; the columns present the directions of the simulated coal face advance. The matrix included the vectors of stress coefficients for each direction, calculated by analogy with the example shown above.

To assess the safety of a selected coal face advance direction, we proposed using a safety criterion, a comparison of safe energy (dimensionless safety criterion [K]). The criterion is determined on the basis of the comparison of data from the seismic station and the ratio of the calculated specific potential activation energy to the specific potential energy of gravity of the overlying rocks E_{grav_sandst} (2) and (3), i.e. [K] is compared with K_{a1} and K_{a2}.

Taking into account the data from Fig. 1 and the inputs on energy levels, we calculated that the boundaries of the II energy level (see Fig. 1, a) were characterized by the specific potential energy in an intact coal seam of 60 kJ/m³ (see Fig. 1, *b*), while the boundaries of the III energy level (see Fig. 1, *a*), by that of 112.5 kJ/m³ (see Fig. 1, *b*).

Let's substitute these values into the numerator in formula (1) as the activation energy. The specific potential energy of gravity remains unchanged. The square brackets below denote that the value is a criterion.

E_{grav_sandst} = 18 kJ/m³.

At W_a = 60 kJ/m³ $[K]_{intact}^{\text{II}}$ = 3.333.

At W_a = 112.5 kJ/m³ $[K]_{intact}^{\text{III}}$ = 6.25.

$[K]_{intact}$ is a safe value corresponding to an intact coal seam. The upper index denotes a reference to the corresponding energy level.

Mining-induced stresses in a rock mass exceed an intact rock strength due to the action of complicating factors. For the transition to the criterion in the conditions of coal extraction we used the fact that in practice relatively safe coal faces at deep levels can be referred to the III stability category according to the studies

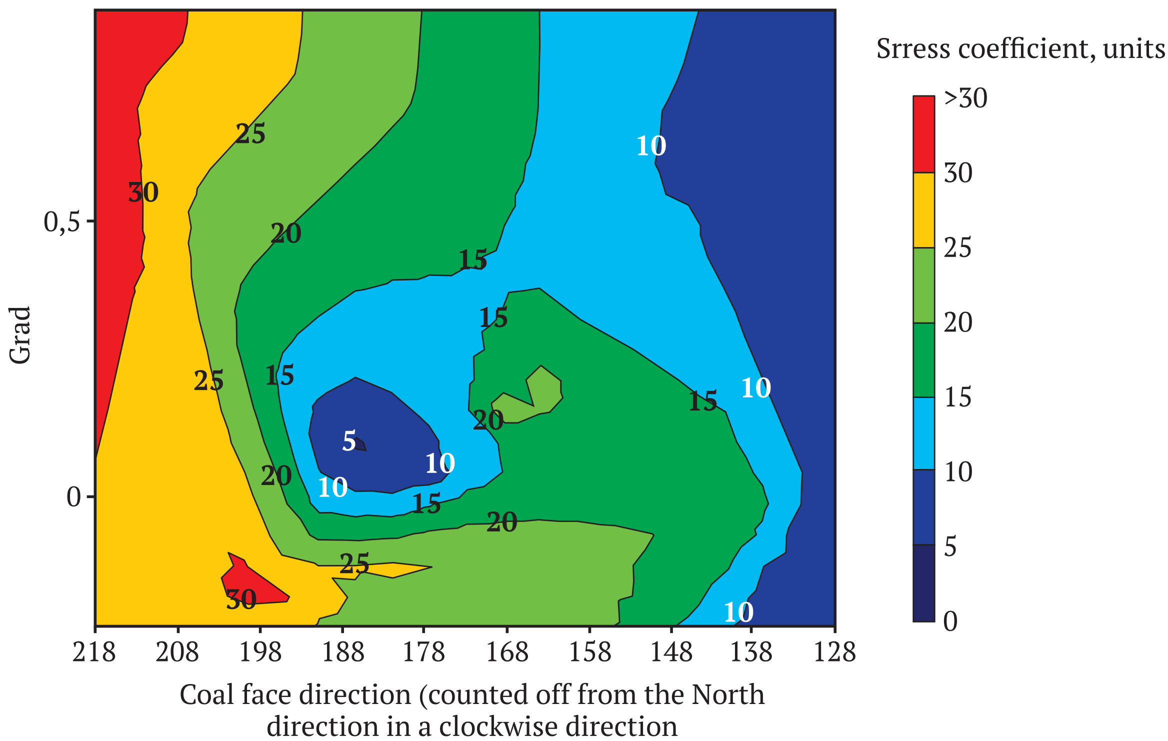

Fig. 8. Isogram of stress coefficient depending on the stress gradient and coal face advance direction

described in [17, 18]. Stability category III is characterized by stabilization of deformation growth after 1–2 weeks. The coefficient taking into account the excess of the actual stresses over the calculated rock strength amounts to 1.61–3.0. Taking into account this coefficient, $[K]_{intact}^{II}$ varies in the range of 5.37–10, while $[K]_{intact}^{III}$ ranges 10.06–18.75. This principle is based on analogy with the recommendations on introducing a coal strength variability factor, presented in normative documentation and Safety rules instructions[2]. The validity of such a transition from an intact rock mass to unstable (disturbed) rocks finds confirmation in laboratory tests conducted by researchers [19].

When changing from an intact rock mass to rocks of stability category III as relatively stable and determining the boundary zone between the disturbed zone in the near-contour rock mass enclosing mine workings and the coal face impact zone we adopted safety criterion $[K] = 10$ at the coal face working stage.

According to Fig. 6, in the conditions of the Komsomolskaya Mine, the safest option is the coal face advance direction between 138 and 128° counter-clockwise from the north direction for any values of deformation modulus and Poisson's ratio. The direction around 188° is also characterized by a lower stress coefficient, but not at all values of deformation modulus and Poisson's ratio. Substantiating the parameters of safe coal extraction at deep levels should be guided by this principle. Insignificant deviations of the angle lead to redistribution of stresses in the face plane and may cause accidents or incidents.

Algorithm for rock bursts forecasting in conditions of coal face work

Based on the above, we concluded that at the stage of a mine design an important prerequisite is selecting safe direction of a coal face advance. In coal seams disturbed by faults, even prior mining, unfavorable conditions arise due to accumulation of potential energy in a rock mass. The excesses of this energy manifest themselves as rock bursts [20, 14]. In coal mines energy manifestations in a rock mass are recorded by sensors sending the data to seismic stations. These manifestations are recorded as events. The above-described example of rock burst forecasting and selecting a safe direction of coal face advance can be written as an algorithm (Fig. 9).

The procedure of the algorithm application is as follows:

1. At the first stage, required data are collected (locations of rock burst manifestation, geological documents, and physical properties of rocks).
2. Then a 2D model is built in a vertical cross-section, taking into account the intersection of the maximum number of faults. The possibility of applying the first assumption (not taking into account the vertical component of a rock pressure) should be confirmed.
3. In addition, the components of rock pressure (horizontal stresses taking into account a side pressure coefficient) are determined in the vertical cross-section. Thus we obtain the boundary conditions for further simulation.
4. Then, a 2D model is built in a horizontal cross-section. Then, the directions of tectonic forces are determined and hazardous zones are identified taking into account the ratio of horizontal stresses to vertical ones. The construction of the 2D model in the horizontal cross-section is performed with the assumption that the extracted coal seam dip angle, height differences, local disturbances (seam crumple, bifurcation, plicative dislocations) are not considered. These seam features are taken into account in a more detailed local forecasting.
5. Further, the probability density function of the number of stress materializations depending on the set of physical property variations in the system of set values “Deformation modulus – Poisson’s ratio” (200 sets) is determined.
6. The behavior pattern of an intact coal seam is calculated using the Lode–Nadai coefficient: generalized tension, compression, and shear. The subsequent selection of a coal face advance direction should be based on the fact that generalized compression should be observed in the potential locations of a coal face construction. A significant part of mining areas meets to generalized compression conditions [20].
7. After the analysis of stresses in an intact rock mass the analysis of stresses in the mining-disturbed rock mass is performed taking into account the mine workings at changing directions of their axes in increments of 10°. The Lode–Nadai coefficient is also calculated in this case in order to identify the pattern of stress redistribution.
8. Then the safety criterion is determined. The safety criterion value corresponding to the most favorable conditions is selected on the basis of comparison of the data of seismic station and the specific potential energy distribution. The value of factor of safety is taken with the correction for a coal seam disturbance due to formation of weakening zones (adjacent to mine workings) and compared with the resulting stress coefficient. Stress coefficient is a value depending on the stress gradient along the normal to a face line.

[2] Industrial safety federal norms and rules "Instruction for dynamic effects forecasting and rock mass monitoring in the course of coal deposit development”. Order #515 of the Federal Service for Ecological, Technological, and Nuclear Supervision of December 10, 2020. Accessed in the Electronic Fund of Legal and Regulatory Documents. URL: https://docs.cntd.ru/document/573264171

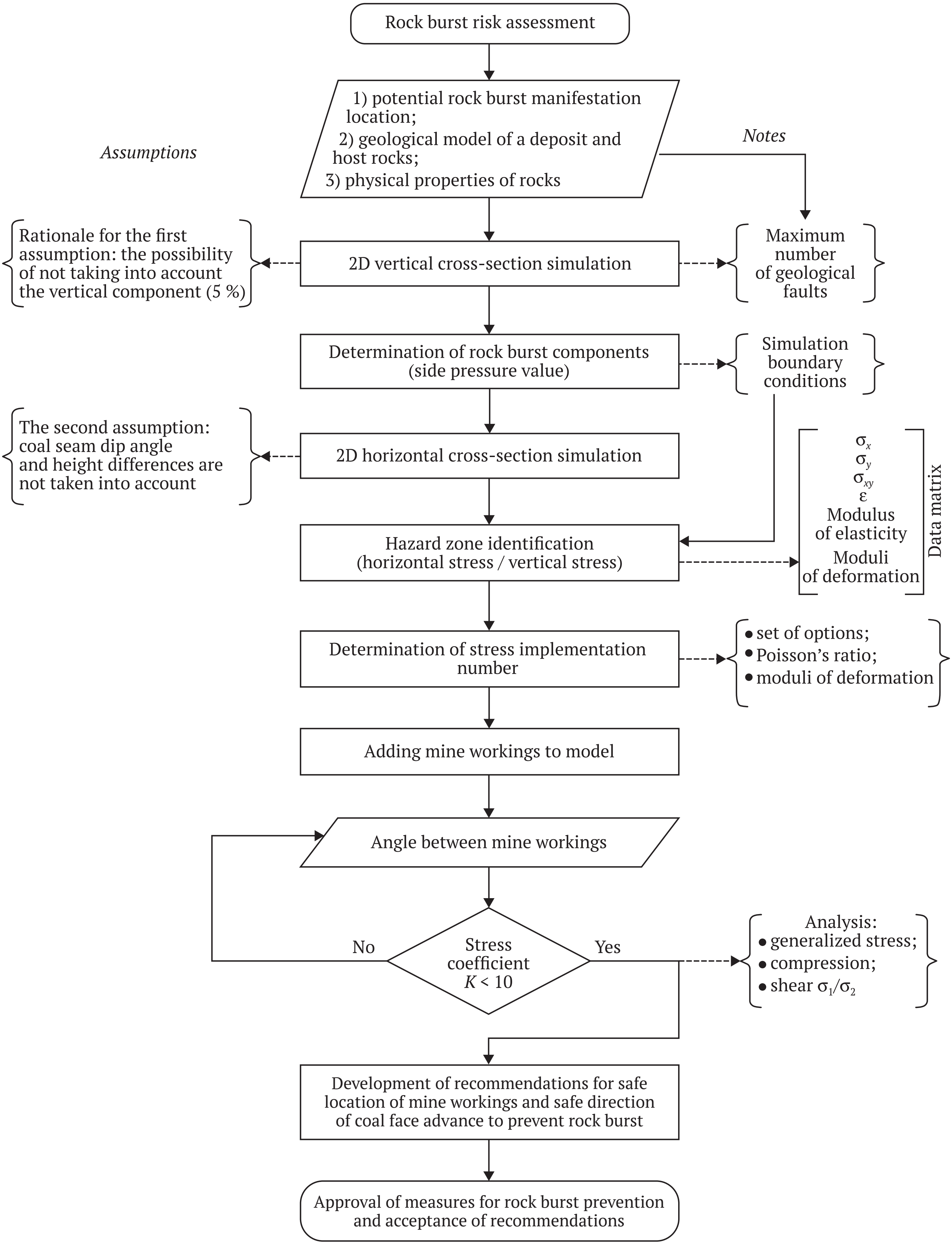

Рис. 9. Алгоритм регионального текущего прогноза горных ударов

9. If the stress coefficient is less than 10, mining is safer in terms of rock burst risk. If the criterion is more than 10, it is recommended to develop additional measures to ensure control and safety of mining.

The presented algorithm is universal for all mining enterprises. Its application is possible at any mine or in any design organization. Special software can be additionally used for its implementation. When using this algorithm for the Komsomolskaya Mine conditions, Plaxis and MathCad software was used.

Conclusion

The developed techniques for rock burst forecasting make it possible to take into account geological faults outside a mine field and the effect of mine workings with their mutual influence, as well as that of a mined-out space.

To estimate the hazard of rock bursts, a criterion, stress coefficient, was introduced. The criterion is determined on the basis of comparison of data from a seismic station and the ratio of the calculated specific potential activation energy to the specific potential energy of gravity of the overlying rocks. The forecast is carried out via estimating the Lode-Nadai coefficient at different directions of coal face advancing.

To implement the technique, an algorithm for current regional rock burst forecasting at coal mines has been developed and tested in the conditions of the Komsomolskaya Mine.

The developed solutions make it possible to improve mining safety.

According to this algorithm, which is based on the developed technique of rock burst forecasting in the conditions of the Komsomolskaya Mine, the safety criterion value was determined to be 10. Besides, the safest direction of a coal face advance to mitigate the risks of rock burst was determined for this mine. The direction between 138° and 128° counter-clockwise from the North direction was identified to be the safest for the Komsomolskaya mine conditions for any values of deformation modulus and Poisson's ratio.

References

1. Malinnikova O., Uchaev D., Uchaev D., Malinnikov V. The study of coal tectonic disturbance using multifractal analysis of coal specimen images obtained by means of scanning electron microscopy. In: *E3S Web of Conferences*. *1st International Scientific Conference "Problems in Geomechanics of Highly Compressed Rock and Rock Massifs" (GHCRRM 2019)*. 2019;129:01017. https://doi.org/10.1051/e3sconf/201912901017

3. Tianwei L., Hongwei Z., Sheng L., Jun H., Weihua S., Batugin A.S., Guoshui T. Numerical study on 4-1 coal seam of xiaoming mine in ascending mining. *Scientific World Journal*. 2015. https://doi.org/10.1155/2015/516095

4. Lan T., Sun J., Batugin A.S., Jia W., Zhang Z. Dynamic characteristics of fault structure and its controlling impact on rock burst in mines. *Shock and Vibration*. 2021;2021:7954876. https://doi.org/10.1155/2021/7954876

5. Lan T., Zhang H., Li S., Batugina I., Batugin A. Application and development of the method of geodynamic zoning according to geodynamic hazard forecasting at coal mines in China. In: *IOP Conference Series: Earth and Environmental Science*. *World Multidisciplinary Earth Sciences Symposium (WMESS 2018)*. 3–7 September 2018, Prague, Czech Republic. 2019;221(1):012088. https://doi.org/10.1088/1755-1315/221/1/012088

6. Markov G.A. *Tectonic stresses and rock pressure in the Khibiny massif mines*. Leningrad: Nauka Publ.; 1977. 213 p. (In Russ.)

7. Lovchikov A.V. A new concept of the mechanism of rock-tectonic bursts and other dynamic phenomena in conditions of ore deposits. *Mining Science and Technology* (*Russia*). 2020;5(1):30–38. https://doi.org/10.17073/2500-0632-2020-1-30-38

8. Yakovlev D.V., Tsirel S.V., Mulev S.N. Regularities of development and technique of rapid assessment of technogenic seismic activity at mining enterprises and in mining regions. *Fiziko-Texhnicheskiye Problemy Razrabbotki Poleznykh Iskopaemykh*. 2016;(2):34–47. (In Russ.) URL: https://www.sibran.ru/upload/iblock/ca1/ca15451a9d2410129c5af3babe2bafef.pdf

9. Yakovlev D.V., Isaev Yu.S., Mulev S.N. et al. "GeoInfoTransSistem (GITS) hardware-software complex in geodynamic and environmental monitoring systems. In: *International Conference "Mining Geophysics"*. June 22–25, 1998. St. Petersburg: VNIMI Publ.; 1998 p. (In Russ.)

10. Kovtanyuk L.V., Panchemko G.L. On compression of a heavy compresible layer of an elastoplastic or elastoviscoplastic. *Medium. Mechanics of Solids*. 2017;52(6):653–662. https://doi.org/10.3103/S002565441706005X

11. Kondner R.L., Zelasko J.S. A hyperbolic stress strain formulation for sands. In: *Proceedings of the 2nd Pan American Conference on Soil Mechanics and Foundation Engineering*. Sao Paulo, Brazil. 1963;1:289–324.

12. Duncan J.M., Chang C.-Y. Nonlinear analysis of stress and strain in soil. *Journal of the Soil Mechanics and Foundation Division*. 1970;96(5):1629–1653.

13. Janbu J. Soil Compressibility as determined by oedometer and triaxial tests. In: *Proceedings of European Conference on Soil Mechanics and Foundation Engineering (ECSMFE)*. Wiesbaden, Germany. 1963;1:9–25.

14. Von Soos P. Properties of soil and rock. In: *Grundbau-Taschenbuch*. Part 4. Ed. 4. Berlin: Ernst & Sohn; 1990. (In German)

15. Ustinov D.V. Impact of the enclosing massif model selection over the results of subway tunnels excavation modelling. *Geotechnics*. 2018;10(5–6):34–50. (In Russ.)

16. Melnikova N.V., Rzhevskii V.V., Protodiakonov M.M. (eds.) *Handbook (cadastre) of rock physical properties*. Moscow: Nedra Publ.; 1975. 279 p. (In Russ.)

17. Trushko O.V. Geodynamic stability assessment for mine workings in deep mines. *Science, Technology and Education*. 2015;(2):58–62. (In Russ.)

18. Trushko O.V., Petrov D.N., Streletsky A.V. Provision of durability of mine workings. *Izvestiya Vysshikh Uchebnykh Zavedenii. Gornyi Zhurnal*. 2012;(2):51–55. (In Russ.)

19. Basov V.V. The study of geomechanical condition of unstable rocks in the vicinity of mine working junctions. *Mining Science and Technology* (*Russia*). 2019;4(1):23–30. https://doi.org/10.17073/2500-0632-2019-1-23-30

20. Kurlenya M.V., Seryakov V.M., Yeremenko A.A. *Technogenic geotechnical stress fields*. Novosibirsk: Nauka Publ.; 2005. 264 p.

Information about the authors

Sergey S. Kobylkin – Dr. Sci. (Eng.), Professor of the Department of Safety and Ecology of Mining, Mining Institute, National University of Science and Technology "MISiS" (NUST MISiS), Moscow, Russian Federation; ORCID 0000-0002-2626-208X, Scopus ID 56209222200; e-mail kobylkin.s@misis.ru

Alexander S. Pugach – Senior Lecturer of the Department of Physical Processes of Mining and Geo-control, Mining Institute, National University of Science and Technology "MISiS" (NUST MISiS), Moscow, Russian Federation; ORCID 0000-0002-9353-4567; e-mail as.pugach@misis.ru, Alpugach@mail.ru

Received 13.03.2022
Revised 08.04.2022
Accepted 27.05.2022

MINING ROCK PROPERTIES. ROCK MECHANICS AND GEOPHYSICS

Research article

https://doi.org/10.17073/2500-0632-2022-2-137-149

Controlling blast energy parameters to ensure intensive open-pit rock fragmentation

U.F. Nasirov[1], Sh.Sh. Zairov[2] ✉, M.R. Mekhmonov[2], A.U. Fatkhiddinov[3]

[1] *National University of Science and Technology "MISiS" (Almalyk Branch), Almalyk, Republic of Uzbekistan*

[2] *Navoi State Mining-Technological University, Navoi, Republic of Uzbekistan*

[3] *Islam Karimov Tashkent State Technical University, Tashkent, Republic of Uzbekistan*

✉ *sher-z@mail.ru*

Abstract

Controlling blast action, in order to increase its energy efficiency in a production blasthole is quite an important issue. This is because it enables the formation of broken rock mass with preset coarseness parameters. Increasing the blast pressure and the time of the blast impact on a rock mass is traditionally recommended as one of the ways to improve the blast action on the rock mass, thus reducing the oversize yield in open pits. One device which enables this approach to a certain extent is a turbulator. The turbulator is fabricated of aluminum plate twisted in a helical fashion around its longitudinal axis. It is mounted in a production blasthole according to a specially designed scheme. The methodology developed to study the stress and strain state of a rock mass when using a turbulator in a blasthole explosive charge allows the size of radial fracture zone and the radius of rock fragmentation to be defined. A method was developed to initiate blasthole charges in a pit blasting block. It includes drilling blastholes, filling them with explosive, installing downhole blasting caps, and blasting using non-electric initiation system. A blasting block is divided into two equal parts (sections), which in turn contain three series of blastholes for short-delay blasting. Blasthole charges are initiated simultaneously in the two parts of the block based on a trapezoidal blasting pattern, thus ensuring meeting detonation waves. In the first series, instantaneous blasting of blastholes located on both ends of the blasting block and forming a trapezoid (in plan view) is carried out. Then after 42 ms, the second series of blastholes (also forming a trapezoid) is detonated. After another 42 ms, the remaining blastholes are detanoated along the perimeter of the blast block in the third series. Implementation of this design with the effect of turbo-blasting for rock fragmentations by blasthole charges at the Kalmakyr deposit of JSC "Almalyk Mining and Metallurgical Complex" has led to the reduction of consumption of explosives, volume of drilling, secondary fragmentation costs, and increased productivity of excavators and mining safety.

Keywords

mining, open pit, blasting, explosives, rock fragmentation, turbo-blast, turbulator, blasthole charges, initiation, JSC "Almalyk Mining and Metallurgical Complex", JSC "Navoi Mining and Metallurgical Complex", Uzbekistan

Acknowledgments

The research was performed within the framework of the Plan of Applied Research Works of Navoi State Mining Institute on the topics: "Development of the technology for forming stable open pit walls with regard to drilling and blasting operations technique" (Project No. BV-Atekh-2018-37).

For citation

Nasirov U.F., Zairov Sh.Sh., Mekhmonov M.R., Fatkhiddinov A.U. Controlling blast energy parameters to ensure intensive open-pit rock fragmentation. *Mining Science and Technology* (*Russia*). 2022;7(2):137–149. https://doi.org/10.17073/2500-0632-2022-2-137-149

СВОЙСТВА ГОРНЫХ ПОРОД. ГЕОМЕХАНИКА И ГЕОФИЗИКА

Научная статья

Управление параметрами энергии взрыва для обеспечения интенсивного дробления горных пород на карьерах

У.Ф. Насиров[1] SC, **Ш.Ш. Заиров**[2] iD SC ✉, **М.Р. Мехмонов**[2], **А.У. Фатхиддинов**[3]

[1] *Филиал Национального исследовательского технологического университета «МИСиС», г. Алмалык, Республика Узбекистан*

[2] *Навоийский государственный горно-технологический университет, г. Навои, Республика Узбекистан;*

[3] *Ташкентский государственный технический университет им. Ислама Каримова, г. Ташкент, Республика Узбекистан;*

✉ *sher-z@mail.ru*

Аннотация

Управление действием взрыва на основе повышения его энергетической эффективности в технологической скважине является актуальной задачей, так как позволяет обеспечить формирование разрушенной горной массы с заданными параметрами крупности. Одним из направлений повышения эффективности взрывного воздействия на горную породу и снижения выхода негабаритов на карьерах традиционно рекомендуется усиление взрывного давления и увеличение времени воздействия взрыва на массив горных пород. Одним из устройств, использование которого позволяет в определенной степени реализовать этот подход является турбулизатор. Турбулизатор изготавливают из алюминиевой пластины, скрученной винтообразно вокруг продольной оси. Монтаж устройства в взрывной технологической скважине осуществляют по специально разработанной схеме. Разработанная методика исследования напряженно-деформированного состояния горного массива при использовании конструкции турбулизатора в скважинном заряде взрывчатых веществ позволила определить размер зоны радиальных трещин и радиус дробления горных пород. Рекомендуется способ инициирования скважинных зарядов взрывчатых веществ во взрывном блоке карьера, включающий бурение взрывных скважин, заполнение их взрывчатым веществом, установление внутрискважинных капсюлей-детонаторов и взрывание неэлектрической системой инициирования. Взрывной блок разделяется на две равные части, которые в свою очередь содержат три серии скважин для короткозамедленного взрывания. Инициирование скважинных зарядов производится одновременно в двух частях блока в виде трапециевидной схемы взрывания с обеспечением встречи детонационных волн. В первой серии с двух концов взрывного блока производится мгновенное взрывание скважин в виде трапеции. Далее во второй серии через 42 мс взрываются последующие скважины также в виде трапеции. Еще через 42 мс по периметру взрывного блока в третьей серии взрываются оставшиеся скважины. Внедрение конструкции с использованием эффекта турбовзрывания при дроблении горных пород скважинными зарядами на месторождении Кальмакыр АО «Алмалыкский горно-металлургический комбинат» позволило снизить потребность во взрывчатых материалах и уменьшить объёмы бурения, снизить затраты на вторичное дробление, повысить производительность работы экскаваторов и безопасность горных работ.

Ключевые слова

добыча полезных ископаемых, карьер, взрывные работы, взрывчатые вещества, разрушение горных пород, турбовзрыв, турбулизатор, скважинные заряды, инициирование, АО «Алмалыкский горно-металлургический комбинат», АО «Навоийский горно-металлургический комбинат», Узбекистан

Финансирование

Исследование выполнено в рамках плана прикладных научно-исследовательских работ Навоийского государственного горного института на темы: «Разработка технологии отстройки устойчиво-конструктивных бортов карьеров с учетом технологии ведения буровзрывных работ» (проект №БВ-А-тех-2018-37).

Для цитирования

Nasirov U.F., Zairov Sh.Sh., Mekhmonov M.R., Fatkhiddinov A.U. Controlling blast energy parameters to ensure intensive open-pit rock fragmentation. *Mining Science and Technology* (*Russia*). 2022;7(2):137–149. https://doi.org/10.17073/2500-0632-2022-2-137-149

Introduction

There are three main approaches to influencing the mechanical effect and controlling rock fragmentation, among known modern blasting optimization techniques [1, 2]:

1) the development of a rational design of explosive charge for effective rock mass fragmentation;

2) the observance of the principle of energy correspondence between the energy expended on rock fragmentation and the energy concentrated in an explosive charge unit;

3) the development of different blasting techniques.

A review of the current condition of drilling and blasting operations, taking into account the regularities of changing rock mass explosiveness [2-7], showed that drilling and blasting performance in these conditions can be improved. This can be achieved by defining the main regularities of the drilling and the effect of blasting parameters on physical-and-mechanical and mining properties of a rock mass, which change with the development depth, and on rock mass fragmentation performance. Other important factors to be defined include the justification of drilling and blasting parameters when using explosives to provide increased blasting performance and safety; the development of efficient blasting methods to improve rock mass fragmentation quality; the development of an integrated safety system for the production and use of explosives, as well as the development of technical and process solutions aimed at controlling blast action based on experimentally established physical phenomenon of increasing its energy and impulse in a blasthole.

At present time even the use of progressive methods of drilling and blasting does not enable the complete elimination of coarse fractions yield (oversize), as evidenced by the experience of breaking hard and very hard rocks in mining operations [8]. The increase of oversize yield from 2.5 to 5 % was found to lead to a reduction in excavator productivity by 20–30 %, while 20 % oversize yield reduces productivity 2.0–2.5 times [9–11]. Special attention should thus be paid to the solution of problems of improving rock mass fragmentation quality and ensuring decrease in oversize yield.

The traditional technique of blasting at deep levels of open pits has run its course. Therefore, more advanced methods need to be implemented, in order to fully ensure the preset quality of rock mass fragmentation. The current techniques for blasting rock mass fragmentation do not provide uniform fragmentation. This leads to a deterioration in rock mass preparation quality and increases excavation costs. When studying the processes of blasting rock mass fragmentation with the use of blasthole explosive charges, special attention needs to be paid to the physical features of their fragmentation depending on the specific structural and strength properties of a blasted rock mass. The use of turbo-blast phenomenon is the most promising area in creating methods of rock fragmentation with asymmetric spatial distribution of blast energy and its maximum concentration depthward a rock mass to be fragmented.

1. Study of the effect of “turbo-blast” in rock fragmentation with blasthole explosive charges

In order to increase the efficiency of blast action on a rock mass and reduce oversize yield in open pits, it is recommended to increase the action pressure and time by using a turbulator, the effect of which is described in detail in [12]. A turbulator is designed to increase the actual coefficient of utilization of the potential energy of a commercial explosive column charge. This is achieved by means of increasing the rate of secondary chemical reactions of an explosive afterburning in a blasthole after the detonation wave passage, until the detonation products reach the free surface.

The basic design of a turbulator is a plate made of steel or aluminum sheet, twisted helically around its longitudinal axis [12] (Fig. 1).

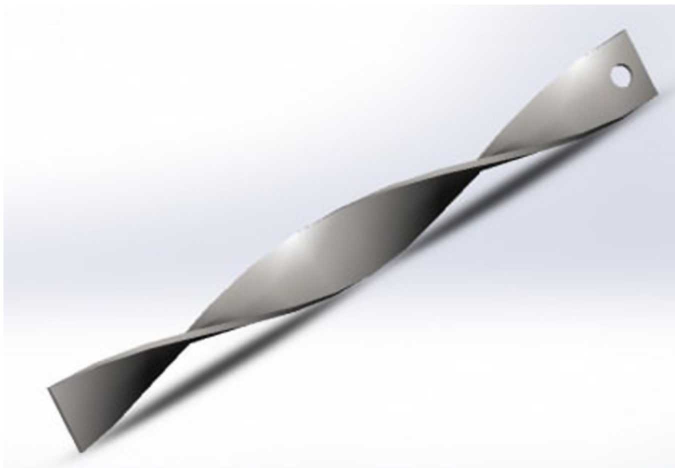

Fig. 1. Basic turbulator design [12]

Turbulator actuation by a detonation wave is presented in Figure 2 [12].

According to Fig. 2, in blasthole 1, detonation of intermediate detonator 2 in explosive 4 forms detonation wave 5 moving toward turbulator 6. The detonation wave passing through the helical plate moves further along the charge – 4.

The detonation wave passing along the turbulator causes turbulization effect. Fig. 2, b shows the resulting pressure at the detonation wave front.

In the turbulator, the pressure and velocity head of high-density detonation products moving behind the wave front arise.

The detonation wave is divided into force components F_x and F_y, whereby the component F_x creates torque around the longitudinal axis of the turbulator, imparting a rotational motion impulse. The component F_y imparts a translational motion impulse along the blasthole to the turbulator. As a result, high-speed rotational-translational motion begins as the detonation wave passes through the turbulator along blasthole *7*.

The high-speed rotational-translational motion causes axisymmetric *8* and longitudinal *9* vortex flows of explosive gases in the blasthole. In front of the turbulator, a gas compression zone arises (zone *10*), and behind it, a depression zone (zone *11*) due to the injection of explosive gases depthward the blasthole. The vortex flows *9* tear off finely dispersed particles (PM) of fragmented rock *17* from the blasthole wall *12* (Fig. 3). The flows are formed in zone *18* due to the blast shattering effect. The PM (particulate matter) concentration decreases towards the blasthole walls and increases towards the blasthole axis. Further, the explosive gases penetrate into the fractures in rock mass *19* [12].

Let us consider the hydrodynamic theory of detonation and shock wave propagation along a turbulator according to the schematic shown in Fig. 4.

Let us assume the following parameters of the medium in front of and behind the shock wave front: pressure P_0 and P_1, density ρ_0 and ρ_1, and temperature T_0 and T_1. We will use the laws of conservation of mass, momentum, and energy to find the relationship between these parameters.

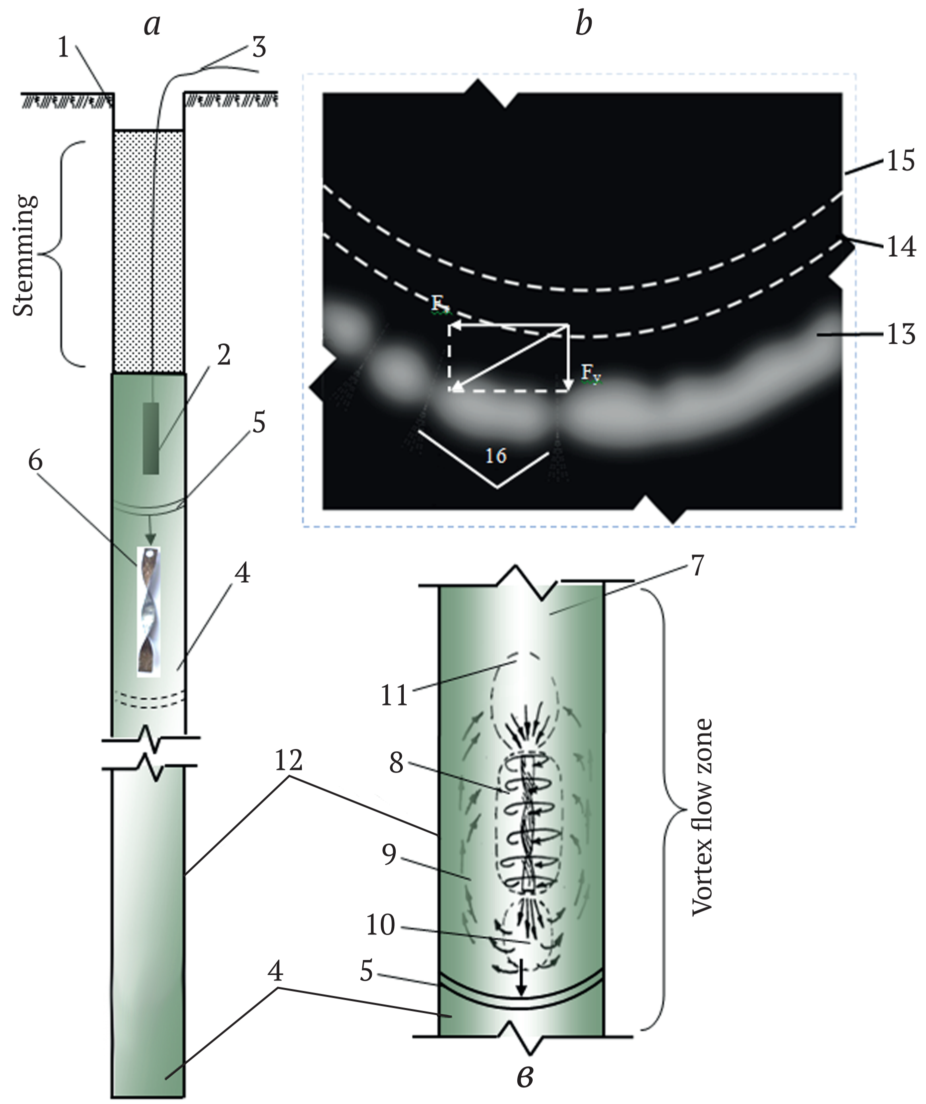

Fig. 2. Schematic of detonation wave action when using a turbulator [12]:
1 – blasthole; *2* – intermediate detonator; *3* – non-electric detonation system SINV; *4* – explosive charge column; *5* – detonation wave; *6* – turbulator; *7* – high-speed translational-rotational motion of a turbulator along a blasthole; *8* – axisymmetric vortex flows of explosive gases; *9* – longitudinal vortex flows of explosive gases; *10* – zone of gas compression; *11* – zone of gas depression; *12* – blasthole wall; *13* – bow shock wave front; *14* – estimated position of the contact surface; *15* – design position of the return wave in the DD; *16* – jets of detonation products penetrating the plasma

eISSN 2500-0632
https://mst.misis.ru/

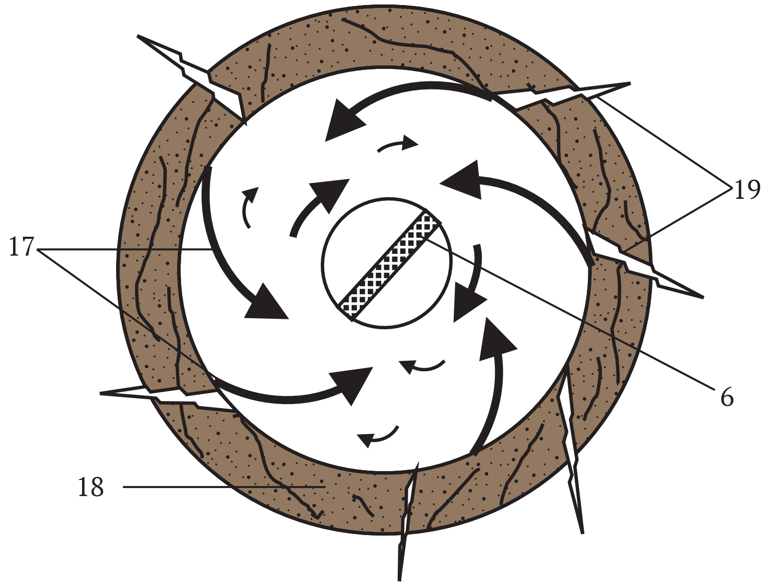

Fig. 3. The process of explosive gas vortex flow formation in a blasthole when using a turbulator:
17 – rock PM; *18* – zone of blast shattering effect; *19* – rock mass fractures

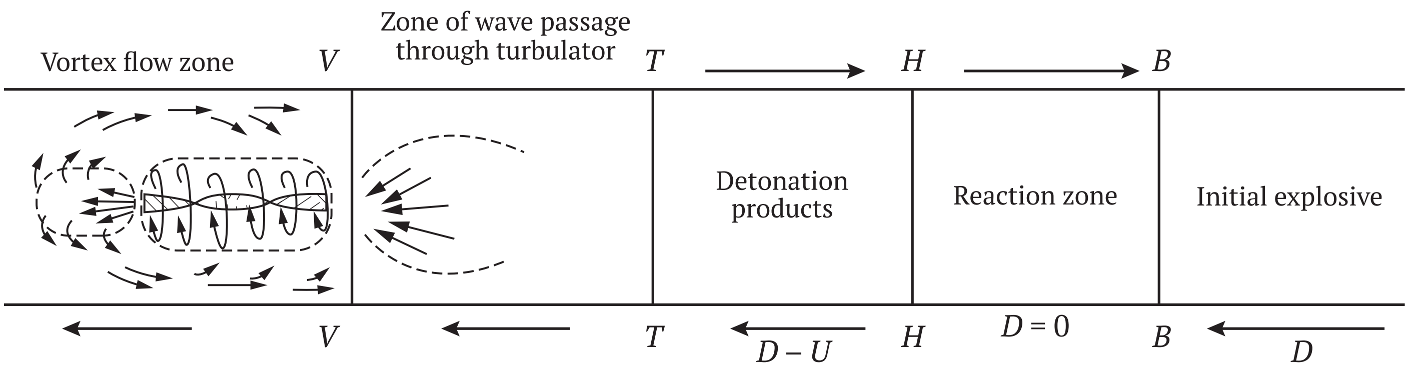

Fig. 4. Scheme of shock wave propagation along a turbulator

During time t the shock wave moves to distance Ut, and the shock wave front moves to distance Dt. The mass of the detonation wave compressed during this time is $\rho_1(D - U)St$, Before compression, the mass was equal to the product $\rho_0 DtS$. From the law of conservation of mass,

$$\rho_0 DSt = \rho_1 (D - U)St, \tag{1}$$

or

$$\rho_0 D = \rho_1 (D - U), \tag{2}$$

where ρ_0 is the detonation wave density before compression, kg/m^3; ρ_1 is the detonation wave density after compression, kg/m^3; D is the initial explosive detonation velocity, m/s; U is the detonation velocity after passing through a turbulator, m/s.

The change in the mass impulse is equal to the impulse of the force acting on it:

$$(P_1 - P_0)St = \rho_0 DStU, \tag{3}$$

or

$$P_1 - P_0 = \rho_0 DU, \tag{4}$$

where P_0 is the initial pressure of gases inside a blasthole, MPa; P_1 is the pressure of gases inside a blasthole after passing through a turbulator, MPa.

Since the process is considered adiabatic, the change in the total energy of the detonation wave mass $\rho_0 DSt$ is equal to the sum of the work of external forces and the energy after passing through a turbulator, i.e.

$$\rho_0 DSt = P_1 USt + E_r + E_{tr}. \tag{5}$$

Let us denote the internal energy of a unit of mass of the detonation wave before and after compression by ε_0 and ε_1, respectively, and the kinematic energy of a unit of mass after compression by $mU^2/2$.

Then:

$$\rho_0 DSt\left(\varepsilon_1 - \varepsilon_2 + \frac{mU^2}{2}\right) = P_1 SUt + E_r + E_{tr}, \tag{6}$$

where E_r is the rotary motion energy, J; E_{tr} is the translational energy, J; S is the blasthole cross-sectional area, m^2.

Let us define the mechanical stress on a blasthole walls when using a turbulator according to the scheme shown in Fig. 5.

We will define the detonation wave length and rotation velocity by means of the following formulas:

$$\Delta S = \alpha R; \tag{7}$$

$$v = \lim_{\Delta t \to 0} \frac{\Delta S}{\Delta t} = \frac{\Delta S}{\Delta t}; \tag{8}$$

$$v = \frac{d(\alpha R)}{dt} = \frac{R d\alpha}{dt} = R\omega, \tag{9}$$

where ΔS is the detonation wave rotation length, m; α is the turbulator rotation angle, deg; R is the turbulator torsion radius, m; v is the detonation wave rotation velocity, m/s; ω is the rotation frequency, Hz; t is the rotation time, s.

We will use a well-known formula for determining kinetic energy, in order to determine rotational and translational motion energies:

$$E_k = \frac{Mv^2}{2}. \tag{10}$$

It follows from equations (8)–(10) that the rotational velocity is equal to $v = R\omega$. Given this expression, we obtain the formula for determining rotational motion energy:

$$E_r = \frac{M\omega^2 R^2}{2}, \tag{11}$$

or

$$E_r = \frac{I\omega^2}{2}, \tag{12}$$

where I – is the moment of inertia, kg·m².

In formula (12) we will take into account the moment of inertia for a turbulator of length l and mass M, i.e. [13]:

$$I = \frac{1}{12} Ml^2. \tag{13}$$

Hence the translational motion energy:

$$E_{tr} = \frac{M\omega^2 l^2}{24}. \tag{14}$$

Substituting expressions (11) and (14) into equation (7), we obtain the equality of the law of conservation of mass:

$$\rho_0 DSt\left(\varepsilon_1 - \varepsilon_0 + \frac{mU^2}{2}\right) = P_1 SUt + \frac{M\omega^2 R^2}{2} + \frac{M\omega^2 l^2}{24}. \tag{15}$$

The mechanical work of a blast in a blasthole when using a turbulator is determined by the formula:

$$A = P_1 SUt + \frac{M\omega^2 R^2}{2} + \frac{M\omega^2 l^2}{24}. \tag{16}$$

The mechanical stress on a blasthole walls is defined as:

$$\sigma = \frac{F}{S} = \frac{PS}{S} = P, \tag{17}$$

where F is the effective force, N; S – the cross-sectional area of a blasthole, m²; P – the mechanical pressure, MPa:

$$P = \frac{A}{\Delta V}, \tag{18}$$

where ΔV is the volume of rototraversingly moving gases, m³:

$$\Delta V = S\Delta l = S(D - U)t, \tag{19}$$

where Δl is the length of rototraversingly moving gases, m.

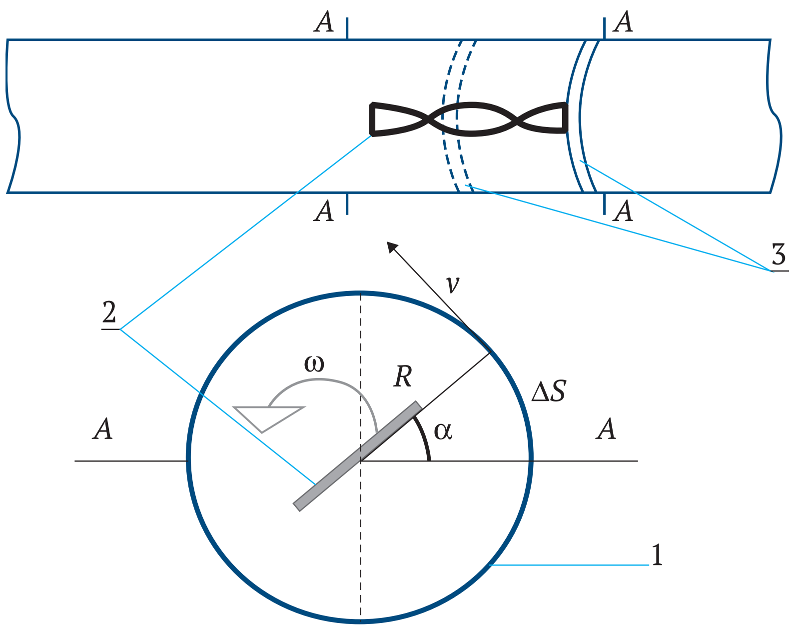

Fig. 5. Scheme for the calculation of mechanical stress on blasthole walls:
1 – blasthole; *2* – turbulator; *3* – detonation wave; *R* – turbulator torsion radius; α – turbulator rotation angle;
ω – detonation wave rotation frequency; *v* – detonation wave rotation velocity; Δ*S* – detonation wave rotation length

Substituting expressions (16), (17), and (19) into (18), we obtain a formula for determining the mechanical stress on a blasthole walls when using a turbulator:

$$\sigma = \frac{P_1 SUt + \dfrac{M\omega^2 R^2}{2} + \dfrac{M\omega^2 l^2}{24}}{S(D-U)t}. \quad (20)$$

We have thus determined the mechanical stress on a blasthole walls when using a turbulator. Implementation of the design with the effect of turbo-blasting for rock fragmentations by blasthole charges reduces the consumption of explosives, the volume of drilling, the secondary fragmentation costs, and increases the productivity of excavators and mining safety.

2. Determining the radial fracture zone size when using a turbulator in a blasthole explosive charge

On the basis of the theoretical assumptions from [14–17] the effect of the physical and mechanical properties of rocks and the explosives energy characteristics on the size of the rock fragmentation zone formed due to a blast when using a turbulator in a blasthole explosive charge was investigated. The mechanism of the fragmentation zone formation is shown in Fig. 6.

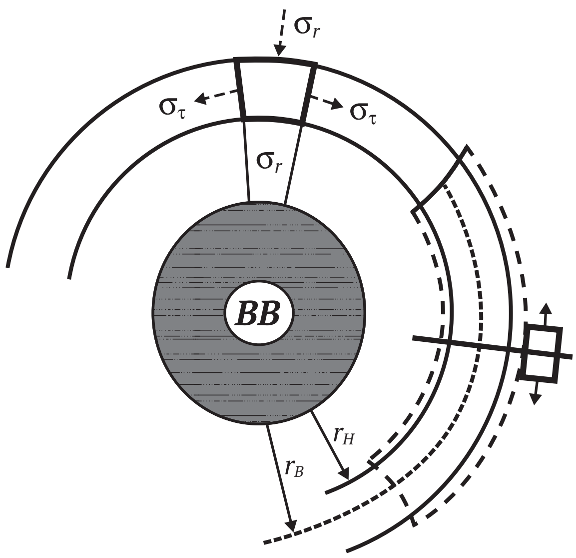

Fig. 6. Mechanism of fragmentation zone formation: σ_r – compressive stresses; σ_τ – tensile stresses

The flow of expanding gases as a result of turbulator action will move into fractures, thus promoting their opening. The expanding gases flow speed is rather high, and the gas in this case can reach the fracture tip. Due to the fact that the gas flow in the fractures is accompanied by hydrodynamic and thermal losses, the pressure will begin to rapidly decrease, becoming insufficient for further fracturing.

Thus, the size of the blast-caused radial fracturing zone will depend on the pressure and strength of the blast detonation products and the elastic properties of the rocks surrounding the charge.

Studies have shown that when using a turbulator in a blasthole explosive charge, the fragmentation zone size does not exceed 3–15 radiuses of the charge. In this regard, the radius of the radial fracturing zone will also depend on the explosive charge radius, the longitudinal wave propagation velocity in a rock mass, and stress.

The radius of the radial fracturing zone is determined by means of the formula [13]:

$$r_{rad} = r_0 C_p \frac{\sqrt{\gamma}}{5\sigma_{comp}}, \text{ m}, \quad (21)$$

where r_0 is the radius of explosive charge, m; γ the rock density, kg/m^3; C_p is the longitudinal wave velocity in a rock mass, m/s; σ_{comp} is the ultimate compression strength of a rock, N/m^2.

When using a turbulator in a blasthole explosive charge, the longitudinal wave velocity in a rock mass is determined taking into account the turbulator rotation angle. Hence

$$C_p = D \cdot cos\,\alpha, \text{ м/с}, \quad (22)$$

where D – is the velocity of detonation of an industrial explosive, m/s; α – is the turbulator rotation angle, deg.

It was found that the longitudinal wave velocity in the rock mass decreases with an increase in the turbulator rotation angle. For instance, at the turbulator rotation angle of 45o, the longitudinal wave velocity in the rock mass is 2,700 m/s.

It is recommended to determine the radial fracturing zone radius when using a turbulator in a blasthole explosive charge by means of the formula:

$$r_{rad} = \frac{0,2Dr_0\sqrt{\gamma}}{\sigma_{comp}} \cos\alpha, \text{ m}, \quad (23)$$

where D the detonation velocity of industrial explosive, m/s; r_0 is the radius of explosive charge, m; γ is the rock density, kg/m^3; σ_{comp} is the rock compressive strength, H/m^2; α is the turbulator rotation angle, deg.

3. Study of rock fragmentation process when using a turbulator in a blasthole explosive charge

According to the energy principle of drilling and blasting parameters calculation [17, 18], the quality of fragmentation, all other things being equal, is conditional on the explosive energy store in the rock mass volume to be fragmented. However, the blast energy can be used in different ways for rock fragmentation. The quality of rock fragmentation has been established to be dependent upon along with the explosive energy store, a number of factors. The most important of these are: rock mass fracturing; charge diameter; blasting pattern; interval, and order; as well as the charge design and type of stemming.

In view of the above, the dependence of the change in the average diameter of a piece of blasted rock mass d_i on the specific explosive consumption q (kg/m^3) when using a turbulator can be expressed as follows:

$$d_i = d_0 \exp(k_{\exp.en} d_0 q).$$

This formula allows for a dependence to be obtained, in order to define the distance between rows of blastholes and between blastholes in a row. This in turn allows the rock fragmentation radius when using a turbulator in a blasthole explosive charge to be determined, depending on the blasting conditions and the required quality:

$$r_{cr.rad} = \sqrt{\frac{pl_{ch}}{mH_l \frac{1}{k_{\exp.en} d_0} \ln \frac{d_0}{d_i}}}, \text{ м}, \quad (24)$$

where p is the capacity of 1 l.m. of blasthole, m; l_{ch} is the explosive charge length in a blasthole, m; m is the separation factor of blasthole charges; H_l is the bench height, m; $k_{\exp.en}$ is the factor taking into account the use of explosive energy for rock fragmentations at specific blast patterns; d_0 is the average diameter of rock mass block on the basis of blockiness (jointing) degree, mm; d_i is the average diameter of a blasted piece of rock, mm.

4. Development of a blasting rock mass fragmentation method with the use of a turbulator

A method of blasting rock mass fragmentation with the use of a turbulator has been developed. The method provides uniform and high-quality blasting rock mass fragmentation, as well as increasing the actual explosive charge potential energy efficiency by means of changing the mechanism of its transmission and increasing the fragmentation process duration.

According to this method, an aluminum plate 2×20×180 mm is twisted in a helical manner around the longitudinal axis by 360° (in a single turn). The plate is mounted vertically in the center of a polyvinyl chloride tube 180 mm long and 100 mm in diameter. Then the tube is sealed at both ends. This creates a device referred to as a turbulator in an air cavity (Fig. 7).

Then blastholes are drilled in the rock mass to be blasted according to a blasting pattern. At the bottom of each blasthole, an intermediate detonator is installed and a small amount of industrial explosive is inserted to completely cover the intermediate detonator (Fig. 8). Then a turbulator is placed into each blasthole and the blastholes are filled with the remaining amount of the explosive, and blasthole stemming and blasting is performed.

Applying the method of blasting rock mass fragmentation with the use of a turbulator enables uniform and high-quality blasting rock mass fragmentation. It also increases the actual explosive charge potential energy efficiency by means of changing the mechanism of its transmission and increasing the fragmentation process duration.

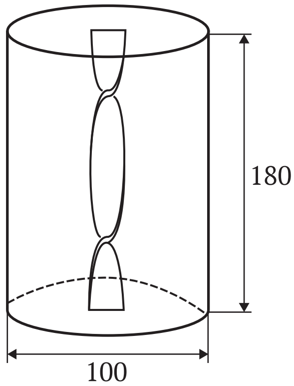

Fig. 7. Design of a turbulator in an air cavity made of PVC tube

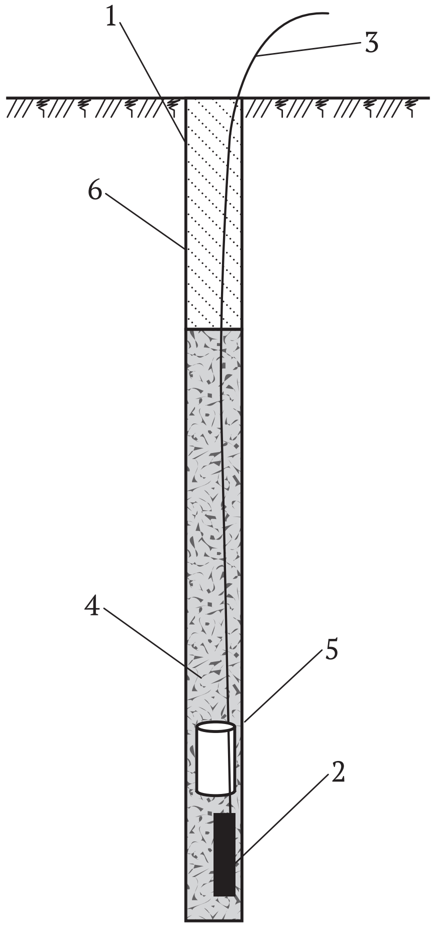

Fig. 8. Design of a blasthole explosive charge with a turbulator for rock mass fragmentation: *1* – blasthole; 2 – intermediate detonator; *3* – non-electric detonation system; *4* – industrial explosive; *5* – air cavity turbulator design; *6* – stemming

5. Development of a method of sectional blasthole initiation

A method of blasthole explosive charges initiation in a blasting block has also been developed. This allows for the duration, frequency, and orientation of blast load application to be regulated. It also increases blast energy utilization for rock fragmentation (Fig. 9).

This method provides for drilling rows of blastholes in a block to be blasted according to a blasting pattern. The blastholes are filled with an industrial explosive, and SINV non-electric detonation system is used for the blasthole charge initiation. The blasting block is divided into two equal parts (sections), and these, in turn, into three series of short-delayed blasting blastholes. The blasthole charges are initiated simultaneously in the two sections of the block based on a trapezoidal blasting pattern. This ensures that the detonation waves meet when moving toward each other simultaneously and provides collision of broken rock lumps. In the first series, the instantaneous blasting of blastholes located at both ends of the blasting block and forming a trapezoid (in plan view) is carried out. Then, after 42 ms, the second series blastholes (also forming a trapezoid) are blasted. In another 42 ms, the remaining blastholes are blasted along the perimeter of the blast block in the third series.

Applying this blasting method enables the effective utilization of blast energy and collision of moving rock lumps. This increases the energy consumption in rock fragmentation, provides preset fragmentation degree and a quality of rock mass preparation for different deposit development designs with minimal material and power consumption.

6. Industrial testing of the methods developed in order to improve the quality of rock mass fragmentation

In accordance with the “Program of research on redistribution of blast energy along the length of a blasthole charge when using the effect of turbo blasting” at Kalmakyr deposit of JSC “Almalyk Mining and Metallurgical Complex”, pilot tests were carried out. They used the new design of blasthole explosive charges with the turbo blasting effect and the method of blasthole explosive charges initiation in a blasting block.

The blasting tests were performed at “Yoshlik-I” open pit, located in the territory of Tashkent Region of the Republic of Uzbekistan at a distance of 1 km to the south of Almalyk city. The open pit produces copper-molybdenum ores. The pit rock mass excavation design capacity is 88.1 million m^3.

The main ore-bearing rocks at “Yoshlik-I” are syenite-diorite (58% of the estimated ore reserves), to a lesser extent diorite (35%), and granodiorite-porphyry (7%). The role of other rocks in the ore bodies’ location is extremely insignificant.

General characteristics of the ores and rocks:
– Protodyakonov hardness index – 10–15;
– Bulk density:
• balance and off-balance ores – 2.6 t/m^3;
• oxidized ore – 2.5 t/m^3;
• rock – 2.44 t/m^3;
– fragmentation index – 1.5;
– pit watering – 65–68%.

A SBSh-250MNA-32 drilling rig performed drilling of blastholes under the Program. ANFO explosive was used in blasting at the mine.

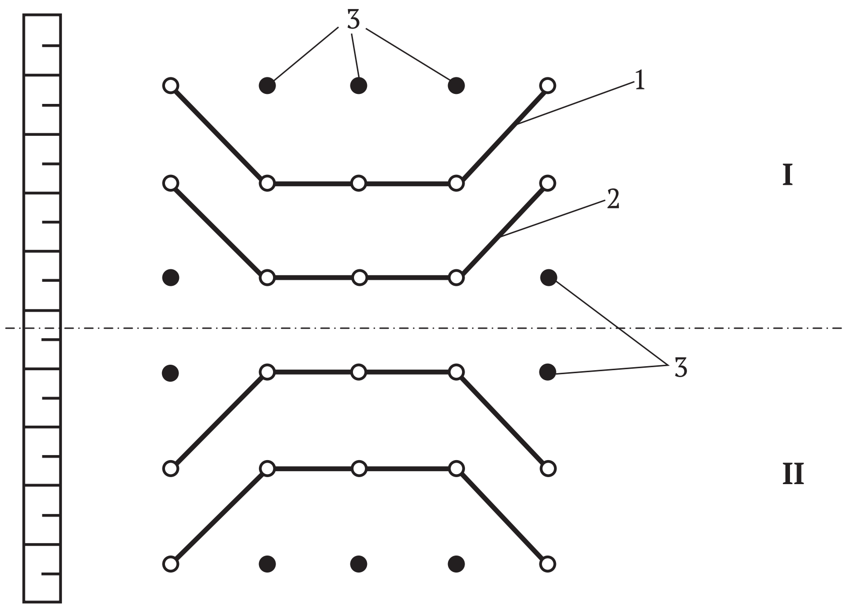

Fig. 9. Blasting pattern in the method of sectional blasthole initiation:
I and II – the first and second sections of blasting block; *1* – the first blasting series with no delay;
2 – the second blasting series with delay of 42 ms; *3* – the third blasting series with delay of another 42 ms

The parameters of the blasthole relieving (fragmentation) charges were calculated in accordance with the "Regulatory Guide for Drilling and Blasting" and "Technical Rules for Blasting on the Surface" [17, 18].

The parameters for the drilling and blasting when using the traditional and developed methods of blasting rock fragmentation are given in Table 1.

Table 1

Drilling and blasting parameters when using the traditional and developed methods of blasting rock fragmentation

Item	Value
Protodyakonov rock hardness index, *f*	10–14
Bench height, m	15
Drillhole depth, m	18
Drillhole diameter, mm	244.5
Blastholes spacing, m x m	7x7
Number of blastholes, pcs.	65
Weight of explosive in a blasthole, kg	588
Explosive type	ANFO
Intermediate detonator type	Almanit
Volume of blasted rock mass, m^3	50,180
Explosive specific consumption, kg/m^3	0.76
Drilling specific consumption, m/m^3	0.0245
Drilling rig productivity, l.m./year	41,800
Quantity of intermediate detonators, pcs.	1

The method of blasting rock mass fragmentation with use of a turbulator was applied, in order to increase the efficiency of blast action on a rock mass and decrease the oversize yield. The use of this charge design changed the energy transfer mechanism allowing the fragmentation process time to be increased. The fragmentation process is determined by a primary compression wave and a system of subsequent stress waves, providing more uniform and high-quality rock mass fragmentation.

The scheme of sequential blasting of blasthole explosive charges with the use of a counter dynamic effect was industrially tested.

According to this scheme, 5 rows of blastholes of 252 mm in diameter were drilled in a blasting block at 5×5 m grid spacing by means of SBSh-250MN drilling rig. At a bench height of 15 m, the blasthole length was 17 m, the stemming length was taken at 5 m, and the charge length was 12 m. The blastholes were filled with ANFO industrial explosive with charge density of 0.85 g/cm^3. The mass of each blasthole charge was 618 kg.

Downhole blasting caps were installed at the bottom of the blastholes (one blasthole – one blasting cap). Delay intervals between the blasthole series were taken at 0.42 ms and 84 ms. The detonation sequence was according to a trapezoidal scheme, ensuring the detonation waves meeting in the center of the blasting block. The initiation of charges in the SINV system was carried out by means of ED-8Zh electrical blasting caps and the main wire of DShE-12 detonating cord. SINV-START served as the source of the explosive pulse for the SINV non-electric detonation system.

The blasting block was divided into two equal sections, I and II with 15 blastholes in each section, and these, in turn, into three series of short-delayed blasting blastholes. Instantaneous blasting of blastholes forming a trapezoid (in plan view) was carried out simultaneously in sections I and II from both ends of the blasting block in the first series. Then, after 42 ms, the second series blastholes (also forming a trapezoid) were blasted. After another 42 ms, the remaining blastholes (the third series) were blasted along the perimeter of the blast block.

The main parameters characterizing the blasting results were the blasted rock mass PSD, and the oversize yield. The results of industrial blastings by means of the traditional (standard) and developed methods are shown in Figs. 10 and 11.

After each blast the broken rock PSD was analyzed while handling. Comparative PSD data for the traditional and developed methods are shown in Table 2 and Fig. 12.

Table 2

Comparative PSD data for the traditional and developed methods of rock fragmentation

Linear size of fractions *d*, mm	Shares of fractions depending on the method of rock fragmentation, %	
	traditional	developed
0–300	20	61.3
301–400	11	12.1
401–500	10	11.2
501–600	16	10.5
601–700	11	2.3
701–800	12	1.6
801–900	11	1
901–1000	5	–
above 1000	4	–

The particle size distribution (PSD) analysis showed that the method developed, when compared to the traditional one, reduced the average lump size by 43 % and the number of oversized lumps by 44 %. Pilot tests showed that the method developed provides uniform rock fragmentation.

Thus, the design with the effect of turbo-blasting in rock fragmentations by blasthole charges reduces the consumption of explosives, the volume of drilling, the costs for secondary fragmentation, while increasing the productivity of excavators and mining safety. Implementing the developed method of sequential

Fig. 10. Results of industrial blasting by means of the traditional rock mass fragmentation method

Fig. 11. Results of industrial blasting by means of the developed rock mass fragmentation method

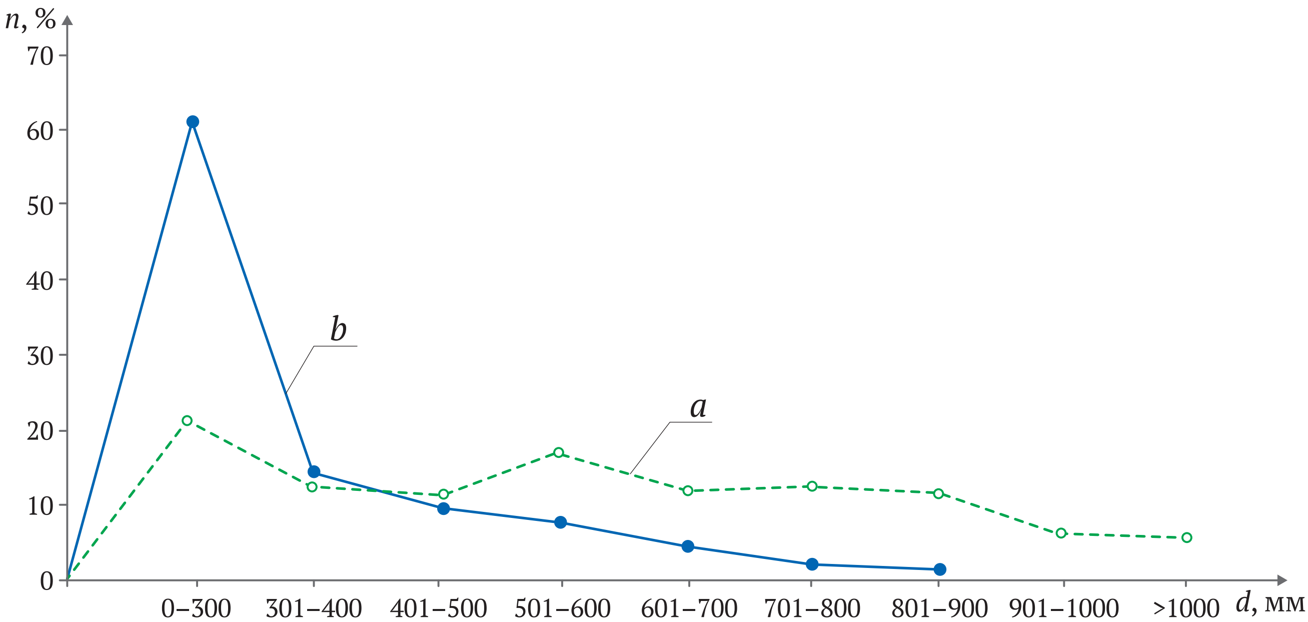

Fig. 12. PSD in the traditional (*a*) and developed (*b*) methods of rock fragmentation

blasting of blasthole explosive charges with the use of the counter dynamic effect enabled effective utilization of blast energy and collision of moving rock lumps. This increased the blast energy consumption in rock fragmentation, and provided preset fragmentation degree and quality of rock mass preparation with minimal material and power consumption.

Conclusions

1. One of the most important components in open-pit mining of mineral deposits is blast action control. This requires a proper understanding of the physical mechanism of the blast effect on a rock mass to be fragmented. Increasing the action pressure and time by means of a turbulator is recommended, in order to improve the efficiency of a blast action on a rock mass and decrease the oversize yield in open pits. A turbulator is designed to increase the actual coefficient of utilization of the commercial explosive column charge potential energy. This is achieved by increasing the rate of secondary chemical reactions of the explosive afterburning in a blasthole after the detonation wave passage until the detonation products reach the free surface.

2. The proposed mathematical model of blast energy redistribution along the length of a blasthole when using the effect of "turbo-blasting" shows how the degree of blast action on a rock mass can be optimized via redistribution of blast energy along the explosive charge length. The mechanical pressure on the walls of a blasthole depends on the following factors: the pressure behind the shock wave front; the blasthole cross-sectional area; the detonation velocity after passage through a turbulator; the shock wave passage time; the length and mass of the turbulator; the rotation frequency; the turbulator torsion radius; and the initial explosive detonation velocity.

3. The physical and mechanical properties of the rock and explosive energy characteristics have an effect on the size of the rock fragmentation zone formed due to a blast, when using a turbulator in a blasthole explosive charge. The size of the radial fracturing zone formed during a blast depends on the pressure of the blast detonation products and strength and elastic properties of the rocks surrounding the charge. The radial fracture zone radius when using a turbulator in a blasthole explosive charge varies in direct proportion to the charge radius, the industrial explosive detonation velocity, the blasted rock density, and the turbulator rotation angle and is inversely proportional to the rock ultimate compressive strength.

4. The method of blasting rock mass fragmentation with the use of a turbulator is recommended. The method provides for the uniform and high-quality blasting rock mass fragmentation, and also increases the actual explosive charge potential energy efficiency by changing the mechanism of its transmission, and increasing the duration of the fragmentation process. A method of blasthole explosive charges initiation in a blasting block is also recommended. This allows the duration, frequency, and orientation of blast load application to be regulated and the blast energy utilization for rock fragmentation to be increased.

5. Use of turbo-blasting for rock fragmentation by blasthole charges and the method of blasthole explosive charges initiation in a blasting block at the Kalmakyr deposit of JSC "Almalyk Mining and Metallurgical Complex" has reduced the consumption of explosives, the volume of drilling, secondary fragmentation costs, and increased the productivity of excavators and mining safety. The particle size distribution (PSD) analysis shows that the methods developed, when compared to traditional ones, reduced the average lump size by 43 % and the number of oversized lumps by 44 %.

References

1. Dubnov L.V., Kolesnichenko I.T. On the energy criterion of explosives performance and some of its consequences. *Gornyi Zhurnal*. 1986;(5):57–61. (In Russ.)

2. Mosinets V.N. Current condition and prospects for the development of technology and methods of blasting work in the USSR's open pits. In: *Blasting Work*. Collected book, № 89/46. Moscow: Nedra Publ.; Pp. 100–109. (In Russ.)

3. Ahmed R. *Comportement et fragmentation dynamique des matérieaux quasifragiles*. Application à la Fragmentation des Roches par Explosifs; Thèse de Doctorat de l'Ecole Nationale Supérieure des Mines de Paris. 2004. 210 p. (In French)

4. Peter B. *Optimisation of fragmentation and comminution at Boliden Mineral, Aitik Operation*. 2005. 179 p.

5. Paine R.S., Holmes, D.K., Clark H.E. Presplit blasting at the Niagara power project. *The Explosives Engineer*. 2003;39(3):72–92.

6. Rossmanith H.P. The mechanics and physics of advanced blasting-waves, shocks, fracture, damage, impact and profit. Short Course. *FragBlast*. 2006;(8). 214 p.

7. Selberg H.L. Transient compression waves from spherical and cylindrical cavities. *Archive for Physics*. 1995;5(7):307–314.

8. Kuzutov B.N., Andrievsky A.P. *New theory and new technologies of rock disintegration by elongated explosive charges*. Novosibirsk: Nauka Publ.; 2002. (In Russ.)

9. Bibik I.P., Rubtsov S.K., Sytenkov D.V. *Control of rock blasting breaking in open pit process flows*. Tashkent: FAN Publ.; 2008. 424 p. (In Russ.)

10. Zairov S.S., Urinov S.R., Nomdorov R.U. Ensuring wall stability in the course of blasting at open pits of Kyzyl Kum Region. *Mining Science and Technology (Russia)*. 2020;5(3):235–252. https://doi.org/10.17073/2500-0632-2020-3-235-252

11. Zairov Sh.Sh., Mekhmonov M.R., Fatkhiddinov A.U. *Improving quality of rock mass fragmentation by blast energy*. Monograph. LAP Lambert Academic Publishing; 2022. 165 p. (In Russ.)

12. Muchnik S.V. *Development and scientific justification of technical and process solutions for control of blast effect in mining industry*. [Ph.D. thesis in Engineering Science.] Novosibirsk: 2000, 308 p. (In Russ.)

13. Rakishev B.R. *Energy intensity of mechanical disintegration of rocks*. Almaty: Baspager Publ.; 1998. 210 p. (In Russ.)

14. Lukyanov A.N. *Development of scientific foundation, research and implementation of methods and means for intensification of technological processes in open-pit mining of hard rock deposits of complicated structure*. [Ph.D. thesis in Engineering Science.] Moscow; 1983. 452 p. (In Russ.)

15. Zairov Sh.Sh., Sharipov Z.S., Mekhmonov M.R., Arzieva S. I. Use of the effect of “turbo blasting” in crushing rocks by well charges of explosives. *Gorniy Vestnik Uzbekistana*. 2021;(4):21–25. (In Russ.) URL: http://gorniyvestnik.uz/assets/uploads/pdf/2021-oktyabr-dekabr.pdf

16. Zairov Sh.Sh., Ravshanova M.H., Mekhmonov M.R., Arziyeva S.I. Use of the effect of “turbo blasting” in crushing rocks by well charges of explosives. *Design Engineering*. 2021;(09):10801–10813.

17. Avdeev F.A., Baron V.L., Gurov N.V., Kantor V.Kh. *Drilling and blasting reference-book on standards*. Moscow: Nedra Publ.; 1986. 511 p. (In Russ.)

18. Avdeev F.A., Baron V.L. et al. *Technical rules for blasting on daytime surface*. Moscow: Nedra Publ.; 1972. 238 p. (In Russ.)

Information about the authors

Utkir F. Nasirov – Dr. Sci. (Eng.), Deputy Director for Research and Innovation, National University of Science and Technology “MISiS” (NUST MISiS) (Almalyk Branch), Almalyk, The Republic of Uzbekistan; Scopus ID 56527108100; e-mail unasirov@yandex.ru

Sherzod Sh. Zairov – Dr. Sci. (Eng.), Professor of the Mining Department, Navoi State Mining and Technology University, Navoi, The Republic of Uzbekistan; ORCID 0000-0002-1513-5683, Scopus ID 56527393000, ResearcherID ABC-5825-2020; e-mail sher-z@mail.ru

Maksud R. Mekhmonov – Doctoral Student, Navoi State Mining and Technology University, Navoi, The Republic of Uzbekistan

Asliddin U. Fatkhiddinov – Doctoral Student, Tashkent State Technical University, Tashkent, The Republic of Uzbekistan

Received 02.02.2022
Revised 14.03.2022
Accepted 25.05.2022

MINING SCIENCE AND TECHNOLOGY (RUSSIA)
ГОРНЫЕ НАУКИ И ТЕХНОЛОГИИ
2022;7(2):150–160
eISSN 2500-0632
https://mst.misis.ru/

MINING MACHINERY, TRANSPORT, AND MECHANICAL ENGINEERING

Research article

https://doi.org/10.17073/2500-0632-2022-2-150-160

Assessment of mine water solid phase impact on section pumps performance in the development of kimberlite ores

N.P. Ovchinnikov
M.K. Ammosov North-Eastern Federal University, Yakutsk, Russian Federetion
ovchinnlar1986@mail.ru

Abstract
Despite innovations in ALROSA's (PJSC) mining and processing complexes under the updated strategy for economic development, practice shows that in recent few years the operating costs of the section pumps at the Udachny underground mine's main drainage have increased significantly. Such an increase could be the result of a concentration of mechanical impurities in the mine water. This study is aimed at the integrated assessment of the impact of mechanical impurities concentration in mine water on the performance of the Udachny underground mine's main drainage section pumps. It is also aimed at studying the feasibility of sinking additional inclined clarifying working-reservoirs. The target goal was achieved by means of visual, analytical, statistical, and other types of research in determining the impact of the concentration of mechanical impurities in mine water on the performance indicators of section pumps of the kimberlite mine's underground drainage facilities. The integrated studies showed that the concentration of mechanical impurities in mine water is the key factor in determining the overhaul life and electricity demand of pumping equipment. The Udachny underground mine's main drainage section pumps overhaul life can be calculated as a linear function of their delivery rates at the moment of taking-down for overhaul. This function is reliably described by empirical expression $Q = -7.5X_6 + 326.67$, where X_6 is the averaged mechanical impurities concentration in the mine water. Calculations showed that reducing the concentration of mechanical impurities in mine water from 17 to 4 g/l would decrease the annual operating costs of the Udachny underground mine's main drainage section pumps by 100 million rubles.

Keywords
diamond mining, underground mine, PJSC ALROSA, Udachny mine, mine drainage, section pumps, wear, groove seals, mechanical impurities, operating efficiency

For citation
Ovchinnikov N.P. Assessment of mine water solid phase impact on section pumps performance in the development of kimberlite ores. *Mining Science and Technology* (*Russia*). 2022;7(2):150–160. https://doi.org/10.17073/2500-0632-2022-2-150-160

ГОРНЫЕ МАШИНЫ, ТРАНСПОРТ И МАШИНОСТРОЕНИЕ

Научная статья

Оценка влияния твердой фазы шахтных вод на эффективность секционных насосов при разработке месторождений кимберлитовых руд

Н.П. Овчинников
Северо-Восточный федеральный университет им. М.К. Аммосова, г. Якутск, Российская Федерация
ovchinnlar1986@mail.ru

Аннотация
Несмотря на принятые нововведения в горно-обогатительных комбинатах АК «АЛРОСА» (ПАО) в рамках обновленной стратегии по экономическому развитию, практика свидетельствует, что за последние несколько лет существенно возросли затраты на эксплуатацию секционных насосов главного водоотлива подземного рудника «Удачный». Такому росту затрат мог способствовать заметный рост концентрации механических примесей в шахтных водах. Настоящая работа посвящена комплексной оценке влияния концентрации механических примесей в шахтных водах на эффективность секционных насосов главной водоотливной установки подземного рудника «Удачный» для технико-экономического обоснования проходки дополнительных наклонных осветляющих резервуаров. Поставленная цель достигается путем проведения визуальных, аналитических, статистических и других видов исследований по установлению степени влияния концентрации механических примесей в шахтных водах на ряд эксплуатационных показателей секционных насосов водоотливных хозяйств подземных кимберлитовых рудников. Комплексными исследованиями доказано, что концентрация механических примесей

в шахтных водах является ключевым фактором, определяющим межремонтный ресурс и электропотребление насосного оборудования. Межремонтный ресурс секционных насосов главной водоотливной установки подземного рудника «Удачный» может быть рассчитан как линейная функция их подачи на момент вывода в капитальный ремонт, изменение которой с высокой степенью достоверности описывается эмпирическим выражением $Q = -7,5X_6 + 326,67$, где X_6 – усредненная концентрация механических примесей в шахтных водах. Расчетным путем установлено, что снижение концентрации механических примесей в шахтных водах с 17 до 4 г/л позволит уменьшить годовые затраты на эксплуатацию насосного оборудования главной водоотливной установки рудника «Удачный» на 100 млн рублей.

Ключевые слова
добыча алмазов, подземный рудник, АК «АЛРОСА» (ПАО), рудник «Удачный», водоотлив, секционные насосы, износ, щелевые уплотнения, механические примеси, эффективность эксплуатации

Для цитирования
Ovchinnikov N.P. Assessment of mine water solid phase impact on section pumps performance in the development of kimberlite ores. *Mining Science and Technology* (*Russia*). 2022;7(2):150–160. https://doi.org/10.17073/2500-0632-2022-2-150-160

Introduction

During the pandemic many domestic mining companies faced sales problems.The above was also true of ALROSA diamond-mining company (hereinafter the Company), whose main production facilities are located in the Mirny district, Western Yakutia. While the demand for industrial and gem-quality diamonds is decreasing, the Company is actively implementing a variety of technological and technical solutions aimed at reducing the costs of mining and processing of rough diamonds as part of its updated economic development strategy.

Innovations implemented at the mining and processing divisions have had a positive effect on the Company's financial position to a great extent. However, at the same time the costs of certain mining process stages continued to grow. The main drainage of the Udachny underground mine is part of such special cases in the mining process flow sheet.

A significant share of the costs of mine drainage pumping equipment (centrifugal section pumps) operating is related to overhauls and electricity consumption. Fig. 1 shows that over the past six years, the costs in these items increased more than 2 times. Thus, there is an urgent need to establish the reasons for such growth of the costs.

The appreciable growth in the concentration of mechanical impurities in mine waters promotes hydroabrasive wear of the liquid end parts, mainly the impeller groove seals (hereinafter groove seals). This can lead to premature deterioration of the pumping equipment performance [1, 2] and can considerably increase the costs.

The adverse impact of abrasive fluid flow on pumping equipment has been noted in historical studies [3–5].

High concentration of mechanical impurities in the pumped out mine water is caused by intensive pollution of drainage routes, along which the mine water moves from the mining levels to the sump galleries.

The main pollution sources are the rock mass, spilled from the conveyors and thickened sludge-slurry, spilled during its LHD hauling from sumps and clarifying working-reservoirs and hoisting to the surface.

At the same time, studies [6, 7] have shown that section pumps often fail due to extensive cavitation damage of the liquid end parts in the process of underground mining.

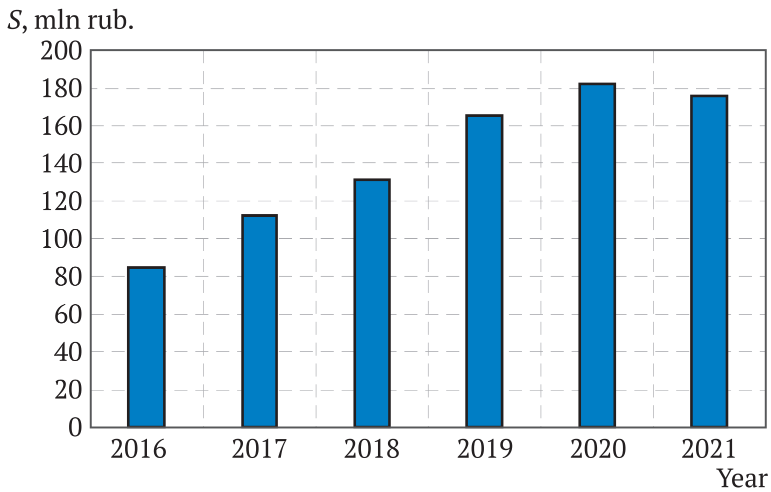

Fig. 1. The Udachny underground mine drainage pumping equipment operating costs by year

Certain papers [8, 9] have demonstrated activation of adhesion wear of section pump casing and rotor parts, typically if the maximum radial clearance in the groove seals has been attained.

The mine water pumped out by the pumps is mainly characterized by high mineralization and pH in the vicinity (above or below) of 7 [10].

In this connection, in the case of sufficient aggressiveness of mine water to metal, metal corrosion of the section pump liquid end parts can occur [11].

The above-mentioned studies supported to the conclusion that the decrease in the durability of the pumps liquid end parts in underground mines and coal mines was caused by complex multifactorial damage. This was due to the complex impact on the metal of hydroabrasion, corrosion, cavitation, and adhesion types of wear. The impact of each of these damaging processes depends on hydrogeological and mining conditions of the specific developed mineral deposit.

The operation services of the enterprise aim to achieve a considerable reduction of solids content at the outlet of the drain sumps of the Udachny underground mine's main drainage (from 17 to 4 g/l). A further aim is to achieve effective dewatering of sludge-slurry deposits via sinking additional inclined clarifying working-reservoirs with a total useful capacity of 7.500 m^3 (Fig. 2). However, the technical solutions implementation bottleneck is due to very high capital costs of about 340 million rubles.

This study is aimed at the integrated assessment of the impact of the concentration of mechanical impurities in mine water on the performance of the Udachny underground mine main drainage section pumps, as well as a feasibility study of sinking additional inclined clarifying working-reservoirs.

The target goal was achieved by means of visual, analytical, statistical, and other research methods to determine the impact of mechanical impurities concentration in mine water on performance indicators of section pumps of the Company's underground mines.

The study subject was section pumps of drainage facilities of the Company's underground mines.

Research techniques

The study of the Udachny underground mine's main drainage section pumps groove seal wear (the JSH-200 and NTsS(K) 350-1100 pump models)

The findings of numerous examinations of the worn-out groove seals showed that they were subject to hydroabrasive wear. This was evidenced by the peculiar waves on the outer surfaces of the impellers and the inner surfaces of the sealing rings, caused by vortex motion of the mine water polluted with mechanical impurities (Fig. 3, *a*–*c*). The largest mechanical impurities at an angle close to the normal, strike the metal causing its deformation in the form of dents and swellings. Smaller mechanical particles moving tangentially, cut the metal layer and the formed swellings [12].

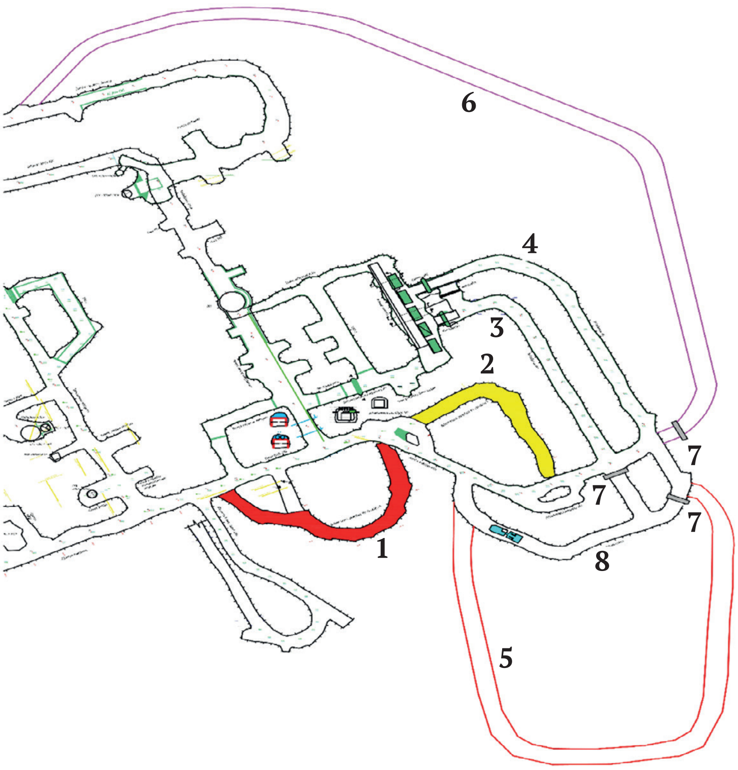

Fig. 2. Proposed main drainage system:
1 – clarifying working-reservoir #3; *2* – clarifying working-reservoir #4; *3* – drain sump #1; *4* – drain sump #2;
5 – design clarifying working-reservoir #5*; 6* – design clarifying working-reservoir #6; *7* – bulkheads; *8* – slurry clarifier

The greatest damage to the metal from contact with mechanical impurities was observed in sites of corrosion, developed on the surfaces of the groove seal parts in the form of local spots (Fig. 4). The corrosion film formed on the parts surfaces is very sensitive to abrasion by mechanical impurities [13].

To a lesser extent, adhesive damage was observed in the failed groove seals. This damage manifested itself in a decrease of the thickness of the impellers collars and sealing rings partially or on the whole surface due to the rubbing of parts against each other (Fig. 5, *a*, *b*). This type of wear is a natural result of critical axial displacement of the rotor in the examined section pumps. This can be caused by the uneven distribution of pressure in the side grooves of the stages due to reaching the limit wear of the groove seals in the hydroabrasive-corrosive working medium. It should be noted that this type of mechanical wear in the section pumps liquid end parts usually indicates an emergency condition of the pumping equipment.

No cavitation wear of groove seals of the inspected pumps was observed. This is explained by their operation with the suction line back pressure. The back pressure ensures that the pump inlet pressure is higher than atmospheric, thus hindering cavitation phenomena development.

The visual inspections of the failed groove seals evidenced that hydroabrasive wear was the prevailing type of their surface wear. This wear was more intensively manifested at the spots of corrosion film formation.

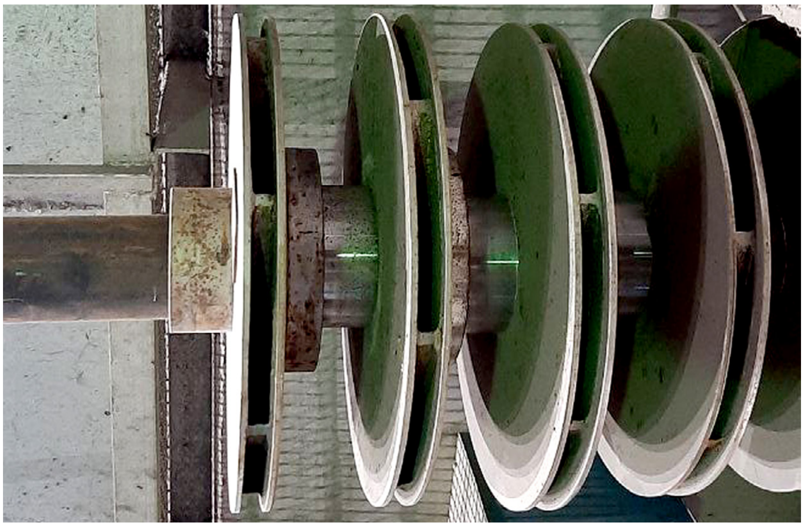

a

b

c

Fig. 3. Hydroabrasive wear of the impeller groove seals:
a – impeller collars; *b*, *c* – sealing rings

Fig. 4. Corrosion film on the surface of the worn impeller collar

Fig. 5. Adhesion wear of impeller grooves and disks

Study of wear of underground diamond mines' section pumps

The overhaul periodicity of section pumps, depending on the intensity of hydroabrasive-corrosion wear of the groove seals surfaces for a given period of time, is conditioned by the effect of the following internal and external environment factors:

- Factors responsible for the abrasive flow velocity: *section pump nominal delivery* X_1 *and delivery head* X_2, *electric motor nominal speed* X_3, *nominal diameter of the impeller groove* X_4, *nominal radial clearance in the groove seals* X_5;
- Factors responsible for the physical-and-mechanical characteristics of the mine water solid phase: *average concentration of mechanical impurities* X_6, *nominal diameter of an abrasive particle* X_7, *its hardness* X_8, *and density* X_9;
- Factors responsible for the mechanical impurities abrasion resistance of the part surfaces: *metal nominal hardness* X_{10}, *averaged mineralization* X_{11}, and averaged mine water pH X_{12}.

The author selected the most significant factors based on the theoretical principles of fluid pumping, hydrogeological conditions of kimberlite ores underground development, and failures of the examined section pumps.

X_1 and X_2 factors were selected from the first group of factors for further study of the hydroabrasive-corrosion wear. The selection of the X_1 factor was due to the fact that it is the best-known parameter which characterizes the kinematics of water movement in a pump liquid end. In addition, in accordance with the theory of hydrotransport, the factor can be considered as a function of the design parameters of the pumps, affecting the speed of the pumped flow, i.e., X_3–X_5 factors. It is for this reason that the above three factors were not taken into account in the further research. X_3 factor exclusion was also due to its value in most of the section pumps in the Company's underground mines was the same, at rated 1.450 rpm.

X_2 factor selection was based on the findings of the visual inspections of the pumps' groove seals. The visual inspections of the section pumps showed that in most cases the hydroabrasive wear of groove seals of the pump stages was almost the same. Theoretically the mechanical impurities have the greatest adverse impact on the parts of the initial stages due to their sharp angular shape. This shape becomes more rounded as they move from the first stage to the last. At the same time the rounded solid particles (grains) in the final stages move at greater fluid pressure compared to the sharp grains in the initial stages. Thus, the impact on a metal of a rounded particle in the higher pressure zones should be compared to its initial sharp shape impact.

From the second group of factors, only X_6 factor was selected. With regard to the other physical and mechanical characteristics of the solid phase in mine water pumped from underground kimberlite mines (the other factors of the group), their values are almost the same. It is for this reason that these factors were not considered in the further studies.

The liquid end parts of the section pumps operating in the Company's underground mines' drainage systems are mainly corrosion-resistant. Evidence of this is their identical operating characteristics, including the steel strength properties. For this reason X_{10} factor was excluded from consideration. Practice shows that mine water pumped from underground diamond mines in terms of its chemical activity to metal is either slightly alkaline or slightly acid brine, depending on the specific mine. Based on the above information, X_{11} and X_{12} factors were selected from the third group of factors.

The performed review and analysis allowed stating the average overhaul life of section pumps T can be represented as a function of the following five factors selected:

$$T = f(X_1, X_2, X_6, X_{11}, X_{12}). \quad (1)$$

The impact of each of the selected factors was determined by means of statistical research.

Statistical studies on the selected factors impact on the frequency of section pumps overhauls

The statistical studies to assess the impact of the selected factors on the T indicator were performed as follows. The weighted average values of the parameters (see formula (1)) were entered into MS Excel spreadsheets, which subsequently formed the correlation fields. Equations of linear regression and their confidence parameters were determined by linear-trend approximation (Fig. 6, *a*–*e*). Then we checked the equations for adequacy on the basis of Fisher's ratio test (F-test) at the confidence level g = 0.05 in the Data Analysis software package.

The confidence factors of the regression equations obtained testified that the T value was mainly governed by X_2 and X_6 factors. These correlation and regression analysis findings are adequate, since the F-significance parameter values in both cases amounted to 0.03. Thus, the studies have confirmed the adverse impact of the mine water solid phase on the frequency of overhaul life of section pumps in the Company's underground mines.

Although the values of the confidence factors of the regression equations where X_{11} and X_{12} factors are function arguments are not very high, it is clear that both these factors also have certain effects on the overhaul life of the Company's underground mines' pumping equipment.

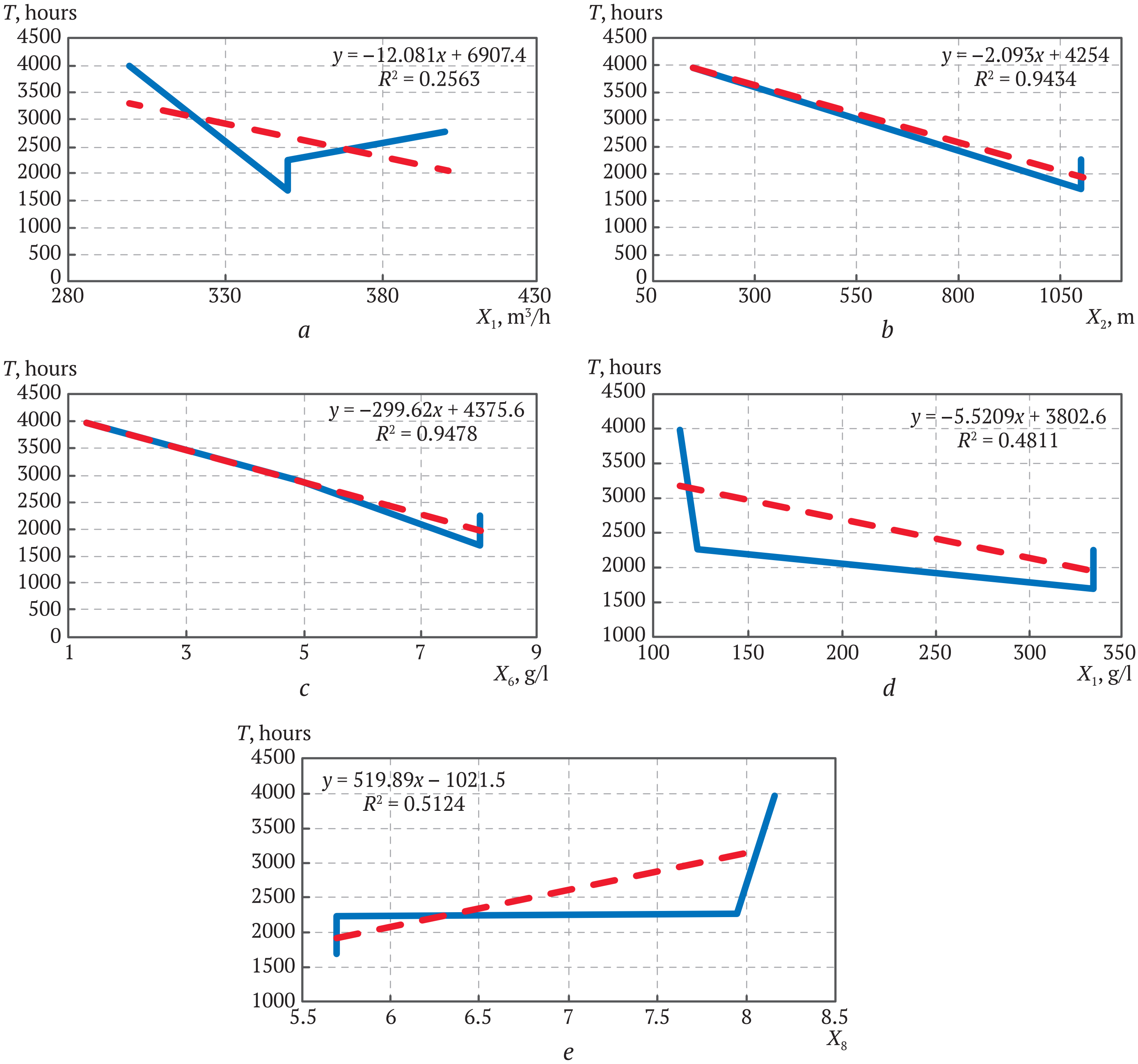

Fig. 6. Average overhaul life of section pumps as a function of rated pump delivery (*a*), rated pressure head (*b*), averaged concentration of mechanical impurities (*c*), averaged mineralization (*d*), and averaged mine water pH (*e*)

It is interesting that the average overhaul life T_r of the section pumps, used in the main drainage system of the Udachny underground mine, decreased to 1625 h, while X_6 factor increased more than two times (from 7 to 17 g/l) (Fig. 7, *a*). At the same time, evaluation by means of the formula obtained from the statistical research (see Fig. 6, *c*), at X_6 = 14 g/l, gave the projected overhaul life value below 200 hours (Fig. 7, *b*).

Due to such inconsistency in the results of the studies, the author conducted additional research.

Reasons for the difference between the actual and evaluated values of the average overhaul life of pumping equipment depending on the concentration of mechanical impurities in mine water

One of the criteria for the removal of a section pump for overhaul is a considerable decrease of its delivery rate (by 30% of the nominal value and more) as a result of increasing the annular slot.

Evaluations (Fig. 8) using the technique described in [14] showed that radial clearance (h) in the section pump groove seals increased by more than 1 mm, their lower limit at operating time *t* of 2250 h, X_6 = 7 g/l; at operating time *t* of 1750 h, X_6 = 9 g/l; at operating time t of 1000 h, X_6 = 16–17 g/l. It should be recalled that the initial radial clearance in the groove seals of the Udachny underground mine's section pumps was about 0.65 mm.

The difference between the actual and evaluated values of the pumping equipment average overhaul life proved to be particularly strong when X_6 = 16–17 g/l.

Thorough analysis of the Udachny underground mine's main drainage pumps operating practice showed that the actual value of Tr parameter did not sufficiently decrease at X_6 = 16–17 g/l when a pump was removed for overhaul after reaching the lower delivery rate *Q* as compared with the previous years (Fig. 9, *a*). Fig. 9, *b* demonstrates that parameters *Q* and T_r are strongly correlated with each other, as indicated by the resulting confidence factor.

The Company argued that the reduction of the delivery rate *Q* in the period of 2019–2021 was due to the need to prevent an excessive number of overhauls of pumps in connection with significant increase in X_6 factor. The correlation and regression analysis showed the strong correlation between the above-mentioned parameters (Fig. 10).

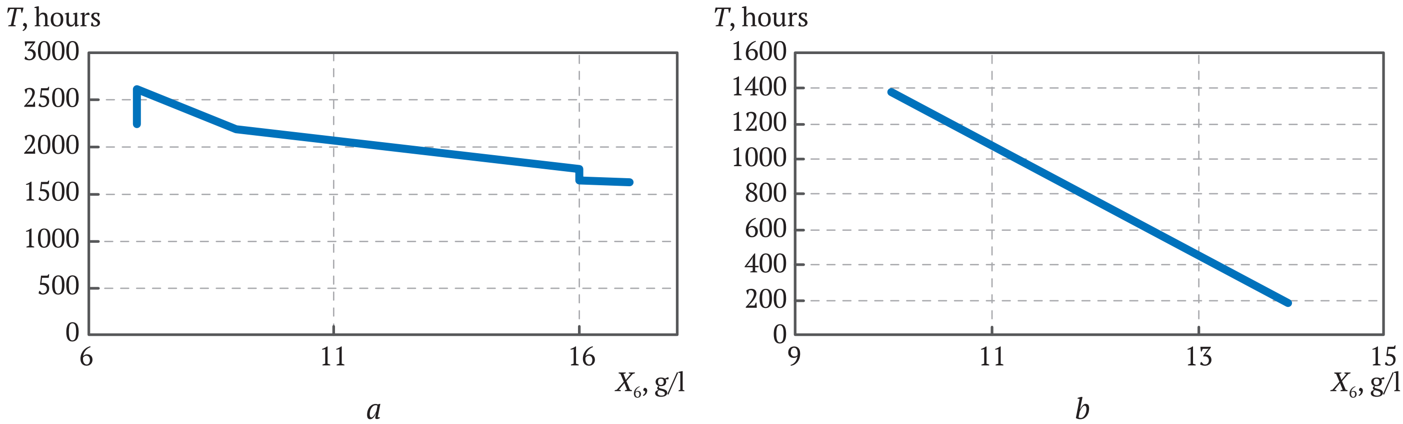

Fig. 7. Comparison of actual (*a*) and evaluated (*b*) values of overhaul life depending on the concentration of mechanical impurities in mine water

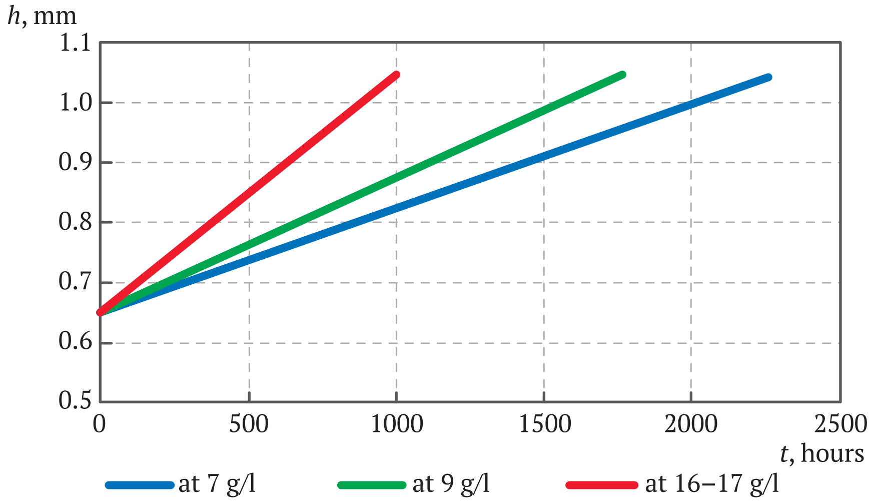

Fig. 8. Radial clearance in groove seals depending on section pump running time

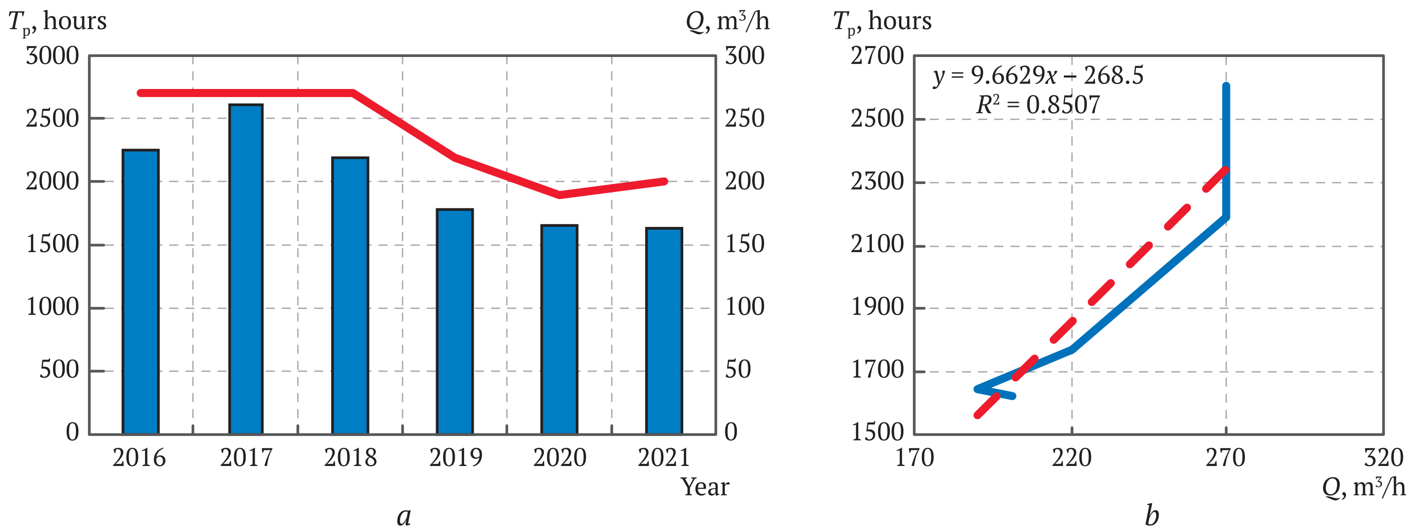

Fig. 9. Time history of section pump average overhaul life and its delivery rate at the moment of pump taking-down for overhaul by year (*a*) and dependence between these parameters (*b*)

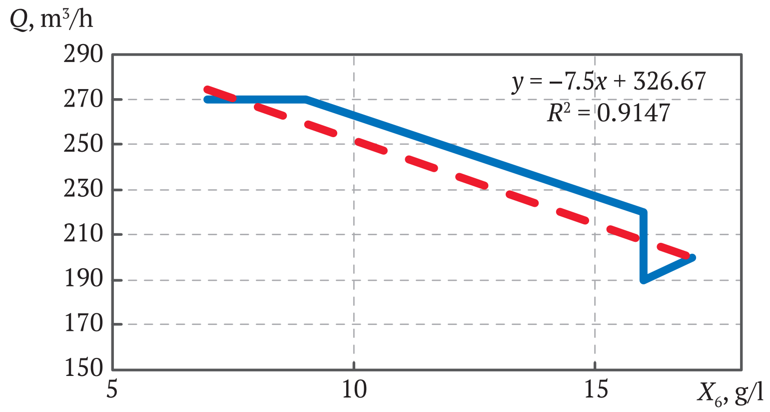

Fig. 10. Section pump delivery rate at the moment of taking-down it for overhaul as a function of averaged concentration of mechanical impurities in mine water

Thus, the overhaul life of the main drainage's section pumps can be calculated as a linear function of their delivery rates at the moment of removal for overhaul. This function is confidently described by empirical expression $Q = -7.5X_6 + 326.67$.

Assessment of energy performance of section pumps when pumping abrasive mine water flow

The laboratory research (Fig. 11, *a*) undertaken according to the technique described in [15] showed that power consumed by centrifugal one-stage pump *P* decreases smoothly, at a rate of 13 %, with a considerable decrease in pump delivery *Q* (by 26 %) due to the liquid end parts wear. At the same time Fig. 11, *b* demonstrates that such a decrease in the delivery rate *Q* is accompanied by significant drop in the pressure head *H*.

In turn, the section pump delivery rate drop by 20–23 % from its nominal value due to intensive wear of groove seals leads to the drop of consumed power by 6.5 % (Fig. 12, *a*). Such a smooth decrease of the power consumed by the section pump at different delivery rates as compared with the single-stage pump can be explained by the relative stability of the pressure head value (997–1008 m). This is caused by the low wear of impeller blades, responsible for the developed delivery rate and pressure, in connection with small size of the pumped solid particles (Fig. 12, *b*). The bulk of mechanical impurities (80–85 %) is represented by −0.05 mm size class.

According to [16] the quantity of mechanical impurities ε, contacting with impeller blades of centrifugal pump, directly depends on their size *d*:

$$\varepsilon = 0.4\sqrt{\frac{0.75}{1 + 0.35 \cdot \frac{\rho_{sol}}{\Delta\rho} \cdot \frac{D}{d}}}, \tag{2}$$

where ρ_{sol} – is density of the mechanical impurities, $\Delta\rho$ – is difference of densities of the mechanical impurities and pure water, D – is impeller diameter, d – is size of solid particle.

In other words, the smallest solid particles are carried away by mine water flow, and do not comeinto contact with impeller blades.

Thus, the pumping of mine water by means of section pumps with worn-out groove seals takes considerably more time when compared with a new or overhauled pump, while its consumed power decreases only slightly. This ultimately leads to significant total increase in power consumption. All this testifies to inexpediency of long-term operation of section pumps at low delivery rates in terms of energy performance.

Findings Discussion

Our research confirmed the adverse impact of intense hydroabrasive wear on the groove seals upon the performance of the section pumps. Fig. 13 shows that the impact of X_6 factor on the total costs in the main cost items S (overhaul and consumed power costs) of the section pumps of the drainage facility can be confidently described by the following empirical expression: $S = 7.6835X_6 + 49.577$. This expression shows that a reduction in the concentration of mechanical impurities in mine water from 17 to 4 g/l leads to a reduction in

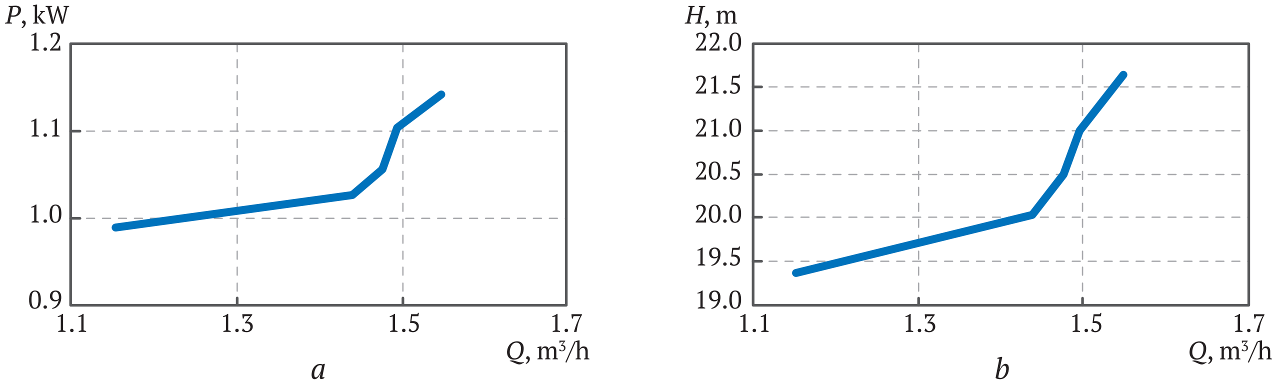

Fig. 11. Consumed power (*a*) and pressure head (*b*) as a functions of a single-stage pump delivery rate

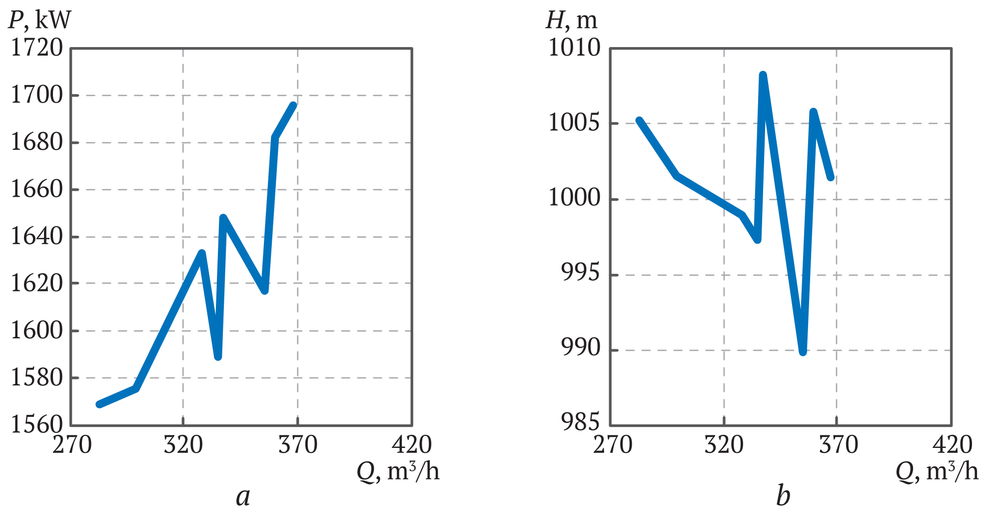

Fig. 12. Consumed power (*a*) and pressure head (*b*) as a functions of a section pump delivery rate

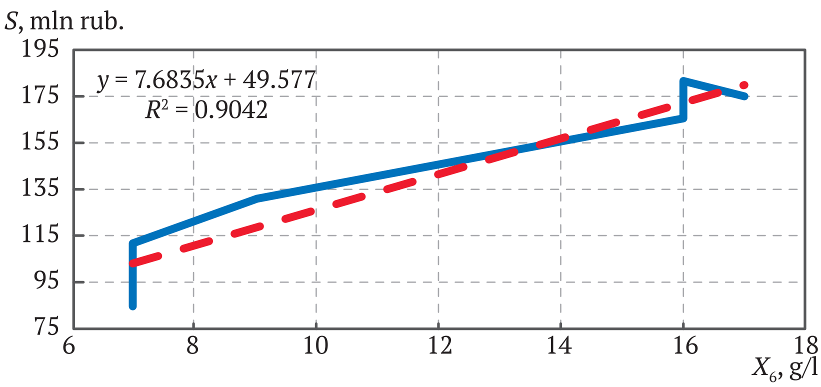

Fig. 13. Total pumping equipment overhaul costs and power consumption as the functions of averaged concentration of mechanical impurities in mine water

the annual operating cost of the Udachny mine's main drainage pumps by 100 million rubles.

Taking into account the expected economic effect of reducing solid phase concentration in mine waters, the capital investments of 340 mln rubles in sinking two design clarifying working-reservoirs will be repaid for less than 3.5 years.

Conclusion

In view of the above the following key conclusions were drawn:

1. The overhaul life of the Udachny underground mine's main drainage section pumps can be evaluated as a linear function of their delivery rates at the moment of their removal for overhaul. This function can be reliably described by the empirical expression $Q = -7.5X_6 + 326.67$, where X_6 is the averaged mechanical impurities concentration in the mine water.

2. Reducing the section pump delivery rate by 20–23 % of its nominal value due to intensive wear of groove seals leads to a drop in consumed power by 6.5 %. The smooth decrease in power consumed by the section pump different delivery rates is due to the relative stability of the pressure head value (997–1008 m). This is caused by low wear of impeller blades due to small size of the bulk of pumped solid particles (−0.05 mm size class).

3. The evaluation showed that a reduction in the concentration of mechanical impurities in mine water from 17 to 4 g/l leads to a reduction in the annual operating costs of the Udachny underground mine's main drainage section pumps by 100 million rubles. Thus, the payback period for sinking two design clarifying working-reservoirs aimed at achieving a significant reduction in solid phase concentration in mine waters will be less than 3.5 years.

References

1. Ovchinnikov N.P., Zyryanov I.V. Assessment of durability of sectional pumps in underground kimberlite mines of ALROSA. *Gornyi Zhurnal*. 2017;(10):41–44. (In Russ.) https://doi.org/10.17580/gzh.2017.10.08

2. Ovchinnikov N.P. Problems of operation of electric pumping sectional type units on kimberlite mines of Alrosa and the ways of their solution. *Bulletin of the Tomsk Polytechnic University. Geo Assets Engineering*. 2018;329(6):66–73. (In Russ.) URL: http://izvestiya.tpu.ru/archive/article/view/2046

3. Dolganov A.V. The influence of hydro-abrasive depreciation of excretory elements on ex-ploitation qualities of rotary pumps at copper and pyrites pits. *Mining Informational and Analytical Bulletin*. 2015;(8):181–186. (In Russ.)

4. Shen Z., Li R., Han W., Quan H. Erosion wear in impeller of double-suction centrifugal pump due to sediment flow. *Journal of Applied Fluid Mechanics*. 2020;13(4):1131–1142. https://doi.org/10.36884/jafm.13.04.30907

5. Serrano R., Santos L., Viana E., Martinez C.B. Case study: Effects of sediment concentration on the wear of fluvial water pump impellers on Brazil's Acre River. *Wear*. 2018;408–409:131–137. https://doi.org/10.1016/j.wear.2018.04.018

6. Palamarchuk N., Timokhina V.J., Palamarchuk T.N. Causes of unsatisfactory operation of the automatic balancing devices of centrifugal high-pressure pumps. *Sbornik nauchnykh trudov Donetskogo instituta zheleznodorozhnogo transporta*. 2016;(42):65–71. (In Russ.)

7. Borodkin N.N., Palamarchuk T.N., Zakharov V.A. Selection and calculation of the basic modes of the parameters of centrifugal pumps to determine the initial stage of cavitation. *Sbornik nauchnykh trudov Donetskogo instituta zheleznodorozhnogo transporta*. 2016;(42):65–71. (In Russ.)

8. Timohin J.W., Palamarchuk T.N. The research results of the axial forces of the rotor and automatic settings. *Sbornik nauchnykh trudov Donetskogo instituta zheleznodorozhnogo transporta*. 2017;(45):32–42. (In Russ.)

9. Dolganov A.., Islentyev A.O., Toropov E.Yu., Churakov E.O. Analysis of effectiveness of dumping devices of mine centrifugal sectional pumps. *News of the Ural State Mining University*. 2014;(2):31–35. (In Russ.) URL: http://www.iuggu.ru/download/2014-2-Dolganov.pdf

10. Dolganov A.V., Timukhin S.A. *Hydroabrasive wear of mine drainage pumps*. Monograph. Moscow: Publishing House of Academy of Natural Sciences; 2016. 180 p. (In Russ.)

11. Sosnovskii S.V., Sel'kin V.P. Effect of transfer medium on wear rate of groove seals of centrifugal pumps. *Journal of Friction and Wear*. 2013;34(2):134–136. (Orig. ver.: Sosnovskii S.V., Sel'kin V.P. Effect of transfer medium on wear rate of groove seals of centrifugal pumps. *Treniye i iznos*. 2013;34(2):171–174. (In Russ.)

12. Ostrovskij V.G., Pesherenko S.N. Calculations of the rate hydroabrasive wear interstage seal oil pump. *Perm Journal of Petroleum and Mining Engineering*. 2012;(5):70–75. (In Russ.) URL: https://ered.pstu.ru/index.php/geo/article/view/1072/553

13. Ostrovsky V.G., Pescherenko S.N. Test bench simulation of corrosion-abrasive disruption of oil pumps guide apparatuses. *Nauchnye Issledovaniya i Innovatsii*. 2010;4(1):86–88. (In Russ.)

14. Litvinenko K.V. *Forecasting ESP technical condition under intensive removal of mechanical impurities*. [Ph.D. thesis in Engineering Science]. Yekaterinburg: Ufa State Oil Technical University; 2016. 24 p. (In Russ.)

15. Ovchinnikov N.P., Vikulov M.A., Bochkarev Yu.S., Dovidenko G. P. Experimental studies of operating properties of pumping unit with worn impeller. *Gornyi Zhurnal*. (In Russ.) 2016;9:61–65. https://doi.org/10.17580/gzh.2016.09.17

16. Menshikov S.S. Improving operating efficiency of suction dredges under conditions of hydroabrasive wear. [Ph.D. thesis in Engineering Science]. St. Petersburg: “Gorny” National Mineral Resource University; 2014. 20 p. (In Russ.)

Information about the author

Nickolay P. Ovchinnikov – Cand. Sci. (Eng.), Associate Professor, Director of the Mining Institute, M.K. Ammosov North-Eastern Federal University, Yakutsk, Russian Federation; ORCID 0000-0002-4355-5028, Scopus ID 57191629443; e-mail ovchinnlar1986@mail.ru

Received 11.01.2022
Revised 22.01.2022
Accepted 01.05.2022

MINING MACHINERY, TRANSPORT, AND MECHANICAL ENGINEERING

Research article

https://doi.org/10.17073/2500-0632-2022-2-161-169

Simulation of loads on operating device of peat-cutting unit with regard to errors in the cutting elements arrangement

K.V. Fomin

Tver State Technical University, Tver, Russian Federation

✉ *fomin_tver@mail.ru*

Abstract

The practice of using units with milling-type operating devices showed their insufficient reliability, which leads to deterioration of the units' performance. The reasons for this are high dynamic loads in structural members, which are caused by external resistance forces on a milling cutter. They have random, sharply variable nature due to structural heterogeneity of a peat deposit, its random physical and mechanical properties, the presence of wood inclusions in it, as well as periodic interaction of blades with the deposit, and many other factors. In this case, the parameters of actual milling cutter, due to manufacturing and installation errors, differ from those specified in the "ideal" design. In addition, wear and irreversible deformations of cutting elements (blades) occur during operation. As a result the position of blades in a cutter body differs from the "ideal" positioning pattern. The purpose of the paper is to develop a model of section moment on a milling cutter when interacting with a peat deposit in the process of technological operations, taking into account the influence of the error of blade positioning on a cutter body. Expressions for calculating the moment spectral density were obtained. Its characteristic features were analyzed. Errors in positioning of cutting elements on a cutter body lead to changes in the magnitude and nature of the load and its frequency content. In this case, new, additional components appear at frequencies multiple of the cutter's angular velocity, enriching the load spectrum and increasing its variance. Their magnitude is determined by the cumulative value of the errors. As an example, an analysis of the influence of the error in positioning cutting elements on the spectral density for the operating device of MTP-42 deep milling machine is given. The study results are of practical value and should be taken into account in the calculation of dynamic loads in designing structural members of milling units, especially if their operating devices have a large number of blades, use fine feeds, and when the natural frequencies of the structural members are equal to or multiple of the angular speed of a milling cutter.

Keywords

peat milling unit, milling cutter, blade positioning errors, probabilistic load model, section moment, spectral density

For citation

Fomin K.V. Simulation of loads on operating device of peat-cutting unit with regard to errors in the cutting elements arrangement. *Mining Science and Technology* (*Russia*). 2022;7(2):161–169. https://doi.org/10.17073/2500-0632-2022-2-161-169

ГОРНЫЕ МАШИНЫ, ТРАНСПОРТ И МАШИНОСТРОЕНИЕ

Научная статья

Моделирование нагрузок на рабочем органе торфяного фрезерующего агрегата с учетом погрешности расстановки режущих элементов

К.В. Фомин

Тверской государственный технический университет, г. Тверь, Российская Федерация

✉ *fomin_tver@mail.ru*

Аннотация

Практика использования машин с исполнительными органами фрезерного типа показывает их недостаточную надежность, что приводит к ухудшению технико-экономических характеристик агрегатов. Причиной этого являются высокие динамические нагрузки в элементах конструкции, которые возникают в результате действия сил внешнего сопротивления на фрезе. Они имеют случайный, резко переменный характер, который вызван структурной неоднородностью торфяной залежи, ее случайными физико-механическими свойствами, наличием в ней древесных включений, а также периодическим взаимодействием ножей с залежью и многими другими факторами. При этом параметры реальной конструкции фрезы ввиду погрешностей изготовления и сборки отличаются от заданных при проектировании. Кроме того, в процессе эксплуатации происходят износ и необратимые деформации режущих элементов. Это приводит к тому, что ножи расположены с некоторым небольшим сдвигом на корпусе фрезы относительно «идеальной» схемы размещения. Цель статьи заключается в разработке модели момента сопротивления на фрезе при взаимодействии с торфяной залежью в процессе выполнения технологической операции, учитывающей влияние погрешности расстановки ножей на корпусе фрезы. Получены выражения для расчета спектральной плотности момента. Проанализированы его характерные особенности. Ошибки размещения режущих элементов на корпусе фрезы приводят к изменению величины и характера нагрузки, ее частотного состава. При этом появляются новые, дополнительные составляющие на частотах, кратных угловой скорости фрезы, обогащая спектр нагрузки, увеличивая ее дисперсию. Их величина определяется суммарным значением ошибок. В качестве примера дан анализ влияния погрешности расположения режущих элементов на спектральную плотность для исполнительного органа машины глубокого фрезерования типа МТП-42. Результаты исследования имеют практическую ценность и должны учитываться при расчете динамических нагрузок в элементах конструкции фрезерующих агрегатов при их проектировании, особенно если рабочие органы имеют большое количество резцов, используют малые подачи и когда собственные частоты элементов конструкции агрегата равны или кратны угловой скорости фрезы.

Ключевые слова
торфяной фрезерующий агрегат, фреза, ошибки расстановки ножей, вероятностная модель нагрузки, момент сопротивления, спектральная плотность

Для цитирования
Fomin K.V. Simulation of loads on operating device of peat-cutting unit with regard to errors in the cutting elements arrangement. *Mining Science and Technology* (*Russia*). 2022;7(2):161–169. https://doi.org/10.17073/2500-0632-2022-2-161-169

Introduction

The use of milling units in peat industry allows increasing productivity and improving the quality of process operations and provides the possibility of their integrated mechanization [1–3].

The practice of using machines with milling type executive bodies showed their insufficient reliability [4, 5]. The reasons for this are high dynamic loads in the structural elements, which result from the action of external resistance forces on a milling cutter [5]. They have random, sharply variable nature [5] due to structural heterogeneity of a peat deposit [6, 7], its random physical and mechanical properties, the presence of wood inclusions in it [5–7], as well as periodic interaction of blades with the deposit, and many other factors [5].

At present, to calculate loads on operating devices, simulation modelling methods using computer technology are used (N.M. Karavaeva, O.A. Golovnina, V.F. Sinitsyn, F.A. Shestachenko) [5]. They are universal, but time-consuming in solving these problems.

The application of experimental methods by means of strain-measuring facilities [8] makes it possible to obtain information about forces and moments and their probabilistic characteristics. However, they are labor-intensive, expensive, and provide information about the load only for a given milling unit in specific operating conditions.

In [5, 9], analytical methods of investigating loading moments on milling-type operating devices were developed. Models of force factors in their interaction with a peat deposit were proposed. Expressions for calculating spectral densities were developed. They take into account the design of a milling cutter, the unit operating modes and the physical and mechanical properties of peat. In [10], approaches for determining mutual spectral moment densities for milling units with several operating devices are considered.

In this case, all the dependences were obtained for an "ideal" operating device, when cutting elements (blades) are positioned in the specified points on the milling body in line with design documentation.

It should be taken into account that the parameters of an actual operating device differ from the design ones due to assembly and manufacturing errors [11, 12]. As a result the position of blades in a cutter body differs from the "ideal" positioning pattern. In addition, wear and irreversible deformations, and even destruction of the cutting elements occur during operation. In this regard, cutting angles, the shape of cutters, their height, the position of cutting edges, and the kinematic characteristics of cutting change [11–13]. This all, in fact, changes both the arrangement of cutting elements (blades) and the conditions of blades interaction with a peat deposit. This causes changes in the magnitudes, nature and frequency properties of the force factors on an operating device and affects the formation of loads in the unit structural members.

Research objectives

The purpose of the paper is to develop models of the formation of loads on an operating device when milling a peat deposit taking into account the influence of errors in blade arrangement on a cutter body and expressions for calculating the moment spectral density.

Research materials, models and methods

The random nature of the section moment arising on an operating device in the process of operation requires the use of approaches of statistical dynamics of mechanical systems [14–16] for analyzing loading of a milling unit and calculating its reliability indicators [16, 17].

The experience of their use in solving similar problems in mining industry [18–20] allows considering one-dimensional and two-dimensional characteristics of loads only when using both analytical and numerical methods [21, 22].

As a rule, probabilistic characteristics of forces and moments, such as mathematical expectation, dispersion and spectral density, are considered [20, 22].

Let us consider a milling cutter with working width B, radius R_Φ, rmilling depth H_Φ, horizontal rotation axis with M cutting planes and K blades in plane.

Position of blades on a milling cutter body is determined by the angles between the reference point and blades in the m-th cutting plane φ_m (an "ideal" operating device) and the angles between neighboring blades in a plane φ_T (in case of uniform arrangement). We will take into account that each cutting element (blade) can be shifted by the value of the error determined by the angle δ_{mk} relative to the "ideal" arrangement of blades (Fig. 1). When a blade is shifted in the direction of blade movement, the magnitude of error has "plus" sign, while in the opposite direction, "minus" sign.

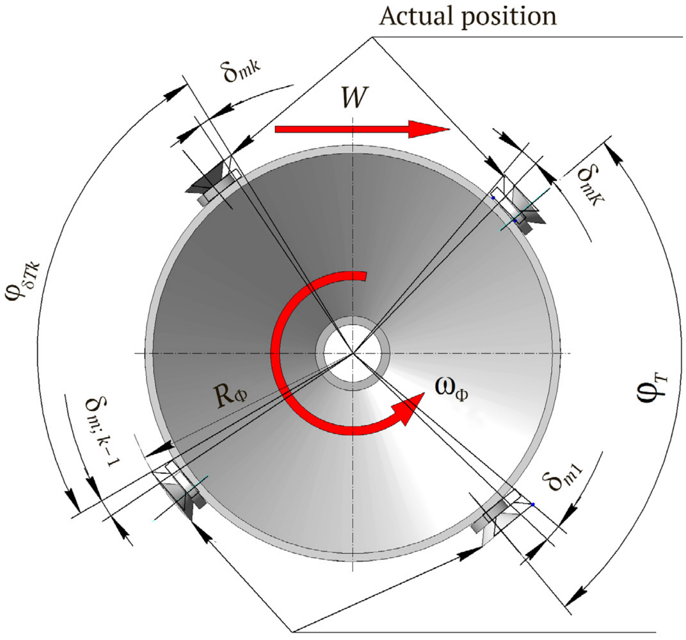

Fig. 1. Error in blades positioning by angle in m-th cutting plane

If a unit depth of milling, operation modes and physical and mechanical characteristics of a peat deposit change rather smoothly during several revolutions of an operating device, so that within one revolution they can be considered to be constant [5, 9], the section moment is described by the following expression:

$$M(t) = \sum_{m=1}^{M} \sum_{n=-\infty}^{\infty} M_{mn}(t - t_m - nT_\Phi; P_{mn}), \qquad (1)$$

where $M_{mn}(t;\, P_{mn})$ – is moment on blades of the m-th cutting plane during one revolution of the operating device; t_m – is time interval between the reference point and the load in the m-th cutting plane $t_m = \varphi_m / \omega_\Phi$; T_Φ – is duration of one revolution $T_\Phi = 2\pi / \omega_\Phi$, where ω_Φ – is angular velocity of the milling cutter; P_{mn} – is random parameters of pulses at the n-th revolution of the operating device in the m-th cutting plane.

Expression (1) can be used to describe the section moment both for an "ideal" operating device and an actual one (taking into account errors of blade positioning on the cutter body). The values of $M_{mn}(t;\, P_{mn})$ will be different in this case.

The amplitude value of the section moment is proportional to the feed [2], the value of which for the "ideal operating device" is $c = W\varphi_T / \omega_\Phi$, and taking into account the blade arrangement error:

$$c_k = W\frac{\varphi_{\delta Tk}}{\omega_\Phi} = W\frac{\varphi_T + \Delta\delta_{mk}}{\omega_\Phi},$$

where W – is speed of advance of a milling unit; $\varphi_{\delta Tk}$ – is angle between the blades in the cutting plane (more precisely between the cutting edges), taking into account the error of their positioning on the milling cutter body (Fig. 1); $\Delta\delta_{mk} = \delta_{mk} - \delta_{m;\,k-1}$ – is the difference between the errors for the adjacent blades in the m-th plane (if $k = 1$, then $k - 1$ corresponds to K).

Correspondingly, for the moment in the m-th cutting plane within one revolution, taking into account the errors of the blades arrangement, the expression takes the following form:

$$M_{mn}(t;P) = \sum_{k=1}^{K} \frac{\varphi_T + \Delta\delta_{mk}}{\varphi_T} M_0\left[t - (k-1)T - \tau_{mk}; P_{mn}\right],$$

where $M_0(t;\, P)$ – is the change of section moment on a blade within the angle of contact with a deposit; $T = \varphi_T / \omega_\Phi$ – is the period of repetition of the interaction of blades in the cutting plane with a deposit; $\tau_{mk} = \delta_{mk} / \omega_\Phi$ – is pulse time delay caused by the error of the k-th blade position in the m-th cutting plane.

Moment (1) is a random function. Its spectral density depends on a milling cutter design, the unit operation modes, the milling depth, which is determined by the terrain and the type of the cutter suspension, the oscillations caused by cutting forces and their imbalance, physical and mechanical properties of the peat deposit and their probabilistic characteristics [5, 9].

The spectral density of the process (1) can be determined from the following relation [23, 24]:

$$S(\omega) = \lim_{N\to\infty} \frac{2}{(2N+1)T} m_1 \left\{ \left| Z^{(k)}(j\omega) \right|^2 \right\} - 2\pi m^2 \delta(\omega), \quad (2)$$

where N – is number of pulses; T is repetition period; $m_1\{\}$ – is averaging sign; $Z^{(k)}(j\omega)$ – spectrum of the k-th implementation of the process (we omit index k hereafter); m is mean value of the process; $\delta(\omega)$ – is delta-function (Dirac function) [24].

Squared absolute value of the section moment spectrum (1) containing $(2N + 1)$ pulses is:

$$\begin{aligned} &\left| Z_M(j\omega) \right|^2 = \\ &= \sum_{m=1}^{M}\sum_{l=1}^{M}\sum_{k=1}^{K}\sum_{s=1}^{K}\sum_{n=-N}^{N}\sum_{i=-N}^{N} S_0(\omega;\, \omega_\Phi; P_{mkn}) S_0^*(\omega; \omega_\Phi; P_{lsi}) \times \\ &\times \frac{\varphi_T + \Delta\delta_{mk}}{\varphi_T} \frac{\varphi_T + \Delta\delta_{ls}}{\varphi_T} \times \\ &\times \exp\left[-j\frac{\omega}{\omega_\Phi}(\varphi_m - \varphi_l) \right] \exp\left[-j\frac{\omega}{\omega_\Phi}(k-s)\varphi_T \right] \times \\ &\times \exp\left[-j\frac{\omega}{\omega_\Phi}(\delta_{mk} - \delta_{ls}) \right] \exp\left[-j\frac{\omega}{\omega_\Phi} 2\pi(n-i) \right], \end{aligned} \quad (3)$$

where the asterisk denotes complex conjugate value; $S_0(\omega;\, \omega_\Phi;\, P)$ – is spectrum $M_0(t;\, P)$:

$$S_0(j\omega; \omega_\Phi; P) = \int_0^{\varphi_k/\omega_\Phi} M_0(t; P) \exp(-j\omega t)\, dt,$$

where φ_k – is the angle of blade contact with peat deposit.

Substituting (3) into (2), considering stationarity of the unit operating conditions (the probabilistic characteristics of parameters depend on the mutual arrangement of pulses only $p = n - i$), using the approaches presented in [5, 9], we obtained an expression for single-sided spectral density of section moment taking into account the errors of cutting element positioning on a cutter body at fixed angular speed ω_Φ:

$$\begin{aligned} S(\omega;\, \omega_\Phi) = &\frac{4}{T_\Phi} \left[\frac{1}{2}\sum_{q=1}^{Q_1} \left[\frac{\partial^2 F_1(\omega;\, \omega_\Phi)}{\partial P_q^2} \right]_m D_q \sum_{m=1}^{M} \mathrm{A}_m(\omega;\, \omega_\Phi) - \right. \\ &- \frac{1}{2}\sum_{q=1}^{Q_2} \left[\frac{\partial^2 F_2(\omega;\, \omega_\Phi)}{\partial P_q^2} \right]_m D_q \sum_{m=1}^{M} \mathrm{A}_m(\omega;\, \omega_\Phi) + \Psi(\omega;\, \omega_\Phi) + \\ &+ \left(F_1(\omega;\, m_q) + \frac{1}{2}\sum_{q=1}^{Q_2} \left[\frac{\partial^2 F_2(\omega;\, \omega_\Phi)}{\partial P_q^2} \right]_m D_q \right) \times \\ &\left. \times \sum_{m=1}^{M}\sum_{l=1}^{M} \exp\left[-j\frac{\omega}{\omega_{\hat{o}}}(\varphi_m - \varphi_l) \right] \mathrm{A}_{ml}(\omega;\, \omega_\Phi)\, \omega_\Phi \sum_{r=1}^{\infty} \delta(\omega - r\omega_\Phi) \right], \end{aligned}$$

where the following notations are introduced:

$$F_1(\omega;\, \omega_\Phi) = \left| S_0(\omega;\, \omega_\Phi; P_{1mn} \ldots P_{Qmn}) \right|^2;$$

$$F_2(\omega;\, \omega_\Phi) = S_0(\omega;\, \omega_\Phi; P_{1mn} \ldots P_{Qmn}) S_0^*(\omega;\, \omega_\Phi; P_{1li} \ldots P_{Qli});$$

$$\mathrm{A}_m(\omega;\, \omega_\Phi) = \sum_{k=1}^{K}\sum_{s=1}^{K} \frac{\varphi_T + \Delta\delta_{mk}}{\varphi_T} \frac{\varphi_T + \Delta\delta_{ms}}{\varphi_T} \times$$

$$\times \exp\left[-j\frac{\omega}{\omega_\Phi}(\delta_{mk} - \delta_{ms}) \right] \exp\left[-j\frac{\omega}{\omega_\Phi}(k-s)\varphi_T \right];$$

$$\mathrm{A}_{ml}(\omega;\, \omega_\Phi) = \sum_{k=1}^{K}\sum_{s=1}^{K} \frac{\varphi_T + \Delta\delta_{mk}}{\varphi_T} \frac{\varphi_T + \Delta\delta_{ls}}{\varphi_T} \times$$

$$\times \exp\left[-j\frac{\omega}{\omega_\Phi}(\delta_{mk} - \delta_{ls}) \right] \exp\left[-j\frac{\omega}{\omega_\Phi}(k-s)\varphi_T \right];$$

Q_1, Q_2 – number of parameters for $F_1(\omega;\, \omega_\Phi;\, P)$ and $F_2(\omega;\, \omega_\Phi;\, P)$, respectively; D_q – is parameters dispersions; $\Psi(\omega;\, \omega_\Phi)$ – is correlational relationship function, taking into account correlations between uniform and different parameters of load pulses, varying both in the direction of unit motion and in a direction transverse to it:

$$\begin{aligned} \Psi(\omega;\, \omega_\Phi) = &\sum_{q<g} \left[\frac{\partial^2 F_1(\omega;\, \omega_\Phi)}{\partial P_q \partial P_g} \right]_m \sum_{m=1}^{M} K_{qg} \mathrm{A}_m(\omega; \omega_\Phi) + \\ &+ \sum_{q<g} \left[\frac{\partial^2 F_2(\omega;\, \omega_\Phi)}{\partial P_{\hat{q}m} \partial P_{gl}} \right]_m \sum_{m=1}^{M}\sum_{\substack{l=1 \\ m\neq l}}^{M} \exp\left[-j\frac{\omega}{\omega}(\varphi_m - \varphi_l) \right] K_{qgml} \mathrm{A}_{ml}(\omega;\, \omega_\Phi) + \\ &+ 2\sum_{q<g} \left[\frac{\partial^2 F_2(\omega;\, \omega_\Phi)}{\partial P_{qmn} \partial P_{gl;n-p}} \right]_m \sum_{m=1}^{M}\sum_{l=1}^{M} \mathrm{A}_{ml}(\omega;\, \omega_\Phi) \sum_{p=1}^{\infty} K_{qgmlp} \times \\ &\times \exp\left[-j\frac{\omega}{\omega_\Phi}(\varphi_m - \varphi_l) \right] \cos\left(\frac{\omega}{\omega_\Phi} 2\pi p \right), \end{aligned}$$

where m_q – are mathematical expectations of the pulse parameters: K_{qg}, K_{qgml}, K_{qgmlp} – correlation and cross-correlation moments of the parameters.

In the case of the parameters stationarity and smoothness of changes, the correlation and cross-correlation moments K_{qgml} and K_{qgmlp} are determined by correlation functions of peat characteristics and working conditions (peat strength, density, and milling depth) in the moments of interaction of blades with the peat:

$$K_{qgml} = K_{Pqsy}\left[(m-l)h \right];$$

$$K_{qgmlp} = K_{Pqsxy}\left[cp; (m-l)h \right],$$

where $K_{Pqsy}(y)$ – are correlation and cross-correlation functions of changes in the characteristics of peat deposit in a direction transverse to the unit movement; $K_{Pqsxy}(x,\, y)$ – are correlation functions of random parameters, taking into account spatial variability of characteristics (both in the direction of movement and in a direction transverse to it); x and y are point coordinates for the corresponding parameters; m, l – numbers of the corresponding cutting planes; h – distance between cutting planes.

Thus, for a milling cutter that has errors in the blade arrangement on the cutter body, new components of the section moment that are multiples of the angular velocity of the cutter rotation arise. While, for the “ideal” operating device, there are loads in the spectrum that are multiples of the recurrence period of the cutting elements interaction with peat deposit [9].

The findings of experimental study [5] confirm such qualitative description of the influence of the error in blades positioning on the cutter body on the frequency composition of resistance forces.

In the process of operation, as a result of the action of a random section moment on the operating device, a random change in the cutter’s angular velocity occurs. Taking this factor into account, spectral density can be described as follows:

$$S_M(\omega)=\int_{-\infty}^{\infty} S(\omega;\ \omega_\Phi)W(\omega_\Phi)d\omega_\Phi,$$

where $W(\omega_\Phi)$ – is ω_Φ distribution density.

Given that [23, 24]:

$$\int_{-\infty}^{\infty} f(x)\delta(cx-x_0)dx=\frac{1}{|c|}f\left(\frac{x_0}{c}\right),$$

for $S_M(\omega)$ we get:

$$S_M(\omega)=\frac{4}{T_\Phi}\times$$
$$\times\left[\frac{1}{2}\sum_{q=1}^{Q_1}\sum_{m=1}^{M}G_{1qm}(\omega)D_q-\sum_{q=1}^{Q_2}\sum_{m=1}^{M}G_{2qm}(\omega)D_q+G_3(\omega;\ \omega_\Phi)+\right.$$
$$+\sum_{r=1}^{R}\left(F_1(r;\ m_q)+\frac{1}{2}\sum_{q=1}^{Q_2}\left[\frac{\partial^2 F_2(r;\ P)}{\partial P_q^2}\right]_m D_q\right)\times \tag{4}$$
$$\left.\times\sum_{m=1}^{M}\sum_{l=1}^{M}\exp\left[-jr(\varphi_m-\varphi_l)\right]\mathrm{A}_{ml}(r)\frac{\omega}{r^2}W\left(\frac{\omega}{r}\right)\right].$$

We introduced the following notations in expression (4):

$$T_\Phi=\frac{2\pi}{\int_{-\infty}^{\infty}\omega_\Phi W(\omega_\Phi)d\omega_\Phi};$$

$$G_{1qm}(\omega)=\int_{-\infty}^{\infty}\left[\frac{\partial^2 F_1(\omega;\ \omega_\Phi)}{\partial P_q^2}\right]_m \mathrm{A}_m(\omega;\ \omega_\Phi)W(\omega_\Phi)d\omega_\Phi;$$

$$G_{2qm}(\omega)=\int_{-\infty}^{\infty}\left[\frac{\partial^2 F_2(\omega;\ \omega_\Phi)}{\partial P_q^2}\right]_m \mathrm{A}_m(\omega;\ \omega_\Phi)W(\omega_\Phi)d\omega_\Phi;$$

$$G_3(\omega)=\int_{-\infty}^{\infty}\Psi(\omega;\ \omega_\Phi)W(\omega_\Phi)d\omega_\Phi.$$

With no errors in positioning cutting elements, i.e. for an “ideal” operating device, taking into account the random change of the cutter angular velocity, we obtain the dependence for the moment spectral density, which is presented in [5, 9].

Expressions (4) give the possibility, at the stage of designing, to assess the influence of errors of cutting elements positioning on the cutter body on the moment spectral density. It presents the input data for analysis of dynamic loads in structural members of a milling unit [5, 14], calculation of reliability indicators [16, 17], and selection of optimal operating parameters and modes.

Analysis of research findings

As an example, let us consider the effect of blade positioning errors on the characteristics of the moment on executive body of a MTP-42 deep milling machine [2]. It is trailed to a T-130B tractor, includes a milling cutter, a drive system, a frame with an impact plate, rear and front rollers [2].

Taking into account that the deep milling machine has an impact plate, which rests on a peat deposit surface [2] and provides a constant milling depth, as well as considering the correlation relations for homogeneous pulse parameters only, we can obtain for spectral density from (4):

$$S_M(\omega)=\frac{4}{T_\Phi}\left[\frac{1}{2}\sum_{m=1}^{M}G_{1qm}(\omega)+G_3(\omega;\ \omega_\Phi)+\right.$$
$$+m_A^2\sum_{r=1}^{R}\left|S_e(r;\ m_q)\right|^2\times$$
$$\left.\times\sum_{m=1}^{M}\sum_{l=1}^{M}\exp\left[-jr(\varphi_m-\varphi_l)\right]\mathrm{A}_{ml}(r)\frac{\omega}{r^2}W\left(\frac{\omega}{r}\right)\right],$$

where:

$$G_{1qm}(\omega)=\int_{-\infty}^{\infty}\left|S_e(j\omega;\ \omega_\Phi)\right|^2 D_A(\omega_\Phi)\mathrm{A}_m(\omega;\ \omega_\Phi)W(\omega_\Phi)d\omega_\Phi;$$

$$G_3(\omega)=\int_{-\infty}^{\infty}\Psi(\omega;\ \omega_\Phi)W(\omega_\Phi)d\omega_\Phi,$$

where m_A, $D_A(\omega_\Phi)$ – are mathematical expectation and variance of the pulse amplitudes [9]:

$$m_A=R_\Phi bc\left(m_\tau\frac{C_T}{\delta^{0,4}}+m_\gamma\frac{m_{\omega_\Phi}^2 R_\Phi^2}{2\cdot 10^3}\right);$$

$$D_A(\omega_\Phi)=R_\Phi^2 b^2 c^2\left[D_\tau\left(\frac{C_T}{\delta^{0,4}}\right)^2+\frac{D_\gamma\omega_\Phi^4 R_\Phi^4}{4\cdot 10^6}\right],$$

where b – is the width of blade interacting with peat; C_T – is coefficient depending on the type of operating device [2]; δ – is average thickness of a chip [2]; m_τ, m_γ, D_γ, D_τ – are mathematical expectations and variances of the yield point τ and density γ of peat; m_{ω_Φ} – is mathematical expectation of the cutter angular speed;

$$\Psi(\omega;\ \omega_\Phi)=\left|S_e(j\omega;\ \omega_\Phi)\right|^2\times$$
$$\times\sum_{m=1}^{M}\sum_{\substack{l=1\\ m\neq l}}^{M}\exp\left[-j\frac{\omega}{\omega_\Phi}(\varphi_m-\varphi_l)\right]K_{qgml}\mathrm{A}_{ml}(\omega;\ \omega_\Phi)+$$
$$+2\left|S_e\left(j\omega;\ \omega_\Phi\right)\right|^2\sum_{m=1}^{M}\sum_{l=1}^{M}\mathrm{A}_{ml}\left(\omega;\ \omega_\Phi\right)\sum_{p=1}^{\infty}K_{qgmlp}\times$$
$$\times\exp\left[-j\frac{\omega}{\omega_\Phi}(\varphi_m-\varphi_l)\right]\cos\left(\frac{\omega}{\omega_\Phi}2\pi p\right),$$

where $K_{Aml}(\omega_\Phi)$, $K_{Amlp}(\omega_\Phi)$ – are correlation moments of the pulse amplitudes,

$$K_{Aml}(\omega_\Phi) = R_\Phi^2 b^2 c^2 \times$$
$$\times\left[D_\tau K_{\tau\perp}\left[(m-l)h\right]\left(\frac{C_T}{\delta^{0,4}}\right)^2 + D_\gamma K_{\gamma\perp}\left[(m-l)h\right]\frac{\omega_\Phi^4 R_\Phi^4}{4\cdot 10^6}\right];$$

$$K_{Amlp}(\omega_\Phi) = R_\Phi^2 b^2 c^2 \times$$
$$\times\left[D_\tau K_\tau\left[(m-l);p\right]\left(\frac{C_T}{\delta^{0,4}}\right)^2 + D_\gamma K_\gamma\left[(m-l);p\right]\frac{\omega_\Phi^4 R_\Phi^4}{4\cdot 10^6}\right],$$

where $K_{\tau\perp}[(m-l)h]$, $K_{\gamma\perp}[(m-l)h]$ – are normalized correlation functions of variation of the yield point τ and density γ of peat in a direction transverse to the milling unit movement; $K_\tau[(m-l);p]$, $K_\gamma[(m-l);p]$ – are normalized correlation functions of the spatial variation (both in the movement direction and in the direction transverse to the movement) of the yield point τ and density γ of peat; $S_e(j\omega;\omega_\Phi)$ – is spectrum of a function describing section moment of unit amplitude on a blade.

The squared absolute value $S_e(j\omega;\omega_\Phi)$ is [9]:

$$\left|S_e(j\omega;\,\omega_\Phi)\right|^2 =$$
$$=\frac{1}{4}\left\{\left|U(\omega-\omega_\Phi;\,\omega_\Phi)\right|^2 + \left|U(\omega+\omega_\Phi;\,\omega_\Phi)\right|^2 -\right.$$
$$\left.-2U(\omega-\omega_\Phi;\,\omega_\Phi)\times U(\omega+\omega_\Phi;\,\omega_\Phi)\cos\varphi_k\right\},$$

where:

$$U(j\omega;\,\omega_\Phi) = \frac{2}{\omega}\sin\frac{\omega\varphi_k}{2\omega_\Phi}.$$

The density of the cutter angular velocity distribution can be calculated using the approaches presented in [5].

MTP-42 has the following design parameters and modes of operation. The cutter diameter is 0.8 m. Its width is 1.7 m. Total number of cutting planes is 29, in each of which four blades are positioned. Dish-shaped blades are mounted on the operating device surface in blade holders [2]. Diameter of a cutting element (blade) is equal to 0.078 m.

The calculation was performed at average milling depth of 0.4 m, yield point of 26 kPa [2], peat density of 890 kg/m^3 [2] (their coefficients of variation were accepted at 10%), milling cutter angular speed of 32.5 s^{-1} having normal distribution density with coefficient of variation of 3%. The unit speed of advance is 0.089 m/s.

The distribution of blade positioning errors relative to the "ideal" positions on the cutter body is shown in Fig. 2.

Fig. 3 shows the moment spectral density without taking into account the blade positioning error ("ideal" operating device), calculated using the expressions obtained in [5, 9]. Fig. 4 presents the moment spectral density taking into account the blade positioning errors.

In Fig. 4, the frequency zones (A and B) lying between the peaks multiples of blades interaction frequencies in the cutting plane are highlighted and presented in separate graphs to show these areas in more detail.

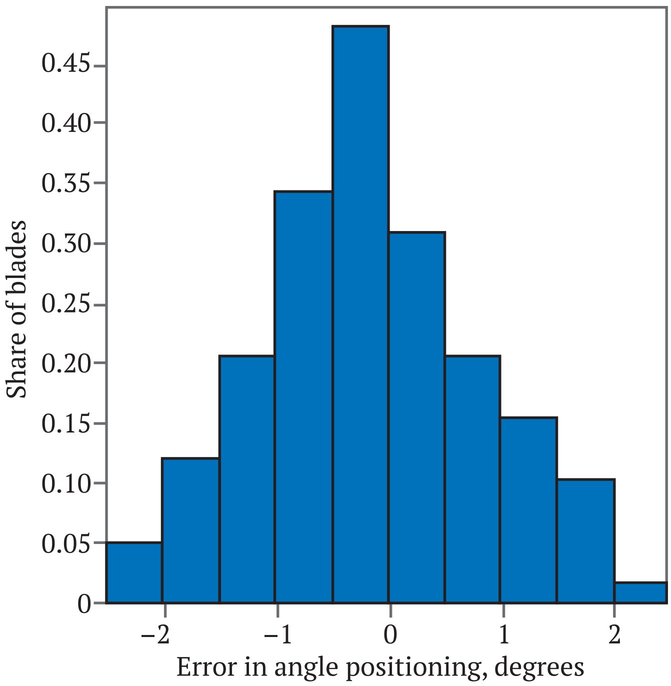

Fig. 2. Distribution of errors of blade positioning on the operating device (X axis – Error in angle positioning; Y axis – Share of blades)

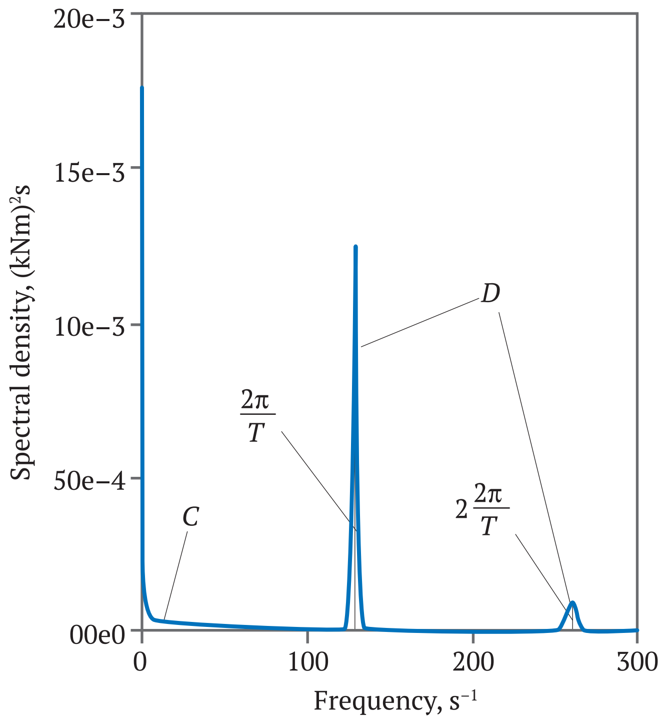

Fig. 3. Moment spectral density for "ideal" operating device

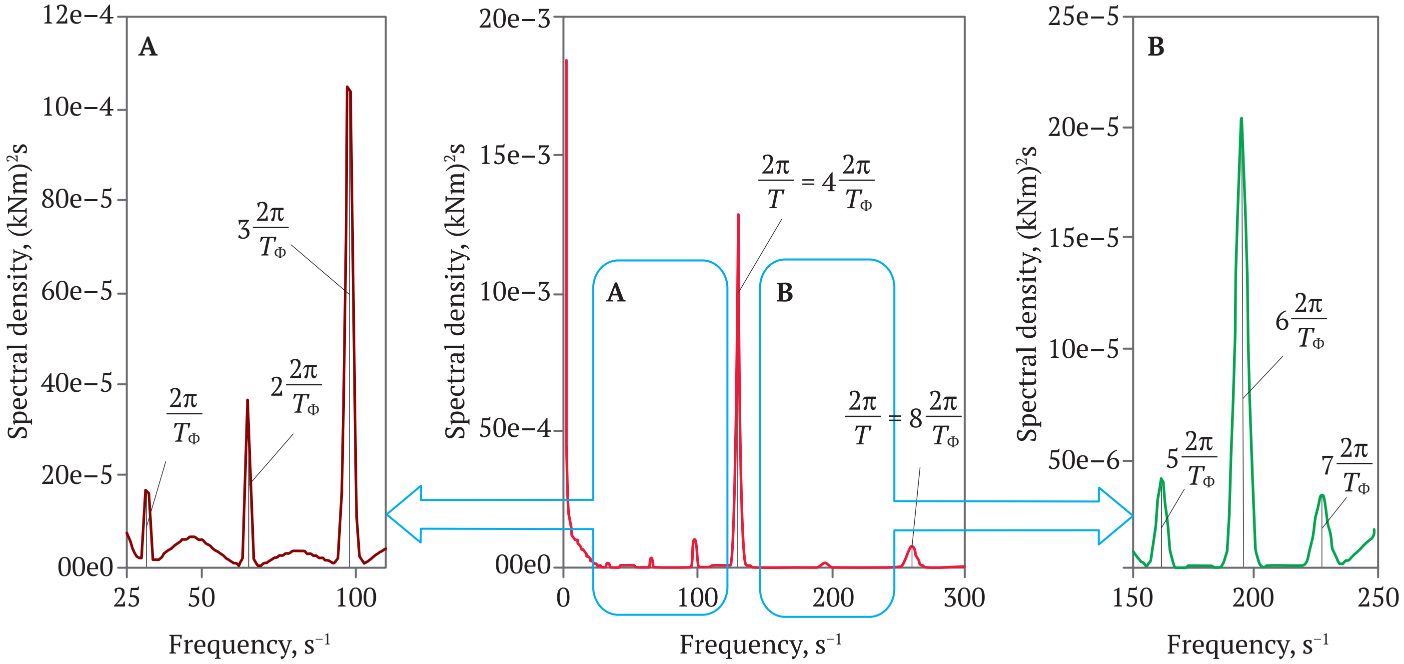

Fig. 4. Section moment (on cutter) spectral density taking into account blade positioning errors

The obtained expressions and calculation results make it possible to highlight some characteristic features of the section moment on a milling cutter.

For the “ideal” operating device, two components can be distinguished in the spectral density (Fig. 3). The first one, the continuous one, is proportional to the variances of the pulse parameters and to the squared absolute value of the section moment spectrum on a blade (*C* in Fig. 3).

Its appearance is defined by correlation functions of pulses parameters, the spectrum of the moment on a blade $S_e(j\omega;\, \omega_\Phi;\, P)$ and the function depending on the arrangement of blades on a cutter [5]:

$$Z(\omega) = \sum_{m=1}^{M}\sum_{l=1}^{M} \exp\left[-j\frac{\omega}{\omega_\Phi}(\varphi_m - \varphi_l)\right].$$

The second part of the spectral density (*D* in Fig. 3) is related to the periodic interaction of blades with peat (kinematic component) [5].

It represents a sequence of peaks, the form of which is determined by a kind of angular velocity distribution density of an operating device, belonging to frequencies $\omega_r = 2\pi r / T$, where $r = 1, 2, 3\ldots$, multiple of the period of blades interaction with a peat deposit. Its value is proportional to the squared mean values of the pulse parameters, spectrum $S_e(j\omega;\, P)$ and depends on the blade arrangement.

Errors in positioning cutting elements on a cutter body lead to changes in value and nature of load, its frequency content (Fig. 4), including appearance of additional components at frequencies multiple of cutter angular speed $\omega_r = 2\pi r / T_\Phi$, where $r = 1, 2, 3\ldots$, enriching load spectrum and increasing its variance. Then the spectral density is proportional to:

$$\sum_{m=1}^{M}\sum_{l=1}^{M}\sum_{k=1}^{K}\sum_{i=1}^{K}\left[1+\frac{\Delta\delta_{mk}}{\varphi_T}\right]\left[1+\frac{\Delta\delta_{li}}{\varphi_T}\right]\exp\left[-j\frac{\omega}{\omega_\Phi}(\delta_{mk}-\delta_{li})\right].$$

Despite its relatively small value, these features should be taken into account if an operating device has a large number of blades and uses fine feeds.

The effect of these additional loads is greatest when the natural frequencies of a unit drive members are equal or multiple to the milling cutter angular speed, because this can lead to resonance phenomena which can increase the dynamic loads in the unit drive members.

Conclusion

Probabilistic models of section moment at an operating device of a milling unit were suggested in the paper, and on their basis analytical expressions for calculating spectral density of the moment, taking into account the impact of errors of blade positioning on the milling cutter body, were obtained. They can be connected with installation and manufacturing errors, deterioration of cutting elements design parameters due to their wear or irreversible deformations during operation.

Errors in positioning cutting elements on a cutter body lead to changes in the magnitude and nature of load and its frequency content. In this case, new, additional components appear at frequencies multiple of the cutter's angular velocity, enriching the load spectrum and increasing its variance. Their magnitude is determined by the nature and cumulative value of the errors.

These facts should be taken into account in the calculation of dynamic loads in designing structural members of milling units, especially if their operating devices have a large number of blades, use fine feeds, and when the natural frequencies of the structural members are equal to or multiple of the angular speed of a milling cutter.

The research findings serve as a basis for the development of methods for dynamic analysis of milling unit structural members, as well as the corresponding mathematical support and software for their computer-aided design systems. Application of CAD will increase the efficiency of new machinery development, reduce the design time, and allow providing recommendations to reduce loads and improve the reliability of structural members of existing units.

References

1. Misnikov O.S. Basic technologies and equipment used for peat deposit development in foreign countries. In: *E3S Web Conf.: III^th International Innovative Mining Symposium*. 26 January 2018. 2018;41(6):01046. https://doi.org/10.105/e3sconf/20184101046

2. Samsonov L.N. *Peat deposit milling.* Moscow: Nedra Publ.; 1985. 211 p. (In Russ.)

3. Kopenkin V.D., Kopenkin L.V., Samsonov L.N. Development of milling machines in peat production (analysis, prospects). *Mining Information and Analytical Bulletin*. 2003;(10):204–207. (In Russ.)

4. Gorlov I.V., Rakhutin M.G. Effect of the presence of stumps on no-failure performance of peat harvesting machines. *Mining informational and analytical bulletin*. 2017;(12):139–145. (In Russ.)

5. Samsonov L.N., Fomin K.B. *Elements of statistical dynamics of peat milling facilities*. Tver: Tver State Technical University; 2005. 168 p. (In Russ.)

6. Mikhaylov A.V., Rodionov E.A., Zvonarev I.E. Analysis of conditions for vertical cutting of peat. *Mining Informational and Analytical Bulletin*. 2019;(1):48–54. (In Russ.) https://doi.org/10.25018/0236-1493-2019-01-0-48-54

7. Michailov A.V., Zhigulskaya A.I., Garmaev O. M. An integrated approach to strip mining of peat. In: *IOP Conf. Series: Earth and Environmental Science*. 2019;378:24–27. https://doi.org/10.1088/1755-1315/378/1/012087

8. Yablonev A.L., Krutov Yu.V. The use of modern digital service stress measurements in the study load of peat machines. *Mining Informational and Analytical Bulletin*. 2016;(8):200–205. (In Russ.) URL: https://giab-online.ru/files/Data/2016/8/200_205_8_2016.pdf

9. Fomin K.V. Method for estimating the spectrum density of the resistance moment on the working body of a peat milling unit. *Journal of Mining Institute*. 2020;241:58–67. https://doi.org/10.31897/PMI.2020.1.58

10. Fomin K.V. Mutual spectral densities calculation of the moments of resistance on the peat milling unit working bodies. *Journal of Mining Institute*. 2021;251:746–756. https://doi.org/10.31897/PMI.2021.5.14

11. Zong X., Guo Q., Kang K., Jia H., He B. Study on Installation Angle of the Milling Wheel Accurate Estimation and Compensation. In: *MATEC Web of Conferences: the 3^rd International Conference on Mechatronics and Mechanical Engineering (ICMME 2016)*. 2017;95:04005. https://doi.org/10.1051/matecconf/20179504005

12. Cheluszka P., Jagieła-Zając A. Determining the position of pick holders on the side surface of the working unit of the cutting machine in the robotic technology of their assembly. In: *IOP Conference Series: Earth and Environmental Science*. 2019;261:012003. https://doi.org/10.1088/1755-1315/261/1/012003

13. Shabaev O.E., Bridun I.I. Technical diagnostics of a roadheader cutting operating device. *Mining Information and Analytical Bulletin*. 2017;(9):94–101. (In Russ.) https://doi.org/10.25018/0236-1493-2017-9-0-94-101

14. Lalanne C. *Mechanical Vibration and Shock Analysis, Random Vibration (Mechanical Vibration and Shock Analysis.* 3^rd Edition. John Wiley & Sons, Ltd; 2014. 595 p. https://doi.org/10.1002/9781118931127

15. Lutes L.D., Sarkani Sh. *Random vibrations: analysis of structural and mechanical systems*. 2004. 635 p.

16. Svetlitsky V.A. *Statistical dynamics and reliability theory for mechanical structures*. Springer, Berlin/Heidelberg; 2003. 452 p. https://doi.org/10.1007/978-3-540-45826-5

17. Gusev A.S. *Probabilistic methods in mechanics of machines and structures*. Moscow: N. E. Bauman Moscow State Technical University Publ.; 2009. 224 p. (In Russ.)

18. Dokukin A.V., Krasnikov Yu.D., Khurgin Z.Ya. *Statistical dynamics of mining machines*. Moscow: Mashinostroenie Publ.; 1978. 238 p. (In Russ.)

19. Krasnikov Yu.D. *Simulation of coal disintegration by cutting tools*. Moscow: Nauka Publ.; 1981. 181 p. (In Russ.)

20. Li X.H., Yu X.W., Ma X.H., Zhao Y.B. Simulation and study of random loads on continuous miner cutting drum. *Advanced Materials Research*. 2011;308–310:1885–8. https://doi.org/10.4028/www.scientific.net/amr.308-310.1885

21. Liu C.S., Li D.G., Chen X.P. Shearer load identification of the load spectrum of the pick based on chaotic characteristics. *Advanced Materials Research.* 2011;199–200:111–114. https://doi.org/10.4028/www.scientific.net/AMR.199-200.111

22. Medolago A.A., Melzi S. A flexible multi-body model of a surface miner for analyzing the interaction between rock-cutting forces and chassis vibrations. *International Journal of Mining Science and Technology*. 2021;31(3):365–375. https://doi.org/10.1016/j.ijmst.2021.03.006

23. Howard R.M. *Principles of random signal analysis and low noise design: The power spectral density and its applications*. Willey; 2002. 310 p. https://doi.org/10.1002/0471439207

24. Levin B.R. *Statistical fundamentals of radio-engineering*. Moscow: Radio i Svyaz' Publ.; 1989. 656 p.

Information about the author

Konstantin V. Fomin – Dr. Sci. (Eng.), Associate Professor, the Head of the Department of Mechanization of Environmental management and Repair of Machines, Tver State Technical University, Tver, Russian Federation; ORCID 0000-0002-8153-1115, Scopus ID 57202900121; e-mail fomin_tver@mail.ru

Received 23.12.2021
Revised 27.01.2022
Accepted 01.02.2022

MINING MACHINERY, TRANSPORT, AND MECHANICAL ENGINEERING

Research article

https://doi.org/10.17073/2500-0632-2022-2-170-179

Justification of geometrical parameters of lining plates for a belt conveyor drive drum

E. Yu. Ziborova[1], V. U. Mnatsakanyan[2] ✉

[1] JSC NPO Istok named after Shokin, Fryazino, Russian Federation

[2] National University of Science and Technology "MISiS" (NUST MISiS), Moscow, Russian Federation

✉ artvik@bk.ru

Abstract

Belt conveyors are widely used in mining industry in open-pit and underground mining for moving bulkload in horizontal and inclined directions to the sites of processing. In order to create the best conditions of frictional contact between a belt and a drum, various methods of drive drum lining are used. The main lining material is rubber of different grades, providing proper coefficient of friction of a belt with a drum (within the range of 0.6–0.62). A drive drum lining material must have high wear resistance, thermal resistance, mechanical strength, ability not to accumulate electric charges on the surface and not to generate dangerous concentrations of toxic components (for example, chlorine gases, carbon monoxide) when heated. The use of ceramic lining opens up great opportunities for increasing lining durability and useful life of high capacity heavy-duty conveyors. The paper presents the results of the study of stress-strain state of belt conveyor drive drum ceramic lining plates. We used *Solid Work Simulation* environment in the study on the basis of the accepted analytical model of plate-belt contact for drive drum with diameter D = 1250 mm, belt width L = 1000 mm, and the belt entering branch tension value S_e = 25400 daN with regard to the value, direction, and nature of the acting loads. On the basis of stress-strain analysis of alumina ceramics lining plates, the favorable geometrical parameters of the plate cleats (projections) and the required properties of lining material ensuring the proper load-carrying capacity at the contact with the belt rubber facing were found. It was established that a plate cleat diameter for heavy duty conditions should be not less than 4.5 mm and its end round R should be within the limits of 0.5–0.6 mm, and, in the base, 0.3–0.4 mm at a cleat height of 1.0–1.4 mm in order to prevent stress concentration in hazardous sections. It was also established that alumina ceramics bending strength must be no less than 350 MPa for effective functioning of rubber-ceramic lining. Simulation of a plate stress-strain state on exposure to alternating loads made it possible to identify characteristic areas with maximum stress concentration, which were foci of crack nucleation. Thus, it became possible to predict lining useful life.

Keywords

belt conveyor, drive drum, ceramic lining, geometrical parameters, working section shape, stress concentration, properties, useful life

For citation

Ziborova E. Yu., Mnatsakanyan V. U. Justification of geometrical parameters of lining plates for a belt conveyor drive drum. *Mining Science and Technology* (*Russia*). 2022;7(2):170–179. https://doi.org/10.17073/2500-0632-2022-2-170-179

ГОРНЫЕ МАШИНЫ, ТРАНСПОРТ И МАШИНОСТРОЕНИЕ

Научная статья

Обоснование геометрических параметров футеровочных пластин приводного барабана ленточного конвейера

Е. Ю. Зиборова[1], В. У. Мнацаканян[2] ✉

[1] АО «НПП «Исток» им. Шокина», г. Фрязино, Российская Федерация

[2] Национальный исследовательский технологический университет «МИСиС» (НИТУ МИСиС), г. Москва, Российская Федерация

✉ artvik@bk.ru

Аннотация

Ленточные конвейеры широко применяются в горной промышленности при открытой и подземной добыче полезных ископаемых для перемещения насыпных грузов в горизонтальном и наклонном направлениях до мест их переработки. Для создания наилучших условий фрикционного контакта ленты с барабаном применяют различные способы футеровки приводных барабанов. Основными футеровочными материалами служат резины различных марок, обеспечивающие должный коэффициент сцепления барабана с лентой, величина которого находится в пределах 0,6–0,62. Материал футеровки приводных барабанов должен иметь высокую износостойкость, термостойкость, механическую прочность, способность не накапливать на поверхности электрических зарядов и при нагреве не образовывать опасных концентраций ядовитых токсических составляющих, например, хлорные газы, окись углерода. Широкие возможности в направлении повышения долговечности футеровок и повышения ресурса тяжелонагруженных конвейеров большой мощности открывает применение керамических футеровок. В статье представлены результаты исследования напряженно-деформированного состояния керамических футеровочных пластин приводного барабана ленточного конвейера. Исследование проводилось с использованием среды *Solid Work Simulation* на основе принятой расчетной схемы контакта пластины с лентой для приводного барабана диаметром D = 1250 мм с шириной ленты L = 1000 мм и величиной натяжения набегающей ветви ленты $S_{нб}$ = 25400 даН с учетом величины, направления и характера действующих нагрузок. На основе анализа напряженно-деформированного состояния футеровочных пластин из алюмооксидной керамики выявлены благоприятные геометрические параметры выступов и требуемые свойства футеровочного материала, обеспечивающие им должную несущую способность при контакте с резиновой обкладкой ленты. Установлено, что диаметр выступов пластин для тяжелых условий эксплуатации должен составлять не менее 4,5 мм, при этом радиус скругления торцевой кромки R желательно выдерживать в пределах 0,5…0,6 мм, у основания – 0,3…0,4 мм при высоте выступа 1,0…1,4 мм, что предотвращает появление концентрации напряжений в опасных сечениях. Установлено, что для эффективной эксплуатации резинокерамических футеровок предел прочности при изгибе алюмооксидной керамики должен быть не менее 350 МПа. Симуляция напряженно-деформированного состояния пластины при воздействии на нее знакопеременных нагрузок позволила выявить характерные участки с максимальной концентрацией напряжений, являющиеся очагами зарождения трещин. Таким образом, появилась возможность прогнозировать ресурс футеровки.

Ключевые слова
ленточный конвейер, приводной барабан, керамическая футеровка, геометрические параметры, рабочий профиль, концентрация напряжений, свойства, ресурс

Для цитирования
Ziborova E. Yu., Mnatsakanyan V.U. Justification of geometrical parameters of lining plates for a belt conveyor drive drum. *Mining Science and Technology* (*Russia*). 2022;7(2):170–179. https://doi.org/10.17073/2500-0632-2022-2-170-179

Introduction

Belt conveyors are widely used in mining industry in open-pit and underground mining for moving bulkload in horizontal and inclined directions to the sites of processing. They belong to continuous transport machines and, as compared with other types of mining transport are characterized by high energy efficiency and productivity [1–3]. The basic trends in belt conveyor development both in Russia and abroad consist, first of all, in increase of their productivity and useful life at the expense of traction stabilization [4, 5], automation of conveyor lines[1], application of powerful drives [6], increasing the length and strength characteristics of the applied belts along with ensuring high level of reliability and durability of driving and guiding assemblies [7–12], increasing the conveyors energy efficiency [13] and transportation efficiency with the use of intermediate drives of various designs [14].

The main traction and at the same time load-carrying body of a belt conveyor is conveyor belt *2*, which moves along a closed circuit (Fig. 1). Drive drum *1* imparts motion to belt via friction gearing.

For providing the best conditions of belt-drum frictional contact, in practice, different ways of drive drums lining are widely used. The main lining material, as

[1] Automation of conveyor lines. URL: http://mydocx.ru/8-5102.html (Accessed date 25.01.2022)

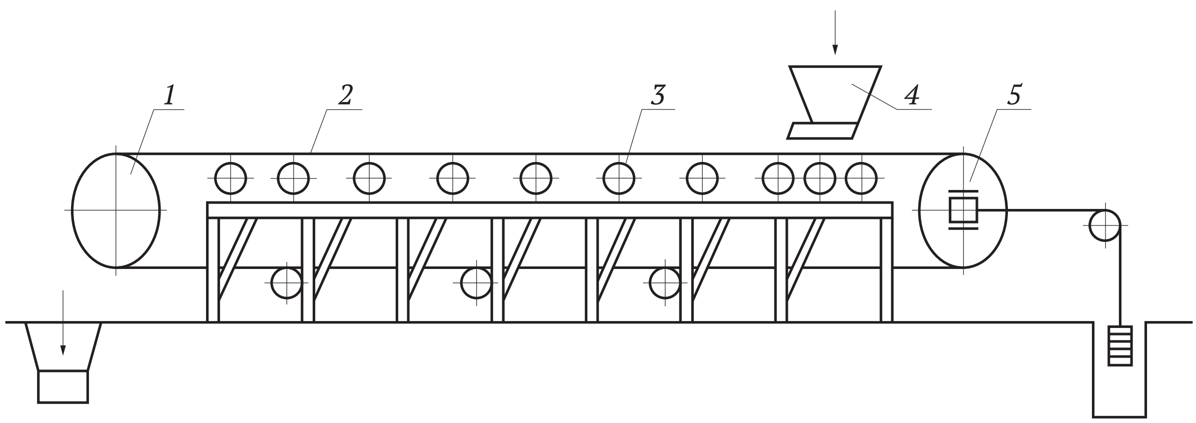

Fig. 1. Belt conveyor schematic:
1 – drive drum; *2* – belt; *3* – belt idlers; *4* – loading device; *5* – tension drum

a rule, is rubber of different grades (Fig. 2, *a*), which ensures proper value of the coefficient of friction between drum and belt (within the range of 0.6–0.62) [1, 8]. The rubber lining disadvantage is sharp decrease in the coefficient of friction in watery conditions. This leads to the belt slipping and loss of traction force.

A drive drum lining material must have high wear resistance, thermal resistance, mechanical strength, ability not to accumulate electric charges on the surface and not to generate dangerous concentrations of toxic components (for example, chlorine gases, carbon monoxide) when heated.

The use of ceramic linings opens up great opportunities for increasing the lining durability and useful life of high capacity heavy-duty conveyors (Fig. 2, *b*). Ceramic lining meets all of the above requirements. For the drums with diameter more than 800 mm, the composite two-three-layer rubber-ceramic, or metal-rubber-ceramic lining is used. Ceramic lining provides the best conditions of friction/friction with partial meshing drum-belt contact with the coefficient of friction of 0.8, which eliminates slippage even at excess moisture in the contact zone and significantly increases the productivity of conveyors, as well as securely fixes a moving belt on a drum width, preventing its slipping[2] [15].

[2] Ceramic plates for drum lining. URL: https://resursbelt.ru/catalog/effektivnost/futerovka/keramika-na-baraban/; Soloviev V. G., Soloviev S. V. Drive drum of a belt conveyor. Patent RU 81949 U1, 2009.

Research objectives and tasks

It is of great practical importance to reduce a belt slip along a drive drum and correspondingly reduce the wear of the belt and the drum surface. In this regard, ceramic lining is the most promising. However, despite their widespread application, there are still a number of urgent problems regarding to the need in increasing their useful life via creation of ceramic plates with a given geometry, improved mechanical and operational properties for the conditions of cyclic loading. Research literature presents recommendations on the selection of geometric parameters of highly elastic lining, while there are virtually no such data for rubber-ceramic lining. A number of leading foreign and Russian manufacturers of composite lining only report about dimensions and height parameters of ceramic plate cleats (projections), the values of which are determined mainly by technological considerations or operating experience[3]. At the same time achieving potential increase in a drive drum traction force and friction coefficient when using rubber ceramic lining first of all requires scientific substantiation of height parameters and shape of a bearing element, which is a cleat

[3] Ceramic plates for drum lining. URL: https://resursbelt.ru/catalog/effektivnost/futerovka/keramika-na-baraban/; T-REXCERA-REX 12x380x10000 rubber-ceramic drum lining. URL: https://centrobelt.ru/conveyor-maintenance/pulley-lagging/ceralag/cera-rex/

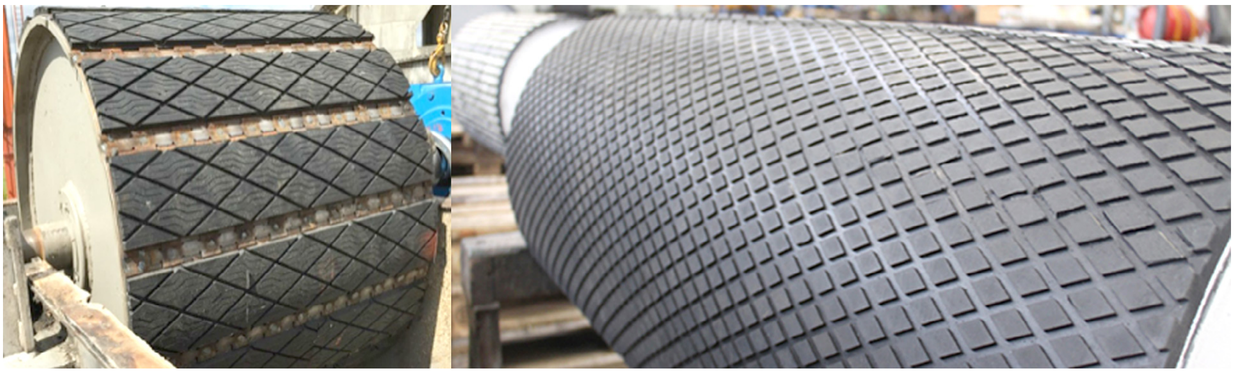

a

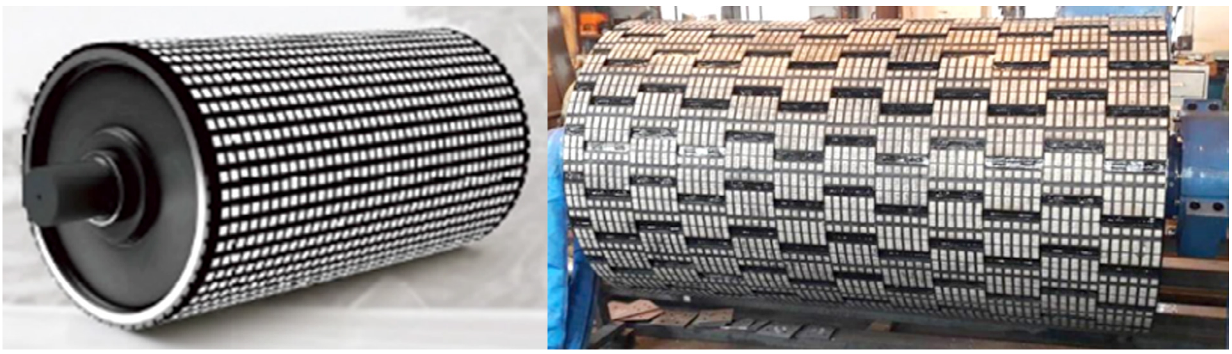

b

Fig. 2. Types of lining:
a – rubber; *b* – rubber-ceramic

immediately contacting with the belt and accepting the main load and providing the required friction during the drive drum rotation. The solution of these problems will allow determining rational parameters of the cleats, providing proper useful life of ceramic plates and, correspondingly, lining useful life along with increasing conveyors' operation and maintenance performance.

Techniques

When traction force is transmitted between a lining and a conveyor belt, the arising forces are described by the following relationship (Fig. 3, *a*):

$$\tau < fN, \tag{1}$$

where f is coefficient of friction between lining and belt; N is the normal force from belt pressure on drum, reduced to unit length ($N = S/R_d$, S is traction body tension force, R_d is drum radius).

In real operating conditions it is accepted to consider the arcs of relative slip (α_s) and relative rest (α_r) (Fig. 3, *b*) [12]. Friction force margin on a drum depends on the ratio of these arcs, while the reserve characterizes slip-free operation of a drive drum. At significant friction force margin (arc α_r) the elastic slippage of a belt relative to a drive drum decreases. As the friction force margin decreases, the slippage increases, and after reaching a certain limit (at $\alpha_s \cong \alpha_r$) the tractive resistance “disappears” and a belt begins to slip relative to a drum. Thus, the traction force is transmitted at the slipping arc, while the arc α_r acts as the traction force reserve. At the same time, as shown in [16, 17], when using elastic lining, some part of the traction force is also transferred at the arc of relative rest.

The influence of geometrical parameters and lining material properties, which ensure drive operation without relative slippage of a belt on a drum, is considered in [12, 16, 17]. In this case the shear of lining with the height H under the effect of distributed forces τ is expressed by the following relation: $\tau = G\gamma$, where G is shear modulus of lining material; γ is angular (shear) strain of lining (Fig. 3, *c*).

The increment of force S at section dx is defined by the equality, where it is assumed that $\gamma = u/H$:

$$dS = B\tau dx = \frac{G}{H}Budx. \tag{2}$$

After a number of transformations in studies [12, 16], traction factor on a lined drum, which carries out the traction force transfer without relative slipping, was expressed by the following formul:

$$\frac{S_e}{S_l} = chml \text{ or } \Phi = chml, \tag{3}$$

Taking

$$m^2 = \frac{G}{EHh},$$

after transformation we have got

$$\Phi = ch\sqrt{\frac{G}{EHh}}l, \tag{4}$$

where c is arbitrary constant, determined by boundary conditions; h is thickness of conveyor belt; l is the arc length of arc of belt contact; H is lining height; G is shear modulus of lining material; E is modulus of elongation.

After transformations, according to [16], the equation takes the form:

$$arch\frac{S_e}{S_l} = \sqrt{(G/H)(B/E_0)}l, \tag{5}$$

where $E_0 = EhB$ is belt longitudinal rigidity; B belt width; S_e and S_l is tension of entering and leaving branches of conveyor belt, respectively.

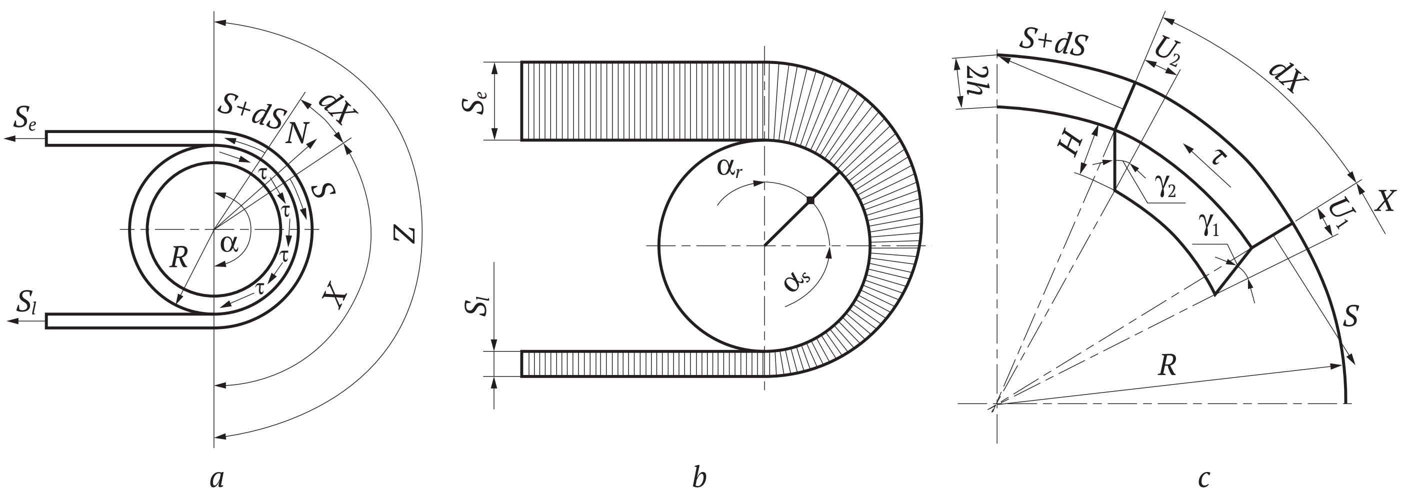

Fig. 3. Schematic of traction force transfer by a drum on:
a – non-weighted, non-stretchable thread; *b* – tensile thread without lining; *c* – tensile thread with lining

It follows from formulas (4) and (5) that, along with a belt material, the lining material rigidity and height parameters have a significant effect on the tractive force value.

The ultimate angular strain of a lining element (Fig. 3, *c*) is defined as:

$$\gamma_{lim} \cong tg\,\gamma_{lim} = \frac{u_0}{G}, \qquad (6)$$

where u_0 is ultimate value of belt strain.

Study [17], devoted to research of highly elastic drum lining parameters, concluded that the increase in thickness of lining and especially its serrated part contributed to the increase of traction ability of a drive drum.

It should be noted that in a ceramic lining, a working element is a plate cleat, the height and diameter of which must be strictly regulated due to ceramics brittleness. Bearing capacity and operating characteristics of lining are first of all defined by stability and integrity of a cleat, therefore substantiation of its height parameters, shape (geometry), and required strength properties is an important applied research task, the solution of which will improve heavy-duty conveyors' performance and efficiency of drive drum lining maintenance and repair.

Cleats take up both by normal and circumferential forces while rotating drum and, consequently, their resistance to rupture determines bearing capacity of lining, especially in the cases when plates are fixed by glue directly on a drive drum shell without elastic rubber base.

As a rule, cleats are distributed over a plate surface at a certain distance from each other, often in chessboard order, which creates a kind of topography for implementation of contact with a belt on the principle of "friction with partial meshing", as well as the possibility of removing water, dirt, and other mechanical particles from the contact zone of plates with the belt. At the same time, the plate-belt contact zones location in single areas of the plate working shape aggravates the loading of each individual element and requires the lining material to have high performance characteristics.

The limiting factors of ceramics application in friction assemblies of belt conveyors are the reduced crack resistance and fatigue strength (bending strength) of the material, caused by heterogeneity of applied ceramics structure, the presence of latent defects and porosity in it.

Increasing plate cleats height is expedient up to a certain value only in order to avoid their rupture under the action of cyclic operating loads.

The interaction of a conveyor belt with a lined drive drum is rather complex process that requires consideration of a large number of factors. The available mathematical apparatus used to identify the relationship between lining strains and circumferential forces is very difficult for engineering calculations, overloaded by a large number of coefficients and often does not allow to take into account all factors [17]. Therefore, computer modeling capabilities were used to solve the tasks.

Currently, in mining, geotechnics, and geophysics, methods of computer simulation and numerical analysis allowing fairly accurate description of various states of technical system elements are widely used to describe and study complex production processes occurring in various mining and geological conditions, as well as solve a number of applied problems in the field of mining machine drives, belt conveyors, and conveyor belts [18–25].

In order to identify favorable geometry of ceramic cleats (inserts), digital models of lining plates were created and the stress-strain state of plate cleats in contact with a belt was investigated taking into account the direction of the existing loads [17]. It was considered that a belt under the action of tangential forces experiences shear strain, and a lining experiences both shear strain in the circumferential direction and compression shear strain in the radial direction (Fig. 4), that is, it occurs in a complex stress-strain state (SSS).

The lining stress-strain state study assumptions were as follows:

– a ceramic lining material is isotropic;

– centrifugal forces are not taken into account;

– at the arc of belt contact with lined drum, Euler's law acts;

– in investigating lining stress-strain state, only steady-state processes are considered;

– shear strains of the elastic part of a lining, into which ceramics is embedded (vulcanized), are low enough and do not exceed 10% of its thickness;

– a belt is assumed to be absolutely elastic.

Computer simulation of the loading process was performed using *Solid Work Simulation* software for lining of drum with diameter D = 1250 mm, belt width L = 1000 mm, and the belt entering branch tension value S_e = 25400 daN. Alumina ceramics with compressive strength of 950 MPa, bending strength of 390–400 MPa, and modulus of elongation E = 374 ГПа. GPa were taken as a material for lining plates. Poisson's ratio ν was taken as 0.3. Shear modulus G was determined by the following formula:

$$G = \frac{E}{2(1+\nu)}.$$

When simulating the contact, the following constraints were taken into account [11]:

– maximum allowable belt tensions at the point of entry on a drum are 0.16–0.25 of the tensile strength of available belts of corresponding width;

– the load on a lining can be up to 1000 kN.

eISSN 2500-0632
https://mst.misis.ru/

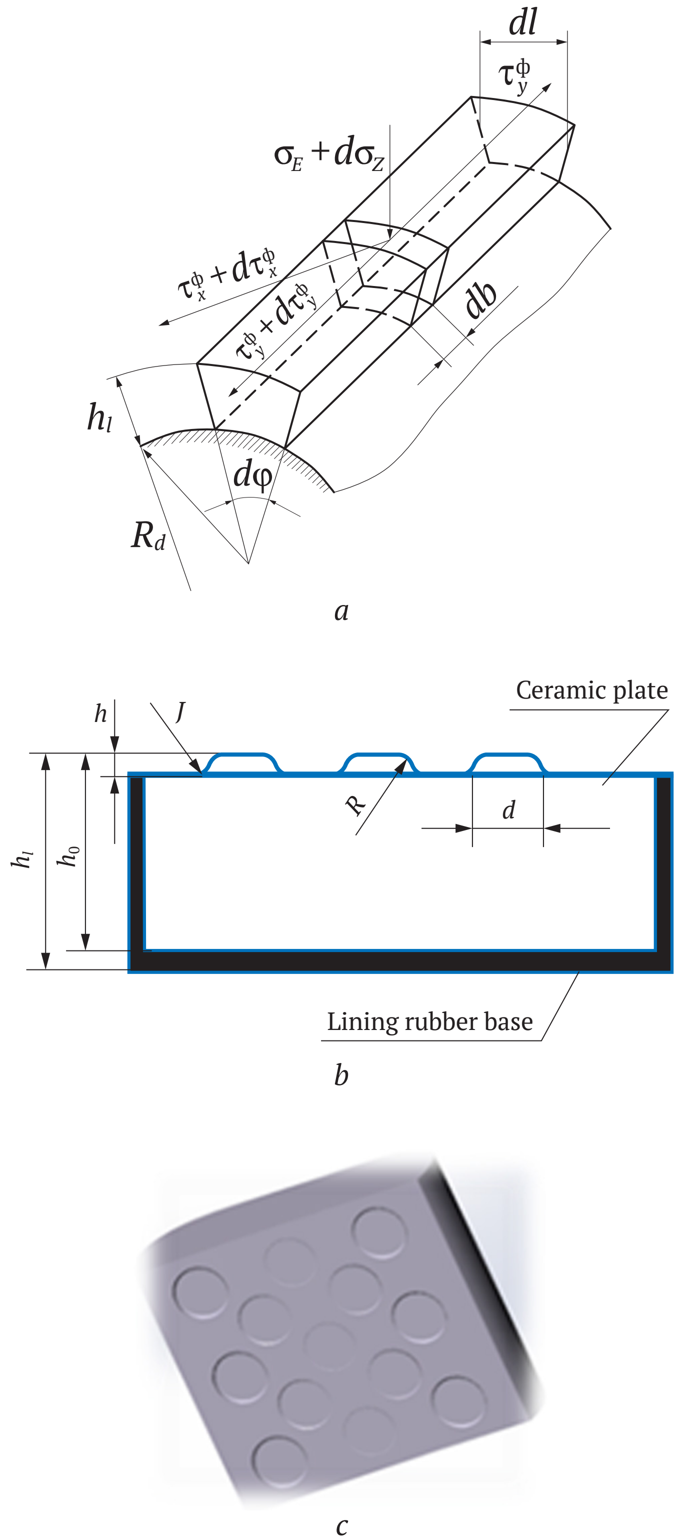

Fig. 4. Schematic diagram for analyzing stress state of elementary sections of a drum ceramic lining (*a*), parameters of ceramic insert (cleat) (*b*) and a digital model of the imprint of ceramic plate cleats in the rubber belt cover due to elastic contact (*c*):
R_d is radius of drive drum; h_l is total lining height; h_0 is ceramic plate height; σ_z – is normal stress; τ_x^ϕ, τ_y^ϕ are tangential stresses in the circumferential direction and across drum width, respectively; *d* and *h* are cleat diameter and height; *J* is radius at the base of a cleat; *R* is cleat end round (end bending radius)

A plate dimensions ($L \times B \times h_0$) were taken as 20×20×8 mm, a cleat diameter *d* varied in the range of 3.0–4.5 mm, a cleat height *h* varied from 1.0 to 2.0 mm, a cleat end round *R* ranged 0.2–0.8 mm, radius at the base of a cleat *r* ranged from 0.2 to 0.4 mm.

The imprint of the digital model working surface on a belt rubber cover, shown in Fig. 4, *b*, evidences that the greatest pressure is experienced by the plate peripheral cleats, which come into contact with the belt and leave the contact when the drum turns.

The maximum specific shear stress on the drum was determined by the following formula [17]:

$$\tau_{\max} = \frac{S_e}{B(R + h_l)}\mu,$$

where S_e is tension of conveyor's entering branch; *B* is belt width; *R* is radius of drive drum without lining; h_l is lining thickness; μ is coefficient of friction.

Findings

The findings of simulation of the stress-strain state of a ceramic plate are shown in Figs. 5, 6, and 7.

Fig. 5 shows solid digital models of the plates with characteristic zones of stress concentration in the most vulnerable points. Thus, the stresses are localized mainly at the base of the cleats (Fig. 5, a), as well as in the middle part of the lower base of the plate. During the operation of ceramic lining defects begin to nucleate exactly in these areas, thus limiting the plate's useful life at insufficient level of mechanical properties, in particular, bending strength. This property determines the fatigue strength of a ceramic plate and, correspondingly, the resistance to cyclic loads. It has been established that effective operation of rubber ceramic lining requires the (plate) alumina ceramics bending strength to be at least 350 MPa, whereas that of the ceramics used in recent lining is 280 MPa only.

At the first stage, the diameter and height parameters of the cleats were investigated. Fig. 6 shows a graph of stress dependency on the height of cleats under the most unfavorable contact conditions and loads at diameters 3.0 mm (curve 1), 3.5 mm (curve 2), 4.0 mm (curve 3), and 4.5 mm (curve 4). The graphs show that stresses increase with increasing the cleats height and reach a maximum at the height of 1.8 mm. The stresses are concentrated at the base of the cleats that leads subsequently to crack nucleation and accelerated failure of the cleats.

Curve 4 indicates a favorable stress field at the bases of cleats 4.5 mm in diameter due to larger cross-section and, consequently, better resistance to strain and cracking under cyclic loading conditions. The stresses simulation findings showed that the height of the cleats 3.0 mm in diameter should not exceed 1.2 mm. At the same time, the height of the cleats 4.5 mm in diameter can vary within the range of 1.0–1.8 mm.

eISSN 2500-0632
https://mst.misis.ru/

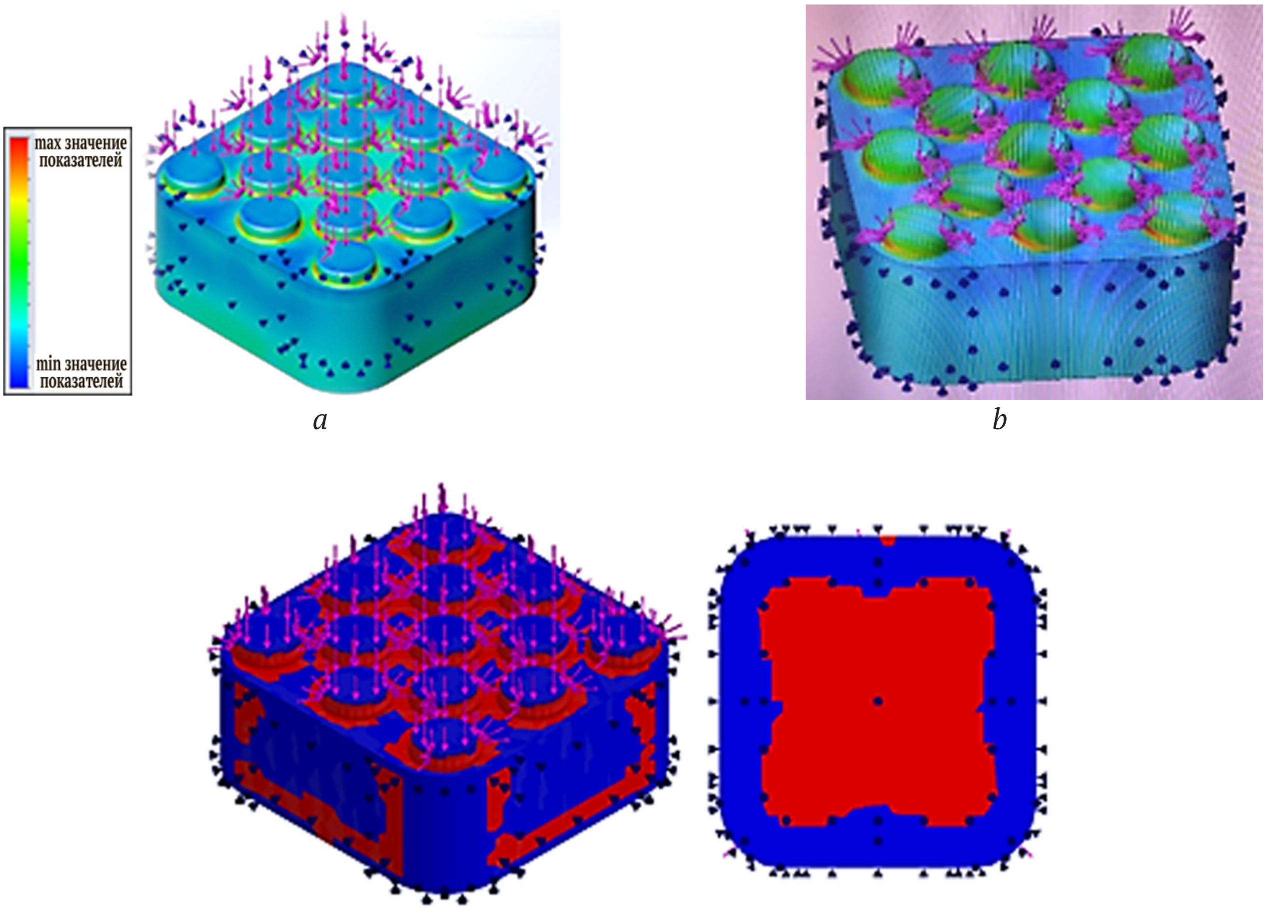

Fig. 5. Simulation of the stress-strain state of digital solid models:
a – when loading cleat 4.5 mm in diameter and 1.4 mm high with radius at the base r = 0,25 mm, end round R = 0,4 mm simultaneously by tangential and normal forces; *b* – when loading cleat 4.5 mm in diameter and 1.8 mm high by tangential force at r = 0,25 mm and R = 0,8 mm; *c* – simulation of stresses under cyclic loading of a plate (areas of fatigue crack nucleation at the cleat bases and in the central zone of the solid part of a plate are shown in red)

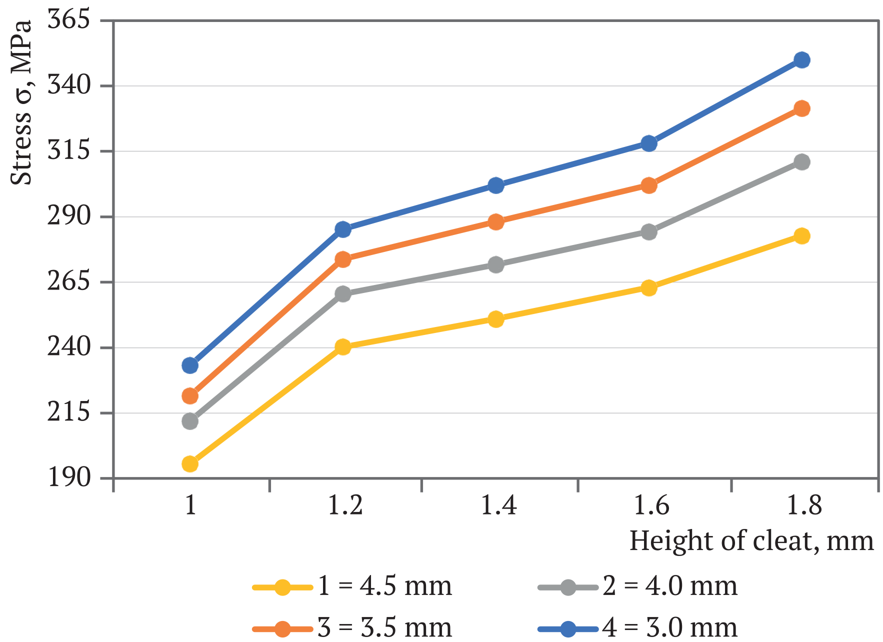

Fig. 6. Stress at plate cleat bases as a function of cleat height and diameter

Fig. 7 shows the results of a numerical experiment with the stresses obtained for various combinations of varied parameters such as a cleat height, round end *R*, and cleat base radius *r*. The analysis was performed for cleats of 4.5 mm in diameter.

The graphs show that significant increase of stresses is observed with decreasing the cleat base radius, and the greater the cleat height, the higher magnitude of the increase. For instance, decreasing *r* from 0.4 to 0.2 mm at h = 1.4 mm and R = 0.3 mm results in increasing stresses from 260 to 340 MPa. At the same time, changing end rounds R results in insignificant changing the near-end stresses.

The numerical experiment data allowed determining the most rational geometrical parameters, which provided favorable conditions for contact of plates with belt under extreme loading conditions. It can be seen from the graphs that the best contact conditions, in terms of the resulting stresses, occur at the following values of geometric parameters: h = 1.0–1.4 mm, R = 0.4–0.6 mm and r = 0.35–0.4 mm.

The research of strain-stress state of ceramic plates allowed producing their digital models (Fig. 8) that made it possible to produce their prototypes with different topography of working section for further experimental research. Fig. 7, *b* shows lining prototypes with ceramic plates embedded (vulcanized) into rubber substrate. The prototypes were made of different fine alumina ceramics grades, which have a dense structure and improved physical and mechanical properties. The plate test results will be presented in the next publications.

Simulation of the stressed state of a ceramic insert (plate) under cyclic load allowed determining the areas of fatigue cracks nucleation (Fig. 5, *c*). The Figure shows that the area of high stress concentration is observed at the cleat bases and in the central part of the lower plate plane. This is probably where fatigue cracks will begin to develop and eventually lead to plate failure.

Conclusion

1. On the basis of stress-strain state analysis of alumina ceramics lining plates, favorable geometrical parameters of cleats and the required properties of the lining material ensuring the proper bearing ca-

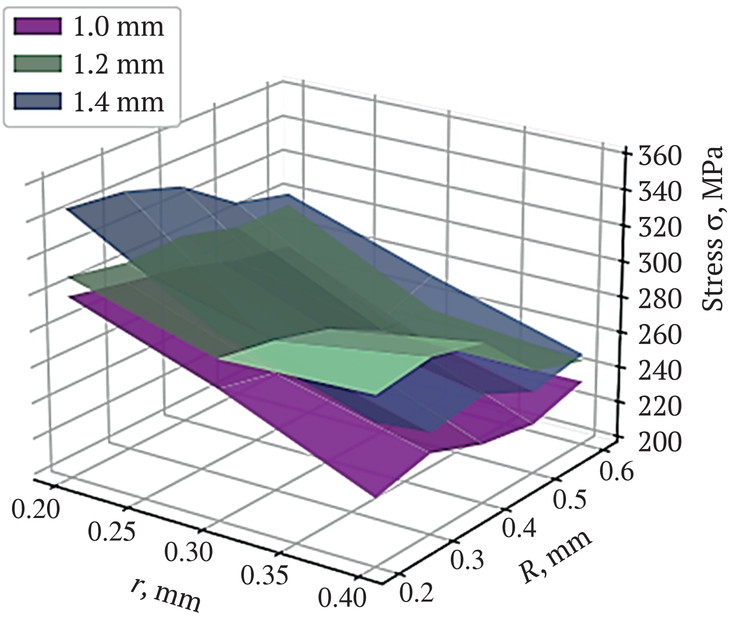

Fig. 7. Stress as a function of geometrical parameters of ceramic plate cleats: radius at the base *r* and end edge *R*

a *b*

Fig. 8. Digital models (*a*) and prototypes (*b*) of ceramic plates for rubber-ceramic lining

pacity at their contact with the belt rubber cover were found. It was established that a plate cleat diameter for heavy duty conditions should be not less than 4.5 mm and the end round R should be within the limits of 0.5–0.6 mm, and, at the base, 0.3–0.4 mm, at a cleat height of 1.0–1.4 mm to prevent stress concentration in hazardous sections.

2. It was also established that the alumina ceramics bending strength must be no less than 350 MPa for effective functioning of rubber-ceramic lining.

3. Simulation of a plate stress-strain state on exposure to alternating loads made it possible to identify characteristic areas with maximum stress concentration, which were foci of crack nucleation. Thus, it became possible to predict lining useful life.

4. Using the obtained digital models of lining plates, production prototypes were produced in the aim of conducting further in-situ tests of lining elements. The production prototypes were made using ultra-disperse alumina ceramics.

References

1. Galkin V.I., Dmitriev V.G., Diachenko V.P. et al. *Modern theory of belt conveyors of mining enterprises*. Moscow: Gornaya Kniga Publ.; 2005. 543 p. (In Russ.)

2. Andreyev A.V., Dyakov V.A., Sheshko E.E. *Transport systems for open-pite mining*. Textbook. Moscow: Nedra Publ.; 1975. 464 p. (In Russ.)

3. Volkov R.A., Gnutov A.N., Dyachkov V.K. et al. *Conveyers*. Handbook. Under the general editorship of Yu. A. Perten. Leningrad: Mashinostroenie Publ.; 1984. 367 p. (In Russ.)

4. Dmitrieva V.V, Aung K.P., Pevzner L.D., Htay W.Z. Development of a mathematical model of belt conveyor with twin-engine drive. In: *International Academic Conference on Engineering, Technology and Innovations (IACETI-2016)*. Beijing, China. 2016. Pp. 5–8. URL: https://worldresearchlibrary.org/up_proc/pdf/454-14765147035-8.pdf

5. Aung K.P. Maintaining traction factor value of belt conveyor with two-engine drive. In: *Third International Conference on Advances in Mechanical and Automation Engineering – MAE 2015*. Rome, Italy. 2015. Pp. 45–48. https://doi.org/10.15224/978-1-63248-080-4-73

6. Polunin V.T., Gulenko G.N. *Operation of heavy-duty conveyors*. Moscow: Nedra Publ.; 1986. 344 p. (In Russ.)

7. Khachatryan S.A. *Problems of reliability of conveyor transport in coal mines*. St. Petersburg: St. Petersburg State Mining Institute (Technical University); 2004. 182 p. (In Russ.)

8. Galkin V.I., Sheshko E.E. Modern tapes for special tape conveyors. *Mining Informational and Analytical Bulletin*. 2016;(S1):382–395. (In Russ.)

9. Solovyh D.J. Computer simulation of the stress state of the belt conveyor drive pulley to assess the durability of welds. *Mining Informational and Analytical Bulletin*. 2015;(1):3–11. (In Russ.)

10. Dmitriev V.G., Asaenko V.V. The character of ring loading of a drive pulley belt conveyor with variable friction coefficient of belt with its surface. *Mining Informational and Analytical Bulletin*. 2011;(2):375–378. (In Russ.) URL: https://giab-online.ru/files/Data/2011/2/Dmitriev_2_2011.pdf

11. Verzhanskiy A.P., Solovykh D.Ya. Belt conveyor drums welded joints endurance assessment. *Ugol'*. 2016;(4):32–36. (In Russ.) https://doi.org/10.18796/0041-5790-2016-4-32-36

12. Dyakov V.A., Shakhmeister L.G., Dmitriev V.G. et al. *Belt conveyors in mining industry*. Under the editorship of A.O. Spivakovsky Moscow: Nedra Publ.; 1982. 349 p. (In Russ.)

13. Mathaba T., Xia X. Optimal and energy efficient operation of conveyor belt systems with downhill conveyors. *Energy Efficiency*. 2017;10(2):405–417. https://doi.org/10.1007/s12053-016-9461-8

14. Trufanova I.S., Serzhan S.L. Improving Transportation Efficiency Belt Conveyor with Intermediate Drive. *Journal of Mining Institute*. 2019;237:331–335. https://doi.org/10.31897/pmi.2019.3.331

15. Ushanova S.E., Ziborova E.Yu. Increasing the durability of friction units for mining equipment and conveyor transport. *Mining Information and Analytical Bulletin*. 2020;5(S15):3–8. (In Russ.) https://doi.org/10.25018/0236-1493-2020-5-15-3-8

16. Mossakovsky V.I., Rudiakov G.Z., Salitrennik V.B. Study of interaction of conveyor belt and elastic lining of a drum. *Izvestiya Dnepropetrovskogo gornogo instituta*. 1967;(48):55–67 (In Russ.)

17. Zharikov V.S. *Study of linings of drive drums for belt conveyors in coal mines*. [Ph.D. thesis in Engineering Science]. Moscow. 1973. (In Russ.)

18. Voznesensky A.S., Kidima-Mbombi L.K. Formation of synthetic structures and textures of rocks when simulating in COMSOL Multiphysics. *Mining Science and Technology (Russia)*. 2021;6(2):65–72. https://doi.org/10.17073/2500-0632-2021-2-65-72

19. Mihailidis A., Bouras E., Athanasopoulos E. FEM analysis of a belt conveyor driving drum. In: *6 BETA CAE International Conference*. 2015. URL: https://www.beta-cae.com/events/c6pdf/2C_2_AUTH.pdf

20. Marasova D., Ambrisko L., Andrejiova M., Grincova A. Examination of the process of damaging the top covering layer of a conveyor belt applying the FEM. *Measurement*. 2017;112:47–52. https://doi.org/10.1016/j.measurement.2017.08.016

21. Rozbroj J., Necas J., Gelnar D., et al. Validation of movement over a belt conveyor drum. *Advances in Science and Technology-Research Journal*. 2017;11(2):118–124. https://doi.org/10.12913/22998624/71183

22. Rybak J., Khayrutdinov M.M., Kuziev D.A., et al. Prediction of the geomechanical state of the rock mass when mining salt deposits with stowing. *Journal of Mining Institute*. 2022;253:61–70. https://doi.org/10.31897/PMI.2022.2

23. Gubanov S., Petsyk A., Komissarov A. Simulation of stresses and contact surfaces of disk rolling cutters with the rock when sinking in mixed soils. In: *XVIII Scientific Forum "Ural Mining Decade" (UMD 2020)*. 2020;177:03008. https://doi.org/10.1051/e3sconf/202017703008

24. Perekutnev V.E., Zotov V.V. Modeling drive wheels of hoisting machines with rubber cables. *Mining Informational and Analytical Bulletin.* 2020;(6):105–114. (In Russ.) https://doi.org/10.25018/0236-1493-2020-6-0-105-114

25. Melezhik R.S., Vlasenko D.A. Load simulation and substantiation of design values of a pin flexible coupling with a flexible disk-type element. *Mining Science and Technology (Russia)*. 2021;6(2):128–135. (In Russ.) https://doi.org/10.17073/2500-0632-2021-2-128-135

Information about the authors

Ekaterina Yu. Ziborova – Design Engineer, JSC "SPE Istok named after Shokin", Fryazino, Russian Federation; e-mail ziborovaekaterina@mail.ru

Victoria U. Mnatsakanyan – Dr. Sci. (Eng.), Professor, National University of Science and Technology "MISiS" (NUST MISiS), Moscow, Russian Federation; ORCID 0000-0001-9276-7599, Scopus ID 6603501339; e-mail artvik@bk.ru

Received 08.02.2022
Revised 14.05.2022
Accepted 30.05.2022

PROFESSIONAL PERSONNEL TRAINING

Research article

https://doi.org/10.17073/2500-0632-2022-2-180-187

VR/AR technologies and staff training for mining industry

M. V. Vavenkov

Ernst& Young LLC. – Valuation and Consulting Services, Moscow, Russian Federation

vavenkov@gmail.com

Abstract

Personnel working at mining enterprises must be prepared to overcome professional difficulties and to possess the professional competencies required not only for the implementation of processes, but above all their safety. Modern digital modeling technologies used in mining activities expand the boundaries of practical training not only for future mining engineers, but also for working specialists. As part of the training process, it is important that the simulation of the mining environment be of a high quality almost indistinguishable from the actual environment. In this context, the development of process solutions based on virtual and augmented reality (VR/AR technologies) is most relevant. Process automation in the conditions of large-scale digital transformation laid the foundations for the development of VR/AR in mining industry. Data analysis shows that VR/AR technologies are the major consumer of IT solutions. They are in fact the integrator, or the highest "IT-transformation", which in practical terms create digital parallel production objects and processes. Further developments in this area may also change some of the existing traditional entities or create new ones, in the training system as well. An example of such an entity, on which the digital future will depend, is the emerging "digital culture". As such it will be applicable not only in the corporate, industry, but also nationally. Despite the diversity of areas in the development of VR/AR technologies, the maximum effect of their implementation is manifested in the development of special skills of personnel in equipment operation. This clearly relates to the need to ensure the efficiency and reliability of technological operations and processes. The interaction between the consumer and producer of VR/AR solutions together with universities allows a number of problems related to the formation of competencies in the future generation of specialists to be resolved. These include: training of university graduates; creation of specialized courses in educational programs; individual higher educational programs; professional development and retraining courses for specialists in the field of VR/AR technologies in mining; involvement of the academic community representatives in the development of practical tasks based on VR/AR solutions, including researchers of different specializations (geology, geophysics, geotechnics, geoinformatics, aerology, geotechnology, mining machinery and equipment, automation, etc.). Other key areas include the dissemination of the best practices of VR/AR usage in the interests of future customers; creation of a common method to assess the effectiveness of VR/AR projects to determine their investment attractiveness; as well as prediction and creation of future technologies.

Keywords

mining, mining engineer, mining engineering education, IT technology, virtual reality, augmented reality, VR/AR technology, processes, process safety

For citation

Vavenkov M.V. VR/AR technologies and staff training for mining industry. *Mining Science and Technology* (*Russia*). 2022;7(2):180–187. https://doi.org/10.17073/2500-0632-2022-2-180-187

ПОДГОТОВКА ПРОФЕССИОНАЛЬНЫХ КАДРОВ. ОРГАНИЗАЦИЯ ИССЛЕДОВАНИЙ

Научная статья

VR/AR-технологии и подготовка кадров для горной промышленности

М. В. Вавенков

ООО «Эрнст Энд Янг – Оценка и Консультационные услуги», г. Москва, Российская Федерация

vavenkov@gmail.com

Аннотация

Персонал, работающий на горных предприятиях, должен быть готов к преодолению профессиональных трудностей, обладать профессиональными компетенциями, которые связаны не только с реализацией технологических процессов, но и прежде всего с их безопасностью. Современные технологии цифрового моделирования горных производств могут расширить границы практической подготовки не только будущих горных инженеров, но и работающих специалистов. В процессе обучения важно обеспечить высокий уровень симуляции производственной горнотехнической среды воспринимаемой человеком практически в качестве реальной. В этом контексте развитие технологических решений на базе виртуальной и дополненной реальности (VR/AR-технологий) становится наиболее актуальным. Основу фундамента развития VR/AR в горном деле заложила глубокая автоматизация технологических процессов в условиях масштабной цифровой трансформации. Анализ данных показывает, что именно VR/AR-технологии становятся потребителем большинства IT-решений, являясь по сути интегратором, или высшим «IT-переделом», практически ведущим к цифровым параллельным производственным объектам и процессам. Дальнейшее развитие событий в этом направлении может изменить и некоторые существующие традиционные сущности или создать новые, в том числе в системе подготовки кадров. Примером таких сущностей, от которых будет зависеть цифровое будущее, может стать формирующаяся «цифровая культура», которая будет применима не только в корпоративном, отраслевом, но и в национальном аспекте. Несмотря на многообразие направлений развития VR/AR-технологий максимальные эффекты от их внедрения проявляются в формировании специальных навыков персонала в работе с оборудованием, что четко увязывается с необходимостью обеспечения эффективности и надежности технологических операций и процессов. Взаимодействие потребителя и производителя VR/AR-решений вместе с университетами позволяет решить класс задач, связанных с: формированием компетенций у будущего поколения специалистов – выпускников университетов; созданием специализированных курсов в образовательных программах, а также отдельных образовательных программ в высшем образовании, курсов повышения квалификации и профессиональной переподготовки специалистов в области VR/AR-технологий в горном деле; вовлечением в процессы разработки практических задач на основе VR/AR- решений представителей академического сообщества – исследователей разной специализации (геология, геофизика, геомеханика, геоинформатика, аэрология, геотехнологии, горные машины и оборудование, автоматизация и т.д.); распространением лучших практик использования VR/AR в интересах будущих заказчиков; созданием единой методики по оценке эффективности внедрения VR/AR-проектов для определения их инвестиционной привлекательности; прогнозированием и созданием будущих технологий.

Ключевые слова
горное дело, горный инженер, горное инженерное образование, IT-технологии, виртуальная реальность, дополненная реальность, VR/AR-технологии, технологии, технологическая безопасность

Для цитирования
Vavenkov M.V. VR/AR technologies and staff training for mining industry. *Mining Science and Technology* (*Russia*). 2022;7(2):180–187. https://doi.org/10.17073/2500-0632-2022-2-180-187

Introduction

Mining is associated with significant process risks, the assessment of which is made complicated by the specific nature of the processes, as well as a high level of natural uncertainty in the description of objects, processes and their models. Despite the achievements of researchers, much of mining is affected by phenomena which are very difficult to predict [1–3]. Throughout the history of mining, there have been major accidents with severe consequences. Mining engineers, for various reasons, felt helpless in their attempts to predict these disasters [2]. Naturally, the most difficult situation lies in the types of geotechnologies associated with underground mining (underground geotechnology, construction geotechnology). This is due to the complicated mining and geological conditions, a significant number of process factors (dust factor hazard, methane content, ventilation systems and many others), as well as particularly difficult working conditions (lack of natural lighting, contamination of the mine atmosphere, significant physical stresses, etc.). The personnel working at mining enterprises must be prepared to overcome professional difficulties and possess professional competencies required not only for process implementation, but their safety [4–6]. It is for this reason that same or very similar disciplines related to mining safety are taught in practically all the curricula for mining engineers training curricula in specialized universities of the world [7]. These include such disciplines as: ventilation (aerology); mining safety; blasting safety; geotechnics; geophysics; methane safety, etc. [8–10]. Naturally, the autonomy of universities leads to different interpretations of these disciplinary areas, but the essence is the same. Everything is aimed at ensuring that the future mining engineer is qualified to make the right decisions in production conditions, in order to ensure effective implementation of processes and to minimize risks of injuries and accidents in general [11–13].

A special role is played by practical training programs in which real production conditions provide theoretical training of future mining engineers who in this way adapt to real working teams, which is of great socio-professional importance [14, 15].

Practical training in education implies the student's activity in the conditions of real production. However, in this case its scope is limited by the duration of training. In fact, in the case of a four-year bachelor’s degree program in mining engineering (international practice), as offered in many countries, there is not a great time resourcefor lengthy practical experience. At the same time, the training of mining engineers-practitioners is extremely important [16]. In Russia and a number of other countries, educational programs in mining engineering are implemented at the level of a specialist's program with 5.5 years program of studies. This forms conditions for the concentration of rather lengthy practical cycles (2–3 months) with the total duration for the whole term of study of more than 7 months [17]. However, even under these conditions there is always themutual desire to increase its scope– both on the part of universities and the employers. Of course, compromises are necessary to achieve the golden mean between the theory and practice. However, modern digital modeling technologies in mining production can expand the limits of practical training of the future mining engineers and working specialists. This is especially true when, for example, a given enterprise is undergoing large-scale modernization associated with upgrading of equipment and process solutions. This concerns not only traditional simulators, whose purpose is to develop the specialized professional skills at the training stage. It is important to provide high quality simulation of the production mining environment as close to the real environment as possible. In this context, the development of process solutions based on virtual and augmented reality (VR/AR technologies) is most relevant [18, 19] in terms of improvement of practical training within the framework of educational programs, including universities.

Areas for VR/AR development in mining

The mining industry is one of the first industries to use VR/AR technologies in its activities. Throughout its historical development, it has had to deal with a broad range of complex economic, operational and now environmental and social challenges. Over the past 10 years, the global mining industry has invested about 0.5 % of its income in research and development into VR/AR technologies[1].

The intense automation of processes in the conditions of large-scale digital transformation laid the foundation for the development of VR/AR in the mining industry [20]. The use of a significant variety of IT solutions at all stages of production cycles of mining enterprises has been observed (Table 1).

Data analysis shows thatVR/AR technology is the primary consumer of these solutions. They are the main integrator, or the highest "IT transformation" leading to the creation of digital parallel production objects. Further development in this area may also change certain traditional entities or create new ones, also in the staff training system. One example, upon

[1] Fade L. How virtual & augmented reality are revolutionizing the mining industry. URL: https://vrvisiongroup.com/how-virtual-augmented-reality-are-revolutionizing-the-mining-industry/

Table 1

World practices of using IT solutions in mining

IT solution	Scope of application	Examples of application, distinctive features
Mining simulators	Simulation training	Simulators place trainees in a controlled production environment
Underground telecommunications	Underground wireless technology	Communication between workers in the mine and the control site on the surface. Real-time data collection of equipment performance allows rapid response to failures and problems
Personnel tracking	Radio frequency identification of miner's metrics	Instantaneous identification of the worker's location to avoid downtime, errors, and human error
Microseismic monitoring	Monitoring of changes in the structural integrity of the working area	Evaluation of the rock mass phenomena severity, determination of geotechnical safety of mine workings and preventive measures before a catastrophic event or accident
Drones [21]	Positioning underground	Displaying of excavation topology, including the condition of their walls surface
Protective equipment	From gas detection devices to clothing that cools personal protective equipment (PPE)	Real time gas sensors. Cooling vests and other clothing items
Mining data	Analysis of data obtained from innovative equipment. Prediction of the state of production processes	Improvement of all production processes, including logistics
VR/AR technologies	Repairs and maintenance, inspection (audit) and work control, training and coaching of employees	Possibility of team training, including practicing of synchronization of operations. Using VR/AR technologies, the staff not only learns and memorizes the order of operations, but also visually practices actions at each stage of work

which the digital future will depend on, could be the emerging digital culture, applicable not only in corporate industry, but also in the national aspect. Digital culture is understood by experts to be a set of competencies which determine the ability to use information and communication technologies for convenience in a digital environment, interaction with society, and digital tasks in professional activities.

According to the study carried out by PwC, the development of digitalization in the industry will require variability and flexibility in terms of professional competencies on the part of the personnel. The accelerated integration of artificial intelligence in the sphere of industrial production and work in dynamic data environments by means of the implementation of IT solutions will require the transition from linear education to lifelong learning[2] [22].

Practice of introducing VR/AR in the mining sector of Russia

Russian mining companies use VR/AR for a range of different purposes. Interesting studies in terms of evaluating the level of introduction of virtual and augmented reality technologies have been conducted by CapGemini and TAdviser (Russian business sector)[3].

The following basic areas were identified:

1) digital methodological support and simulators for assembly and integration processes for equipment of high-level complexity (virtual training centers);

2) simulators for working in the conditions of elevated hazard;

3) support for the activities of operating personnel (remote expert);

4) evaluation of the load and operating modes of equipment in real time;

5) assessment of the suitability of virtual models to the real physical characteristics and parameters of equipment and processes;

6) creation of archives, including visual ones;

7) solving the problem of visualization of a “digital twin”, also from different and hard-to-access positions and conditions;

8) virtual and visual description of hazardous production zones.

Companies are faced with a wide range of problems, including process, expert and educational ones. Many of these problems are associated with ensuring

[2] Geissbauer R., Lübben E., Schrauf S., et al. How industry leaders build integrated operations ecosystems to deliver end-to-end customer solutions. URL: https://www.strategyand.pwc.com/gx/en/insights/industry4-0/global-digital-operations-study-digital-champions.pdf

[3] Market of industrial VR/AR solutions in Russia Research of TAdviser. URL: https://www.tadviser.ru/index.php/Статья:Рынок_промышленных_VR/AR-решений_в_России_(исследование_TAdviser)

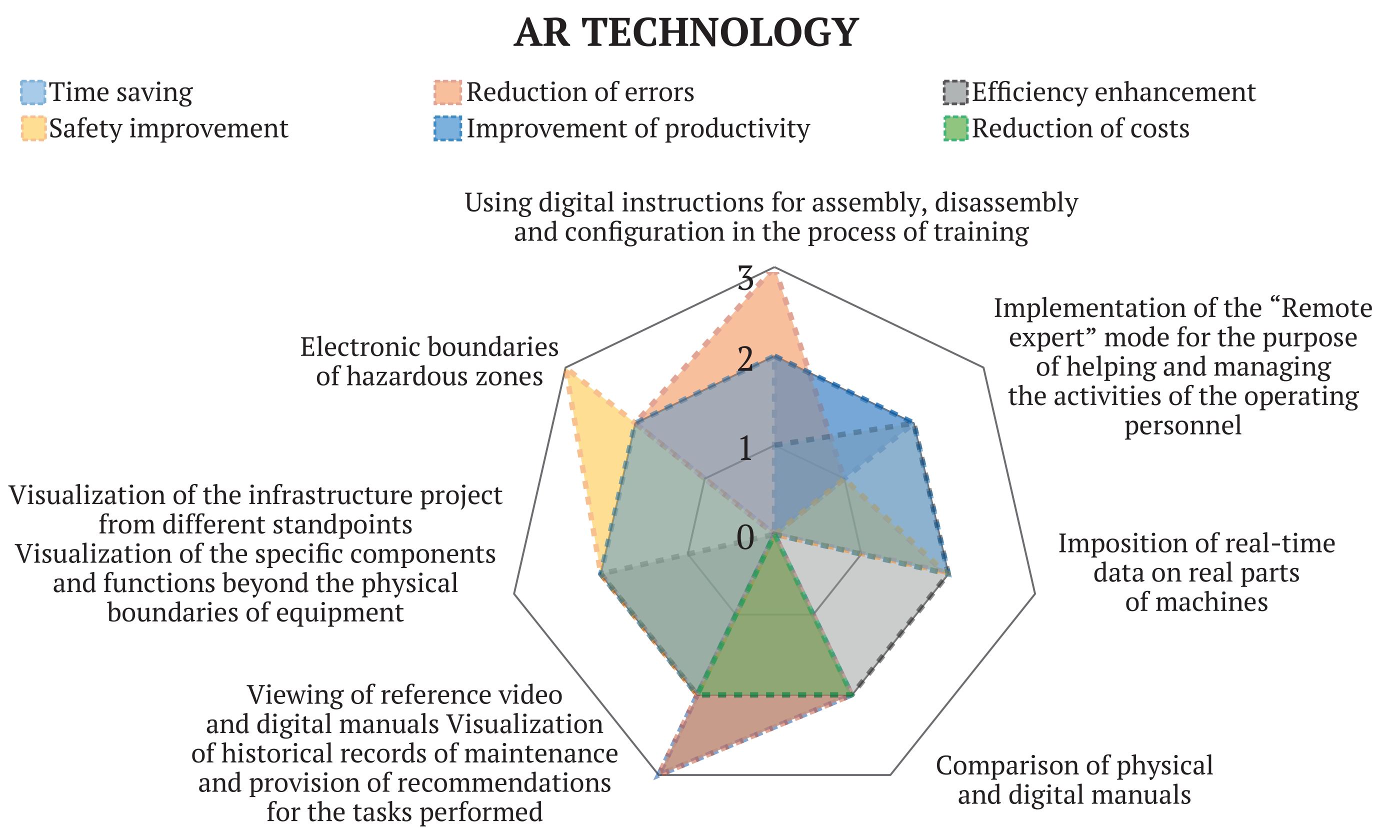

Fig. 1. Expected and real effect from the introduction of AR technologies (according to TAdviser research data)

safety in the conditions of hazardous technological production. There is a class of companies which have been developing corresponding competences through existing corporate centers and/or committees. These include: SIBUR; Severstal; GazpromNeft; EVRAZ; and Magnitogorsk Iron and Steel Integrated Works (MMK). Alrosa and the Siberian Coal Energy Company (SUEK) are also working in this area.

We will provide data with assessment of effects from implementation of VR/AR technologies in the mining complex of Russia (Figs. 1, 2).

This data indicates that the maximum effects of implementing VR/AR technologies are manifested in the formation of special skills of the personnel in working with equipment. This is clearly linked to the efficiency and reliability of technological operations and processes.

Examples of VR/AR solutions in the mining and metallurgical industries are presented in Table 2.

Some of the main challenges faced by companies when implementing VR/AR projects at mining enterprises are:

– significant financial costs required to build the necessary digital infrastructure to implement and adapt VR/AR technologies;

– lack of scalable solutions;

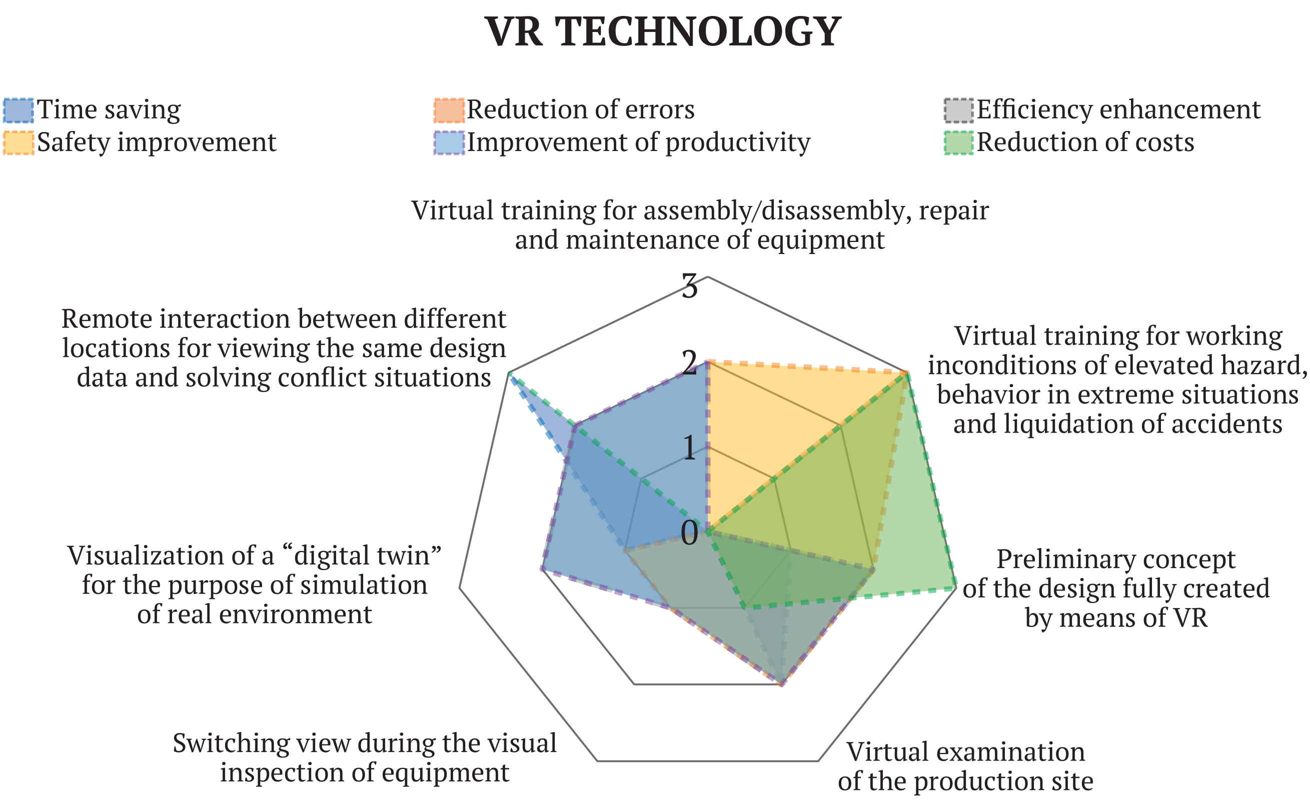

Fig. 2. Expected and real effect from the introduction of VR technologies (according to TAdviser research data)

Table 2

Examples of practical use of VR/AR in Russia

Company in Russia	SIBUR	Gazpromneft	Severstal	Magnitogorsk (MMK)	Evraz
Examples of use	Systems “Remote expert”, “Digital assistant”, interactive training, training in handling hazardous reagents	Systems “Remote expert”, “Digital assistant”, interactive training, training in handling hazardous reagents, virtual technological maintenance	Interactive instructions for disassembling and detection of flaws in pumping equipment, practicing of safety procedures and work in emergency situations, VR shop of the Cherepovets Metallurgical Complex	Virtual training in working in a high-risk environment. Virtual training for behavior in extreme situations and emergency response	Virtual examination of the production site

– lack of methods for calculating the efficiency of implementing such solutions. This introduces uncertainty into the parameters of investment projects;

– limited access to advanced process solutions;

– limited competence of the human potential (lack of qualified personnel at all levels)[4].

Role of VR/AR in training staff for the mining industry

In the context of the mining industry, the main advantages of the AV/VR technology are that it allows training in an environment close to reality, as well as the simulation of virtual scenarios [23]. Obviously, the introduction of virtual and augmented reality technologies in educational programs will require new methodological approaches which will take into account the level of specialists' training, their individual qualifications (installer, operator, dispatcher, mine rescuer, etc.), the number of trainees, and the new role of the teacher, etc. Evaluating the applicability of individual AR and VR technologies, developers also offer mixed MR solutions [24].

The training of operators and maintenance workers of sophisticated equipmenton simulators includes:

1) the process of continuous theoretical training;

2) working on simulators where practical situations at workplaces are practiced;

3) control of knowledge, skills and abilities;

4) working with instructions based on VR/AR solutions;

5) error correction, reinforcement of the correct action algorithms.

Approaches to the implementation of complex VR/AR solutions in the main educational programs for training industry specialists (bachelors, specialists and masters) are presented in a completely different way. A future mining engineer (the higher education level is specialist) should be prepared not only to undertake practice on simulator systems, but also be able to generate complex solutions based on expert evaluations in technological cycles or processes. In this regard, the use of VR/AR technologies in the mining engineer educational process need to be clearly linked with his/her future labor functions. Global practice shows that the best solutions for the formation and development of competencies in the field of the VR/AR environment are implemented by mining enterprises in partnership with universities.

The role of universities as the main concentrators of knowledge is associated with the requirements and expectations of industrial partners. This also involves the development of innovative educational programs and technologies. Universities not only train young specialists, bachelors and masters, but also transfer advanced competencies to the existing staff of enterprises. This in turn allows universities and advanced companies to build long-term partnerships. An indisputable advantage of universities is the state support, including financial support. This can lead to universities becoming centers of technological solutions based on VR/AR technologies. Modern state support of universities in Russia is based on the principles of co-funding of projects by business, which ensures the relevance of projects for the real economy. This approach also allows companies to receive financial support in the form of targeted subsidies from the federal budget under the national projects "Education" and "Digital economy" (subproject "Digital technologies") for the development of VR/AR technologies.

Conclusions

1. Virtual and augmented reality technologies recreate the comprehensive conditions and processes of mining production in high quality, contributing to the formation of professional competencies of personnel of various levels and qualifications. It is worth noting the special role of VR/AR technologies in ensuring the safety of mining operations.

2. Interaction between producers, consumers of services and their cooperation with universities play a great role in the development of VR/AR technologies. Such alliances allow a class of problems related to the formation of competencies in the future generation of specialists to be resolved. These include: the training of university graduates; creation of specialized courses in educational programs, as well as individual higher educational programs; and professional development and retraining courses for specialists in the field of VR/AR technologies in mining. Another outcome is the formation of the corresponding staff potential in general in the industry and not only on a corporate level. This also requires the involvement of the academic community in the development of practical tasks for VR/AR solutions. The researchers engaged in study come from a range of specializations: geology; geophysics; geotechnics; geoinformatics; aerology; geotechnology; mining machinery and equipment, as well as automation, inter alia. This also creates conditions for critical analysis and the improvement of specific solutions. The best practices of VR/AR usage are disseminated in the interests of future customers (market development) and contribute to the creation of a common method to assess the effectiveness of VR/AR projects, thus determining their investment attractiveness, predictability and the creation of future technologies.

[4] Why AR is more promising for the industry compared to VR? URL: https://news.myseldon.com/ru/news/index/221068050

References

1. Ushakov K.Z., Kaledina N.O., Kirin B.F. *Safety of mining operations and mine rescue*. Textbook. Moscow: MGGU; 2002. 487 p. (In Russ.)

2. Kabanov E.I., Korshunov G.I., Kornev A.V., Myakov V.V. Analysis of the causes of methane explosions, flashes and ignitions at coal mines of Russia in 2005–2019. *Mining Informational and Analytical Bulletin*. 2021;(2–1):18–29. https://doi.org/10.25018/0236-1493-2021-21-0-18-29

3. Pelipenko M.V., Balovtsev S.V., Aynbinder I.I. Integrated accident risk assessment in mines. *Mining Informational and Analytical Bulletin*. 2019;(11):180–192. (In Russ.) https://doi.org/10.25018/0236-1493-201911-0-180-192

4. Krechmann Y.U., Plien M., Nguen T.H.N., Rudakov M.L. Effective capacity building by empowerment teaching in the field of occupational safety and health management in mining. *Journal of Mining Institute*. 2020;242:248–256. https://doi.org/10.31897/pmi.2020.2.248

5. Puchkov L.A., Petrov V.L. The system of higher mining education in Russia. *Eurasian Mining*. 2017;(2):57–60. https://doi.org/10.17580/em.2017.02.14

6. Petrov V.L., Krupin Yu.A., Kochetov A.I. Evaluation of professional education quality in mining and metallurgy: New approaches. *Gornyi Zhurnal*. (In Russ.) 2016;(12):94–97. https://doi.org/10.17580/gzh.2016.12.19

7. Sui W.H. Safety geology and geological education for mining engineers. Global View of Engineering Geology and the Environment. In: *Proceedings of the International Symposium and 9th Asian Regional Conference of IAEG*. Beijing, China, 24–25 September 2013. Pp. 563–567. https://doi.org/10.1201/b15794-90

8. Bakum Z., Tkachuk V. Mining engineers training in context of innovative system of Ukraine. *Metallurgical and Mining Industry*. 2014;6(5):29–34. https://doi.org/10.31812/0564/425

9. Mischo H., Brune J.F., Weyer J., Henderson N. Mine disaster and mine rescue training courses in modern academic mining engineering programmes. *Journal of the Southern African Institute of Mining and Metallurgy*. 2014;114(12):987–992.

10. Henderson N.R., Mischo H., Brune J.F. Student mine rescue in today's: Mining engineering curriculum. *Mining Engineering*. 2014;66(2):33–37.

11. Kizil M.S. New developments in the Australian mining education. *Madencilik*. 2017;56(1):33–40.

12. Kazanin O.I., Sergeev I.B. Training a modern mining engineer: Objectives of universities and professional communities. *Gornyi Zhurnal*. (In Russ.) 2017;(10):75–80. https://doi.org/10.17580/gzh.2017.10.16

13. Czaja P. World trends in human resource education for mineral engineering and mining. *Inzynieria Mineralna*. 2018;19(1):179–188. https://doi.org/10.29227/IM-2018-01-29

14. Vercheba A.A. Personnel training for the mining and geological sector of Russia. *Mining Science and Technology* (*Russian Federation*). 2021;6(2):144–153. (In Russ.) https://doi.org/10.17073/2500-0632-2021-2-144-153

15. Lushpey V.P., Makishin V.N. Training of mining engineers at the Far East Federal University. *Gornyi Zhurnal*. 2015;(3):96–100. (In Russ.) https://doi.org/10.17580/gzh.2015.03.16

16. Haupt G., Webber-Youngman R.C.W. Engineering education: An integrated problem-solving framework for discipline-specific professional development in mining engineering. *Journal of the Southern African Institute of Mining and Metallurgy*. 2018;118(1):27–37. https://doi.org/10.17159/2411-9717/2018/v118n1a4

17. Chernikova A.A., Polukhin O.N., Petrov V.L., et al. National university of science and technology MISIS: Contribution to rise and development of mining industry in the Belgorod Region. *Gornyi Zhurnal*. 2014;(8):24–29. (In Russ.)

18. Abdelrazeq A., Daling L., Suppes R., Feldmann Y. Virtual reality mine: A vision for digitalised mining engineering education. In: *Mining Goes Digital – Proceedings of the 39th international symposium on Application of Computers and Operations Research in the Mineral Industry, APCOM 2019*. 2019. Pp. 17–24. https://doi.org/10.1201/9780429320774-3

19. Lindblom A., Laine T.H., Rossi H.S. Investigating Network Performance of a Multi-user Virtual Reality Environment for Mining Education. In: *Proceedings of the 2021 15th International Conference on Ubiquitous Information Management and Communication, IMCOM 2021*. 2021. https://doi.org/10.1109/IMCOM51814.2021.9377356

20. Clausen E., Sörensen A., Uth F., Mitra R. *Assessment of the Effects of Global Digitalization Trends on Sustainability in Mining Part I: Digitalization Processes in the Mining Industry in the Context of Sustainability*. Aachen: Bundesanstalt für Geowissenschaften und Rohstoffe; 2020. URL: https://ecominingconcepts.cl/wp-content/uploads/2021/03/digitalization_mining_dustainability_part_I_en.pdf

21. Kim M.L., Pevzner L.D., Temkin I.O. Development of automatic system for unmanned aerial vehicle (UAV) motion control for mine conditions. *Mining Science and Technology* (*Russian Federation*). 2021;6(3):203–210. https://doi.org/10.17073/2500-0632-2021-3-203-210

22. Kazanin O.I., Marinin M.A., Blinov A.M. Professional retraining in the staffing system for the mining enterprises. *Bezopasnost' Truda v Promyshlennosti*. 2021;(7):79–84. (In Russ.) https://doi.org/10.24000/0409-2961-2021-7-79-84

23. Daling L. M., Khodaei S., Thurner S., et al. A decision matrix for implementing AR, 360° and VR experiences into mining engineering education. In: Stephanidis C., Antona M., Ntoa S. (eds.) *Communications in Computer and Information Science*. Communications in Computer and Information Science. Springer Science and Business Media Deutschland GmbH. 2021;1420:225–232. https://doi.org/10.1007/978-3-030-78642-7_30

24. Abdelrazeq A., Daling L., Suppes R., et al. A virtual reality educational tool in the context of mining engineering – the virtual reality mine. In: *13th International Technology, Education and Development Conference*. Valencia, Spain. 11–13 March, 2019. Pp. 8067–8073. https://doi.org/10.21125/inted.2019.2002

Information about the author

Mikhail V. Vavenkov – Specialist, Ernst & Young – Valuation and Advisory Services LLC, Moscow, Russian Federation; ORCID 0000-0002-5829-7076; e-mail vavenkov@gmail.com

Received 08.03.2022
Revised 03.06.2022
Accepted 04.06.2022